SURFACE JUNCTION THERMAL PROBE FOR TRANSIENT MEASUREMENTS – CONCEPTUAL DESIGN TO FIELD APPLICATIONS

A thesis

Submitted in Partial Fulfillment of the Requirements for the Award of the Degree of

DOCTOR OF PHILOSOPHY

By

Sumit Agarwal

DEPARTMENT OF MECHANICAL ENGINEERING

INDIAN INSTITUTE OF TECHNOLOGY GUWAHATI

JUNE 2018

Dedicated to my parents

Mr. Mahabir Prasad Agarwal and
Mrs. Radha Devi Agarwal,
Sister, Rajni Agarwal, and
Brother, Mr. Ashish Agarwal and his family

Whose endless faith and blessings always
Inspired me to move forward

.

DECLARATION

I hereby certify that the work compiled in this dissertation is the outcome of the research work, performed by myself, else stated, under the guidance of **Prof. Niranjan Sahoo**.

Any part of this work has not been submitted for the award of any degree, diploma, associate-fellowship, fellowship or its equivalent to any university or institution.

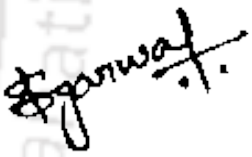

Sumit Agarwal

Registration No. 126103005

Department of Mechanical Engineering

Indian Institute of Technology Guwahati

Department of Mechanical Engineering
Indian Institute of Technology Guwahati
Guwahati-781039, India

CERTIFICATE

It is certified that the work contained in the thesis entitled **"Surface Junction Thermal Probe for Transient Measurements – Conceptual Design to Field Applications"** by **Mr. Sumit Agarwal**, a student, in the department of Mechanical Engineering, Indian Institute of Technology Guwahati, India, for the award of the degree of the Doctor of Philosophy, has been carried out under my supervision and, that this work has not been submitted elsewhere for the degree.

Date: 13/06/2018

Prof. Niranjan Sahoo
(Supervisor)
Professor
Department of Mechanical Engineering
Indian Institute of Technology Guwahati
Guwahati-781039, Assam, India

ACKNOWLEDGEMENTS

Foremost, I would like to offer my heartfelt gratitude to my supervisor, **Prof. Niranjan Sahoo**, who has constantly supported me throughout my research work with his patience, motivation, enthusiasm and colossal knowledge whilst allowing me the room to work in my own way. His guidance has created a big impact during my research work till the completion of this thesis. Briefly, I could not have imagined having a better advisor for my doctorate study. I would also convey my deepest regard to **Dr. Vinayak N Kulkarni** for guiding and giving me his expert opinion towards my research work and beyond, which remains invaluable to me. Furthermore, the financial support rendered by **Dr. Balkrishna Mehta** during my PhD work is highly appreciable. I am also deeply indebted to the **Director** of Indian Institute of Technology Guwahati and sincerely acknowledge for providing me with such a wonderful environment for the inception of my research career.

Besides my supervisor, I would like to thank the doctoral committee members, **Prof. Ujjwal Kumar Saha**, **Dr. Ganesh Natarajan** and **Dr. Tapas Kumar Mandal**, for their encouragement, valuable suggestions, and insightful comments throughout my seminars, which has always directed me towards a meaningful thesis work.

I am very thankful to all the faculty and staff members of the Mechanical Department and **Dr. Amit Shelke** from Civil Engineering Department for furnishing their whole-hearted support in the entire course of my stay. Further, a special appreciation for the senior technician and support staff of the Department for their valuable help namely, **Mr. Nip Borah**, **Mr. Rituraj Saikia**, **Mr. Monuranjan Dowarh**, **Mr. Saiffuddin Ahmed**, **Mr. Sanjib Sarma**, **Mr. Jiten Basumatary**, **Mr. N.K Das**, **Mr. Mrinal Sarma**, **Mr. Dilip Chetri**, **Mr. Nabajyoti Dutta** and **Mr. Raju Talukdar**.

My sincere gratitude to my spiritual Guru **His Holiness Sri Sri Ravi Shankarji** who has been a beam of light in the darkest of times by showering me with the teachings of yoga and meditation. This has helped me immensely to remain calm and distress in every situation. I am perhaps a better version of myself for his blessings. A special mention to **Mr. Ankit Dave**

who was the reason behind me being a part of Art of Living. His act has proven to be a big epiphany for me and shall remain a part of who I am today.

It would be fitting for me to mention my art of living family for teaching the way of life and in turn became an integral part; namely **Dr. Atreyi Ghosh**, **Miss Sarrika Dawar**, **Dr. Bhanita Sharma, Dr. Brajesh Rawat**, **Dr. Vinaya MM**, **Mr. Dhanuvardhan Singh Jhala**, **Mr. Ankit Kumar**, **Mr. Raju Ram Jhakar**, **Mr. Durgesh Kumar**, **Mr. Mrinmoy Dutta**, **Mr. Sachin Aglave**, **Mentor Mr. Virat Chirania and Mr. Vivek Agarwal**, **Miss Garima Chabbra**, **Miss Ila Verma**, **Miss Harsha Choudhary**, **Miss Deepika Bishnoi**, **Miss Ruchika Goyal**, **Mr. Rishi Agarwal**, **Mr. Arvin Tanwar**, **Mr. Nayan Mangal**, **Mr. Rachit Srivastava**, **Mr. Naman Pal**, **Mr. Prashant Singh, Mr. Bikash shah** and **Miss Anju Modi.**

I would deeply thank all my fellow lab-mates in Aerodynamic Laboratory: **Dr. Rakesh Kumar**, **Dr. Ravi Kumar Peetala**, **Dr. P Ramesh Babu**, **Dr. Shrutidhara Sarma**, **Mr. Soumya Ranjan Nanda**, **Mr. Saibal Kanchan Barik**, **Mr. Anil Kumar Rout**, **Mr. Santosh Kumar Hota**, **Mr. Minelik Walle**, **Miss Priyanka Dash**, **Mr. Siddhant Parvat**, **Mr. Siddharth Kar**, **Mr. Hrishikesh Kumar Singh**, **Mr. Manish Sonkar**, **Mr. Amar Singh**, **Mr. Himansu Sahoo** and **Mr. Mahesh Chandra Bharti** for all the valuable discussions and sleepless nights we had to work together. Without them, my journey here perhaps would have been less fun.

The moral support boosted by my seniors, fellow mates and sports family namely, **Mr. Sourabh Sharma**, **Mr. Rasmi Ranjan Behera**, **Dr. Bhaskor Jyoti Bora**, **Dr. Azd Zayoud**, **Dr. Sachin Singh**, **Dr. Jitendra Kumar Patel**, **Dr. Jai Manik**, **Dr. Mohit Sahu**, **Mr. Anupam Alok**, **Mr. Kelli Durgaprasad**, **Miss Rapur Janani Shruti**, **Mr. Vaibhav Jaisawal**, **Mr. Rajendra Soni**, **Mr. Shatrughan Prasad Jaiswal**, **Miss Sangjukta Devi**, **Mr. Rajeev Anupoju**, **Mr. Kishore Gajrani**, **Dr. Anand Agarwal**, **Mr. Shyam Trivedi** , **Mr. Hemanshul Garg**, **Mr. Anshul Garg**, **Mr. Gaurav Kumar**, **Dr. Ambesh Kumar Jha**, **Mr. Milan Krishna Singha Sarkar**, **Mr. Ravi Kumar**, **Mr. Rahul Kumar Chaurasia**, **Mr. Subrat Kotoky**, **Mr. Mukul Parmanand**, **Mr. Vinod Pandey**, **Mr. Arun Kadian**, **Mr. Vinay Kulkarni**, **Mr. Yashojit Kumar**, **Mr. Bikash Kumar Naik**, **Mr. Akash Raj**, **Mr. Himanshu Mishra**, **Mr. Yashwardhan Panwar**, **Mr. Debarshi Mallick**, **Mr. Asif Iqbal**, **Mr. Subra Shankar Kalita**, **Mr. Amit Rathi**, **Mrs. Priyanka Rathi**, **Mr. Parag Kamal Talukdar**, **Mr. Sudhansu Kumar Behera** and **Dr. Kalpajyoti Borah.** Your valuable discussion, team talk, on and off field sledging,

glory days shall all be a part of my good memories. A special mention of my alter ego friends **Mr. Shuvayan Brahmachary**, **Mr. Siddesh Desai** and **Mr. Snehasish Panigrahy**, for enriching my life with the bond of friendship. Our late night gossips, impromptu gathering and the evening "chai" holds something indelible.

My sincere thanks also go to **Prof. Viren Menzes** for offering me an opportunity to visit Shock Tunnel Laboratory, Aerospace department of Indian Institute of Technology Bombay and conduct valuable experiments and giving indispensable insights for the research work. A special mention of **Mr. Kiran Joy Irimpan**, a doctorate student and a good friend along with **Mr. Jadhav** and **Mr. Amol** for helping in every possible aspect during the visit.

I am deeply indebted to the **Gas Turbine Research Establishment** (**GTRE**), **Bengaluru**, with particular mention of **Dr. Sanjay Barad** (**Scientist**, **G**) and **Mr. Vishwanath K** (**Technical Officer 'D'**) from the Strain Gauge Laboratory for guiding and helping in the successful implementation of the experiment. Along with **Mr. T.N. Suresh** (**Scientist**, **G**), **Dr. Dilip Kumar** (**Scientist**, **E**), **Dr. Jitendra Chauhan** (**Scientist**, **C**), **Mrs. Chitra J** (**Technical Officer 'C'**), **Mr. Thimmaraya Setty** (**Technical Officer 'B'**) and **Mrs. Poornima S** for the in-numerable support they provided during my visit, which remains invaluable.

Last but not the least, I owe my profound gratitude towards my parents **Mr. Mahabir Prasad Agarwal** and **Mrs. Radha Devi Agarwal**, my brother and sister-in-law **Mr. Ashish Agarwal** and **Mrs. Yogita Agarwal**, my sister and brother-in-law **Mrs. Rajni Agarwal** and **Mr. Rajesh Agarwal** for being the constant guiding, and supporting force throughout. I also owe thanks to my close friends **Mr. Nimit Jain**, **Mr. Sandeep Jain**, **Mr. Debajit Das**, **Mr. Sahidul Alam**, **Mr. Hardik Ranka**, **Mr. Sammi Kashyap**, **Mr. Rahul Kumar Jaiswal** and **Mr. Mainak Dutta** for being their always as supporting and inspiring force in all the difficult times.

Sumit Agarwal
Indian Institute of Technology Guwahati
June 2018

List of Publications from This Thesis Work

Book Chapter:

1. **Agarwal S** and Sahoo N (2016) Exhaust gas flow field simulation of an internal combustion engine for a thermal sensor, *Fluid Mechanics and Fluid Power – Contemporary Research*, pp.195-203. [doi: https://doi.org/10.1007/978-81-322-2743-4_20]

Journals:

1. **Agarwal S** and Sahoo N (2018) An experimental investigation towards calibration of a shock tube and stagnation heat flux determination, *International Journal of Aerodynamics (IJAD)*, 6(1), 18-40. [doi: 10.1504/IJAD.2018.10010824]

2. **Agarwal S**, Irimpan KJ, Sahoo N, Menezes V and Desai S (2017) Comparative performance assessments of surface junction probes for stagnation heat flux estimation in a hypersonic shock tunnel, *International Journal of Heat and Mass Transfer*, 114, 748-757. [doi: https://doi.org/10.1016/j.ijheatmasstransfer.2017.06.109]

3. Nanda SR, **Agarwal S**, Sahoo N and Kulkarni V (2017) Shock tube as an impulsive application device, *International Journal of Aerospace Engineering*, 2010476. [doi: https://doi.org/10.1155/2017/2010476]

4. **Agarwal S**, Sahoo N and Singh RK (2016) Experimental techniques for thermal product determination of coaxial surface junction thermocouples during short duration transient measurements, *International Journal of Heat and Mass Transfer*, 103, 327-335. [doi: https://doi.org/10.1016/j.ijheatmasstransfer.2016.07.062]

5. **Agarwal S** and Sahoo N (2018) Stagnation point heat flux measurement in the shock tube using coaxial surface junction thermocouple, *Journal of Energy Heat and Mass Transfer (JEHMT)*, (under review)

6. **Agarwal S** and Sahoo N (2017) Determination of instantaneous surface heat flux inside the combustion chamber of an internal combustion engine using coaxial thermal probe, *Journal of The Institution of Engineers (India): Series C*, (under 1st review).

Conferences:

1. **Agarwal S** and Sahoo N (2017) Surface junction temperature probe in shock tube flows, *24th National and 2nd International Conference on Heat and Mass Transfer (IHMTC)*, 27-30 December, BITS Pilani Hyderabad, India.

2. **Agarwal S** and Sahoo N (2016) Comparative analysis of stagnation point heat flux over a hemispherical model using different types of thermal sensors in the shock tube, *4th National*

Symposium on Shock Waves (NSSW), 25-26 February, Karunya University, Coimbatore, India.

3. **Agarwal S** and Sahoo N (2015) Coaxial surface junction thermocouple for transient measurements in the combustion chamber of an internal combustion engine, *International Conference on Advances in Energy Research (ICAER)*, 15-17 December, IIT Bombay, India.

4. **Agarwal S** and Sahoo N (2015) Stagnation point heat flux measurement in the shock tube using coaxial surface junction thermocouple, *23rd National and 1st International Conference on Heat and Mass Transfer (IHMTC)*, 17-20 December, Thiruvananthapuram (ISRO), India.

5. **Agarwal S** and Sahoo N (2015) A coaxial surface junction thermocouple – fabrication and testing in internal combustion engine, *Frontier Energy Research with Industry Academia Partnership (FERIAP)*, March 20-21, IIT Guwahati, India.

6. Shrutidhara S, **Agarwal S** and Sahoo N (2014) Numerical and experimental study for measurement of exhaust gas temperature and heat flux using thermal sensors in an internal combustion engine, *Sixth International Conference on Theoretical, Applied, Computational and Experimental Mechanics (ICTACEM)*, December 29 – 31, 2014, IIT Kharagpur, India.

7. **Agarwal S**, Siddhant P and Sahoo N (2014) Numerical analysis of a coaxial surface junction thermocouple for temperature measurement in the exhaust of an internal combustion engine, *5th International and 41st National Conference on Fluid Mechanics and Fluid Power (FMFP)*, December 12-14, IIT Kanpur, India.

8. **Agarwal S**, Siddhant P and Sahoo N (2014) Fabrication and static calibration of a coaxial thermocouple for short-duration transient measurement, *3rd National Symposium on Shock Waves (NSSW)*, February 21-22, IIT Bombay, India.

Abstract

One of the most crucial requirements of a traditional thermal probe is its ability to accurately reproduce thermal quantities of interest such as transient surface temperature history and heat flux data when engaged in a transient environment. Some of the prominent fields where thermal sensors have been subjected to are Internal Combustion (IC) engine, heat exchanger, steam/gas turbines, shock tunnel/tube applications etc. As such, a thermal sensor is required to operate upon harsh conditions such as impact load in shock tube/tunnel for short duration, pulsating load in IC engines, continuous high temperature load in gas turbine applications etc. Moreover, upon inevitable structural failure, it is highly desirable to reproduce the probe with a minimum investment of paraphernalia cost. Lastly, it is vastly noble if the same cost-efficient and robust thermal probe can be shown to serve the dual purpose of accurate measurement of temperature data as well as the low/high frequency measurement.

Focussing on the need for advancement in high-speed measurement techniques and the requirement to bridge the gap listed in the above paragraph, an attempt has been made to develop an in-situ thermal sensor, which would serve the primary purpose of accurate measurement of heat transfer history as well as frequency measurement.

Considering the hypersonic flows, which are produced for short duration timescale in impulse facilities such as shock tunnels, free-piston shock tunnels and expansion tubes. The test times are in the order of few milliseconds in the shock tunnels and for expansion tubes, it is still less (in the range of 50 μs). The fundamental measurements in these facilities include the prediction of aerodynamic forces and surface heating rates for various generic aerodynamic configurations. During the force/heat transfer measurements in short duration facilities, the model never attains steady state due to very less test times available for experiments. In continuation, the measurement diagnostics must account for this fact while recovering the histories of an unknown force and surface heat transfer rates. Therefore, the fundamental experiments involve localized measurements of temperature histories for surface heating measurements. These sensors has to be mounted in flush on any generic aerodynamic models under study. In this backdrop, the thermal sensors such as coaxial surface junction thermocouples (CSJT) and thin film gauges (TFGs) are highly useful in recovering transient surface temperature. Subsequently, with appropriate heat conduction modelling, the convective surface heat loads on the aerodynamic surfaces can be predicted from the recorded temperature history.

Usually, the transient measurement of temperatures is performed by mounting the thermal sensors embedded on the surface of the heated material. The surface heat fluxes are then

estimated from the temperature history, analytically/numerically by various heat transfer modelling (such as one-dimensional/ two-dimensional/axisymmetric). Moreover, there certain practical situations in which it may not be feasible to keep the thermal sensors on the surface; rather they are mounted at some interior points inside the medium, where inverse heat transfer modelling helps one to estimate the temperature history at that particular location. The thermal sensors such as coaxial thermocouples are advantageous in the manner that it can be mounted in any harsh condition. The thermocouples design involves two dissimilar metals, which are joined together to form a junction and when exposed to a temperature gradient, a corresponding voltage is generated (Seebeck effect). The voltage difference generated can be measured and the corresponding temperature gradient is estimated with the help of the sensitivity of the sensor. The purpose of this thesis is to get greater insight into the fabrication of coaxial surface junction thermocouples, which includes modelling, its calibration, XRD analysis, real-time experimental exposure for supersonic and hypersonic speed, into the internal combustion engine and lastly into the gas turbine engine applications.

Greater efforts have been laid down to acquire good expertise in the fabrication of CSJTs and ultimately develop CSJT in the form of the product. The initial phase of research includes designing of the coaxial thermocouple, which caters carrying out simulation to validate the dimension of the sensor as well as the assumption of one-dimensional heat conduction for semi-infinite theory. Further, based on the simulation results, various sensors namely, E (chromel-constantan), K (chromel-alumel), T (copper-constantan) and J (iron-constantan) types are fabricated in the laboratory. In continuation, X-Ray Diffraction (XRD) analysis has been attempted to study the deformation characteristics of the surface junction.

Further, calibration study based on known temperature and known heat flux has been performed. The known temperature based calibration (static calibration) is carried out to determine the sensitivity of the individual thermocouple using the oil-bath experimental set-up as well as the alumina-based fluidized bath. Additionally, the known heat flux based calibration included the exposure of the fabricated sensor to a known wattage of the laser source, with an intention to determine gauge response in real-time experiments.

Furthermore, few calibration methodology has been undertaken to estimate the thermal product value, which is a property of the material and is a variable under highly transient measurement. The thermal sensor does not predict heat flux directly, it rather gives the voltage-time signal, which with further post-processing gives the heat flux. The heat flux equation (Duhamel Superposition Equation) includes the thermal product value. It is highly desirable to estimate thermal product value for individual thermocouple, as uncertainties up to 25% can be

incorporated. Few of the experiments are executed using the Water droplet technique and Water plunging technique and, also using the shock tube based technology for the determination of thermal product.

The latter part of the study includes exposure of the thermal sensor to the real-time flow environments such as shock tube for studying the low supersonic environment heat flux estimation, shock tunnel for hypersonic flow based heat flux determination, internal combustion engine to study the heat flux phenomenon inside the combustion chamber and for the exhaust environment. Lastly, the study focuses on the detection of combustion instability (screech phenomenon) in the gas turbine engine, to check the capability of thermal sensor beyond heat transfer measurement along with the packaging assembly of the thermal sensor.

CONTENTS

Nomenclature

A	Area (m^2)
E	Gauge thickness (m)
v,u	Velocity (m/s)
a_1	Speed of sound in the driver section of the shock tube (m/s)
a_4	Speed of sound in the driven section of the shock tube (m/s)
c	Specific heat (J/kg-K)
c_p	Specific heat capacity of the test gas (J/kg-K)
C_i	Mass concentration of species *i*
ρ	Density (kg/m^3)
ρ_e	Density at the edge of the boundary layer (kg/m^3)
h	Enthalpy (J/kg)
k	Thermal conductivity (W/m-K)
p	Pressure (N/m^2, bar)
p_∞	Freestream pressure (N/m^2, bar)
p_4 , p_1	Pressure in the driver and driven section of the shock tube (N/m^2, bar)
p_5	Pressure in the driven section of the shock tube after the shock reflection (N/m^2, bar)
p_e	Pressure at the edge of the boundary layer (N/m^2, bar)
Q	Heat Transfer Rate (W)
$\dot{q}$	Heat Flux (W/cm^2, W/m^2)
$\dot{q}_S$	Instantaneous surface heat flux (W/cm^2, W/m^2)
$\dot{q}_\circ$	Stagnation heat flux (W/cm^2, W/m^2)
S	Sensitivity (μV/°C)
M_S	Shock Mach number
$M_{S,t}$	Theoretical shock Mach number
$M_{S,e}$	Experimental shock Mach number

M_R	Reflected shock Mach number
$M_{R,t}$	Theoretical reflected shock Mach number
$M_{R,e}$	Experimental reflected shock Mach number
γ_1, γ_4	Specific heat ratio in the driver and driven section of the shock tube
d	Spacing between two atomic planes (m)
θ	Bragg's Angle
λ	Incident electron beam wavelength ($\overset{\circ}{A}$)
T	Instantaneous temperature (K, °C)
T_{amb}, T_∞	Ambient/freestream Temperature (K, °C)
T_1, T_4	Temperature of the driven and driver section of shock tube (K, °C)
T_5	Temperature in the driven section of the shock tube after the shock reflection (K, °C)
T_S	Surface temperature history (K, °C)
T_W	Water droplet temperature (K, °C)
$T_\circ$	Total temperature (K, °C)
r_i	Inner radius of spherical vessel (m)
s	Surface
S_i	Species production($kg / m^3 s$)
u	Velocity in y direction (m/s)
$\tilde{u}_i$	Diffusion velocity in x direction
v	Velocity in y direction (m/s)
$\tilde{v}_i$	Diffusion velocity in y direction
w	Thickness of spherical vessel (m)
Pr	Prandtl number
R_n	Nose radius of the hemisphere (m)
R	Universal gas constant (J/kg-K)
Y_i	Mass fraction of species i

α	Thermal diffusivity (m^2/s)
$\alpha_\circ$	Thermal expansion (K^{-1})
$\beta(TP)$	Thermal Product ($\sqrt{\rho ck}$, $Jm^{-2}s^{-1/2}K^{-1}$)
β_W	Thermal Product of water ($Jm^{-2}s^{-1/2}K^{-1}$)
β_t	Theoretical Thermal Product ($Jm^{-2}s^{-1/2}K^{-1}$)
β_e	Experimental Thermal Product ($Jm^{-2}s^{-1/2}K^{-1}$)
$\beta_{t,E}$	Theoretical Thermal Product E-type CSJT ($Jm^{-2}s^{-1/2}K^{-1}$)
$\beta_{t,J}$	Theoretical Thermal Product J-type CSJT ($Jm^{-2}s^{-1/2}K^{-1}$)
$\beta_{e,E}$	Experimental Thermal Product E-type CSJT ($Jm^{-2}s^{-1/2}K^{-1}$)
$\beta_{e,J}$	Experimental Thermal Product J-type CSJT ($Jm^{-2}s^{-1/2}K^{-1}$)
μ_e	Dynamic viscosity at the edge of the boundary layer (Ns/m^2)
τ	Time in seconds (s)
σ_h	Hoop Stress (N/m^2)
$\left[T_s(t)\right]$	Rise in temperature (K)
$\left(\Delta T_s/\Delta t\right)$	Temperature gradient (K/s)

Abbreviations

2-D A-C	2-Dimensional model with Alumel inside and Chromel outside
2-D C-A	2-Dimensional model with Chromel inside and Alumel outside
3-D A-C	3-Dimensional model with Alumel inside and Chromel outside
3-D C-A	3-Dimensional model with Chromel inside and Alumel outside
AC	Alternating Current
AEDC	Arnold Engineering Development Centre
AFR	Air-Fuel Ratio
ATDC	After Top Dead Centre
AUSM	Advection Upstream Splitting Method
AWG	American Wire Gauge
BNC	Bayonet Neill–Concelman
BTDC	Bottom Top Dead Centre

CA	Crank Angle
CFD	Computational Fluid Dynamics
COV	Coefficient of Variation
CSJT	Coaxial Surface Junction Thermocouple
CW	Continuous Wave
DART	Delft Aerospace Re-entry Test Vehicle
DAS	Data Acquisition System
DC	Direct Current
DHFG	Direct Heat Flux Gauge
DI	Direct Injection
EDX	Electron Discharge X-ray
EGT	Exhaust Gas Temperature
EMF	Electromotive Force
FEA	Finite Element Analysis
GUI	Graphical User Interface
HCCI	Homogenous Charge Compression Ignition
HFA	Heat Flux Array
HFM	Heat Flux Micro Sensor
HST	Hypersonic Shock Tunnel
ICE	Internal Combustion Engine
IHCP	Inverse Heat Conduction Problem
IIR	Infinite Impulse Response
IMEP	Indicated Mean Effective Pressure
INA	Instrumentation Amplifier
IR	Infrared
IRT	Infrared Thermography
ITO	Indium Tin Oxide
LIF	Laser Induced Fluorescence
LIP	Laser-Induced Phosphorescence
NDE	Non-Destructive Evaluation
PMMA	Polymethyl Methacrylate
RTD	Resistance Temperature Detector
SEM	Scanning Electron Microscope

STS	Surface Temperature Sensor
SWL	Shock Wave Laboratory
SWBLI	Shock Wave Boundary Layer Interaction
TCR	Temperature Coefficient of Resistance
TDC	Top Dead Centre
TFG	Thin Film Gauge
TFTC	Thin Film Thermocouple
TSP	Temperature Sensitive Paint
TLC	Thermochromic Liquid Crystal
TP	Thermal Product
USHAS	Unstructured Solver for Hypersonic Aerothermodynamics Simulations
VCR	Variable Compression Ratio
UV	Ultraviolet
WD	Water Droplet
WP	Water Plunging
XRD	X-Ray Diffractometry

List of Figures

List of Tables

CHAPTER 1

Introduction

1.1 Preface

The field of heat transfer is marked to represent a good portion of both art and science, which is true for the measurement; necessitating one to have a good understanding of the flow physics. It is that discipline of thermal engineering, which has to deal with the generation, conversion and exchange between two physical systems. Further, it is an important aspect/issue considering from engineering design point of view, ranging from cooling chips of a data acquisition system to the protection of re-entry space shuttle. With appropriate modelling, one can predict indirectly the quantity of heat transferred between any two systems, which can be either steady/transient. All the modes of heat transfer involve some classical means of modelling with measurement of temperature as one of the essential criteria for all the modelling techniques, which ultimately predicts the heat flux.

All naturally occurring processes in the universe change with respect to time which complicates the process of heat transfer and makes it a challenge for appropriate prediction of transient temperature data. Many a times, it is not possible to expose the temperature sensors directly in the flow fields due to experimental constraints. In some cases, the sensors need to flush mounted to capture instantaneous rise in temperatures and thereby predicting step/impulse heat loads. Even though, projecting/flush/exposing the probe is not always a feasible option, capturing transient temperatures under different thermal loading environments is very vital for accurate prediction of heating rates. With proper heat transfer modelling, inverse heat transfer techniques one can achieve the desired objective for prediction of heating rates.

The global intentions of the dissertation work remain focused on the design, in-house fabrication, and calibration of heat transfer gauges for real-time applications in transient flow environment pertaining to areas such as low supersonic environment (shock-tube), hypersonic facilities like shock tunnel, afterburner transient temperature of the gas turbine engine, internal combustion engine. This chapter includes the brief historical background with some classical measurement techniques for heat flux.

1.2 Heat Transfer

Heat transfer is concerned with two things, one temperature and other flow of heat. Here, temperature represents the amount of thermal energy available, whereas heat flow represents the movement of thermal energy from place to place. It is the transition of thermal energy from between two objects at different temperatures by satisfying second law of thermodynamics till thermal equilibrium between the objects. When an object or fluid is at a different temperature than its surroundings or another object transfer of thermal energy occurs in such a way that the body and the surroundings reach thermal equilibrium this means that they are at the same temperature. Where there is a temperature difference between objects in proximity, transfer of heat between them can never be stopped, it can only be slowed. A convenient definition of heat transfer is energy in transition due to the temperature difference. The transfer of heat takes place in three different modes: *conduction, convection,* and *radiation* (*Fig. 1.1*). All modes of heat transfer require the existence of a temperature difference.

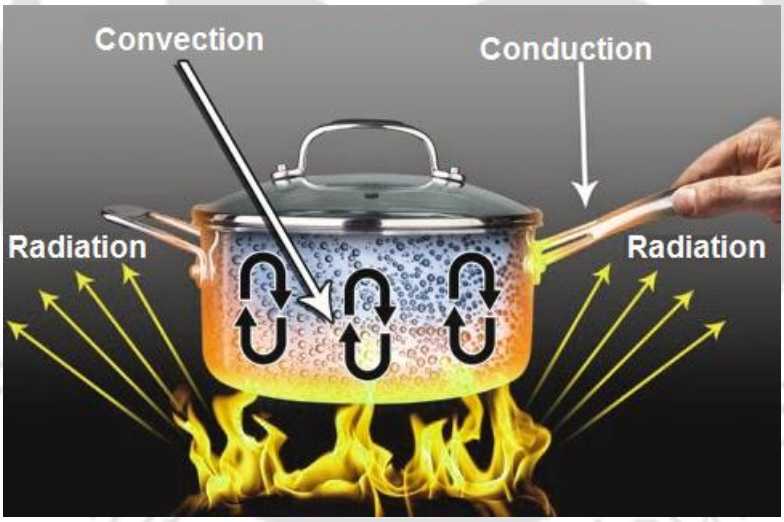

Fig. 1.1: Schematic highlighting the modes of heat transfer (*https://me-mechanicalengineering.com/modes-of-heat-transfer/*)

Conduction is the transfer of energy from the more energetic particles of a substance to the adjacent less energetic ones as a result of interactions between the particles. In gases and liquids, conduction is due to the *collisions* and *diffusion* of the molecules during their random motion. Convection happens in the fluid in one or two mechanisms: random molecular motion, which is termed as diffusion or bulk fluid motion of a fluid carries energy from place to place. It can be either forced through as for example pushing the flow along the surface or natural as that which

happens through buoyancy. Radiation occurs when heat energy is transfer through electromagnetic phenomenon, for which sun is one of the common important source. It happens between surfaces with different temperature, even if there is no medium, between them as long as they face each other.

1.3 Transient Heat Transfer

Heat transfer is energy in transit due to the temperature difference. Whenever there exists a temperature difference in a medium or between media, heat transfer occurs. The basic requirement of heat transfer is the presence of temperature difference. This transfer of thermal energy may occur under steady or unsteady state conditions. If the temperature of a body does not vary, it is said to be in steady state; but, if there is an abrupt change in its surface temperature, it (body) attains an equilibrium temperature or a steady state after some period. During this period the temperature varies with time and the body is said to be in an unsteady or transient state. The term transient or unsteady designates a phenomenon, which is time-dependent. *Conduction of heat in unsteady state refers to the transient conditions wherein the heat flow and the temperature distribution at any point of the system vary continuously with time.* Transient heat transfer is used in a variety of broad areas of applications such as internal combustion engines, gas turbines, aircraft and aerospace industries, heat treatment of metals, various shock applications etc.

1.3.1 Transient Heat Conduction in Semi-Infinite Solids

A semi-infinite solid is an idealized body that has a *single plane surface* and extends to infinity in all directions. This idealized body is used to indicate that the temperature changes in the part of the body in which we are interested (the region close to the surface), due to the thermal conditions on a single surface. The earth, for example, can be considered to be a semi-infinite medium in determining the variation of temperature near its surface. In addition, a thick wall can be modelled as a semi-infinite medium if we are interested in the variation of temperature in the region near one of the surfaces, and the other surface is too far to have any impact on the region of interest during the time of observation. For short periods of time, most bodies can be modelled as semi-infinite solids since heat does not have sufficient time to penetrate deep into the body, and the thickness of the body does not enter into the heat transfer analysis. For example, a steel piece of any shape can be treated as a semi-infinite solid when it is quenched rapidly to harden its surface.

1.3.2 One-Dimensional Heat Conduction

In most of the heat conduction situations, the temperature variation is significant only in one direction while its effect in other two Cartesian coordinates are negligible. The Fourier's Law of heat conduction can be readily applied (*Eq. 1.1*)

$$q = -K\frac{\partial T}{\partial x} \tag{1.1}$$

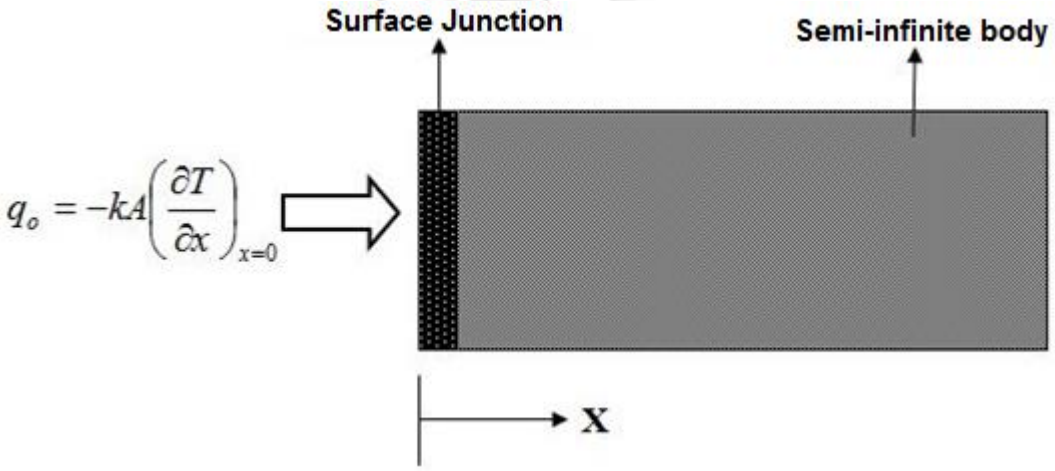

Fig. 1.2: One-dimensional heat conduction

The general form of one-dimensional heat conduction equation can be written as,

$$\frac{\partial^2 T}{\partial x^2} = \frac{1}{\alpha}\frac{\partial T}{\partial t} \tag{1.2}$$

Considering the substrate to be a semi-infinite solid maintained at an initial temperature T_i and is suddenly exposed to a constant surface heat flux q_o and the temperature distribution in the solid is assumed to be a function of time ('α'being the thermal diffusivity).

The initial and boundary condition becomes:

$$T(x,0) = T_i \tag{1.3}$$

$$\frac{q_o}{A} = -k\left[\frac{\partial T}{\partial x}\right]_{x=0} \quad for \quad t > 0 \tag{1.4}$$

The solution for this case is given by

$$T - T_i = \frac{2q_0\sqrt{\frac{\alpha t}{\pi}}}{kA}\exp\left(\frac{-x^2}{4\alpha t}\right) - \frac{q_o x}{kA}\left(1 - erf\,\frac{x}{2\sqrt{\alpha t}}\right) \tag{1.5}$$

For $x = 0$, the *equation (1.5)* reduces to

$$T = T_i + \left(\frac{2q_o}{k}\right)\sqrt{\frac{\alpha t}{\pi}} \tag{1.6}$$

1.3.3 Transient Temperature Measuring Device

In general, most of the transient devices, measure the temperature-time history during the time scale of interest and the heating rates are subsequently predicted from the temporal data. Some of them are a thermocouple, thin film gauge, coaxial surface junction thermocouple (CSJT), liquid crystal thermography, infrared thermography, phosphor thermography, temperature sensitive paints (TSP) etc.

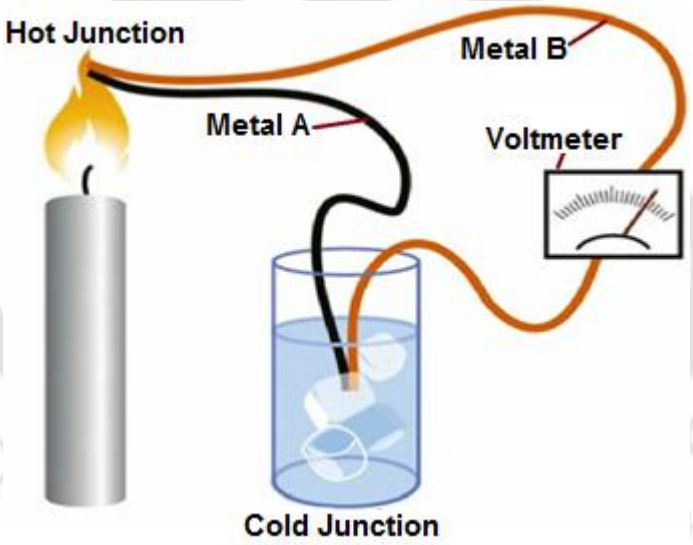

Fig.: 1.3: Schematic of a conventional thermocouple

A *thermocouple* is a junction between two dissimilar metals that produces a voltage difference related to a temperature difference (*Fig. 1.3*). Thermocouples are the widely used temperature sensor for measurement and control and can also be used to convert heat into electric power. They are inexpensive and interchangeable, fitted with standard connectors and can measure a wide range of temperatures Any junction of dissimilar metals will produce an electric potential related to temperature. Thermocouples for practical measurement of temperature are junctions of specific alloys which have a predictable and repeatable relationship between temperature and voltage.

Different alloys are used for different temperature ranges. Properties such as resistance to corrosion may also be important when choosing a type of thermocouple. When the measurement point is far from the measuring instrument, the intermediate connection can be made by extension wires which are less costly than the materials used to make the sensor. Thermocouples are widely used in science and industry; applications include temperature measurement for gas turbine exhaust, diesel engines, and other industrial processes.

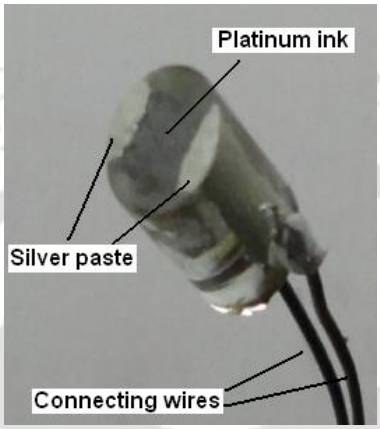

Fig.: 1.4: Thin-wall heat transfer gauge [*Kumar et al. 2011*]

Moving on to another class of sensors, which are based on semi-infinite theory are broadly categorized as *thin-film sensors* (TFGs), *thin-skin calorimeter gauges*, and *thick-wall gauges*. All the sensors are utilized to capture transient temperature signals mostly in short duration impulse facilities. The basic methodology for the sensors are similar (uniform slab), such a way that a high conducting sensing element are mounted on the insulating substrate (*Fig. 1.2*). When a constant heat flux is applied on the sensing surface, the element measures the instantaneous surface temperature, parabolic in nature. The measured temperature in general are complexly related to the heat transfer coefficients, in which measurements are usually carried out with geometries such that only one spatial coordinate needs to be considered. In *thin-film gauge* (TFG), the film is so thin such that the measured temperature is same as that of surface temperature (*Fig. 1.4*). A TFG is a resistance temperance detector which is a combination of a high conducting (sensor) and a lower conducting material (substrate) [*[1]Sarma et al., 2016; [2]Sarma et al., 2016; Sarma, 2017*]. It operates on the simple principle that penetration of heat pulse from the high conducting material to the low conduction one is very small during the time span of measurement. A typical TFG consists of a high conducting metal (platinum, nickel, gold, silver etc.) mounted on an insulating substrate (quartz, machinable ceramics etc.) as shown in *Fig. 1.4.*

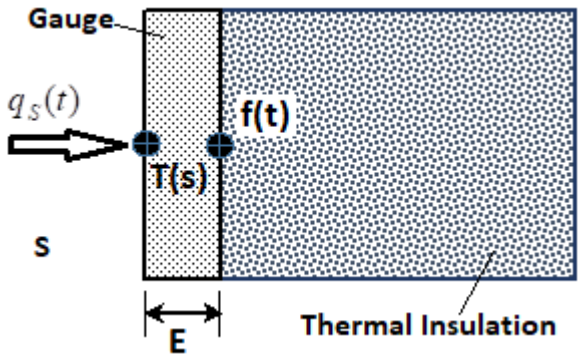

Fig. 1.5: Thin-skin calorimeter

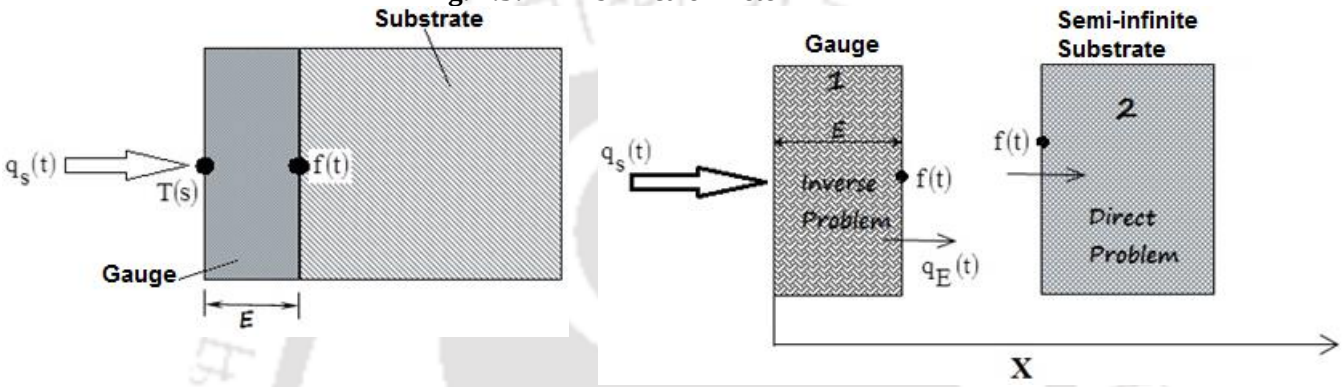

Fig.: 1.6: (a) Thick-wall gauge; (b) sub-division of thick-wall gauge

Considering the *thin-skin calorimeter gauges*, the element in the sensing junctions are very thin, which are nothing but thin metal plates with thermocouple wires welded to form a surface junction. The rate of surface temperature rise in this case is approximately equal to the rate of mean temperature rise at the interface; enabling one-dimensional heat conduction to be applied in order to extract the heat flux from the mean temperature variations (*Fig. 1.5*). Contrary, in the *thick-wall gauges*, the heat received by the gauge is largely stored within the gauge as shown in *Fig. 1.6 (a)* while only a small portion is transferred to the substrate. In this regard, the surface heat flux is related in a more complex way than in the case of the thin-skin calorimeter. The instantaneous surface temperature $f(t)$ of the substrate is measured at $x = E$. The problem is to calculate the front surface temperature and the heat flux at $x = 0$ given the measured temperature at a point $x = E$. The given problem can be sub-divided into two separate problems, one of which is a direct problem, as shown in *Fig.1.6 (b)* and the other part as an Inverse-problem. The semi-infinite body from $x = E$ to $x = \infty$ can be analyzed as a direct problem because the boundary conditions at both boundaries are known $T_2(E,t) = f(t)$ at $x = E$.

Thermochromic liquid crystals (TLC) are materials that change their reflected colour as a function of temperature, when illuminated by white light; hence, reflect visible light at different wavelengths. In the term thermochromic, thermo means temperature and chromic means colour. A bright and stable white light source is required to obtain accurate and reliable reflected light intensity from a 'TLC' coated surface. The light source must be void of infrared (IR) and ultra-violet (UV) radiation. Any 'IR' energy present in the incident light will cause radiant heating of the test surface. Extended exposure to 'UV' radiation can cause rapid deterioration of the 'TLC' surface (*Fig. 1.7*). This causes the surface to produce unreliable colour temperature response performance. Consistent light source settings and lighting viewing arrangements between calibration and actual testing are essential to minimize colour-temperature interpretation errors.

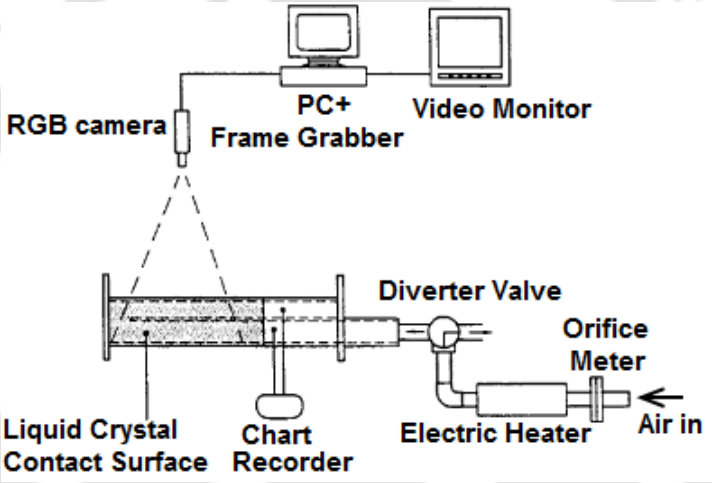

Fig. 1.7: Schematic of Liquid crystal assembly [*Ekkad and Han, 2000*]

Infrared thermography helps one to measure and interpret the transient temperature field prevailing over the surface of the body under observation. The general philosophy/principle for the technique lies in the fact that the internal structure of the inspected object and its blemishes will have a different thermal behaviour. The defect, if any, on the body will affect the flow of previously applied heat source, giving a heated and a cold surface, resulting in temperature difference on the surface of the body as captured by the infrared camera. The application of IRT is based on two approaches, active and passive. The active scheme requires external spur to be applied on the specimen of interest with an objective to create thermal contrast on sub-surface defects. On the other hand, for the passive, the specimen in focus should be at different temperature. The IRT has a response time in the range of few microseconds. *Figure 1.8* shows the

schematic of the working principle of the IR thermography highlighting the complete process. Infrared thermography is a proactive troubleshooting and predictive maintenance tool.

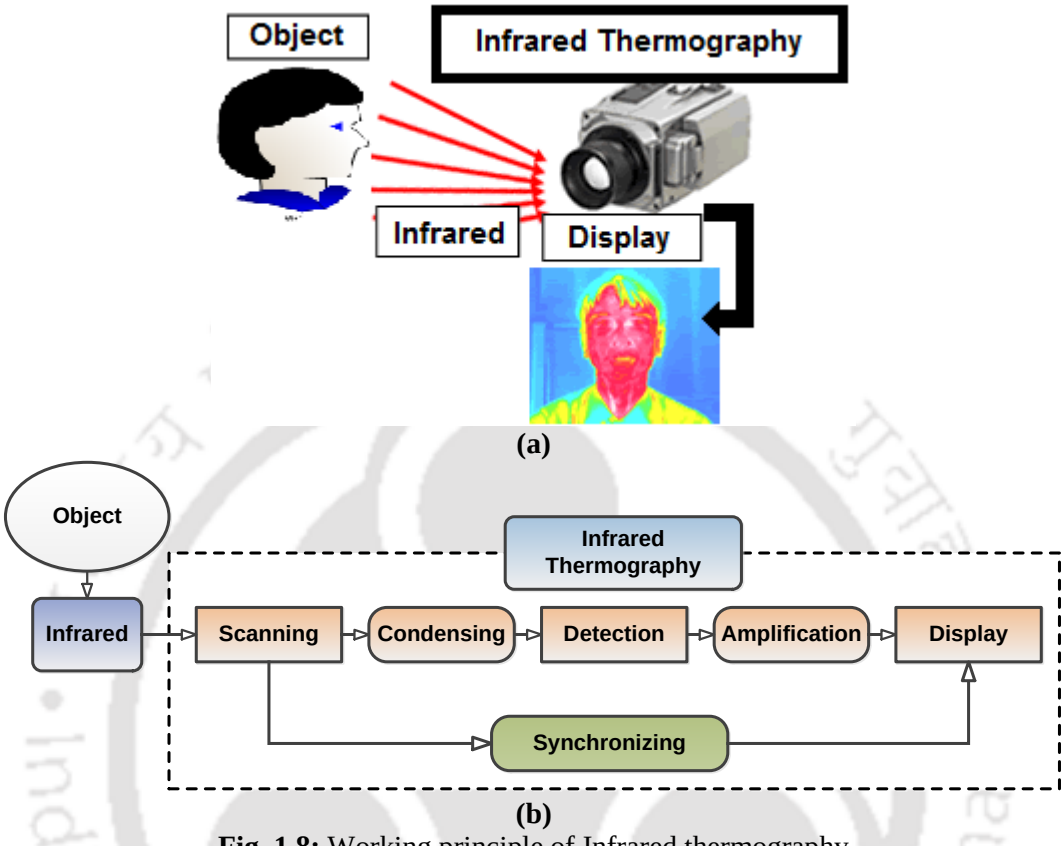

Fig. 1.8: Working principle of Infrared thermography

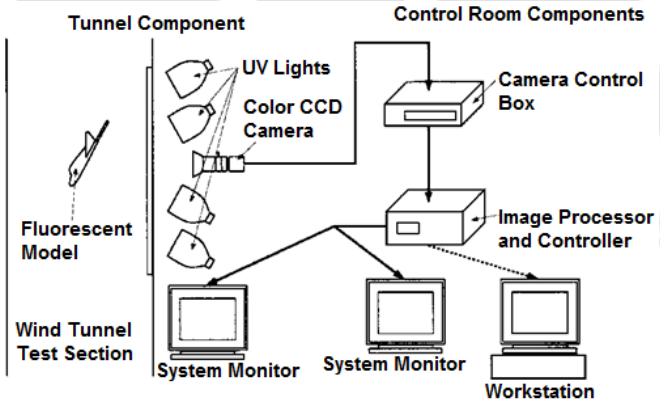

Fig. 1.9: Set-up for Phosphor Thermography [*Merski, 1999*]

Thermographic phosphors have been used in fibre-optic thermometry system for testing of electronic systems. Surface fluorescence of a *thermographic phosphor* is induced by ultraviolet (UV) radiation. The phosphor absorbs UV energy, because of which electrons are raised from lower energy state to the higher state, which changes certain characteristics of the emitted light

highlighting the change in temperature. Phosphor (fine white/pastel-coloured inorganic powder) is an optical method for surface temperature measurement. In general, Phosphor thermography is a laser-induced fluorescence technique utilized for remote sensing of rotating components within the adverse environment. The application of which includes the combustion engine, analysing the condition and temperature of motor and generator, turbine engines etc. *Figure 1.9* shows the schematic of a typical Phosphor thermometry set-up.

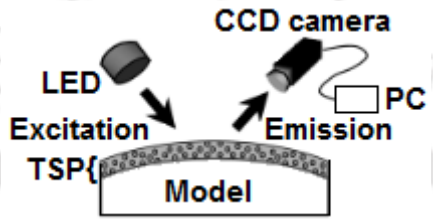

Fig. 1.10: Schematic representation of the temperature sensitive paints [*Nagai et al., 2008*]

The principle on which *temperature sensitive paint* (TSP) work depends on the oxygen quenching of luminescence from the paint. The photodetector measures the light intensity emitted by the paint and correlates it to the transient temperature variations. The molecules inside the sensor become excited electronically to an elevated energy state when illuminated by light at an appropriate wavelength. The transient surface temperature is provided based on the photochemical reaction. In general, TSP is nothing but coating which consists of sensor molecules dispersed in a polymer binder. *Figure 1.10* shows the schematic of the typical temperature sensitive set-up.

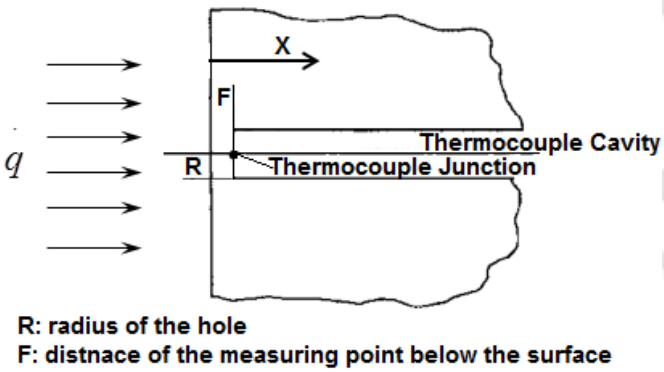

(a) **(b)**

Fig. 1.11: Schematic of null-point calorimeter [*Santos et al., 2009*]

Null point calorimeter falls in the category where that measures transient temperature variation at the point of some distance from the actual exposure of the surface, where there is

difficulty in measuring the transient temperature actually at the surface. The null point as seen in the *Fig. 1.11* is the point at which $x = F$ and $R = 0$. The sensor captures the transient temperature history and by using inverse mathematical model, one can infer heat flux. The measured temporal history is assumed to be same as that of the surface**.**

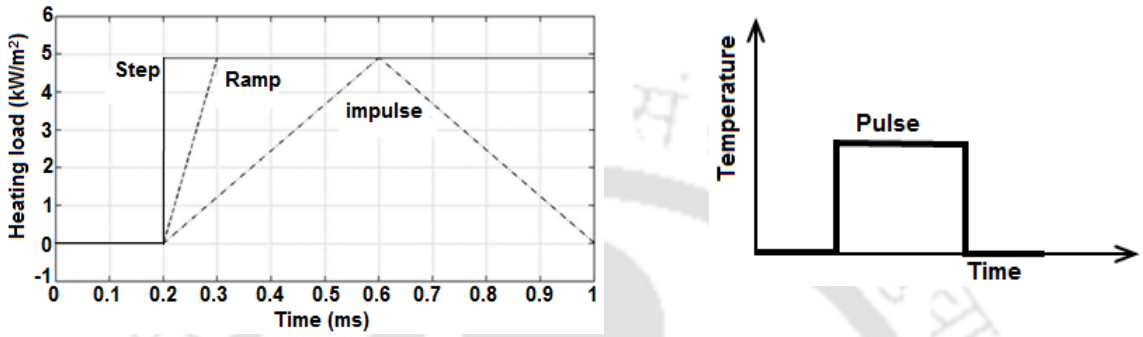

(a) **(b)**

Fig. 1.12: Typical nature of signal for different flow conditions

The demand of *Coaxial Thermocouple* for an instrument to measure transient temperatures in a short time duration flow (few microseconds) arises in numerous heat transfer investigations particularly in internal combustion engine (pulsating/periodic load), aerodynamics facilities (continuous and blow-down type), gun barrels, gas turbines and in boiling experiments and many such experimental facilities. In aerodynamic impulse testing facilities (such as shock tunnels), the heating load is characterized by step/impulse load (*Fig. 1.12-a*). In internal combustion engine applications, the nature of the flow is pulsating/periodic (*Fig. 1.12-b*) and the determination of temperatures and heat fluxes in the combustion chamber are significant parameters because they provide information about the engine healthiness. Because of their simplicity and comparatively rapid response, fine wire thermocouples usually are employed. However, in certain applications, fine-wire thermocouples are unsatisfactory because of their lack of strength and difficulties in positioning the junction at the point of interest. In addition, the minimum size of the junction, which affects the rate of response, usually is limited to the wire diameter. The coaxial surface junction thermocouple is different when compared with conventional thermocouple, as in conventional one there is a point junction and in coaxial there is a thin-film surface junction which helps one to capture the heat flux.

Coaxial thermocouples are available for different standard sizes. The CSJTs being surface temperature detector, qualify itself for capturing the transient temperature signals. They are usually

formed from inner wire of negative elements with an outer annulus of the positive element, with both elements being electrically insulated by a layer of epoxy-resin along the length of the element. The CSJT provide a unique facet of having a surface junction, formed in its construction process through plastic deformation by abrading of one thermocouple material over the other material using an abrasive blade. The artificially created micro-scratches helps one to respond during short duration timescale of application. The thermocouple allows a mounting through the wall, which is important for the accurate measurement of a rapidly changing surface temperature. Some application requires direct measurement of transient wall temperature, which makes it a challenge. In this case, the probe material should have thermal properties, which matches to those of the surrounding wall as nearly as possible. This necessitates the requirement for determining convective heating rates by performing a fast surface temperature measurement with the help of a coaxial thermocouple. Usually, the thermocouple is fixed in the wall by glueing at the rear part of the element. Installation by a thread is also possible for higher operating temperatures. Of course, installation is also possible in a blind hole in the test wall to measure the internal material temperature at a known location.

The coaxial temperature probe has distinctive advantages:

(i) It is easily constructed with low cost compared to the commercial one

(ii) The sensing surface can be restored from time to time if damaged (i.e., losing its linearity with temperature) during the experiment;

(iii) It has fast response characteristics with a less rise time,

(iv) It is stable and repeatable in dynamic calibration experiments;

(v) It can easily be fitted to any model surface (cone, cylinder, sphere, etc.) due to its small size and sturdy design.

The most important factor that determines the performance of the thermocouples (such as accuracy, response time and repeatability) is the quality of the junction. The method of forming the thermocouple junction makes the gauge very robust and suitable for the application in harsh environmental conditions. As an example, the impact of high-speed particles transported by a fluid has, in general, no influence on the operation of the thermocouple. Coaxial thermocouples are of different types depending upon the materials used for the fabrication. Some of them are *Type K*: Chromel-Alumel, *Type E*: Chromel-Constantan, *Type J*: Iron-Constantan, *Type T*: Copper-

Constantan, *Type N*: Nicrosil-Nisil, etc. *Fig. 1.13* shows the schematic of a typical coaxial surface junction thermocouple.

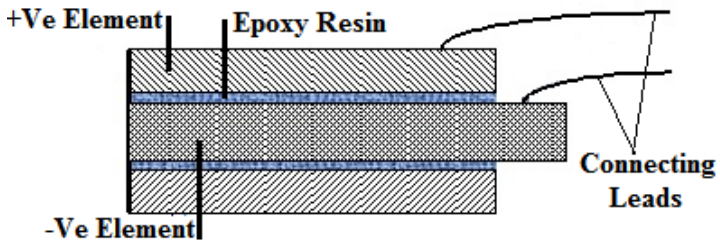

Fig. 1.13: Schematic of coaxial thermocouple

1.4 Delineation of the Dissertation Work

The dissertation work mainly focuses on the design, development, calibration of coaxial surface junction thermocouple and further, real-time application in the environment such as low supersonic speed (shock-tube), hypersonic facilities (shock-tunnel), the internal combustion engine and gas turbine engine. The *First chapter* of the thesis describes the background of the work on the usage of the transient heat flux and its associated measurement devices. It emphasizes on the various categories of the measuring devices and selection of one for the current study. The *Chapter 2* gives the exhaustive literature survey and finally, describing the objective of the present set of investigation along with its motivation. *Chapter 3* describes the numerical modelling of such sensors using commercial package (ANSYS-Thermal Transient) to validate the use of the assumption theory of one-dimensional heat conduction into semi-infinite solid and in turn strikeout an appropriate dimension for the thermal sensor. Additionally, the chapter elaborates on the mathematical details of the recovery tool using various fitting techniques such as linear, polynomial and cubic-spline based methods for one-dimensional heat equation; along with methodology to design a coaxial surface junction thermocouple. *Chapter 4* gives the details of the fabrication of the coaxial surface junction thermocouple along with the characterization of the sensor using X-ray Diffractometry technique to highlight the plastic deformation of the thermocouple material at the junction. In conjunction, calibration methodology using both temperatures with oil-bath technique (sensitivity determination) and constant heat flux technique with a laser of constant wattage have been worked out. *Chapter 5* describes the experimental techniques for the thermal product ($\sqrt{\rho ck}$) estimation for millisecond timescale using the water-droplet and water-plunging methods for the fabricated thermocouple. *Chapter 6* dwell on the

comprehensive investigation for installation of shock tube and its experimental calibration. In addition, estimation of stagnation point heat flux in the shock-tube using the in-house fabricated coaxial thermal sensors. *Chapter 7* focuses on a comparative study using thermal sensors to estimate stagnation point heat flux in the hypersonic facilities such as shock tunnel. *Chapter 8* investigates the feasibility of the use of coaxial surface junction thermocouple to measure heat flux inside the combustion chamber of an internal combustion engine and further, at the exhaust port of the engine. *Chapter 9* explores at another possible application of coaxial surface junction of thermocouple beyond heat flux measurement in the rig of the gas turbine engine and in combination to develop coaxial thermocouple as a product. Lastly, concluding remarks and future scope of the work are presented in *Chapter 10*.

CHAPTER 2

Survey of Literature

2.1 Preface

Measurement of transient heat transfer is considered one of the most prolific phenomena in high-speed flows, internal combustion engines, gas turbines and many such areas. The high-speed flows bear complexities due to the thin shear layer, high temperature, and inviscid-viscous interaction. The launch vehicles or missiles encounter this flow regime and hence need special attention in their design phase. A paradigm shift can be noticed in their development over a short span of time due to the stimulus need for space exploration and faster global transportation. In addition, the challenge ahead of research community lies in encountering the impulsive mechanical as well as thermal loading for the safety and cheaper space flights. The recent advances have led to the development of ground-based impulse facilities, which includes shock tunnels, free-piston shock tunnels, and expansion tubes [*Kulkarni and Reddy, 2008; Morgan, 1997; Stalker 1967*].

Considering the transient short duration applications, a fast response sensor such as thin-films sensor and coaxial surface junction thermocouple (CSJT) are best suited for the transient conditions. Furthermore, with respect to the high-speed flow applications, the sensors response time becomes more crucial, pertaining to the time scale of measurement. The coaxial surface junction thermocouple is more robust than the thin-film but is less sensitive as compared to the thin-film gauges. For measuring relatively low heat fluxes in clean environment conditions, thin-films are recommended, but for measurement in harsh conditions, thermocouples are advised. The transient measurements are usually performed using thin-films gauges, temperature sensitive paints, coaxial thermocouples for which the response time falls in the range of few microseconds. Keeping this vista in mind, a thorough literature survey has been carried out in order to get an insight of the current development status in the area of co-axial surface junction thermocouple (CSJT). The literature survey has been undertaken to keep in mind eight broad categories namely:

1. Mathematical modelling of transient heat transfer measurement
2. Construction and calibration of coaxial surface junction thermocouple
3. Estimation of calibration parameters (Thermal product)
4. Utilization of shock tube as an impulsive experimental tool
5. Heat transfer measuring gauges

6. Application of coaxial surface junction thermocouple (internal combustion engine, hypersonic facilities, gas turbine)
7. Simulation-based study, and
8. Lastly, the assessment is focused on the work undertaken in IIT Guwahati considering advancement of coaxial surface junction thermocouple.

2.2 Mathematical Modelling for Transient Heat Transfer Measurement

Schultz and Jones (1973) described in detail the techniques, essential for measurements in short duration and rapidly varying flow environment. The author had comprehended the study to estimate heat flux in short duration facility focusing on three basic gauges such as a thin-skin calorimeter, thick-skin calorimeter and thin-film.

Kidd (1993) investigated the recent progress in techniques which include thermal analysis applied to transducer concept, improved heat flux fabrication methods etc., employed in the measurement of very high heat-transfer rates in re-entry-type facilities at the Arnold Engineering Development Centre (AEDC). Further, the graphical illustrations of the results of extensive thermal analyses of the null-point calorimeter and *coaxial surface thermocouple* concepts with application to measurements in aero-thermal test environments were presented. In addition, the time response experiments and absolute calibration of the null-point calorimeter and coaxial thermocouple were performed in the laboratory from intermediate to high heat flux levels.

Chen and Hsu (1995) developed a *micro thermocouple* probe whose response time is better than 1 ms, capable of detecting *transient* surface temperatures. The obtained transient temperature data were utilized to determine the time-varying *heat flux* under liquid contacts. The instantaneous surface heat fluxes were found to vary by orders of magnitude during the milliseconds of liquid residence at the hot surface. The value of average heat flux obtained during liquid contact was found to fall in the range from 10^5 to 10^7 W/m^2 for water at atmospheric pressure, with temperature up to 450 °C. The ravages of this investigation indicated that the process of heat transfer during the short duration of direct liquid contacts may be quite complex; the earlier works have shown that the frequency and duration of liquid contacts in transition boiling were functions of the wall superheat and fluid sub-cooling. In addition, the investigation revealed that the time-averaged heat flux during liquid contact was also strongly affected by wall superheat.

Taler (1996) defined the unified mathematical techniques of *transient* methods for measuring the surface heat transfer rates. Mainly, three heat flux gauges were discussed: *thin film*, thick-wall gauges placed on *semi-infinite* substrates and thin-skin calorimeters. The idea was to present a simple and accurate method for determination of the time-varying heat transfer coefficient (or heat flux) given an accurate temperature history of the body at a selected point beneath the surface. By solving the inverse heat conduction problem for the gauge, the measured interior temperature measurements were converted into local instantaneous heat transfer coefficients. The result of the inaccuracies in the measurement of the interior temperature was eliminated by using cubic spline smoothing or digital filtering of the raw interior temperature data prior to using it in the inverse heat conduction analyses. In general, the technique led to the development of closed-form equations for instantaneous surface heat flux or heat transfer coefficient.

Gulhan (1999) explained the fundamentals of heat transfer measurement techniques in high enthalpy flows. In addition, different heat flux measurement techniques were discussed with special focus on the design aspects. Further, a mathematical model for heat flux rate evaluation and application limits of each sensor type, in order to provide a useful and practical script for the reader with respect to the choice of an adequate sensor type for different requirements. Furthermore, sensor calibration and comparative measurements using different heat flux sensors in the arc heated facility was presented.

Battisti and Bertolazzi (2001) reported a data reduction procedure for heat transfer measurements in short duration facilities. Single and double layer thin film thin-film sensors were utilized for this purpose. A simple finite element discretization was implemented and its ability to accurately reconstruct signals of known testing functions (as Heaviside signal with superimposed fluctuations) was checked. The obtained results seem to confirm the performance of the code presenting a very accurate signal reconstruction at a very low sampling frequency. Once the assumption of semi-infinite slab becomes invalid (i.e. leading edge of blades), the numerical discretization such as finite element approach becomes non-negotiable. Lastly, it was suggested to develop a 2-D scheme in order to consider problems where lateral conduction effects cannot be neglected, and the evaluation of the influence of heat flux generated by Joule effect into the sensor becomes important.

Schrijer (2003) investigated the hypersonic flow over an axisymmetric compression corner, with its related boundary layer separation as a reattachment phenomenon. The investigated model was DART (Delft Aerospace Re-entry Test vehicle), a re-entry demonstrator vehicle, designed and developed at the Faculty of Aerospace engineering of TU Delft. The vehicle, a blunted cone-flare made of Makrolon, was designed to be fully reusable with the task to collect the aero-thermodynamic flight data and test new thermal protection system concepts. Transient heat transfer measurements were conducted in a short duration hypersonic facility at Mach 9, and Schlieren visualization was used as a complementary tool. An infrared camera, which operated in the line-scan model to obtain an adequate sampling rate was used to get the surface temperature variation in time. Four different data reduction methods were used to get the heat flux data from the surface temperature. The result obtained with the different methods were within a maximum tolerance of about 10%.

Vasiliki (2005) developed two measurement techniques based on the applications of the *thin film sensors*. The first method involves the determination of wall heat transfer with two-layer gauge and the other technique involved measurement of flow temperature using dual thin film probe. The techniques were utilized in short duration tunnels of the Von Karman Institute (VKI) under-engine representative conditions and were able to resolve both time-averaged component and time-resolved component i.e. the periodic blade passing events at ~5-7 kHz with harmonics up to 50 kHz. Furthermore, to find out the wall *heat flux* with the two-layer gauge, the unsteady conduction equations were solved in the two-layer substrate using the measured value of the wall temperature as a boundary condition.

Buttsworth et al. (2005) formulated a one-dimensional transient heat conduction model to evaluate the transient surface heat flux from the measurements of surface temperature using an eroding ribbon surface thermocouple. The junction of the thermocouple was formed with low thermal inertia just near the surface by the use of abrasive wear. The impulse response was captured with the help of laser excitation; it was noted that the response of particular sensors may vary if new junctions were created with abrasive wear. In addition, the response of the sensors seemed to deviate substantially from the one-dimensional model and varied from the sensor to sensor. The impulse response was further simulated with greater conformity using a two-dimensional finite element model, but three-dimensional effects were also seen to be significant. The impact of these

variations on the derived heat flux was assessed for the case of measurements in an internal combustion engine; when the measured impulse response was used to derive the surface heat flux, the apparent reversal of heat flux during the expansion stroke does not occur. It was observed that for the time scales less than 0.1 ms, different thermocouple junctions created on the same sensor can produce very different responses, also for time scales between 0.1 ms and 1 ms, different junctions can still influence the sensor response, but the response was typically more consistent for time scales less than 0.1 ms. In short, the use of either one-dimensional/two-dimensional models for the sensor response will lead to substantial errors in the inferred heat flux results.

Saravanan et al. (2009) utilized a platinum *thin-film* gauge to study experimentally the surface convective heating rate on a missile shaped body flying at hypersonic. In addition, the effects of fins on the surface heating rates of missile frustum were investigated. The experiments were performed in a hypersonic shock tunnel at Mach number of 5.75 and 8, having stagnation enthalpy of 2 MJ/kg with 0° angle of attack. Further, the measured stagnation-point heat-transfer data compared well with the theoretical value, estimated using Fay and Riddell expression. Furthermore, the measured heat-transfer rate with fin configuration was slightly higher than that of the model without fin; the normalized values of experimentally measured heat transfer rate and Stanton number compared well with the numerically estimated results.

Hubble and Diller (2010) described the development and evaluation of a novel hybrid method for obtaining heat flux measurements. It was noted from the obtained result that by combining the spatial and temporal temperature measurements of a heat flux sensor, the time response, accuracy, and versatility of the sensor could be improved. Further, sensors utilizing the hybrid method were able to make heat flux measurements on both high and low conductivity materials. In addition, by changing, the thermal conductivity of the backing material by four orders of magnitude caused only an 11% change in sensor response i.e. the hybrid method can enhance the time response of heat flux sensors. Furthermore, the temporal response was seen can increase by a factor of 28 compared with a standard spatial sensor. The developed hybrid method was tested both numerically and experimentally on high and low conductivity materials and it demonstrated significant improvement compared with operating the sensor as a spatial or temporal sensor alone.

2.3 Construction and Calibration of Coaxial Surface Junction Thermocouple

Kovacs and Mesler (1964) conducted an experiment to study the response of a *surface thermocouple* as a function of size and the type of junction using a 200 J flash tube as a high-intensity transient heat source. A very thin surface junction gave an abnormally high surface temperature during the initial temperature rise and thick junctions gave a temperature response similar to that of a thermocouple embedded at some depth from the surface. The correlation of the observed surface temperatures to the measured heat flux showed good agreement between the experimental observations and the theoretical predictions.

Kendall et al. (1967) investigated on the possible methods of increasing the sensitivity capabilities for determining the *heat transfer rates* associated with the wind tunnel testing. The existing techniques involving *surface thermocouple* materials do not provide the temperature sensitivity for low heat transfer rates, which leads the necessity of using surface thermocouple fabricated from semiconductors materials such as germanium. The calibration of the developed sensor has resulted in 35 times increment in sensitivity than that of the chromel-constantan thermocouple.

Lee et al. (1982) conducted experiments to detect liquid contacts on a high-temperature surface during film and transition boiling regimes using a *micro-thermocouple* probe. The experiment highlighted that the response of the probe, its associated data recording and processing circuits were sufficiently quick, to estimate the quantitative measurements of individual liquid contacts. It permits the calculation of contact frequencies and durations, and of average vapour with respect to liquid contact time fractions. The results indicated that for pool boiling, with the quenching of high temperature copper block, the liquid contact time fraction increased from 10% to 65% in 7 s as the block surface temperature cooled from 483 K to 418 K respectively.

Charles et al. (1984) developed a fast response high temperature and high pressure resistant thermocouple. The *thermocouple* was made up of two thin wires (W5Re and W26Re) embedded in fused alumina. A thin film of molybdenum provided the electrical contact at the hot Junction in the transducer. The obtained response (1 ms or less) under dynamic conditions of temperature and pressure (explosion) were in good agreement with the values calculated using simulation. The tip of the sensor can withstand temperatures of up to 1900 °C and pressures of several thousand bars. Considering its structure, the sensor could be inserted in the wall of an enclosure subjected to high

pressures and hence, could be utilized to determine thermal response inside autoclaves during reactions, in the cylinders of internal combustion motors, in jet nozzles or in the combustion chamber of ballistic missiles.

Yust and Kreider (1989) developed a transparent *thin film thermocouple* by reactive sputtering which has a Seebeck coefficient of 0.14 $mV.K^{-1}$. The developed sensors positive leg is indium tin oxide (ITO) and the negative leg is ln_2O_3. The In_2O_3 and ITO thin films were tested with sputtered thin film platinum to obtain their individual thermoelectric potentials. The stability of the transparent thermocouple at 1175 K was found to be ±2% for 132 h in air and ±2% at 575 K.

Jessen and Gronig (1990) presented a new method for the manufacture of *thin film gauges* using ceramic substrates (ZrO_2) with two sintered platinum wires. The sensor showed good mechanical strength and sensitivity. The sensor if damaged can be refurbished with a layer of new film or polishing the damaged surface. The testing of the sensor was accomplished using the shock-tunnel. The calibration was carried out and notably, the pulse calibration has demonstrated remarkable repeatability and accuracy.

Schreck et al. (1993) worked on the comparison of two calibration techniques for *thermocouples* for the transient application. The sensor could be utilized for measurement of transient surface temperatures with high spatial resolution and sensitivity. The first technique is a steady-state technique, was an elegant method to achieve temperature calibration independent of the geometry, the thermal properties of the bulk material, the laser power, and the absorption coefficient of the surface, and uses a focused laser beam with a diameter of 3 μm as a point heat source. This technique consists of two steps. The first step involved was an absolute but spatially averaged temperature measurement with a resistive temperature sensor. In the second step, the un-calibrated thermocouple junction was translated to resolve the spatial temperature profile generated by the laser spot. Both measurements were combined to provide an absolute calibration, which was independent of the thermal properties of the imbedding material and of the absorbed laser power. The second calibration technique was based on a dynamic measurement, which was a theoretical model to describe the heat diffusion to allow a fit for the experimental data. To implement this technique, they fabricated a small electrical heating element close to one of the junctions and with the dynamic calibration; the time-resolved response of the thermocouple to a short heat pulse was

recorded. A least-square fit with a simple model of heat diffusion to the measured response yields both the temperature calibration of the thermocouple and the heat diffusivity of the imbedding medium. The obtained temperature calibration of the thermocouple with the dynamic technique was in good agreement with the steady-state calibration.

Holmberg and Diller (1995) evaluated a new method of in-situ *heat flux gage* calibration to utilize in convective facilities with high heat transfer and fast time response. A Heat Flux Microsensor (HFM) was utilized to simultaneously measure time-resolved surface heat flux and temperature from two sensors fabricated on the same substrate in a shock tunnel. Further, demonstrated a method for estimating gage sensitivity and frequency response from the data generated during normal transient test runs. The shock tunnel data were processed using one-dimensional semi-infinite conduction model based on measured thermal properties for the gage substrate for verification of heat flux sensitivity. The results matched well with the gage calibrations performed in convection at the stagnation point of a free jet and that done by the manufacturer using radiation. Furthermore, a finite-difference model of the transient behaviour of the heat flux sensor was presented to demonstrate the first-order response to a step input in heat flux. The HFM recorded the heat flux response with an estimated time constant of 6 μs, which demonstrates a frequency response covering DC to above 100 kHz.

Sanderson and Sturtevant (2002) developed and tested a new form of a *thermocouple*. The design involved the utilization of tapered fit between two coaxial thermocouple elements. The developed sensor has a response time of the order of 1 μs and was suitable for measuring large transient heat flux in hypervelocity wind tunnels. Further, to demonstrate the operating principles and assess the errors associated with the finite thickness of the surface junction asymptotic analysis were utilized. A spectral de-convolution method was utilized in order to infer a mean square optimal estimate of the surface heat flux from time-resolved surface temperature measurements and the signal developed is applicable to transient heat flux gauges of all type. The measurement of the heat flux about the forebody of a cylindrical body in a hypervelocity flow was carried out to demonstrate the functioning of the gauge. The measured heat flux was compared with the established theoretical predictions, to obtain statistical estimates of the repeatability of the technique.

Heichal et al. (2005) fabricated a *thin film thermocouple* to measure the rapid surface temperature change. A fine wire of Constantan was inserted vertically into a hole drilled through a steel plate and held in place by ceramic cement that acted as an electrical insulator. In addition to that, a thin conductive film was deposited on the surface to provide an electrical connection between the steel substrate and the thermoelectric wire. Then the developed sensor was calibrated and the result showed that the thin film sensors could detect a temperature rise of over 200 °C in less than 10 ns produced by a laser pulse focused on the junction. Further, the sensors were utilized to measure transient surface temperature distribution under an impacting droplet of molten aluminium. In conclusion, the developed thermocouple could be built on any metallic substrate and can be deposited on either smooth or polished surface and several sensors can be spaced close together.

Ewing (2006) fabricated a thin-film *heat flux* array (HFA) which expanded the capabilities of currently available technologies for heat flux measurement. The developed array utilized a direct measurement technique that allowed the sensor to be placed on any surface and take measurements on any fluid. In addition to that, use of thin-film technology gives the array a first order time constant of 32 ms for arrays built with a 50 μm Kapton resistance layer. Additionally, the calibration of the array brings forth an average sensitivity of 42 $\mu V/(W/cm^2)$, which was sufficient output for most applications. Lastly, a design was accomplished using the custom bank of electronics to boost the signal and counteract capacitance effects inherent to the gage's design.

Mohammed et al. (2008) demonstrated the design technique of K-type *CSJT* and associated fabrication difficulties. In addition, the microstructural analysis and the chemical characterization (which included SEM and EDX analysis), were carried out to verify the surface morphology and to qualitatively evaluate the CSJT materials composition. The results from EDX point analysis concluded the presence of the alumel and chromel compositions over the entire surface of the CSJT. The performance of the developed sensor for measuring the surface temperatures and heat transfer rates under transient conditions were demonstrated using the UNITEN's shock-tube facility. The obtained results have shown a time response of the order of microseconds and confirmed the suitability for making the transient heat transfer measurement. It was concluded that additional studies using different types of thermocouples as well as different Mach numbers with different locations in shock-tube are necessary for demonstrating and improving the construction technique.

Kumar et al. (2011) worked on the in-house fabrication and calibration of *platinum thin-film sensors*. The experiments were carried out applying step heat load on the thin film sensor, using laser light of known wattage. The recorded transient temperature data were processed for estimation of laser wattage using numerical and analytical models. The signals were also predicted using ANSYS by applying a known heating load using one-dimensional transient heat conduction solver. The agreement of the numerical simulation with the analytical was quite good and satisfactory within ±2% accuracy. Encouraging agreement of these predictions has demonstrated the success of the designed calibration set up and cost-effective means of in-house fabrication of thin film sensors.

[1]Mohammed et al. (2011) presented a dynamic calibration technique for *coaxial temperature* probes. The probe was successfully designed and fabricated in-house. The transient response for heat transfer measurement was carried out in the hypersonic test facility. The developed sensor has a response time of 50 μs and rise time of the order of 0.3 μs. The junction for the probe was made from two scratching technique namely abrasive paper of different grit sizes and scalpel blades of different thickness. The sensors were tested and calibrated in the test section and end wall of the UNITEN shock tube facility at different axial and radial locations. Additionally, the effects of Mach number, different working fluids were also studied. It was concluded from the calibration technique that the TP of a particular sensor depends on Mach number, junction scratch technique, and junction location, as well as on the enthalpy conditions. Furthermore, calibrated coaxial temperature probe using the scalpel blade technique with a particular blade size gives consistent thermal product values and so, does not require an individual calibration; for a coaxial temperature probe whose junction was created using the abrasive paper technique with different grit sizes, a calibration for each coaxial temperature probe is likely to be needed. From the thermophysical properties of different temperature sensors it was revealed that there were 23% error if it was taken from the available literature, but from the study presented here, it was reduced to 10%. Moreover, the probe performance was significantly influenced by the *gap thickness, insulating method, junction location and junction formation technique;* electrical insulation has a larger impact on the sensor performance and the gap between the elements should be minimized to 10 μm. In addition, it depicts that the effective junction location would be closer to the insulating layer when the abrasive paper technique was utilized with those created with scalpel blades. Lastly,

the helium-air gas combination used in the shock-tube gave the highest temperature rise compared to other working fluids.

D'Aleo and Prasser (2012) described the construction, calibration and testing of a *thin film platinum RTD* arrays on glass substrates developed using the photolithographic technique. The fabrication involved an array of resistive temperature detectors (RTDs), based on a micropatterned thin film platinum resistor has been built. The sensors were located on a glass substrate (40×53 mm^2), which has the platinum resistors and the electrical contact leads are embedded. The operational temperature range was below 0 °C up to 200 °C. The temperature coefficient of resistivity (TCR) was found to be 0.0011 $°C^{-1}$ with a high correlation coefficient. The thermal time constant of the sensor has been verified at about 30 ms. The sensors can be utilized to measure and characterize in terms of frequency and amplitude of thermal fluctuations at the inner wall of T-junction pipelines to evaluate the heat flux through the wall and thus the heat transfer coefficient.

2.4 Estimation of Thermal Product

Lyons and Gai (1988) found a novel method for determining the thermal product $(\rho ck)^{1/2}$ of *thin film or surface thermocouple* type heat transfer gauges. The method utilises optical technique using a known power laser. The obtained values of $(\rho ck)^{1/2}$ were comparable favourably to those obtained by previous authors. The comparison was accomplished utilizing two types of heat transfer gauge. One was a NASA manufactured palladium thin-film gauge on a MACOR substrate (*Miller et al., 1985*). The other was a surface thermocouple with the coaxial symmetry of type K (Chromel-Alumel); it was manufactured by the ASEA Corporation of Sweden and is referred to as type YL641015 (*Gai et a1., 1985*). Both the gauges were installed side by side along the stagnation line of a cylinder in a cross-flow and were exposed to the same hypersonic high enthalpy stream for the duration of about 500 μs in a free-piston-driven shock tunnel.

Gatowski et al. (1989) characterized several types of *surface-temperature sensors* based on the thermal properties and response times for evaluation of their capabilities as transient heat flux sensors using a rapid compression machine. A radiometric technique and a laser-pulse technique were utilized to measure the thermal properties and response time of various surface-temperature sensors. It was observed that the measured heat flux was affected by the thermal properties of the

sensor substrate. The tested sensors were the eroding and vacuum-deposited metal surface thermocouples, platinum thin-film resistance thermometers and spot-welded surface thermocouples. In addition, Spot-welded surface thermocouples give erroneous results for convective heat transfer because of heat-conduction effects from the bare lead wires extending into the boundary layer. The comparison of the heat flux histories measured in the rapid compression machine by a platinum thin-film resistance thermometer on a ceramic substrate to those measured by an eroding surface thermocouple on a cast-iron substrate suggested that significant errors in the heat flux measurements. The reason could be because of material mismatch between the sensor body and the walls of the test section. In nutshell, systematic error leads one to conclude that the use of ceramic-substrate probes in heat transfer studies with an otherwise metal test section was undesirable, despite the superior signal-to-noise characteristics they possess.

Buttsworth (2001) experimentally determined the response of *K-type* surface junction *thermocouples* using a water droplet calibration technique (for millisecond times scales) and a shock tube (for microsecond time scales). Different junctions formed by scalpel blade scratches and abrasive paper were investigated. When scratches from scalpel blades were used to form the junction, the thermal product (TP) identified from the water droplet calibrations consistently differs by approximately 20% depending on whether the junction was made on the chromel or alumel substrate, in accord with existing thermal properties data. However, the shock tube calibrations indicate that for scalpel-scratched junctions, there was considerable variability in thermocouple response time due to effective junction depth variations produced during construction. On the other hand, junctions formed with abrasive paper produced rise times consistently less than 1 μs, but the water droplet and shock tube experiments both indicated significant variability in the effective TP of the made gauges. Moreover, the consistency in TP for scalpel-scratched junctions for millisecond timescales and the capriciousness for junctions created with abrasive grit for both the millisecond and microsecond timescales were attributed to the differences in the effective proximity of the junction to the insulation between chromel and alumel substrates. For junctions created with abrasive grit, the effective TP was approximately 30% smaller for microsecond timescales than it was for a millisecond. Further, the insulation was likely to have a more significant influence for junctions created with abrasive grit than for scalpel scratched junctions; because the effective junction location would be much closer to the insulation

in the abrasive grit case because the physical scale of the plastic deformation was much finer when abrasive grit was used.

[1]Mohammed et al. (2010) presented the dynamic calibration technique for evaluating the thermal product values of different scratched *temperature sensors*. Mainly, two types of scratch such as abrasive papers with different grit sizes and scalpel blades with different thicknesses to form the sensor junction were used. The sensor was tested in a shock tube facility operating under different conditions; the result shows that the TP of sensors depends the Mach number, surface junction scratch technique, junction location as well as on the enthalpy conditions. Furthermore, it was noticed that using scalpel blade technique with a particular blade size gives consistent thermal product values and so it does not require an individual calibration. However, for sensors whose junction created using the abrasive paper technique with different grit sizes, a calibration for each sensor is likely to be needed and hence, the effects of thermophysical properties on the TP were greatly examined. The sensor performance was influenced by the way of forming the surface junction; the TP for alumel is larger than that of chromel by approximately 17.33%. The results obtained have provided useful and practical data for TP values for different scratched temperature sensors and were beneficial to the experimentalists in the field and can be used for accurate transient heat transfer rate determination. In addition, the calibration technique used shows that the response time of these sensors is on the order of microseconds (less than 50 μs) and it has a rise time less than 0.3 μs. The literature further includes a numerical technique for evaluating the transient heat flux history from the measured temperature-time signal.

[2]Mohammed et al. (2010) obtained practical data for thermal product values of *E-type CSJT* for accurate transient heat transfer measurements under hypersonic flow conditions. The data were evaluated using different scratched temperature sensors. Further, the effect of using different scratch techniques (abrasive papers and scalpel blades) to form the sensor's junction were also investigated. It was observed that the TP of a particular sensor depends on the Mach number, junction scratch technique, junction location and enthalpy conditions. The results demonstrated that using different scratched technique would produce different TP values. The accurate TP value depends on whether the junction formed where actually located on the positive, or the negative or on both and on its proximity to the thin insulating layer. It was observed that there were apparent differences between the thermal product for junctions formed on chromel element and those

formed on constantan element; the TP value for constantan element was larger than that of chromel element by approximately 15.1%.

[2]***Mohammed et al. (2011)*** reported the effect of different scratch techniques on the *thermal-product* (TP) value of temperature sensors using a dynamic calibration technique in a shock tube facility. They utilized abrasive papers and scalpel blades to form the junctions on the temperature sensors. It was outlined that TP of a particular sensor was found to be dependent on the flow Mach number, junction scratch technique, junction location, and also on the enthalpy conditions. Further, using different scratch techniques normally results in different thermal-product values of sensors; the exact TP value depended upon whether the junction was located on the positive or negative element or on both, and on the proximity to the junction to the thin insulating layer between the two elements. The temperature sensors scratched with scalpel blades of appropriate thickness showed consistent thermal-product values, requiring no individual calibration. However, calibration for each temperature sensor whose junction was prepared using abrasive papers with various grit sizes is likely to be needed. The thermal product for alumel was larger than that of chromel by approximately 17.33%. The experimental procedure used in the present study has yielded practical data on characteristics of scratched temperature sensors; these data can be utilized for accurate measurement of *transient heat transfer* under hypersonic flow conditions.

[3]***Mohammed et al. (2011)*** depicted the experimental technique to evaluate the thermal product (TP) values of rugged and fast response *temperature probes* for hypersonic aerodynamic experiments mainly by using abrasive papers with different grit sizes and scalpel blades with different thicknesses, to form the probe junction. A shock Tube facility was utilized for testing and calibrating the developed probe. The outcome of the experimental results showed that TP of a particular sensor depends on Mach number, junction scratch techniques, junction location as well as on enthalpy condition. The effect of the thermophysical properties of different substrates on the temperature sensor thermal product was examined, and some new correlation equations for evaluating the temperature sensor thermophysical properties were derived for getting accurate results. It was identified that depending on the scratch techniques, individual calibration is not required for sensors whose junction are made from scalpel blade, but individual calibration is necessary for junction formed with abrasive grits. A significant difference between the thermal products for junctions formed on the alumel and chromel elements using the scalpel blade

technique ranged up to about 17.33%. The accurate thermal product value of a particular TP depends upon junction location on the positive/negative element or on both and upon its proximity to the thin insulating layer between the two elements.

2.5 Utilization of Shock tube as an Impulsive Experimental Tool

Spadaccini and Colket (1994) comprehended a thorough investigation to determine ignition delay characteristics for mixtures of methane with ethane, propane, butane and for a typical mixture of natural gas fuel. The experiments were conducted at an equivalence ratio of 0.45-1.25, a temperature range of 1300-2000 K and at a pressure range of 3-15 atm. In addition, the combined data of all the mixtures were utilized to study/predicting the ignition delay characteristics of binary methane-hydrocarbon mixtures and multi-component natural gas mixtures in terms of its temperature, initial fuel and oxygen concentration. Further, a chemical kinetic modelling was performed to estimate the ignition mechanism for lower temperatures and different fuel concentrations, and to permit extrapolation of data; in turn predicting the effect of using vitiated air for combustor testing.

Doolan and Morgan (1999) proposed a new free-piston driver type for expansion tube in the already existing shock tube facility. The facility was such that it would act as a two-stage free-piston driver in which driver gas was compressed in two distinct stages with a unique compound piston design. In addition, a quasi 1-D numerical model was developed for the compression process, which agrees well with the driver tube experimental results. In nutshell, the demonstrated facility has the capability of driving hypervelocity expansion tubes.

Bhaskaran and Roth (2001) carried out a detailed review on the use of the shock-tube facility as means of chemical kinetics study highlighting all the limitations and in turn, suggestions with major focus on the diagnostic techniques. In nutshell, the applicability of shock –tube as a high temperature wave reactor for kinetic studies in both homogeneous and heterogeneous systems were highlighted.

Duff and Blackwell (2003) developed several different high explosives driven shock tube as a cradle of short duration, supersonic, high pressure pulses for its usage to load large, massive objects with accelerations up to many thousand g's; particularly for its usage in order to simulate strong

blast effects on hardened structures. The author presented a detailed design module with experimental measurements on few numbers of configuration resulting in a good agreement with the calculations. The developed facilities can produce peak dynamic pressure in the range of 70 to 2000 bar for halftime duration from a few hundred microseconds to several milliseconds.

Persico et al. (2005) proposed a procedure for dynamic calibration of fast-response pressure probes using the shock tubes flows resulting from the incomplete burst of the diaphragm. In general, the partial opening of the diaphragm results in deviation of the results as predicted from the originated step signal. It was observed that the energy integral of the perturbations decreases with the increase in the distance from the diaphragm.

Jagadeesh (2007) illustrated the usage of shock wave as an industrial application device with a major focus on shock wave assisted cell transformation, preservative injection into bamboos, sandal oil extraction, and removal of micro size dust from silicon wafer surfaces. The facility was developed at the Shock Wave Laboratory (SWL) in the Aerospace department of IISc Bangalore. The author has successfully injected deoxyribonucleic acid into the Escherichia coli and Agrobacterium cells using the underwater shock wave generator. Further, with the use of vertical shock wave reactor, water-soluble chemical preservative (copper-chrome-arsenic) were successfully injected into bamboos. In addition, a remarkable result was observed while exposing sandalwood to shock wave resulting in 40 % reduction in time for extraction of oil.

Nachiketa et al. (2015) investigated a deformation study on the AA5086 aluminum alloy using shock wave deformation with an impulse input of ~0.2 Ns. The analysis includes the microstructure, bulk texture and the hardness of the materials. The shock deformation revealed characteristics texture evolution with the high brass component. In short, the work revealed the viability of the high-velocity forming of AA5086 aluminum alloy with a shock wave.

Andreotti et al. (2015) successfully tested the performance characteristics of a double diaphragm shock-tube facility in order to investigate the structural response. The simulation was accounted with several different finite element models of increasing complexity in order to cater various sources of dissipation including the partial diaphragm opening and the shock tube vibration. The study revealed that the most significant sources of dissipation include the diaphragm opening process.

2.6 Heat Transfer Measuring Gauges

Rose (1958) developed a heat transfer gauge for measurement of extremely high heat transfer in shock tubes rates occurring under the quasi-transient conditions. The instrument works on the calorimetric principle and was made possible by the short steady state times inherent in shock tubes. The author reported in detail the operating principle and the experimental experiences with the calorimetric gauges. The developed sensors were utilized to experimentally measure the laminar and turbulent heat transfer rates at velocities up to satellite speeds (approx. 7925 m/s). In addition to that, heat transfer rates as high as 40 kW/m^2 have been encountered in these experiments.

Miller (1985) reported the principle uncertainty associated with the use of thin-film gauge on the MACOR substrate in a hypersonic wind tunnel. The result included uncertainty with both MACOR thermal properties and variation of those properties with respect to the temperature. In succinct, the influence of shock strength on stagnation point heating at low Reynolds numbers was illustrated.

O'Brien (1990) described an experimental technique to measure time-resolved heat flux in a steady-flow ambient temperature facility with a high frequency response using thin-film gauges. The test facility includes a rotor-wake heat transfer model which was preheated and suddenly injected into an established steady flow. The thin-film gauges were deposited on the test surface. The experiment was successful in the determination of desired information on the effects of wake passing on stagnation region heat transfer. The technique, however, fails to capture continuous heat flux signals.

Hager et al. (1991) worked on estimating the performance characteristics of a heat flux micro-sensor fabricated out of micro-fabrication techniques. The developed gages were small, had a high frequency response, could measure high heat flux and the output was directly proportional to the heat flux. Basically, the gages consisted of a thin thermal resistance layer sandwiched between many thermocouple pairs on a glass and silicon substrates, in turn, forming a differential thermopile. The complete analysis was carried using 1-D transient finite difference model of the six layers comprising the gage plus the substrate.

Lu and Wilson (1994) conducted a review of the basic operating principles of a number of short duration facilities such as shock tunnel, gun/free piston tunnel and expansion tube, with an emphasize on the recent developments to improve the understanding and operation of such facilities.; which will result in an improved ability to interpret test data.

Babinsky and Edwards (1996) developed a technique to measure surface heat transfer rate in short duration hypersonic wind tunnel using the colour response of the encapsulated thermochromic liquid crystal. The experiments are conducted for an axisymmetric compression corner at Mach number 5 and in turn compared with the surface thermocouple measurements.

Robert and East (1996) highlighted the use of thermochromic liquid crystal for heat flux measurement in short duration hypersonic facilities. The detail regarding the model construction, liquid crystal calibration, and image acquisition and analysis were focused. It was observed that despite having inherent limitations in the technique, it was able to capture high spatial resolution data within acceptable uncertainty. The developed technique had an invaluable tool for comprehending data of complex flows.

Hubner et al. (2002) measured surface temperature and heat transfer rate on a generic indented cone model in short duration hypersonic flow using the time-dependent high speed imaging and luminescent coating techniques (TSP). The experiments were performed on 48-inch shock tunnel and LENS I tunnel facilities at Calspan- University of Buffalo Research centre on to a Mach number ranging from 9.5-11.1 and Reynolds number of $1.4 \times 10^5 – 3 \times 10^5$ m^{-1} within a run time of less than 10 ms. Further, it was desirable to utilize camera technology, which enables to increase the number of the captured frame without distorting the outline performance characteristics.

Nagai et al. (2008) studied the relationship between the temperature sensitive paint layer thickness and the measurement accuracy of the heat flux on the aerodynamic model. The experimental model was tested at a Mach number of 10 in the Japan Aerospace Exploration Agency's 0.44 m hypersonic shock tunnel. A comparison between the temperature sensitive paint data and conventional thermocouple data depicted that the measurement error changed with a thickness of the paint layer. The experiment was further repeated with a 3-dimensional model to validate the temperature sensitive paint of optimum thickness. A complex heat flux pattern was observed, which is caused by the shock-wave/shock-wave interaction.

Liu et al. (2009) depicted on the analytical means for Temperature Sensitive Paint (TSP) measurements to obtain quantitative global heat flux diagnostics in the hypersonic environment on important physical phenomena such as laminar-turbulent transition, near-surface stationary vortices and separation. The exact transient solution for 1-D time-dependent heat conduction equation is obtained using Laplace transform for a thin-polymer on a semi-infinite base. Further, simulations and experiments were conducted to validate the analytical method and to access the relevant factors regarding the measurement uncertainty. The experiments were repeated considering *Huber et al. (2002)* experimental model. Additionally, an analytical method was applied to the heat flux measurements on a Nylon cone conducted in the Boeing/AFOSR Mach-6 Quiet Tunnel at Purdue University.

Peng et al. (2016) comprehended on the simultaneous measurement of transient flow using fast responding pressure and temperature sensitive paints in the long-duration hypersonic tunnel. The experiments were conducted on a standard model (HB-2) at Mach 5. The data for both pressure and temperature were recorded at 500 Hz using the high-speed camera. Based on the TSP results a time-dependent temperature correction was applied on the PSP data; while the heat flux was calculated using time-resolved temperature field using a 1-D semi-infinite heat conduction model. According to the study, the PSP/TSP has great potential for unsteady flow diagnostics in hypersonic flows.

2.7 Application of Coaxial Surface Junction Thermocouple

2.7.1 Internal Combustion Engine

Alkidas (1980) evaluated *transient heat flux* at four positions on the cylinder head of a four-stroke single-cylinder spark-ignition engine. The tests were performed for both fired and motored operation of the engine. The analysis has been carried out with engine speed as a primary operational variable. The obtained results showed that the heat flux varies considerably with the position of measurement, can be principally attributable to spatial variations of the temperature and velocity fields in the combustion chamber. The initial high rate of increase of heat flux was noted at each position of measurement correlated with the calculated time of arrival of the flame at that position with fired conditions; in comparison, for motored operation of the engine, the increase of heat flux during the compression stroke occurs simultaneously at the four positions of

measurement. During the last stage of the expansion process prior to the opening of the exhaust valve, the magnitude of the heat flux is independent of spark setting. Further, as expected the peak heat flux was found to increase with increased engine speed.

Alkidas and Myers (1982) measured *heat-flux* on the cylinder head and liner of a four-stroke, single-cylinder, and Spark-Ignition engine. The heat transfer was examined with the variation of air-fuel ratio and volumetric efficiency. The results showed that the magnitude of the heat flux was highest at near-stoichiometric composition, whereas at either leaner or richer composition the heat flux decreased. In addition, an increase in volumetric efficiency from (40 to 60)% resulted in an increase in peak heat flux of about 30%. The large cycle-to-cycle variation in the measured heat flux occurred at the time of the initial high rate of heat flux, which relates to the cycle-to-cycle variation of flame propagation in the combustion chamber. Likewise, the calculated amount of heat transferred to the walls of the combustion chamber during the closed portion of the engine cycle (intake valve closing to exhaust valve opening) was in good agreement with the corresponding values obtained from the heat-flux measurements.

Alkidas and Cole (1985) experimentally measured the *transient surface heat flux* on the cylinder head of a divided-chamber diesel engine. The operational parameter for the engine used was examined and was found to be: engine speed (1000 to 3000 r/min), fuel/air ratio (0 to 0.040), and combustion timing (TDC to 10° ATDC). The found local heat flux histories were significantly different and the anomaly for that was largely for the spatial non-uniformity of the fluid motion and combustion. Both the local time-averaged and local peak heat fluxes decreased with decreasing speed and load. Retarding the combustion timing beyond TDC resulted in decreasing the peak heat flux in the antechamber, increasing the peak heat flux in the main chamber. The reason could be attributed to the relative increase in the portion of fuel that burns in the main chamber with retarded combustion timing. For motored conditions, the highest heat flux was measured in the antechamber due to the presence of high swirl flows. On the other hand, for fired conditions, the highest heat flux levels were measured at the location in the main chamber between the valves and in line with the throat of the antechamber. The obtained result for the fired condition was due to the convective action of the high-temperature combustion gases exiting in the antechamber during the early stages of the expansion stroke.

Assanis and Badillo (1989) have carried out a finite element modelling of various fast-response thermocouple design. Owing to the small differences between the thermal properties of thermo-elements and metal engine components, the standard coaxial thermocouples were able to measure transient temperatures of the metal components only within an accuracy limit of 98%. Furthermore, it was observed that this small error in temperature measurement was leading to a 30% errors in the iron surfaces with respect to its indicated peak-to-peak-temperature swings; which resulted in 30 % error in the measurement of heat-flux rate pertaining to iron surfaces. Further, the obtained heat-flux errors could even be larger, if the coaxial thermocouple were used for measurements in aluminium or ceramic surfaces. Additionally, increasing the thin-film thickness on the surface of coaxial thermocouple could result in overcoming the anomalies in the measurement of heat-flux. The proposed design was capable of capturing very precise heat-flux measurements in ceramics.

Assains et al. (1993) designed a Chromel-Alumel overlapping *thin-film thermocouple* (TFTC) for transient heat transfer measurements in ceramic-coated combustion chambers. The developed TFTC have been successfully developed using various metallurgical techniques and were calibrated against a standard thermocouple. The uniform deposition of thin-film over the plug surface was analysed using SEM. The result evaluated at room temperature and after annealing the plug at 1000 °C for two hours, showed no evidence of delamination or cracking on the ceramic surface, the lead wires, or around the periphery of the ceramic/metal interface. The developed TFTC were tested in a diesel engine combustion chamber operating at 1900 rpm and at full load. The sensor measured a mean temperature of 613 K with a cyclic swing of 55 K for a ceramic-coated chamber surface. The obtained result displayed a dramatic reduction in transient heat flux into the surface with the application of the ceramic coating.

Rakopoulos and Mavropoulos (2000) experimentally studied the transient engine surface temperature and instantaneous heat-flux in the combustion chamber walls of a direct injection air-cooled four-stroke diesel engine. A novel experimental installation was developed, in which the engine transient signal was separated into two parts viz., short and long-term responses, and their discrete signal processing into two independent data acquisition system. In addition, a pre-amplification unit for the fast response thermocouple, appropriate heat-flux sensors, and an innovative object-oriented control code was designed and fabricated. A one-dimensional heat

conduction with the Fourier analysis was used, for the analysis of instantaneous engine cylinder and exhaust pipe heat-flux. The result of heat-fluxes of the engine cylinder, exhaust manifold, together with the engine indicator diagram revealed the mechanism governing the transient heat transfer. Furthermore, the engine speed has very little impact on the cylinder head peak heat-flux; the heat-flux from the exhaust manifold continues to rise with the increasing speed of the exhaust gases. The wall surface temperature gives a significant shift, showing its peak value approximately at 10°CA after the appearance of the peak of cylinder head heat-flux and the indicated gas pressure respectively.

Nijeweme et al. (2001) carried out a study to understand the phenomenon of heat transfer from wall to the combustion chamber in the expansion stroke during the instantaneous heat flux measurement. Twelve different fast response thermocouples were employed on the wall of the combustion chamber of the four valve, single cylinder spark ignition engine. A CFD simulation was attempted to support the experimental results. The obtained results have clearly shown that the change in cylinder pressure causes a phase shift of the heat flux forward in time.

Chana et al. (2003) successfully measured the heat transfer rate on the piston surface and cylinder head exposed to the combustion gases using platinum *thin-film resistance thermometers*. The sensor has a frequency response of around 100 kHz and thus can track the heat transfer rate changes on the piston surface and cylinder head adequately. The measurement taken with engine motored and at low load were discussed and presented for a number of positions on the piston and cylinder head. The investigation has clearly demonstrated the use of thin film gauges for taking heat transfer measurements in a spark ignition engine operated at realistic conditions. The measured peak heat transfer level on piston and cylinder head were found to be of the order of 2.5 MW/m^2 and were seen varying significantly from cycle to cycle. The technique was suggested as a working diagnostic tool for engine development.

Kar et al. (2004) developed a method for measuring the instantaneous exhaust gas temperature using *thermocouples*. Usual normal thermocouples do not measure the instantaneous exhaust gas temperature, which was because of their limited dynamic response. For that reason, a thermocouple compensation technique has been developed to estimate the time constant in situ. The developed method was commissioned in a simulation study and a controlled experiment (air-

rig experiment) with a reference temperature. The study has shown that the signal bandwidth has to be restricted to nullify the amplification of noise in the temperature reconstruction. In addition, a comparison between two independent pairs of thermocouples has shown that the temperature variations at frequencies up to 80 Hz could be recovered. The medium load results agree with a previous study, which used fast response thermometers with a bandwidth of about 50 Hz. However, the results at low load and two different speeds have highlighted the need to do some *1-D unsteady flow simulations*, in order to gain more insight into the exhaust process.

Chang et al. (2004) carried out an experimental study to provide a qualitative and quantitative insight into gas to wall heat transfer in a gasoline-fuelled Homogeneous Charge Compression Ignition (HCCI) engine. *Fast response thermocouples* were embedded in the piston top and cylinder head surface to measure the instantaneous wall temperature and *heat flux*. The obtained heat flux measurements at multiple locations showed some small spatial variations, which confirms the relative uniformity of in-cylinder conditions in an HCCI engine operating with premixed charge. As a result, the spatially-averaged heat flux epitomizes well the global heat transfer from the gas to the combustion chamber walls in the premixed HCCI engine, as confirmed through the gross heat release analysis. The heat flux measurements were used for assessing several existing heat transfer correlations; the Woschni expression, which is one of the most popular models, was shown to be inadequate for the HCCI engine. The reason for which was cited to the flame propagation term, which was not appropriate for the HCCI combustion. A modified model was proposed, which resulted in significant improvement in the prediction of heat transfer in a gasoline HCCI engine and showed very good agreement over a range of conditions.

Yusaf et al. (2005) predicted the *transient heat flux* during combustion in a spark ignition engine using a quasi-one-dimensional engine cycle simulation program on MATLAB® tool using Graphical User Interface (GUI). A two-zone heat release model was utilized to model the combustion process inside the combustion chamber, Using the variable specific heats, fuel, air and burned gas properties were calculated throughout the engine cycle. The Woschni heat transfer model was used to determine the transient heat flux inside the combustion chamber due to the change in the in-cylinder gas temperature and pressure during combustion. The obtained numerical results were compared with the experimental measurements and good agreement was obtained. The difference between the numerical and theoretical assumptions was mainly due to the

assumptions of the mass fraction for burned and unburned gas region. Four *thermocouples* were positioned at an interval of 5 mm along with a ray from the spark plug location on the engine head. The thermocouples were able to capture the heat flux release by the burned gas to the wall during the combustion process including the cycle-to-cycle variations. Additionally, the pressure sensor was installed at the engine head to capture the pressure change throughout the cycle. From the application point of view, the model could prove to be a very handy tool to investigate the quality of combustion in the combustion chamber.

Marr et al. (2009) designed a *fast response thermocouple* for measuring the surface temperatures of aluminium components in ICE combustion chambers. The use of the aluminium substrate as one of the thermocouple metals and the use of a thick copper layer as the hot junction at the surface were the key features of the design. The copper equalizes the hot junction temperature with the surrounding aluminium to correct the differences in thermal properties between the two materials. The designed thermocouple is a modified form of the thermocouple developed by *Heichal et al. (2005)*, in which addition of a thick copper layer at the surface to conduct heat away from the constantan wire was the primary modification. Furthermore, the FEA determined the optimum thickness of the copper layer to be deposited which should be between 100 and 125 µm. Additionally, the thermocouple should be able to measure average surface temperatures within 0.19 °C when worked under typical SI engine heat flux conditions; the magnitude of temperature swings within 6% of true values. After the FEA, the optimized thermocouple was tested in an SI engine and the obtained results displayed the same trends as the FEA at measuring average temperatures and temperature swings, which suggested that the thermocouple was performing as predicted. The experimental engine testing of the thermocouple displayed the trends predicted by the FEA and the results suggested that the thermocouple were accurate at measuring average temperatures and temperature swings.

Morey and Seers (2010) carried out an experimental study to measure the exhaust gas temperature. The intention was to monitor the in-cylinder combustion process of a spark-ignition engine for achieving better fuel economy and further reducing the pollutant emissions. The measurement of exhaust gas temperature was carried out with a small diameter thermocouple (25.4 µm or 0.001 in.), while the in-cylinder pressure was measured using a pressure transducer. In addition, cycle-by-cycle variations of the measured exhaust gas temperature were compared to IMEP variations

for groups of cycles. The experimental results showed that both the coefficient of variation of maximum temperature and the coefficient of variation of indicated mean effective pressure followed the same trend.

Torregrosa et al. (2012) validated an innovative experimental facility to estimate *heat fluxes* on a modified Diesel single cylinder combustion chamber. The methodology was for evaluating the influence of some of the engine parameters on local engine heat transfer behaviour under motored steady-state conditions. The study was divided into two main parts; the first part included the design and setting of an experimental bench to reproduce diesel conditions and perform local-instantaneous temperature measurements along the walls of the combustion chamber using fast response thermocouples. Secondly, to develop a procedure using one-dimensional Fourier analysis for treatment of temperature signal and calculation of local heat flux. Further, the thermodynamic diagnosis model was employed to characterize the modified engine with the newly designed chamber. The measured data resulted in greater understanding of the local behaviour of heat transfer in an internal combustion engine, and the influence of engine parameters on local instantaneous temperature and heat flux. It was observed that the heat transfer through the combustion chamber is strongly affected by the air consumption, as air mass flow rises heat flux peaks also rises.

2.7.2 Hypersonic Facilities

Kendall (1957) conducted an experiment on a flat plate with sharp leading edge in the GLACIT 127 by 127 mm with Mach number 5.8 in the hypersonic shock tunnel. The measurement of the induced pressure was calculated with the help of the orifice in the plate surface. At various distances from the leading edge, the profiles of Mach number, velocity, mass flow, pressure and momentum deficiency were calculated from the impact pressure normal to the surface. A very good observation was made from the obtained results.

Fay and Riddell (1958) worked on the reduction of boundary layer equations to a set of non-linear ordinary differential equations at the stagnation point. Two methods of numerical solution were developed considering the fact that chemical reactions proceed slowly in a manner such that the thermochemical equilibrium is not achieved. The first method included the equilibrium case and the other for the non-equilibrium one. The numerical results were correlated with the parameters

entering the numerical formulation, with an intention not to depend on physical assumptions. The catalytic and non-catalytic wall surfaces were considered for the non-equilibrium boundary layer. It was observed that with the use of simple correlation formula, the heat transfer through the equilibrium boundary layer can be evaluated; further, the obtained heat transfer is unruffled by the non-equilibrium state of the boundary layer. A closed equation was proposed to model the convective and catalytic heat flux at the stagnation point of an aero-shell.

Kendall and Dixon (1966) measured surface temperature histories on various aerodynamic configurations in the McDonnell Hypervelocity Impulse (Hot Shot) Tunnel using thin film surface thermocouples. In addition, a computer program was designed to compute the heat transfer rate from the temperature history of the surface thermocouple. The instrument resulted in measuring heat transfer rates ranging from 0.1 to 900 W/cm^2. Additionally, low heat transfer rates of 0.1 and 1.0 W/cm^2 have been determined within ±10% uncertainty with instruments utilizing Pyrex and Chromel substrates, respectively. The surface temperature thermocouple has proven to be a useful tool for the determination of heat transfer rates experienced in the McDonnell Hypervelocity Impulse Tunnel.

Modarress and Azzazy (1989) presented a review of the modern experimental techniques focusing on the diagnostic tools (measurement of velocity, density, and detection of boundary layer transition) for high-speed flow measurements. The techniques for detecting boundary layer includes the flow visualization, thin-film, optical and holographic interferometry, and infrared imagery.

Olivier et al. (1995) described the techniques for surface heat flux measurement in shock-tunnel applications. Considering the same model, a coaxial thermocouple was used for high heat flux measurement and a thin-film gauge for low heat flux measurement. Further, the coaxial thermocouple is equipped with a pressure tap, which allows the measurement of heat flux and surface pressure almost at the same location. The necessary flow conditions were monitored using a combined Pitot pressure and stagnation point heat flux measurement on a sphere. The reason behind the development of the probe was such that the measurement of free stream static pressure for hypersonic facilities was not very important to determine the free stream dynamic pressure, mass flux or total enthalpy, etc. It was rather important to characterize the thermodynamical and

chemical state of the free stream in high enthalpy facilities, as free stream static pressure were very sensitive to high temperature relaxation effects.

Simmons (1995) attempted to emphasize on the utilization of available instrumentation technique and future developments in short duration high enthalpy hypersonic test facilities with a major focus on free-piston shock tunnels. Major issues were addressed such as free stream calibration, surface measurements on models, flow visualization, laser diagnostics and accuracy.

Reddy et al. (1996) reported an extensive review on the hypersonic test facilities being established at IISc Bengaluru. The tunnel has been extensively utilized to measure the data on various aerodynamic bodies of interest at hypersonic Mach number in the range of 4-13. The details of measurements attempted during the period 1975-1995 along with its performance capabilities of HST1 has been presented in this report. The study, in fact, highlighted the suitable capabilities of the hypersonic shock tunnel in a future space mission to India.

Jagadeesh et al. (2000) carried out experiments to measure forebody surface convective heat transfer rates over large-angle blunt cones at a Mach number of 5.75. It was observed that when the stagnation enthalpy is doubled, the heating rates in the stagnation zone increased by five fold. The obtained results are utilized to develop an appropriate analytical model for estimating the heating rate distributions over the large angle blunt cone. In addition, the results were compared numerically using axisymmetric Navier-Stokes solutions at a 0° angle of attack.

Itoh et al. (2001) experimentally studied the non-equilibrium hypersonic aerodynamics of HOPE using the high enthalpy shock tunnel HIEST. The study was carried out in the enthalpy range of 8-14 MJ/kg, with the result highlighting maximum pitching moment likely to be caused by non-equilibrium at a moderate enthalpy of 14 MJ/kg. In conclusion, the non-equilibrium effect with oxygen dissociation occurs mostly at moderate or high enthalpies condition particularly for re-entry vehicles whose main body and the wing was much larger than blunt-nosed part such as that of HOPE.

Marini (2001) computed a study to understand the phenomenon of shock wave/boundary layer laminar interactions over compression ramp with sharp leading edge using numerical simulation and its validation with the experimental results. The simulations cover a wide range of Mach

number and Reynold number. The results revealed that the mechanical and thermal load over compression ramp strongly depends on the ramp angle, wall temperature assumption and on the geometric configuration. Additionally, the quantitative prediction depends on the grid resolution besides the correctness of the employed physical and numerical modelling.

Stalker et al. (2005) reported on the use of shock tunnel as a tool to study the operation of scramjet-powered configurations at sub-orbital velocities above 2 km/s. Further, considering hydrogen as fuel, combustion heat release study on a constant area duct were successfully reviewed. It was observed that the skin friction was predicted successfully using the existing theories of turbulent boundary skin-friction, when combustion of hydrogen occurred outside the boundary layer, while the reduction in skin friction was noticed for combustion within the boundary layer. The experiments validated the use of shock tunnel for stagnation enthalpies near 3 MJ/kg.

Sahoo et al. (2005) studied experimentally on the effectiveness of film cooling technique in order to reduce convective heating rates on a large angle blunt cone flying at hypersonic Mach number and further its effect on the aerodynamic characteristics. The experimental investigation is carried out utilizing a 60°Apex-angle blunt cone with an internal mounted accelerometer balance system for measuring aerodynamic drag; an array of surface mounted platinum thin-film gauges for measuring heat transfer rates on a low stream Mach number of 5.75 with a stagnation enthalpies 1.16 MJ/kg and 1.6 MJ/kg with and without gas injection. It was observed that an increment of 12% in the aerodynamic drag coefficient with helium injection; while considering other gases the increment were 27%.

Sahoo et al. (2006) conducted an experimental investigation over a 60° apex-angle to measure aerodynamic forces and fore-body convective surface heat transfer rates at a nominal Mach number of 5.75 in the hypersonic shock tunnel HST2. An aluminium model incorporating a three-component accelerometer-based balance system was used for measuring the aerodynamic forces and an array of platinum thin-film gauges deposited on thermally insulating backing material flush mounted on the model surface. It was observed that there was a variation in the measured value of the drag coefficient varies by about ±6% from the theoretically estimated value based on the modified Newtonian theory, while the axisymmetric Navier–Stokes computations over predict the drag coefficient by about 9%. Finite element analysis of model- balance assembly at 0° angle of

attack was carried out to choose appropriate rubber bushes for achieving free-floating model conditions in the test section. Besides, the normalized value of measured heat transfer rates at 0° angle of attack was about 11% higher than the theoretically estimated values.

Sahoo (2007) carried out an experimental study on a 60° apex-angle to study the feasibility of simultaneous measurement of drag and aerodynamic heating in a shock tunnel. A three-component accelerometer balance system was used to measure the drag whereas platinum thin film gauges were used for heating rate measurements on the surface of the blunt cone model. As every ground test and flight test data have unique test conditions, so the importance of simultaneous measurement was realized by measuring both drag and heating rates under unique test conditions during gas injection (viz., air, carbon dioxide, argon and helium) at the nose of a blunt cone model flying at Mach 5.75, in a IISc hypersonic shock tunnel (HST2). The maximum reduction of surface heating rates of 40% were noted in the vicinity of stagnation point with carbon dioxide injection, whereas the aerodynamic drag was enhanced by (12-25)%. Furthermore, conducted a flow visualization experiments on the blunt cone model using electric discharge technique to reveal the shock structure in the hypersonic flow field.

Tashiro et al. (2007) described an experimental technique to determine the response function of a thermocouple using a short acoustic pulse wave. A pulse of 10 ms was generated in a tube filled with 1 bar helium gas and the subsequent temperature was measured using the thermocouple. Further, the reference temperature was deduced from the measured pressure on the basis of a laminar oscillating flow theory. The response function of the thermocouple was obtained as a function of frequency below 50 Hz through a comparison between the measured and reference temperatures. The obtained response function with the pulse method agreed good with that obtained using the conventional method with the use of a continuous acoustic wave.

Menezes and Bhat (2010) designed and tested a robust, reproducible, and is highly inexpensive chromel-constantan coaxial surface junction thermocouple in a hypersonic freestream of Mach 8 in a shock tunnel to measure the transient temperature on the surface of a body. The developed coaxial thermocouple was of diameter 3.25 mm, and flush-mounted on the surface of a hemisphere of 25 mm diameter. The preliminary test results indicated that the thermocouple is quite sensitive to low temperature-rarefied freestream, and has a response time of a few microseconds (≈ 5 μs) to

meet the requirements of short duration transient measurements. The obtained data were well comparable with the numerical and analytical results.

[3]Mohammed et al. (2010) described the design, fabrication, and evaluation technique of fast response Surface Temperature Sensor (STS). They fabricated STS of chromel-constantan elements (which is of Type-E) with 2.2 mm and 0.8 mm in diameter. The STS was calibrated using shock tube facility for measuring the transient surface temperature and heat transfer rate. It was proved from this experiment that the STS response time is very short of the order of fewer than 50 μs and a rise time of the order of 0.5 μs. The investigation has clearly demonstrated that the use of miniature STS enables measurements of transient surface temperature in a shock tube facility. The results have significant implications for the design of transient heat transfer experiments with microsecond time scales using STS. The effect of the thermal product (β) for each STS could be evaluated and investigated according to its scratch type to form the surface junction since there was an uncertainty about 25% of the thermophysical properties if it was taken from other open literature.

Irimpan et al. (2015) fabricated the coaxial surface junction thermocouple of E-type for its application in an ultra-short duration, hypersonic impulse facilities. The said thermocouple was designed, fabricated, validated and standardized against a more proven platinum thin-film gauge. The study was carried on a hemispherical model in a hypersonic freestream of Mach 8. The study revealed that a cold junction compensation can be eliminated pertaining to the use of the CSJT in the impulse facilities such as that of shock tunnel. Furthermore, the experiment proved the performance, ruggedness of the sensor to be an effective impulse heat-flux sensor. In addition, the measured heat-flux agreed well with the one predicted by the *Fay and Riddell* equations. The developed sensor has a response time of the order of 25±10 μs; although the sensitivity of CSJT was less compared to the thin-film but can be an assured alternative to the thin-film gauge.

Desikan et al. (2016) demonstrated the design, calibration and testing of a K-type (3 mm length and 1.6 mm diameter) thermocouple (slightly tapered) in hypersonic test facilities having Mach number of 5.75 and total enthalpy of 0.92 MJ/kg to measure the stagnation point heat flux on a hemispherical body. The obtained result was in good agreement with the Fay-Riddell value within an accuracy of 5.5%.

Srinivasan et al. (2016) worked on measuring fore-body and stagnation point heat flux using E-type thermocouple and platinum thin-film gauge on a typical crew model at Mach number of 5.8 and 8 having an enthalpy range of 1.5–3.73 MJ/kg in a combustion-driven shock tunnel. It was observed for fore-body heat flux for a range of the angle of attack (0-20°). It shows that the stagnation point heat flux moved towards the bottom and the top surface experiences lower heat flux. The heat flux value has been noticed to be low at the base level of the crew and minimum at the centre of the model. In addition, it was identified that the obtained heat flux was 50 % higher than the Fay-Riddell correlation for dissociated air with Newtonian correlation, which leads to the utilization of modified Fay-Riddell correlation incorporating the experimentally obtained velocity gradient. The obtained result seemed to be at a variance of 14.25%. With further introduction of dissociation factor, the difference reduced to 9.46%. The proper choice of the transport properties and the velocity gradient plays an important role in accurately predicting the stagnation point heat flux.

2.7.3 Gas Turbine

Lefebvre et al. (1960) briefly described the heat transfer process occurring in the gas turbine and correlated a general equation for flame-tube temperature. The effectiveness of the equation comes handy to analyze the effect of flame-tube temperature on the aircraft flight conditions such as conditions of pressure, inlet temperature, and air-mass flow and further on the combustion chamber design. They conducted experiment to validate the relevance of the derived equation.

Dunn and Stoddard (1979) successfully conducted experiments to obtain heat transfer rate distribution using thin-film heat transfer gage on the first stage stationary inlet nozzle of the AiResearch TFE -731-2 engine. The experimental set-up consists of a helium-driven shock tube as a source of high temperature and high pressure driving a nozzle test section mounted near the exit of the primary shock tunnel nozzle, extending the set-up to a shock tunnel reservoir tank. The set-up has the capability to produce data on the cascade loses.

Martinez-Botas et al. (1995) attempted to measure the heat transfer on the aerofoil surfaces of a large annular cascade of high-pressure nozzle guide vanes using transient liquid crystal technique in the Oxford University Cold Heat Transfer Tunnel. The measurement was accomplished by coating the interesting surface with a narrow band of thermochromic liquid crystal and the

subsequent cooler crystal change was recorded using the CCD video camera. The coefficient of heat transfer was obtained by solving the one-dimensional heat transfer equation for all the points of interest with 7% uncertainty.

Piccini et al. (2000) described a method to calculate *the surface heat flux* from direct-heat-flux gauge (DHFG) temperature traces. The design comprises of an insulating layer mounted on a metal substrate. The sensor measures the heat flux across the insulating layer by capturing the top surface temperature employing a sputtered thin-film gauge (TFG) and the metal temperature using a thermocouple. The TFGs are platinum temperature sensors with a physical thickness less than 0.1 μm and were instrumented on the insulating layer. In addition, the thermal properties and the ratio of the thickness over the thermal conductivity of the insulating layer have been calibrated. The author presented a detailed method of analysis for calculating the surface heat flux from DHFG temperature traces. Moreover, the advantages of the DHFG included its high accuracy, its wide range of frequency response (from dc to 100 kHz) and, most significantly, that there was no requirement for knowledge of the structure of the metal substrate. The DHFGs applied on the gas turbine nozzle guide vane, were successfully tested in the Oxford Cold Heat Transfer Tunnel.

Seyfried et al. (2005) investigated on the characterization of the afterburner of a full-size aircraft using optical/laser-based techniques. The tests were conducted at the Volvo Aero Corporation mainly using the thermographic phosphors and fuel visualization at different engine running conditions. A Laser-induced Fluorescence (LIF) based fuel visualization technique was utilized to study the extent of unburned fuel that exits the afterburner. Additionally, measurement of two-dimensional surface temperatures on the outlet nozzle of the afterburner was carried out using the Laser-Induced Phosphorescence (LIP) from thermographic phosphors. Besides, the outcome from the emission spectrum suggested that the use of phosphors with phosphorescence in the low UV-region would be highly beneficial for increasing the signal to noise ratio and, further improvement of the measurement precision.

Khalid and Kontis (2008) reported on the use of phosphor thermometry as a diagnostics tool in high temperature application and its development over the years. The areas of the application included the measurements in the engine, hypersonic wind tunnel, pyrolysis studies, determination of droplet/spray/gas temperature etc. The technique is a non-contact type as in extremely difficult

conditions it becomes challenging to utilize thermocouple. The method has been flexible and was able to measure temperature where it becomes challenging for the conventional methods.

2.8 Simulation Based Study

Buttsworth (2002) measured transient response using a two-dimensional finite element analysis on an erodible-ribbon element heat gauge. The work results depict that the two- dimensional transient heat conduction effect have a significant influence on the surface temperature measurements made with these devices. Further, for the ribbon element gauge and time scales of interest in IC engines studies, using a one-dimensional analysis (and hence a single value of $\sqrt{\rho ck}$) would lead to substantial inaccuracy in the derived heat flux measurement. It is incorrect to assume that the response of the gauge was governed by the thermal properties of the surrounding materials for the timescale of interest. The thermal properties of the surrounding materials do have an impact, but the properties of the insulation and thermocouple materials make an important contribution to the net response. In addition, it becomes inappropriate; if one treats, the data produced using this type of erodible thermocouple as one-dimensional for the time scale of interest in IC engine experiments. As significant lateral conduction occurs for events with scales between about 1 ms and 10 ms (or more), which can result in an apparent (negative) overshoot in a response when the eve of heating is reduced (if the analysis assumes one-dimensional behaviour). More importantly, there are certain limitations of the present modelling using non-semi-infinite boundary conditions. The material properties particularly for the insulating material with one special type of erodible thermocouple (a ribbon element configuration) was considered.

Mohammed et al. (2007) numerically investigated the transient response of erodible surface thermocouples using a two-dimensional finite element analysis. The study was focussed on four types of base metal erodible surface thermocouples were considered, namely, K (alumel-chromel), E (chromel-constantan), T (copper-constantan), and J (iron-constantan) types respectively with each having a thickness of 50 mm. The practical implication lies in the utilization of internal combustion engine studies and aerodynamics experiments. A step heat flux was applied on the surface of the thermocouple, assuming the heat transfer within the devices as one-dimensional. The surface temperature histories were predicted at different positions along the thermocouple. Further, the normalized surface temperature histories were evaluated at the centre of the

thermocouple for different types at different response time. The thermocouple response to different heat flux variations was considered considering a square heat flux with 2 ms width, a sinusoidal surface heat flux variation width 10 ms period and repeated heat flux variation with 2 ms width. The two-dimensional transient heat conduction effects have a significant influence on the measured surface temperature. In addition, the surface temperature of the mica and thermocouple materials rises faster than that of the dural, because of the lower values of thermal product for the mica and thermocouple materials.

John et al. (2013) developed a 2-D finite volume based in-house CFD solver to study the shock wave boundary layer interaction (SWBLI) and its associated changes in wall properties for ramp induced flow breakdown. In nutshell, it can be said that an attempt was made to comprehend the laminar boundary layer separation in the presence of ramp-induced shock wave including the leading edge bluntness, considering surface heat transfer rates, wall skin-friction coefficient and wall pressure distribution. From the investigation, it was observed that the ratio of wall temperature to freestream stagnation temperature were the governing parameter for SWBLI instead of the individual temperatures. Further, an increase in Mach number seemed to suppress the upstream influence resulting in a decrement in the extent of separation.

Desai et al. (2016) made an attempt, to numerically study the chemical non-equilibrium effects in high enthalpy flows by employing a finite volume based unstructured inviscid flow solver. They carried out simulations for a variety of cases like unsteady wave propagation in a shock tube, 2-D computations, and axisymmetric flows. The limitations of conventional non-dimensional numbers were portrayed in predicting the flow features and flow properties in the presence of reactions.

2.9 Research Undertaken at IIT Guwahati

Sahoo and Peetala (2010) successfully attempted to estimate heat flux out of the temperature data, obtained from a nickel film sensor for a supersonic flight test. Mainly three different curve fitting techniques were utilized to recover temperature data history of real-time flight using piecewise linear fit, polynomial fitting and cubic-spline method. A one-dimensional transient heat transfer modelling was employed to infer heat flux from the temperature history. The results had shown that the polynomial and cubic-spline technique matches very closely, with piecewise linear fitting slightly under-predicting the peak surface heat flux values.

Kumar et al. (2010) described the methods of designing and fabricating a fast response *thermocouples and a thin film gauges* (TFG) for transient measurement. Both the thermocouple and thin film gauge were calibrated under same experimental conditions using the oil-bath technique. The calibration results proved that the hand-made sensors could be utilized to accurately measure the surface temperature and heat transfer rates in transient facilities.

Peetala and Sahoo (2011) carried out an investigation on the effect of sensor thickness on surface heat flux measurement during flight measurement. The measurements were estimated considering the temperature histories obtained from the nickel thin film sensor, mounted on quartz crystal, during a flight test. Further, heat flux was estimated from inverse methods using the analytical solution as well as control volume approximation. Later, the experimental data were discretized using the cubic spline method. The results were validated with the standard benchmark data using the thin-film gauge analysis based on a semi-infinite assumption for one-dimensional medium. It was observed that there were no significant changes in the measured surface heat flux between the inverse and thin-film analysis. Furthermore, it was noticed that when the thickness of the thin-film was increased 100 times during numerical simulation of inverse methods, the peak surface heat flux increased by 20%. It was observed that the inverse methods heat balance equations based on control volume were relatively easy and reduces computational time compared to that of analytical solutions.

Kumar et al. (2011) fabricated platinum based thin film sensors and further calibrated by applying step heat load using the laser light of known wattage. Four different step heat load were applied to the TFG and subsequent transient data were captured. Numerical simulation were performed to support the experimental investigation. The estimated results have shown the satisfactory demonstration of the developed calibration set-up and cost effective means of in-house fabrication of thin-film sensors.

Kumar and Sahoo (2012) proposed fabrication of different types on thin film gauge (TFG) using high conducting platinum and nanomaterials. The sensors were prepared by depositing high conducting gauge material on the insulating surface such as Pyrex, Macor and Quartz. Oil-bath based calibration set-up were utilized to obtain the sensitivity of all the TFGs and a comparison

study were drawn among the sensors. The obtain results suggested that the use of carbon nanomaterial and graphene enhanced the sensitivity as compared to only platinum based sensors.

Kumar et al. (2012) explored the possibility of using thin film gauges for short duration transient measurements with pure conduction mode of heat transfer. A simple calibration set-up was used to supply known heat flux of different magnitudes to the thin film gauges that were fabricated in-house with platinum as sensing element and Pyrex as an insulating substrate. The experimentally recorded temperature signals from the gauges were compared with simulated temperature histories obtained through finite element analysis, performed using ANSYS. The transient temperature data were discretized using the cubic-spline technique. Furthermore, convoluted integral of one-dimensional heat conduction equation was used to predict the surface heat flux and comparison of it with input heat loads. The developed calibration setup was seen to be very useful for conduction based measurements of thin film gauges. The obtained signals for temperatures and surface heating rates were seen to match well within a reasonable uncertainty of ±2%. In general, conduction based calibration explored the feasibility of using thin film gauges in various inter-disciplinary applications.

Kumar and Sahoo (2013) worked on the design and in-house fabrication of a K-type *coaxial thermocoupl*e and thereafter performed dynamic calibration using simple laboratory instruments. There were two methods, where the known step load loads were applied through radiation and conduction modes of heat transfer. The radiation and conduction based experiments for step-heating loads were almost analogous to the heating environment experienced by any aerodynamic model in short duration impulse facilities and in flights. The surface heat fluxes (measured temperature histories) have been successfully predicted, and compared with input loads using one-dimensional heat conduction modelling. The recovered value for the heat flux from the laser-based and conduction based calibration experiments was comparable within 4% and 6% respectively from its true input heat load. In addition, finite element based numerical study was performed to compare the experimental results. The obtained simulation results were within an accuracy of ±0.3 % from the experimental value.

Peetala et al. (2013) predicted heat flux from the temperature signals obtained from the in-house built finite volume computational solver, and experimental data (shock tunnel and flight testing)

using one-dimensional heat conduction modelling and Laplace transform techniques. Three different discretization techniques were used namely piecewise linear fitting, polynomial fitting and cubic spline for the temperature signal. The obtained results have shown encouraging trends and magnitude from all the methods for smooth or non-noisy temperature signals. The applicability of polynomial based fitting was seen to be restricted only to the smooth temperature signals due to the qualitative prediction of heat flux or discontinuous or noisy temperature signals. Further, for trend based prediction and quantification of heat flux, spline based fitting techniques were found to have upper hand for all temperature data. Additionally, lower order (linear spline) were equally effective to higher order spline but were limited to short duration measurement.

Sahoo and Kumar (2016) successfully fabricated three types of thermal sensors namely TFG made out of platinum, TFG made of platinum mixed with CNT and chromel-alumel coaxial surface junction thermocouple. The sensors were calibrated in-house using an oil-bath calibration set-up. A comparison study was shown using a sudden step heat load in convection mode for a 200 ms time duration. All the sensors predicted the surface heat flux well within the range of ±4%.

2.10 Summary

From the thorough literature, considering the international and national status of the work, that there is still enormous room to explore various aspects related to the aforementioned topic, which needs a special attention. The survey was carried out on various aspects as mentioned, related literature gap was analyzed and it can be summarized in the following points.

- With respect to application of coaxial surface junction thermocouples there are very limited works on E-type, T-type and J-type CSJT. Hence there is a need to focus the attention, as they have higher sensitivity than a K-type thermocouple.
- The determination of thermal product (TP/β) (i.e., $\sqrt{\rho ck}$) values, which is essential for the determination of heat-flux value from the obtained temperature-time history, have not been focussed much.
- The surface morphology is another important area which needs attention
- In the past, mostly there are limited studies on K-type CSJTs and thin-film gauges for their usage only in impulse facilities. Still there is ample scope of exploring other types of CSJTs

for wide range of applications. Thus, the focus of the investigation is to fabricate different types of CSJT with their implementation on real-time scale experiments.

2.11 Objective of the Thesis

The core objective of the work involves **Design, in-house fabrication, calibration of Coaxial Surface Junction Thermocouple for real-time applications in transient flow environment**. In order to achieve the key objective, the work is categorized into few sub-categories, which are listed as follows:

- **Fabrication of Coaxial Surface Junction Thermocouple (CSJT):** The design of the various coaxial thermocouple, which involves simulation to validate the dimension of the sensor (*Chapter 3*). The sensors are developed and fabricated in the laboratory with deformation characteristics details of the sensing surface (*Chapter 3* and *Chapter 4*)
- **Calibration of CSJT (temperature and surface heat flux):** The calibration methodology is conducted to check the feasibility of developed sensors (*Chapter 4*). It is broadly classified into two categories, based on, "known temperature" and "known heat flux input". Here, the "sensitivity" of the sensor is obtained for the known temperature (static mode of calibration), and linearity in voltage signal is checked. Before the sensor are exposed to the real-time experiment such as impulse facilities, it is desirable to calibrate the thermal sensor with similar nature of heat load such as exposing the sensor to a certain known heat input (Dynamic mode of calibration)
- **Determination of Thermal Product for CSJT:** The measurement of transient surface temperature and heat flux are very important requirements in umpteen-heat transfer research. The heat transfer sensor basically captures temperature histories and thereafter heat flux histories are estimated. For a short duration study, the heat flux calculations are carried out using one-dimensional semi-infinite medium solution for a step change in temperature. The equation for heat flux includes the "thermal product" estimation, which is a property of the sensing material. The dynamic calibration for each of CSJT is highly desired for accurate estimation of TP as uncertainties up to 25% can be introduced when the thermophysical values of materials are directly taken from the literature. Analyzing all the aspects, few experiments are attempted by using "water droplet" and "water plunging" techniques (*Chapter 5*).

- **Real-time application-based study of CSJT for Heat Flux Measurement:** The sensors are used to capture transient heat flux in real time experiments. The present work is focused on the real-time based study such as stagnation point heat flux estimation in a low supersonic environment such as that of shock-tube (*Chapter 6*); heat flux estimation in the short duration hypersonic facilities such as shock tunnel (*Chapter 7*); instantaneous heat flux measurement in the combustion chamber of the internal combustion engine (*Chapter 8*), qualitative detection of "screech phenomena" in a gas turbine engine (*Chapter 9*),
- **The packaging of Coaxial Thermal Probe:** In order to have a product-oriented thermal sensor for real-time testing, some important aspects of packaging involving curing process and integrating it with a barrel for housing the sensors are discussed (*Chapter 9*).

Figure 2.1 throws basic insights into the work carried during the entire curriculum. The flowchart highlights the path followed for achieving the desired objective.

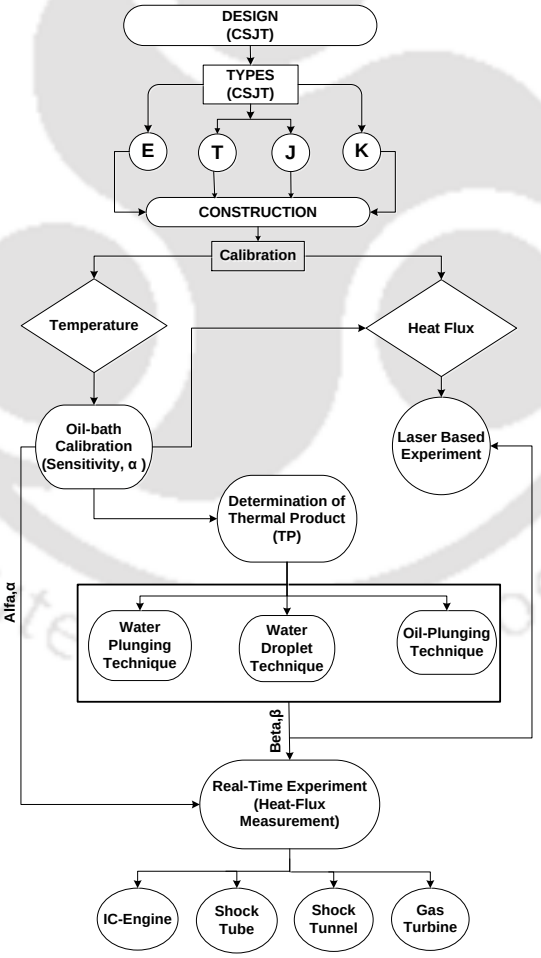

Fig. 2.1: Flowchart highlighting the entire thesis work

CHAPTER 3

Designing and Modelling of Coaxial Surface Junction Thermocouple

Compendium:

With the passage of time, there is a sense of interest among the research community for the measurement of transient heat flux. Thus, it has necessitated the desire to understand in detail the heat transfer phenomena prevailing in the transient environment. Despite the progress in the field of heat transfer measurement, there is still an umpteen requirement to accurately capture the transient phenomena high-speed flow environment, internal combustion engine, gas turbine etc. The surface heat flux estimation for short duration transient study is essence of all these research requirements. The estimation of proper temporal nature of heat load and precise quantification of heat fluxes are the roots of a typical temperature sensor during transient measurements. This chapter presents the numerical modelling of two-dimensional and three-dimensional sensor configurations with an emphasis on instantaneous heat loads experienced by the sensor. These simulations are carried out to estimate the gauge dimensions and directionality of heat flow across Cartesian coordinate systems during the short duration measurement time scale of 1s. Further, the assumption of semi-infinite slab theory of one-dimensional heat conduction during short duration flows has been validated. As there is no direct means for estimation of surface heat flux, the measured transient temperature is processed and converted into heat flux based on one-dimensional transient heat conduction theory. It is also necessary for any analytical modelling to have a closed form solution for any experimental measured temperature data. Additionally, mathematical details with respect to one-dimensional heat conduction equation for recovery of heat flux in relation to fitting in terms of linear, polynomial and cubic-spline based methods are discussed. Keeping the zeal of continuous improvement and the need for the transient measurement of temperature in harsh environment of short duration; the chapter discusses the complete methodology for selection of coaxial thermal probe for transient temperature measurement and subsequent heat flux determination.

3.1 Introduction

In recent times, the hypersonic research has been in major focus due to the marathon development in the field of hypersonic re-entry vehicle, reusable launch vehicles, and orbital transfer vehicles. Further, understanding the transient surface temperature and the heat flux measurement are also one of the important requirements in these research fields. Estimation of the surface heating rate from the short duration transient temperature data has always been of interest in scientific and engineering research particularly in the area of aerodynamics [*Jagadeesh e al., 2000; Reddy et al., 1996*]. Considering the design aspect of the hypervelocity aerodynamic vehicles, the accurate measurement of heat transfer rate in the high-speed over the aerodynamic body remains a real challenge as the heat varies with the cube of the velocity [*Anderson, 2000*]. The flow regime in the high-speed environment is very small of the order of few millisecond or even lesser for almost all aerodynamic facilities [*Sahoo et al., 2006*].

Considering the short duration facilities, the transient temperatures are usually measured with very special type of thermal sensors with high response time, by mounting the thermal sensor on to the aerodynamic body of interest and exposing it to high-speed environment. The heating loads are mostly characterized as step/impulse load given the time of exposure. However, there are no direct methods available which enables one to measure the heat flux. In most of the experiments conducted in impulse aerodynamic facilities (shock tunnel, expansion tubes etc.), the transient temperature data are acquired using various types of temperature sensors and subsequently, surface heat transfer rates are computed by appropriate modelling. The thermal sensor must account for the rapidly varying flow environment and should have very fast response characteristics. Thin-film gauge and coaxial surface junction thermocouple based heat flux measurement are the two most suited classical techniques utilized to account for the heat flux as the response timescale is very high [*[1]Sarma et al., 2016; Kumar et al., 2011; [3]Mohammed et al. 2010; Sanderson and Sturtevant, 2002*]. Furthermore, with respect to the high-speed flow applications, the sensors response time becomes more crucial, pertaining to the time scale of measurement. The coaxial surface junction thermocouple is more robust than the thin-film, but is less sensitive as compared to the thin-film gauges. For measuring relatively low heat fluxes in clean environment conditions, thin-films are more suited, but for measurement in harsh conditions, thermocouples are advised [*Olivier and Gronig, 1995*]. The TFGs encounters high shear and its

film gets eroded with almost every blow-down, which urges for frequent replacement. Considering the thin-film gauges, the construction of coaxial thermal sensors is very simple and can be made in the laboratory itself [*Buttsworth, 2001*].

The transient measurement can also be achieved using non-intrusive techniques such as temperature sensitive paints [*Nagai et al., 2008*] and thermography [*Ireland and Jones, 2000; Ekkad and Han, 2000*], thin-skin thermocouple [*Miller, 1981*], null-point calorimeter [*Powars et al., 1972*], and calorimeter type transducer [*Ledford et al., 1968*]. Considering the temperature sensitive paints (TSPs), working on the principle of light intensity emitted from paint, which is captured by a photodetector and, correlated with the transient variation of temperature. The classical approach of measuring the transient temperature in the hypersonic facilities such as wind tunnel were carried out using the thermochromic crystal technique [*Nagai et al., 2008*]. Each mentioned techniques hold its own pros and cons. In addition, the thin-skin calorimeter, are not recommended for many facilities for its lack of strength and difficulties in positioning the sensors. On the other hand, non-intrusive technique suffers from clumsy calibration technique.

With respect to the high-speed flow applications, the sensors response time becomes more crucial, pertaining to the time scale of measurement. Coaxial surface junction thermocouple (CSJT) and thin-films sensor are best suited for the transient conditions. The thin-film gauges (TFGs) are mainly made by depositing a thin-film of temperature sensitive material (gold, silver, platinum, etc.) over an insulating substrate (Macor, Pyrex, etc.). The film thickness is usually of the order of few nanometer to micrometers [*Sarma, 2017; [1]Sarma et al., 2016; [2]Sarma et al., 2016*]. The TFGs are mostly passive sensors powered by external current source for which there is a change in resistance (and voltage) due to temperature change on the gauge surface. The parameter “temperature coefficient of resistance (TCR)” relates the variation of voltage with respect to temperature. On the other hand, coaxial thermocouples are considered most effective for day-to-day transient measurements. The coaxial sensors work on the principle of Seebeck effect, i.e. whenever the surface junction is exposed to the temperature difference, an electromotive force is developed, which is related to temperature using the effective “sensitivity value” [*Kumar and Sahoo, 2013*]. For aerodynamic measurements, the gauges are flush mounted on the body of interest. Considering transient measurement in very short duration timescale of application, the

coaxial sensors are a special class of thermal sensors for which the choice of appropriate material with respect to its application, is very important.

In view of all aforementioned facts, the present chapter begins with estimating the gauge dimension and validating the semi-infinite one-dimensional heat conduction equation through numerical modelling. The numerical study is carried out considering the sensor model as both two-dimensional (2-D) as well as three-dimensional (3-D). Further, analytical modelling to discretize the temperature-time history as captured by the thermal sensor has been discussed. As known earlier, there is no direct technique, which predicts heat flux directly; the obtained temporal history has to be processed to estimate the heat flux. And, obtaining heat-flux from the temperature signal follows some data reduction techniques and few assumptions [*Sundqvist, 1992; Schultz and Jones, 1973; Cook and Felderman, 1966*]. Three discretization technique namely, Linear fitting, Least-Square (polynomial) and Cubic-Spline based fitting has been elaborated in detail, which can be utilized to process the transient temperature data with the help of an in-house numerical code developed on MATLAB® and eventually estimate the heat flux. Once the numerical validation and modelling are done, the step is taken to understand the design methodology to depending on that factor one should choose to fabricate the thermocouple.

3.2 Numerical Simulation

Prior to carrying out any experimental studies on the thermal sensor, it is paramount to justify the underlying assumption of 1-D heat conduction on a semi-infinite body. i.e. the physical length scale of the thermal sensor (model) along the longitudinal direction needs to be identified/established before it can be used for the fabrication of the coaxial thermocouple. With that intention, a numerical experiment is planned with the commercially available software ANSYS (*Transient Thermal Model*) v 14.5. Apart from this, we also perform additional studies are performed to obtain the basic understanding of the coaxial thermocouple.

The schematic model of the coaxial surface junction thermocouple (*Fig. 3.1*) via geometry module in ANSYS (*Transient Thermal Model*), are shown in *Fig. 3.2(a-b)*. The thermocouple materials (chromel and alumel) with 10 mm long and diameter 3.25 mm with sensing surface junction of surface of 20 μm and epoxy resin (Teflon) thickness of 0.094 mm, is considered as domain of heat flow. The choice of surface junction thickness of 20 μm is mainly attributed due

to the fast response characteristics as reported in the literatures. A transient simulation has been performed for a duration of 1 s with constant heat flux of 1000 W/m^2, applied on the top surface of the thermal probe.

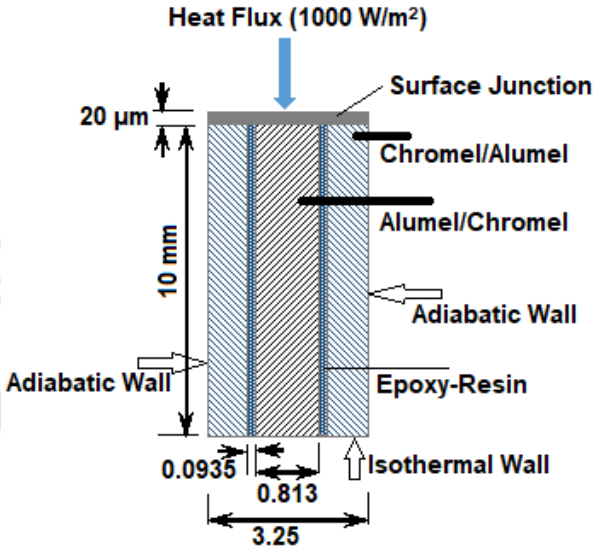

Fig. 3.1: Schematic shows the geometry of the coaxial surface junction thermocouple

Furthermore, the side walls/surface were considered *adiabatic*, the bottom wall/surface is assumed as *isothermal* with temperature equal to room temperature of 300 K. Finally, simulations were carried out considering two case study as illustrated in the *Fig. 3.1*, namely

i) Alumel (A) formed the annulus and chromel (C) of inner wire,

ii) Chromel (C) formed the annulus and Alumel (A) of the inner wire.

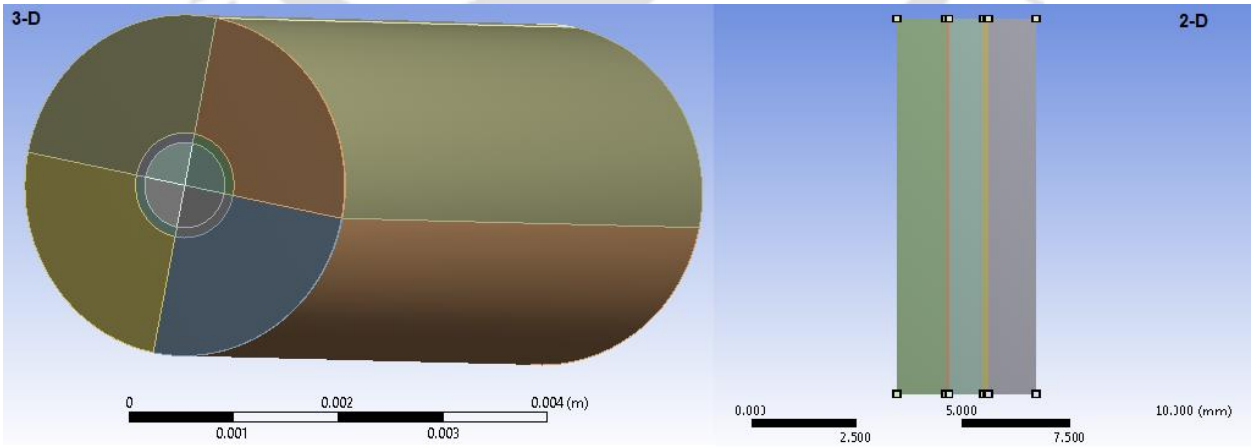

Fig. 3.2: Computation domain of coaxial surface junction thermocouple

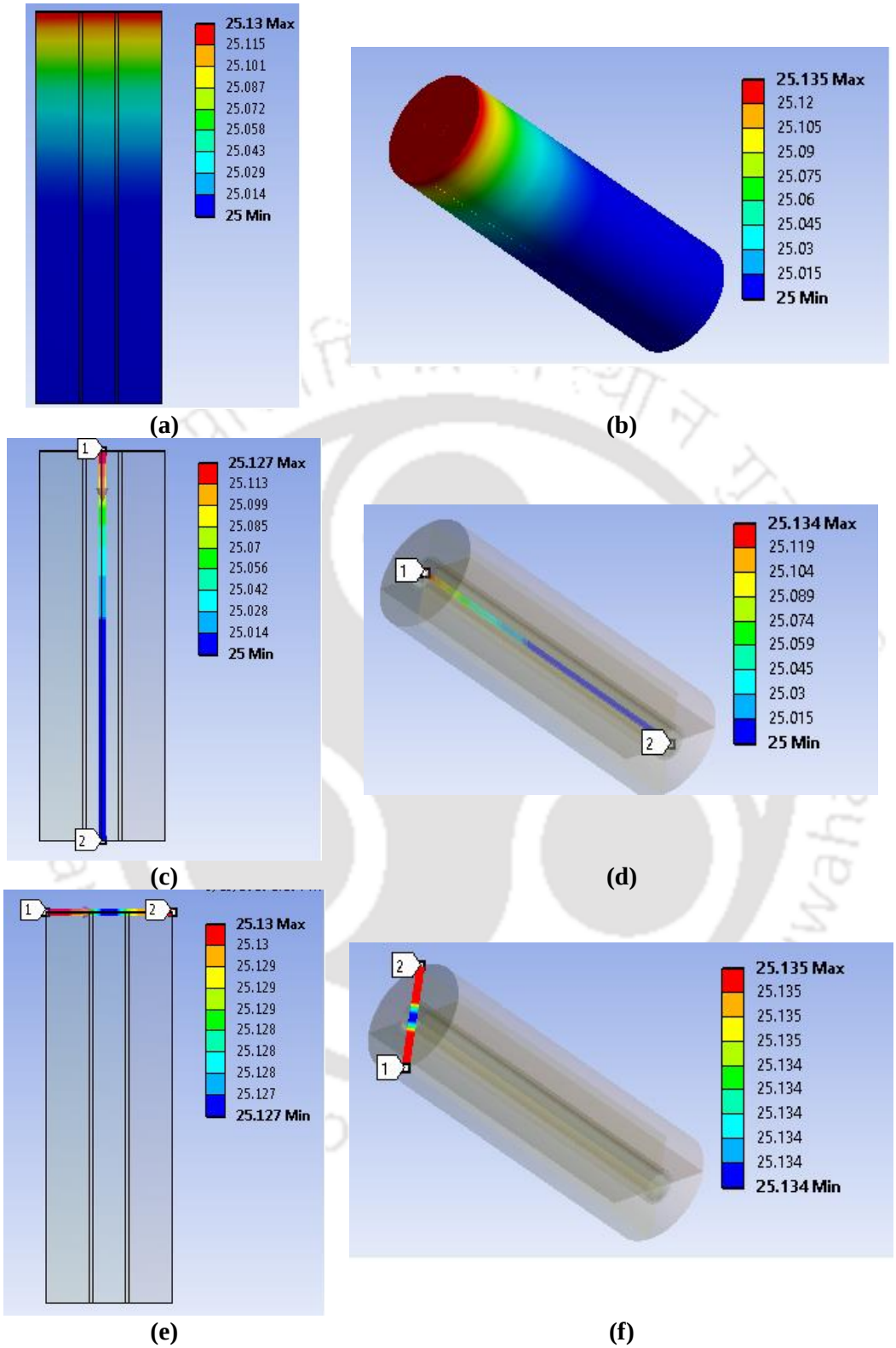

Fig. 3.3: (a-b) Temperature contour in 2-D and 3-D model; (c-d) variation of temperature along the length for both model; and (e-f) variation of temperature along the radial direction for both model

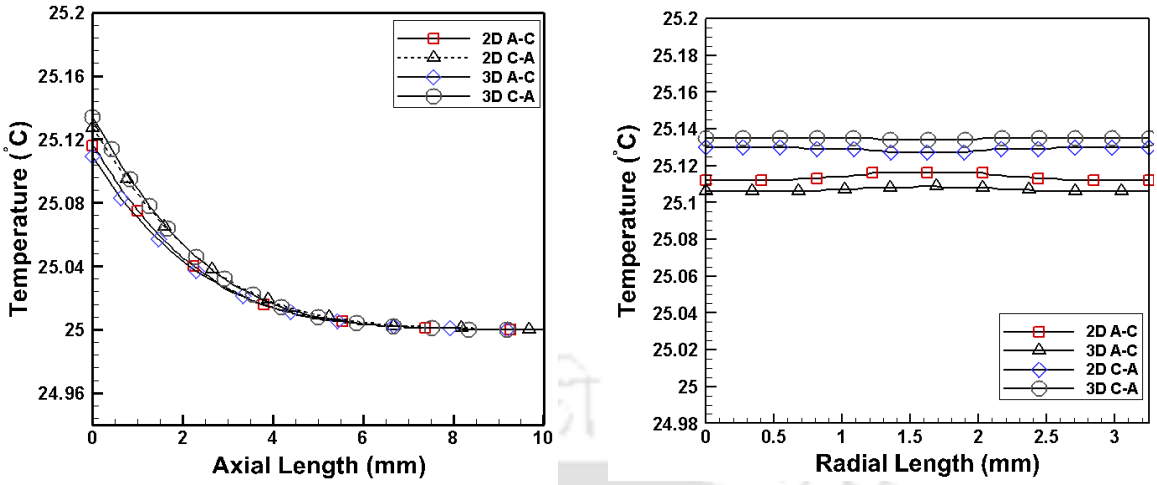

Fig. 3.4: Temperature variation for coaxial thermocouple sensor: (a) longitudinal direction; (b) lateral direction

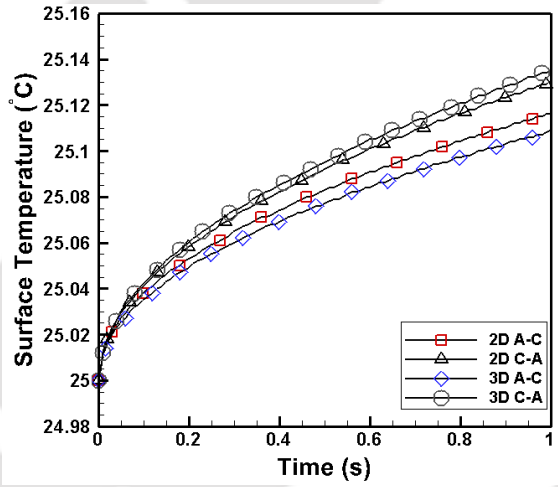

Fig. 3.5: Typical variation of temperature as captured by the coaxial thermal probe

One of many available method of meshing which aid in creating structured mesh, is the use of *multi-zone* method of meshing. The main intention is to choose good quality mesh, besides checking its element quality, skewness, orthogonality etc. starts from generating structured mesh with *quadrilateral* cells, as opposed to *tetrahedral* unstructured cells. To facilitate *multi-zone* method of meshing in ANSYS, one needs to first divide the entire computational domain into sub-domains or blocks. This can be easily done by creating imaginary planes, otherwise known as slices, which assist in dividing the domain into further parts (*Fig. 3.2*). Once the domain has been divided into sub-divisions, the line-segment encompassing each block is then divided into chosen number of divisions, to locally define the *mesh sizing*. The amount of divisions varied according

to the kind of grid that was chosen for the grid-independence study i.e. *grid 1* (coarse), *grid 2* (medium), *grid 3* (fine). The number of *computational volumes* (*nc*) or cells for each grid are (*grid 1= 38080 & 71500, grid 2 = 53317 & 147840 and grid 3 =83490 & 237600*). For the numerical simulation performed herein, it was observed that the choice of grid-size does not influence the final solution to a significant amount. In other words, the grid-size chosen for the simulation were fine enough to obtain grid-independent solutions for both 2D and 3D test-cases. The above observations augers well with the reports of *Wei et al. 2006*. Following this, one can select individual blocks one after another to create the structured mesh containing only quadrilateral cells. However, a time-step independent study (*0.5 ms, 1 ms and 2 ms respectively*) has also been carried out and it was observed that both the simulation study are time-step independent (*Figs. 3.6 (a-b)*).

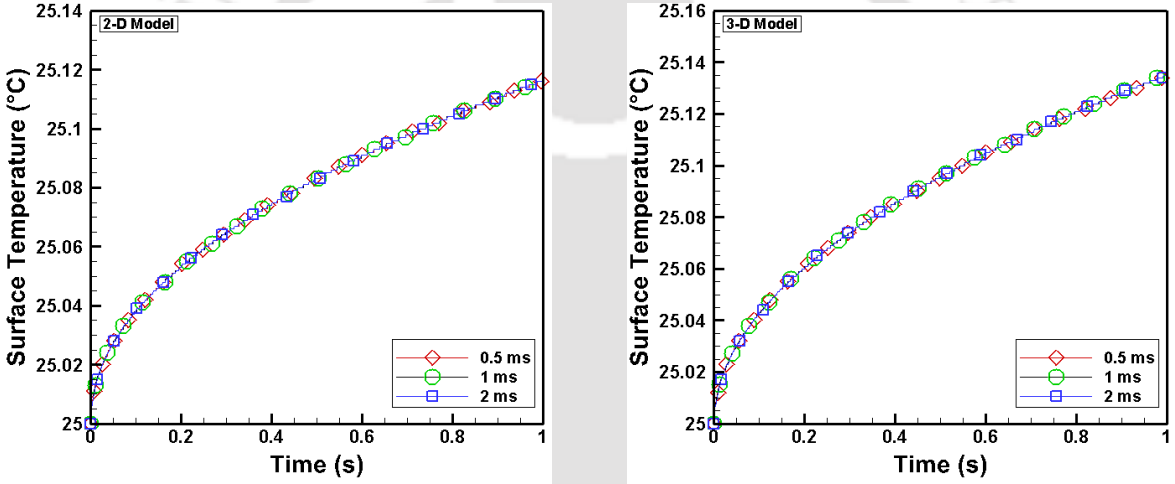

(a) **(b)**

Fig. 3.6: Typical time-step independence study for the simulation model

It is seen from the obtained results (*Figs. 3.3 (a-d)*) that for both 2-D and 3D models, the depth of penetration of temperature is limited to a certain length. Same inference can again be drawn from *Fig. 3.4(a)*, which shows the variation of the temperature along the length of the substrate at time 1s. Appreciable change in temperature is only observed till a length of 6 mm approximately (measured from the film-substrate junction), and hence it can be asserted that the chosen length of the substrate does not violate the assumption of the 1D heat conduction for semi-infinite geometry when subjected to transient condition of 1s. From *Fig. 3.4(b)*, it can be observed that the lateral variation of temperature is negligible for both 2D and 3D model, which is true partly because adiabatic wall assumption was considered along the side wall/surfaces. In continuation, it was qualitatively also seen the overall estimation of output generated from the simulation were

independent on the polarity of the material i.e. selection of outer material as chromel or alumel. Lastly, it is seen from *Fig. 3.5*, that the temperature-time history trend clearly depicts a parabolic behaviour, which is also in agreement with literature [*Holman, 2001*].

3.3 Theoretical Modelling of Heat Flux Measurement

The principle on which thermal sensors namely, thin-film and coaxial sensors work, have been synoptically reviewed by *Schultz and Jones (1973)*. These thermal sensors measure transient temperature histories and in turn, the heat flux is predicted thereafter by using suitable one-dimensional heat conduction modelling. Heat transfer plays a vital role in many industrial and environmental applications. In case of hypersonic vehicles, convective heat transfer plays a very pivotal role. There are no direct methods, which enable us to measure the convective heating rate, it can only be measured from transient temperature-time history captured by the thermal sensor. In short, milliseconds time scales, the surface heating rates from transient temperatures can be recovered through appropriate modelling of Duhamel superposition equation with the assumption of one-dimensional heat conduction [*Cook and Felderman, 1966*].

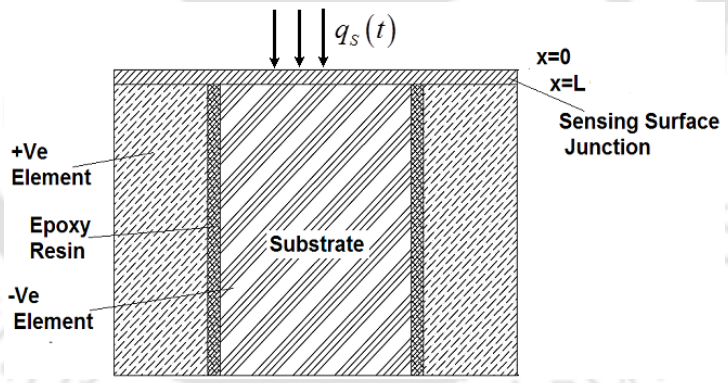

Fig. 3.7: Schematic of one-dimensional heat conduction model

Further, it is desired to base the surface heating rate from the transient temperature obtained at the surface of the thermal sensor as seen in *Fig. 3.7*. In addition, as explained through the numerical simulation in *section 3.2*, the thermal penetration distance during experimental run times is small compared to the linear dimension of the gauge, therefore, the system can be modelled by considering unsteady, linear conduction of heat in a one-dimensional semi-infinite solid [*Taler, 1996*].

$$\frac{\partial^2 T_1}{\partial x^2} = \left(\frac{\rho_1 c_1}{k_1}\right)\frac{\partial T_1}{\partial t} \tag{3.1}$$

$$\frac{\partial^2 T_2}{\partial x^2} = \left(\frac{\rho_2 c_2}{k_2}\right)\frac{\partial T_2}{\partial t} \tag{3.2}$$

The suffix 1 and 2 in *Eq. (3.1)* and *Eq. (3.2)* depicts the sensing surface and the substrate material of the heat flux gauges.

In order to have uniform initial conditions, if a heat load of $q_S(t)$ is applied instantly, the transient temperature of the coaxial sensor will be $T_S(t)$. Therefore, referring to *Fig (3.1)* initial and boundary condition can be written as follows:

Initial conditions: $t = 0$ *and* $0 \le x \le l_2;\ T(x,0) = T_{amb} = 300\,K$

$$\text{Top wall: } x = 0, t > 0; \dot{q}(0,t) = \dot{q}_S(t)$$

$$\text{Interface: } x = l_1, t > 0; \dot{q}_{S1} = \dot{q}_{S2} = \dot{q}_S \tag{3.3}$$

$$\text{and, } T_1 = T_2 = T_S(t)$$

$$\text{Bottom wall: } x = l_2, t > 0; T(l_2,t) = 300\,K$$

Now, solving the *Eq. (3.1)* and *Eq. (3.2)*, considering the thermal properties of the coaxial sensors as constant, the heat flux $\dot{q}_S(t)$ passing through the surface $x = l_1$ is calculated using the Duhamel's superposition integral as given below [*Taler, 1996; Carslaw and Jaeger, 1959*].

$$\dot{q}_S(t) = \frac{\beta}{\sqrt{\pi}}\int_0^t \frac{1}{\sqrt{t-\tau}}\frac{d\{T_s(\tau)\}}{dt}d\tau \ ;\ \beta = \sqrt{\rho c k} \tag{3.4}$$

There are certain assumptions for evaluating the heat flux from the governing equation as given in *Eq. (3.4)*. The assumptions hold good only if,

(i) the temperature measured by the sensing element/film is identical to the substrate surface temperature,

(ii) the substrate of the sensor does not undergo any lateral heat conduction and the heat is only conducted in the normal direction of the substrate, and

(iii) due to very small experiment time scale, the thermal properties of the substrate are treated as constant.

All the calorimetric gauges rely on transient surface temperature histories for prediction of surface heat flux by using *Eq. (3.4)*. In many instances, the "Thermal Product (TP)" values are generally assumed from theoretical estimates, which are either thermal properties of the substrate (in the case of thin film gauges) or the surface junction (for CSJTs). In any case, the accuracy of surface heat flux predications mainly depends on the correctness of TP values as well as the acquisition of transient surface histories from CSJTs.

For using the above-mentioned *Eq. (3.4)*, it is desirable to have a closed form solution of transient temperature data and the estimation of the value of the thermal product (β). In the present case, three different discretization techniques namely, linear fit, polynomial fit and cubic-spline based techniques have been employed to study further and estimate a closed form solution [*Sahoo and Peetala, 2010; Schultz and Jones, 1973*].

$$\dot{q}_L(t) = \frac{\beta}{\sqrt{\pi}}\left[\frac{T(t)}{\sqrt{t}} + \frac{1}{2}\int_0^t \frac{T(t)-T(\tau)}{(t-\tau)}\right]; \beta = \sqrt{\rho c k} \tag{3.5}$$

Since, the thickness of the surface junction is small and further the same heat flux must leave the substrate, so the surface heat flux (i.e. at x=0) can be assumed as $\dot{q}_L(t) = \dot{q}_S(t)$.

The *Eq. (3.5)* is the most effective form of temperature data analysis when the heat transfer rate is not constant. In many practical cases, the function in the *Eq. (3.5)* cannot be described by a simple expression; so, it is essential to perform numerical integration by discretizing the temperature data. The obtained temperature-time history out of the thermal sensors can be utilized to smoothen the data using three different curve fitting techniques namely, piecewise linear, least square and cubic spline.

The piecewise linear function is assumed for temperature if the surface temperature between successive times is assumed to vary linearly with time data [*Sahoo and Peetala 2011; Sahoo and Peetala, 2010; Cook and Felderman, 1966*].

$$\{T_2(\tau)\}_{linear} = T_2(t_{i-1}) + \frac{T_2(t_i)-T_2(t_{i-1})}{\Delta t}(\tau - t_{i-1}) \tag{3.6}$$

$$\text{Where, } \tau = t_i = i(t/n) = i\Delta t;\ i = 0,1,2,3,.....,n \tag{3.7}$$

The factor '*n'* is the number of temperature data points recorded by the acquisition system, during the experiment. The simplified expression for *Eq. (3.5)* is given as below;

$$\left\{\dot{q}_L(t)\right\}_{linear} = 2\sqrt{\frac{\rho_2 c_2 k_2}{\pi}}\sum_{i=1}^{n}\frac{T_2(t_i)-T_2(t_{i-1})}{(t_n-t_i)^{1/2}-(t_n-t_{i-1})^{1/2}} \tag{3.8}$$

Further, polynomial-based data discretization techniques can also be utilized for obtaining the heat flux:

$$\left\{T_2(t)\right\}_{poly} = A_0 + A_1 t + A_2 t^2 A_3 t^3 + \ldots\ldots\ldots\ldots\ldots + A_m t^m = \sum_{i=0}^{m} A_i t^i \tag{3.9}$$

Additionally, the heat flux value can be evaluated using the following equation

$$\left\{\dot{q}_L(t)\right\}_{poly} = 2\sqrt{\frac{\rho_2 c_2 k_2}{\pi}}\left(\left[A_1\sqrt{t} + \sum_{i=2}^{m} iA_i t^{((2i-1)/2)}\right]\left[1+\sum_{k=1}^{i-1}\frac{(-1)^k}{(2k+1)k!(i-1-k)!}\right]\right) \tag{3.10}$$

With the help of regression analysis and matrix inversion technique, the coefficients $A_0, A_1, A_2, A_3, \ldots\ldots\ldots\ldots A_m$ can be obtained using the relation as given by the researcher *Taler (1996).*

The analysis deals with polynomial fitting for estimation of surface temperature and heat flux. The major flaw of *Eq. (3.10)* lies in the accuracy of the polynomial fitting; as only, the calculation of high-order derivatives are allowed using the polynomial fitting of higher order, which may not reproduce the real data points, especially when taken into consideration that the time spread of the fitted data is large. In addition, one more technique is utilized to fit the experimental data points given by the cubic-spline method, the mathematical expression of which follows:

$$\begin{aligned}&\left\{T_S(\tau)\right\}_{spline} = a_{1,i} + a_{2,i}(\tau-\tau_i) + \frac{1}{2}a_{3,i}(\tau-\tau_i)^2 + \frac{1}{6}a_{4,i}(\tau-\tau_i)^3 \\ &\left(for\ \tau_i \le \tau \le \tau_{i+1}, i = 1,2,3,\ldots\ldots,M\right)\end{aligned} \tag{3.11}$$

where, $T_S(\tau)$ is the surface temperature history.

The constants in the *Eq. (3.11)* can be evaluated using the following expression:

$$a_{1,i} = T_2(\tau_i);\ a_{2,i} = T_2^{'}(\tau_i);\ a_{3,i} = T_3^{''}(\tau_i);\ a_{4,i} = T_4^{'''}(\tau_i) \tag{3.12}$$

The surface heat flux for the spline technique can be discretized in the following form:

$$\left\{\dot{q}_L(t)\right\}_{spline} = \left[2\sqrt{\frac{\rho_2 c_2 k_2}{\pi}} \sum_{i=1}^{M-1} \left\{ \begin{array}{l} V_i\left(P_i^{1/2} - R_i^{1/2}\right) - \\ \frac{W_i}{3}\left(P_i^{\frac{3}{2}} - R_i^{\frac{3}{2}}\right) + \\ \frac{a_{4,i}}{10}\left(P_i^{\frac{5}{2}} - R_i^{\frac{5}{2}}\right) \end{array} \right\} + 2\sqrt{\frac{\rho_2 c_2 k_2}{\pi}} \left(\begin{array}{l} V_M - P_M^{\frac{1}{2}} - \\ \frac{W_M}{3} P_M^{\frac{3}{2}} + \frac{a_{4,i}}{10} P_M^{\frac{5}{2}} \end{array} \right) \right] \sqrt{S_t} \qquad (3.13)$$

$$P_i = \tau_{M+1} - \tau_i;\ R_{i=}\tau_{M+1} - \tau_{1+i};\ F_i = a_{1,i} + a_{2,i}P_i + \frac{a_{3,i}}{2}P_i^2 + \frac{a_{4,i}}{6}P_i^3;\ V_i = \frac{dF_i}{d\tau_{M+1}};\ W_i = \frac{d^2F_i}{d\tau_{M+1}^2}; \qquad (3.14)$$

S_t = time scaling factor

A numerical algorithm is developed in-house using MATLAB® for discretization of temperature data (*Eq. (3.11)*) and subsequent computation of surface heat flux using the numerical algorithm (*Eq. (3.13)*) from the known values of thermal properties [*Sahoo and Peetala, 2010*].

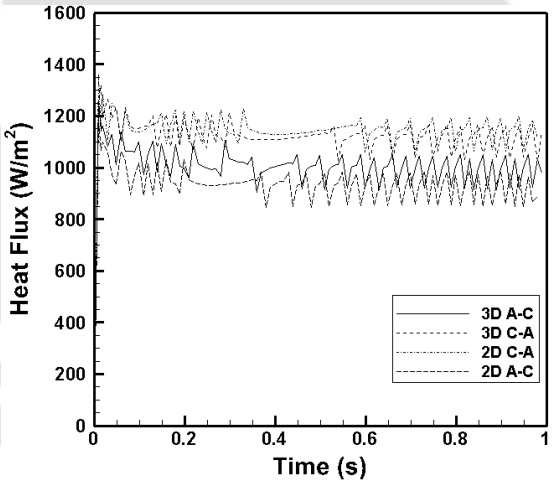

Fig. 3.8: Variation of heat flux extracted from the CFD simulation using the in-house developed code

Furthermore, the obtained temperature signal from the CFD simulation as shown in *section 3.2*, i.e. for both 2-D and 3-D geometry under a step input time of 1 s, are processed through the in-house code for checking the validity of the ANSYS model. A cubic spline discretization technique as per *Eq. (3.11)*, were considered to discretize the present set of data (*Fig. 3.8*). The results produced a heat flux value, which is approximately equal to 1000 W/m^2, same as the input value given to the CFD with an uncertainty of ±5 %. The correctness of simulation is thus validated from the obtained heat flux histories, which is in close approximation to the given input. In

nutshell, it validates the assumption of choosing the dimension of the coaxial surface junction thermocouple to be appropriate. For all the fabrication process, a length of 10 mm is considered for the thermal probe.

3.4 Design of Coaxial Surface Junction Thermocouple

Once the numerical validation and modelling of the sensor have been carried out successfully, the sensor is processed for designing with appropriate dimension. *Bendersky (1953)* initially proposed the concept of the coaxial thermocouple, which is nothing but a small wire coated with a thin layer of aluminium oxide insulation. A coaxial surface junction thermocouple works on the principle that when two dissimilar metals joined, an emf is generated [*Seebeck effect*]. The design process involves two major steps:

- Selection of materials.
- Of surface junction Formation.

3.4.1 Selection of Materials

There are few factors that need to be considered while selecting the material combinations for thermocouples, which are justified as follows:

1. A sufficiently higher **electromotive force** should be produced with the connection of the combination of the thermocouple materials, resulting in the correctness of measurement.
2. A **fast response** should be ensured with the combination of the materials. The result ensures that there is sufficient emf generated with every degree change in temperature.
3. It should ensure higher **stability** over a specified range of temperature.
4. The material should be resistant to **oxidation**, which is essential for material utilized at a higher temperature.

On the basis of above factors for K-type thermocouple, Chromel-Alumel materials are used, Chromel-Constantan are used for E-type thermocouple, Copper-Constantan for T-type, Iron-Constantan for J-type etc. and so on.

Although nickel is the major constituent of type-K elements, there are significant differences in the thermophysical properties of Chromel and Alumel materials. The density of both

the material are almost equal, but Alumel has higher thermal conductivity than Chromel. Chromel is considered as positive material and Alumel is considered as negative one, but surface junction thermocouples can be formed with an inner wire of either the positive or negative thermocouple element, and an outer annulus of the other thermocouple material.

Table 3.1: Properties of thermocouple materials [*Caldwell, 1962*]

Material	Density (kg/m^3)	Specific heat (J/kg-K)	Thermal Conductivity (W/m-K)	Thermal Product ($Jm^{-2}s^{-1/2}K^{-1}$)
Chromel	8730	447.83	17.846	8352.83
Alumel	8600	523.336	27.463	11117.66
Teflon	2250	1400	0.25	887.411
Constantan	8900	390	19.5	8227.1
Copper	8960	386	401	37684.765
Iron	7870	450	80.4	16874.139
Nicrosil	8530	460.2	13	7143.638
Nisil	8585	500	23	9936.17

Table 3.2: Properties of Coaxial Thermocouple Sensors [*Caldwell, 1962*]

Materials	Types	Constituents	Temperature Range (°C)	Density (kg/m^3)	Specific heat (J/kg-K)	Thermal Conductivity (W/m-K)	Theoretical Thermal Product (β_t) ($Jm^{-2}s^{-1/2}K^{-1}$)
Chromel	K	Ni: 89-90 %, Cr: 9-9.5 %, Si: up to 0.5 %, Fe: 0.02-0.65 %, Mn: 0.01-0.8 %	-200 to 1350	8665	486	22.65	9735
Alumel		Ni: 94-96 %, Si: 1-1.5 %, Al: 1.3-2.5 %, Mn: 1.8-3.25 %					
Chromel	E	Ni: 89-90 %, Cr: 9-9.5 %, Si: up to 0.5 %, Fe: 0.02-0.65 %, Mn: 0.01-0.8 %	-150 to 750	8815	419	18.67	8670
Constantan		Cu: 55 %, Ni: 45 %					
Copper	T	-	-200 to 350	8930	388	210.25	11600
Constantan		Cu: 55 %, Ni: 45 %					
Iron	J	-	-40 to 750	8385	420	49.95	13700
Constantan		Cu: 55 %, Ni: 45 %					

For E-type thermocouple, Chromel is the positive material and Constantan is the inner material i.e. negative. An insulator separates the two thermocouple elements from each other, thus not allowing any heat to transfer from one element to another, maintaining high strength and toughness. Teflon/Araldite is used as an insulator as its thermal conductivity is very low (lower is the value of 'k', better is the insulation). *Table 3.1* gives the insight to the typical properties of all the thermocouple materials. Further, *Table 3.2* highlights the essential properties of the coaxial thermal sensors material [*Mohammed et al., 2007*].

3.4.2 Surface Junction Formation

For measurement of accurate temperature, thermocouples are best-suited techniques used universally for many years. It has the capability of measuring/operating over a wide range of temperature and are reasonably cheap. The quality of the junction is in-turn the most important factor that determines the performance of the thermocouple such as *accuracy*, *repeatability* and *response time*, respectively. The conventional thermocouple, mostly suited for steady state application, is the one in which two dissimilar metals are joined together to form a junction; the type of the thermocouple is classified based on the materials used and on the range of applications such as K, E, T, J, N-types etc. Furthermore, coaxial surface junction thermocouple is the one in which, one thermocouple element is swaged over the other with an electrical insulation in between that is, it is a surface junction, not a point junction (*Fig. 3.9*). The thin junction required for quick sensing is obtained by slightly abrading one thermocouple element over the other with a scalpel blade/abrasive grit and this abrasion results in plastic deformation of one material over the other. The greater care needs to be taken for the preparation of the surface, as junction preparation is more of an art rather than a process. Being coaxial, the thermal sensors can be fitted on any surface with ease.

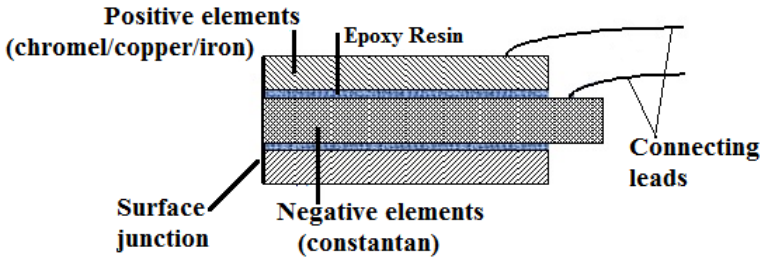

Fig. 3.9: Schematic representation of surface junction probes

3.5 Summary

The detailed numerical simulation, heat flux modelling and thereafter design methodology of coaxial surface junction thermocouple has been presented in this chapter. Firstly, a complete analogy based on numerical simulation has been done to find the required dimension of the thermal sensor for which the semi-infinite assumptions holds good. The study has been carried out to simulate the thermal penetration depth for the thermal probe in 2-dimensional as well as 3-dimensional models. The study revealed that there was no significant variation in the lateral direction and a linear decrement in the temperature has been observed along the length of the sensor. Once the numerical simulations are done and semi-infinite theory is validated, the thermal probe can be modelled as a case of unsteady, linear conduction of heat in a one-dimensional semi-infinite solid. Three curve fitting is followed in the present case namely, linear fitting, polynomial fitting and cubic-spline fitting in order to obtain a closed form solution. An in-house of numerical code using MATLAB® has been developed, based on the discretization technique, and subsequently, employed to estimate the heat flux. The temperature-time history obtained from the numerical were discretized using the cubic-spline fitting with constant thermal properties, to obtain heat flux in order to validate the given input heat flux during CFD. Once, validating the design module of the thermal sensor, the step is taken forward to follow a certain methodology to design the coaxial thermal probe. The proper prediction of temporal nature of heat load and an accurate quantification of heat flux is the major requirement for a typical thermal probe. The design of thermal probe basically follows some important criteria such as selection of proper material, surface junction preparation, and appropriate epoxy resin. The design of the coaxial thermal sensor involves swaging of one thermal element over the other. It basically involves two dissimilar metals which are joined together to form a junction, the junction when exposed to a certain temperature gradient, a voltage is generated (Seebeck Effect).

CHAPTER 4

Fabrication and Calibration of Coaxial Surface Junction Thermocouple

Compendium:

Coaxial surface junction thermocouples have fast response characteristics and are the most cost effective thermal sensors for dynamic temperature measurements as compared to its counterparts. They can be easily fabricated in the laboratory based on the requirements of temperature ranges and utility with respect to practical applications. Numerical, analytical modelling with focus on the design of the thermal sensor of coaxial type includes the work of previous chapter. For usage of these probes in short duration experiments, a cylindrical probe of 10 mm long and 3.25 mm diameter is adequate for which there is minimal penetration of heat in lateral direction. Thus, one-dimensional heat conduction theory with semi-infinite substrate can be applied for the probe for short duration experiments up to 1 s. This chapter emphasizes on the comprehensive and systematic fabrication methodology for the coaxial surface junction thermocouple along with its characterization to qualitatively account for the plastic deformation that is happening at the surface of the thermocouple. In order to effectively use surface junction probes in real time applications, the experimental calibration in terms of temperature and heat flux is very essential. Being the resistance temperature detectors (RTD), the voltage-temperature relationship (preferably linear) is obtained through a parameter known as "sensitivity". Further, the probes must predict actual transient heat flux from temperature histories when flush mounted on the surfaces during real time experiments. Hence, the probes must be calibrated for known heat fluxes. This chapter includes the experimental calibration techniques for all the fabricated sensors. The static calibration setup uses a hot temperature bath for which experimental data are obtained and subsequently linearity of voltage change with respect to the temperature variation are observed for the thermocouple materials used during sensor fabrication. Subsequently, the transient heat flux is estimated from the temperature history by using one-dimensional heat conduction modelling. The dynamic calibration of the thermal probe involves exposure of the sensor with a known heat load typically achieved by means of a laser source. These two experimental calibration techniques are the major focus of this chapter. Before using the gauge directly in the impulse facility, it is desirable to calibrate the gauges in the laboratory using similar nature of known heat load, in order to account for the errors estimated in the ground- based experiments.

4.1 Introduction

Many transient surface temperature applications such as aerodynamic vehicles, gun barrel, an internal combustion engine (continuous type), gas turbines etc., needs a fast response thermal probe as it always remains a challenge to obtain highly accurate data when it comes to accomplishing flight mission. The generation of data in short duration facilities such as shock tunnel becomes a task as the real gas effects are simulated for re-entry or aerothermal studies, which caters the need to have heat flux sensors as it is of paramount interest for the designing of the thermal protection system. Now, considering the case of the internal combustion engine, the measurement of heat flux/transient temperature plays an important role considering the design of combustion chamber, estimating the performance, efficiency, engine emission characteristics helping in designing the cooling requirement of a particular engine.

The heat flux measurement is a derived quantity. When the short duration transient temperature is measured, they are converted into the heat flux using one-dimensional semi-infinite heat conduction equation [*Schultz and Jones, 1973*]. The semi-infinite theory depicts the fact that acquired heat flux does not influence the temperature at the rear end of the substrate. However, there exist many contemporary techniques, which involves transient surface temperature measurement namely, temperature sensitive paints (TSP) [*Nagai et al., 2008; Liu and Sullivan, 2005; Nakakita et al., 2003*]**,** platinum thin film gauges [*[1]Sarma et al., 2016; Kumar et al., 2011*], null point calorimeter [*Kidd 1992*], thin skin thermocouple [*Kidd, 1985*], coaxial thermocouples [*Desikan et al., 2016; Irimpan et al., 2015; Kumar et al., 2013; Menezes and Bhat, 2010; Mohammed et al., 2008; Sanderson and Sturtevant, 2002*]. Additionally, there are non-intrusive techniques involved, but they are still in its earlier stages, which requires an incommodious calibration procedure [*Merski, 1999*]. Each of the techniques holds certain pros and cons. Thin-film gauges have a higher response, but the sensor encounters high shear, which leads to frequent replacement of the same. Nevertheless, coaxial surface junction thermocouples are easy to fabricate, are lesser sensitive compared with its counterpart TFG, but have high resistance to shear. Being miniature in size, they could be mounted on any surface. If the thermal sensor can be fabricated in-house, then in turn, it makes the sensor cost effective.

The present investigation revolves around describing the technique and fabricating the fast response thermal probe namely, E, T, J and K-type respectively, considering all the desired

parameter as explained in *Chapter 3*. Further, the CSJT are characterized using EDX technique to justify the plastic deformation that happens during the formation of the junction at the thermocouple surface. Lastly, the fabricated thermal sensors are calibrated using two methods namely, constant temperature source (static calibration) and constant heat flux mode (dynamic calibration). For short duration impulse facilities, the dynamic based calibration is not very well established. Before utilizing the sensor on the surface of interest, it is essential to calibrate the thermal probe with the similar nature of heat load in order to account for the error in the case of the actual experiment. The method includes exposing the thermal probe to a known input wattage using laser source in the range of 1.5-6 W respectively.

4.2 Fabrication of Coaxial Thermal Sensors

Since many years, conventional thermocouples are best-suited universal techniques, for measuring the steady-state temperatures and have point junction. In contrast, the CSJTs have surface junction where one thermocouple element is swaged over the other with an electrical insulation in between them. The thin surface junction over the sensor is achieved by abrading one thermocouple element over the other using a scalpel blade. The micro-scale plastic deformation of one material over the other helps for quick response during short duration measurements. In the present study, four different types of coaxial thermal sensors are fabricated namely E, J, T and K-types respectively. The reason for choosing the mentioned type of thermal probe is purely based on their sensitivity, availability and to comprehensively study a comparative assessment in a different heating environment of interest. Considering, the fabrication methodology of E-type CSJT, it includes chromel and constantan wires of diameters *3.25* mm and *0.813* mm, respectively (*Fig. 4.1-a*). As numerically verified in the previous chapter, an appropriate length of about 10 mm of the outer material (chromel) is considered prior to the assembly of the sensor while a slightly higher length is taken for the inner material (constantan), to keep the overall length of the sensor as small as possible. In order to avoid the electrical contact between the two thermocouple elements, a thin layer of epoxy resin *(approximately 0.0935 mm)* is put on the entire inner material. In the chromel wire, a hole of 1 mm is drilled with the help of a drill bit and the constantan wire with a thin layer of epoxy resin is inserted, so as to tightly fix the assembly. Once the assembly is fixed, the junction on the surface is formed with the help of a scalpel blade, by slightly abrading constantan element over the chromel material. Although the process can also be achieved by using abrasive paper of

various grit sizes; but the present study includes scalpel blade for all the junction preparation. Thus, it forms a micro junction of 20–24 μm thickness of both the metals only on the surface. A qualitative information about this micro junction is noticed during EDX analysis highlighted in subsequent sections in this Chapter. Both the surface junction thickness with very low thermal mass and plastic deformation characteristics are in line with literature findings [*Menezes and Bhat, 2010; Mohammed et al., 2008*]. The resistance of the sensing surface is continuously monitored with the help of multimeter, which typically falls in the order of 1 Ω. The quantitative information of junction thickness and the resistance ensure the plastic deformation with very low thermal mass and inertia [*Irimpan et al., 2015; Menezes and Bhat, 2010; Mohammed et al., 2008*]. Towards the end of fabrication, the connecting leads (Aluminium alloy wire coated with Teflon) are fitted on the thermocouple element, which can be achieved by either of the ways that is through spot welding or by soldering the lead.

The spot welding method is preferred in the present case (evaluated through experiments) as it gives more rigidity and bonding of lead wires on the thermocouple material. Finally, it is wrapped with Teflon for protecting the connections from any thermal penetration, which is essential for a transient heat flux gauges. Similar fabrication procedure has been followed for other types of thermal sensors namely, J (*iron-constantan*), T (*copper-constantan*) and K (*chromel-alumel*)-types respectively. The dimension of inner and outer material remains same for all the cases with an exception for J–type CSJT, which includes outer material iron of *2.5* mm diameter. Further, in case of K-type CSJT inner material (alumel) of diameter *0.813* mm is chosen instead of constantan. *Fabrication of coaxial thermocouple of T-type is a real challenge as copper is highly sensitive material; drilling a hole in the copper has to be done with real care as a large amount of heat is generated during the drilling process which leads to the breakage of the drill bit. Secondly, connecting the leads wire to the T-type surface is another challenge.* For the case of copper as its highly conducting, so soldering becomes a tough task, secondly, the spot welding set-up is capable of producing 200 J of energy, which is lesser for the case of spot welding on the T-type material as it requires 1000 J of energy for creating a spot weld. For the present case, soldering method has been employed in case of T-type for connection of lead wires. The fabrication of CSJT is an art rather than a method. *Figures 4.1(a-d)* show the fabricated coaxial thermal sensors along with the schematic of the thermocouple assembly.

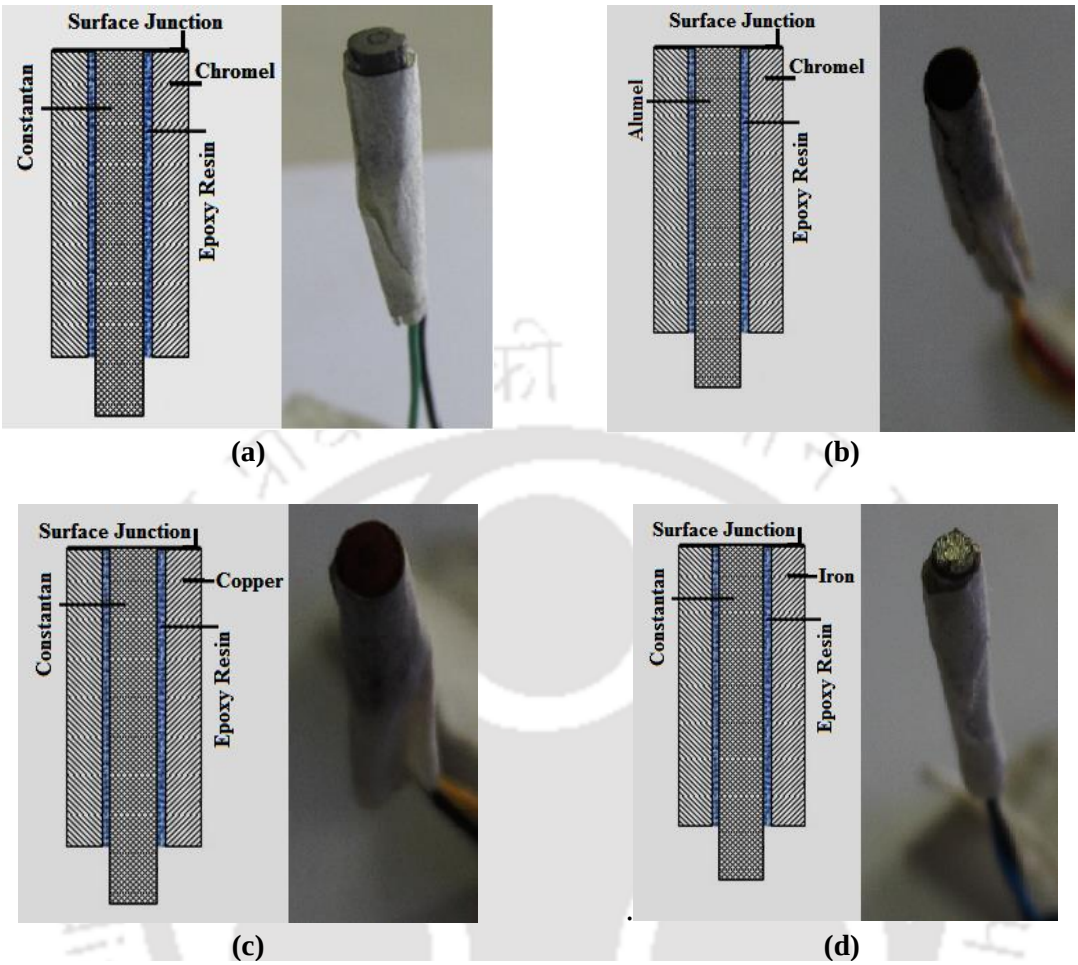

Fig. 4.1: Schematic and pictorial representation of the in-house fabricated CSJT namely, (a) E-type, (b) K-type, (c) T-type, (d) J-type

4.3 Characterization of Coaxial Surface Junction Thermocouple

4.3.1 Electron Discharge X-ray (EDX) methodology

EDX is an analytical technique utilized for chemical characterization and elemental analysis of a sample. The method depends on the use of X-ray excitation/spectrum emitted by a solid sample, which is bombarded with a focused beam of electrons. Approximately almost 95% of the solid material is crystalline, which helps one to obtain the diffraction pattern owing to the interaction of X-ray with the crystalline structure. A unique pattern is observed for a particular crystalline structure, which gives the advantage of using a mixture of substance, as it would result in same pattern/peak irrespective of the mixture. A diffraction pattern containing the information about the atomic arrangement within the crystal is obtained with the scattering of X-rays from the atoms [*Fultz and Howe, 2008*]. The spacing $'d'$ between two atomic planes is calculated using the Bragg's

law as seen *Fig. 4.2*; where n is an integer, 'λ'is the incident electron beam wavelength and $'\theta'$ is the Bragg's angle.

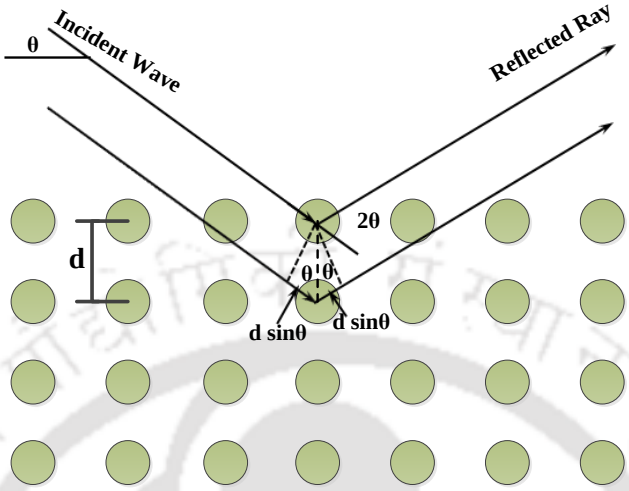

Bragg's Law $n\lambda = 2d \sin\theta$

Fig. 4.2: Schematic of X-ray diffraction mechanism

4.3.2 EDX on test sample

A test sample is prepared to study the deformation of thermocouple material created at the junction of the thermal sensor. The XRD study is intended to qualitatively estimate the formation of surface junction created because of the abrasion process as explained in *section 4.1*. It is believed that a junction at the surface of the thermal sensor has been created because of the deformation of one thermocouple over the other. A three set of sample has been prepared for the present investigation namely, chromel material, constantan material, prepared thermal sensor [*Figs. 4.3(a-b)*].

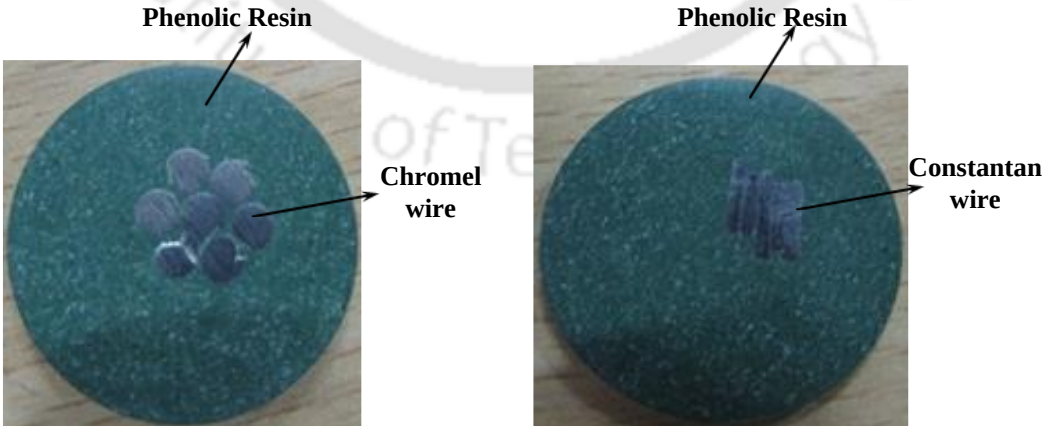

(a) **(b)**

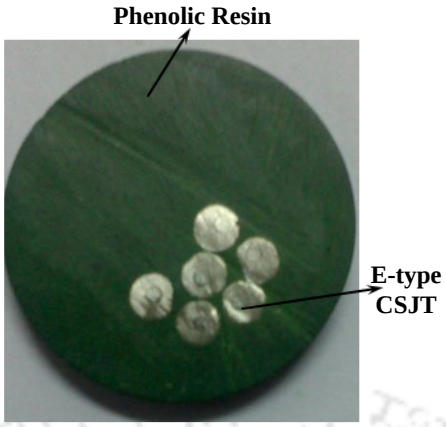

(c)

Fig. 4.3: Mould created for the experiment using phenolic resin (a) chromel wire, (b) constantan wire, and (c) E-type CSJT

The composition of the chromel material is roughly 90 % Nickel, 10 % Chromium. Constantan material contains 55 % Copper, 45 % Nickel roughly [*Caldwell, 1962*]. Initially, a small length (approx 3 mm) of chromel and constantan material are considered. A hot moulding press is utilized to create a mould with phenolic resin as seen in *Figs. 4.3(a-b)*. An E-type CSJT has been chosen to carry out the study, for which mould has been created in a similar manner. The fabrication process for E-type (*6 nos*) is similar to as explained in *section 4.1*, except that the overall length of the sensor is not more than 4 mm. Special care needs to be taken for the formation of the surface junction as the sensor size is pretty small.

Moreover, the connectivity between the two-thermocouple material is constantly monitored using the multimeter. The EDX set-up has a limitation such that it can hold a specimen not more than 3 mm in thickness.

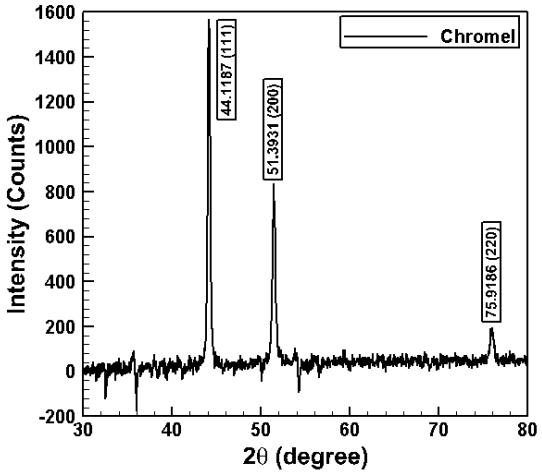

(a)

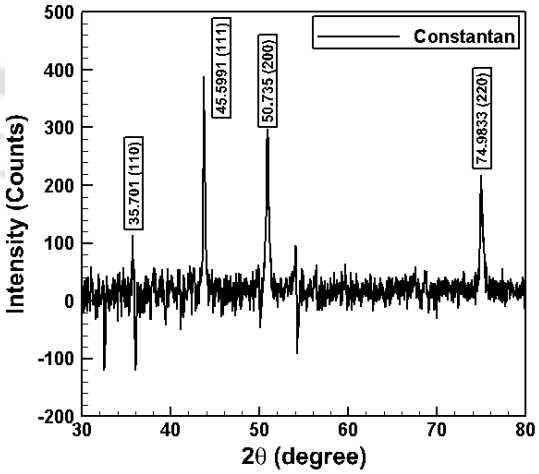

(b)

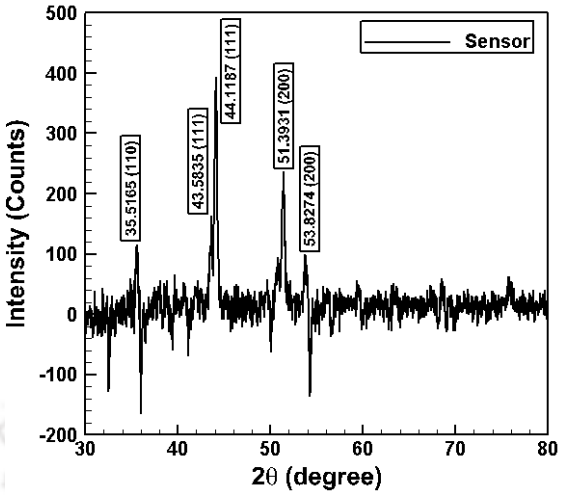

(c)

Fig. 4.4: XRD pattern for (a) Chromel wire, (b) Constantan wire, and (c) E-type sensor

As the EDX specimen has a limitation of holding a material of thickness not more 3 mm, the sensor length is reduced by polishing the surface till it reaches 3 mm approx.

All the material surface are polished to get a smoothen surface using the polishing machine. The test is performed on X-ray Diffractometer (XRD) with Cu-Kα radiation of wavelength 1.54059 $\overset{o}{A}$ (*Make: PANalytical-XPERT*). The system has generated a voltage of 40 kV and current of 30 mA. The XRD spectrum is acquired in a 2θ range of 30 to 80º using a scan step size of 0.03º with a time per step of 0.5 s.

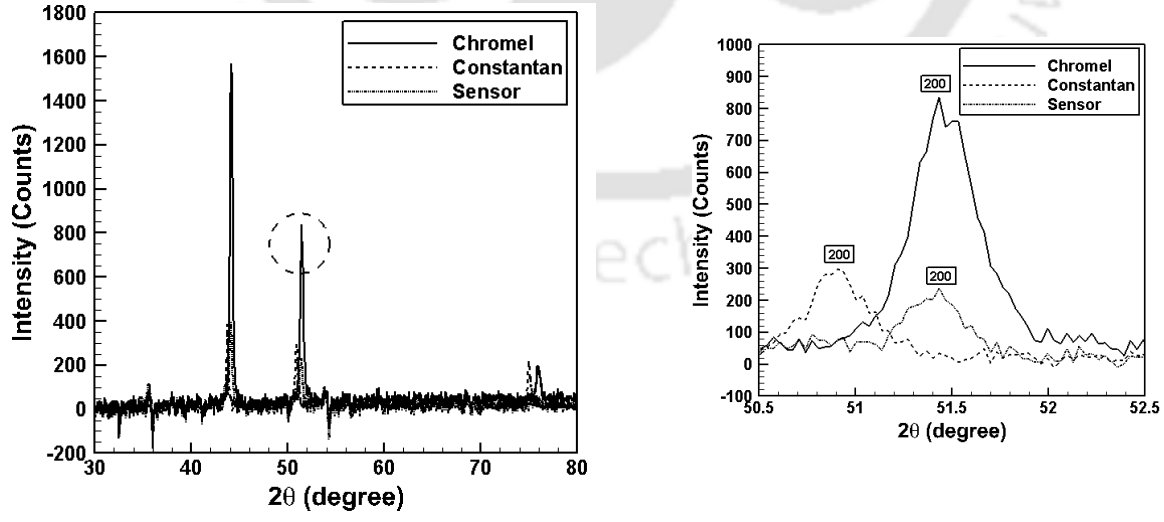

(a) **(b)**

Fig. 4.5: Comparative plot highlighting the XRD pattern

Before getting the actual result, a sample test run is taken to get the XRD of the phenolic resin, so that the resin effect is nullified while taking the actual sample test. *Figures 4.4(a-c)* show the XRD pattern of Chromel wire, Constantan wire and E-type CSJT respectively. The selection rule for checking the '*hkl*' value has been taken from the literature [*Fultz and Howe, 2008*]. Clearly, it can be observed from the graph that there is a certain change in the peak value as captured in case of sensor sample, when compared with individual thermocouple material. *Figure 4.5* shows the comparative plot of the sample, which successfully justifies the plastic deformation that is taking place due to abrasion of one material over the other.

4.4 Calibration of Thermal Sensors

4.4.1 Constant source of temperature

As discussed, the coaxial surface junction thermocouples are the most widely used thermal sensor for measurement and control. The CSJT can generate the voltage signals without any external current source i.e., it is an *active* sensor, whereas the thin-film sensors require an external current source to actuate it i.e., called *passive* sensors. Resistance temperature detector (RTD), industrial type sensors available are usually encased in probes or in plugs; they come in a variety of shapes and sizes. Most commercial sensors available tend to be quite large and have a relatively slow response time. In general, the commercial sensors are mostly used to monitor temperature rise or heat transfer over a relatively long period of time. The application involving such cases normally does not require elaboration of specification involving response time, sensitivity and self- heating data. In turn, the manufacturers do not provide information for sensors to qualify for application involving high speed research. In addition, all these factors restrict commercial sensors to be unstable for application involving gas dynamics research. The custom built sensors, however, holds the advantage such that it can be contoured to the shape of the test model; but the cost involved for such sensors are high and the sensors are mostly destroyed only by few shots. It will be very expensive and rather impractical to replace such thermal sensors. In this regard, construction of handmade sensor and the calibration of such sensors are very much essential. The CSJTs produce a voltage signal corresponding to the temperature change in the medium. Typically, this variation is linear and slope of the ''voltage-temperature" graph is defined as ''sensitivity" of the thermocouple (*S*). By static calibration, one intends to find the sensitivity of the thermal sensor and in turn the precession and accuracy of the measuring device. The sensitivity of the

thermocouple is the most important parameter responsible to link the voltage variation with the temperature change of the medium. The study of the variation in the output with respect to the inputs is known as the ***Sensitivity***. It depends on materials temperature and crystal structure.

In general, the typical sensitivity and the significance of different types of conventional thermocouples have been listed as follows:

a) Chromel- Constantan (*E-type*): It has a sensitivity of about *68* µV/°C. It is mostly suited for cryogenic uses and it is non-magnetic with a temperature range of -50 °C to 740 °C.

b) Chromel-Alumel (*K-type*): It is a general-purpose sensor, which has a sensitivity of about *41* µV/°C. It operates in the very wide range of temperature -200 °C to 1350 °C.

c) Copper-Constantan (*T-type*): It is best suited for working in the temperature range of -200 °C to 350 °C. It has a sensitivity of around *43* µV/°C.

d) Iron-Constantan (*J-type*): It operates in the temperature range of -40 °C to 750 °C. It has a sensitivity of about *50* µV/°C. The restricted range in temperature can be associated with the Curie point of iron, which is 780 °C.

e) Nicrosil-Nisil (*N-type*): It has a sensitivity of about *39* µV/°C. It has an operating range from -270 °C to 1300 °C. Due to its stability and oxidation resistance, it is suitable for wide range of operation. It is suited for application such as a nuclear reactor.

If ΔT is the difference in temperature and ΔV is the thermoelectric voltage between the two ends of the material, then the sensitivity of the material can be calculated as,

$$Sensitivity, S = \frac{\Delta V}{\Delta T} \tag{4.1}$$

The calibration of the thermocouple is performed by an “oil-bath based experimental technique” that provides gradual step rise in temperature [*Kumar and Sahoo, 2013*]. The calibration rather the experiment is mainly performed to check the linearity between the change in voltage signals with the corresponding changes in temperature across the sensing the material during up-scaling and down-scaling process i.e., during heating and cooling process. Before the sensor is fabricated, the bare wire (locally purchased) must be calibrated, to ascertain the sensitivity of the sensor to be

fabricated. The calibration of the sensor prior to fabrication is essential as the sensitivity of the thermocouple depends on the material property, not on the formation of the surface junction. If we consider the calibration of the E-type thermocouple, bare chromel wire of 3.25 mm and constantan wire of 0.813 mm, having 1 m in length is taken. A small hole is drilled at the top of the chromel wire and the constantan is press-fitted inside the drilled chromel wire so that the connectivity is maintained. The setup consists of a *heater*, an *oil-bath*, a *scientific thermometer*, two *beakers* and *Data Acquisition System* (DAS). One end of the thermocouple wire is inserted in the beaker and the other end is kept inside the ice-bath so as to maintain the reference junction temperature in this case as 0 °C, and further, it is connected to the DAS, for acquiring the change in voltage. In this method, hot air is produced in a beaker (where the thermocouple is placed), by heating oil kept in another container as shown in *Fig 4.6*. The thermocouple experiences convective heating through the hot air inside the beaker placed in the oil bath. The oil is heated using a constant temperature water bath. Further, a scientific thermometer is mounted in the beaker along with the thermocouple to manually record the temperature of the air during heating and natural cooling. Sufficient care is taken to minimize the heat losses from various other sources. DAS (Agilent 34970A), having a sampling frequency of 2 GHz, is used to monitor the change in voltage across the sensor for corresponding changes in temperature. The air is heated from 30 °C to 75 °C with a step change of 5 °C and the temperature, as well as the voltage change, are recorded. The process is repeated during cooling with the same value of step change in temperature. Before noting the final readings, the bath temperatures are monitored at several locations to ensure the uniform temperature gradient in the entire region of hot air. In the present experiment, the entire procedure was repeated three times in order to check the repeatability of the thermocouple.

The calibration result consists of three set of readings, taken both for heating and cooling process and the average value is plotted thereafter as shown in *Fig 4.7*, which is for E, T, J, and K-types thermocouples respectively. From the graph, it is quite evident that the calibrated thermocouple wires for different types have good repeatability. The graph provides a satisfactory linear variation of voltage with the change in temperature. The calibrated thermocouples namely, E, T, J and K-types respectively as observed have a Sensitivity of *58.96* µV/°C, *28.47* µV/°C, *43.82* µV/°C and *36.02* µV/°C respectively. The specifications of the instruments used for the calibration process is elaborated in *Appendix C*.

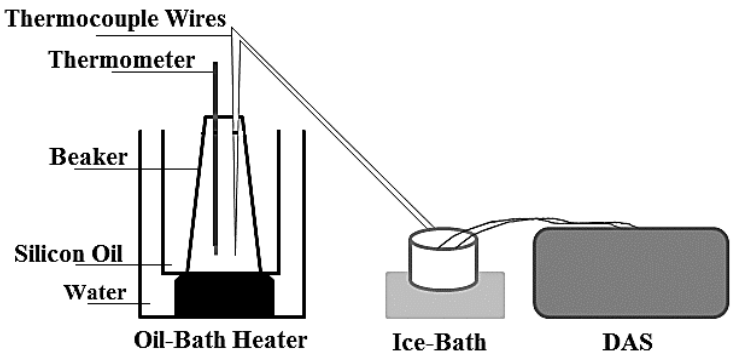

Fig. 4.6: Schematic of oil-bath based calibration set-up with known temperature

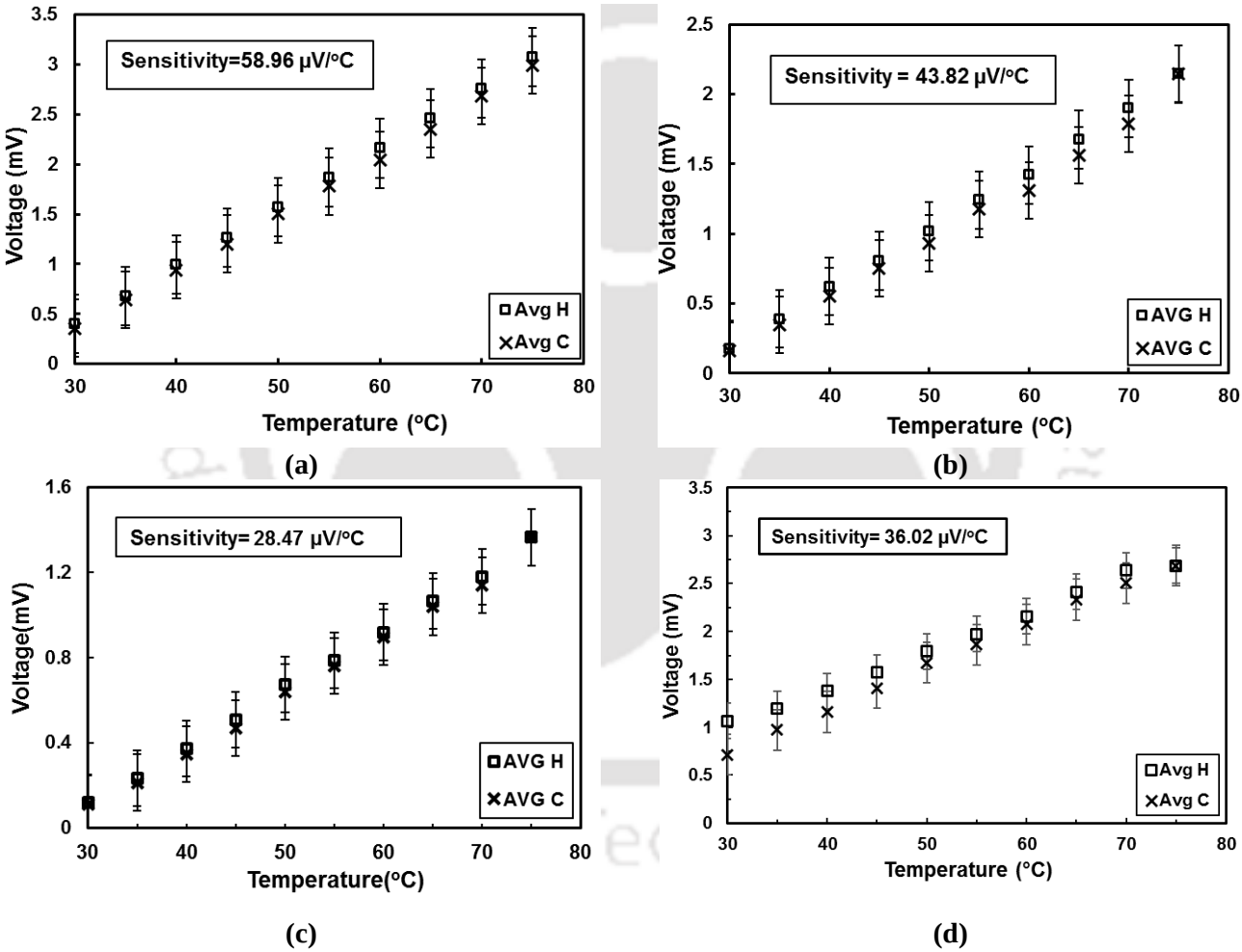

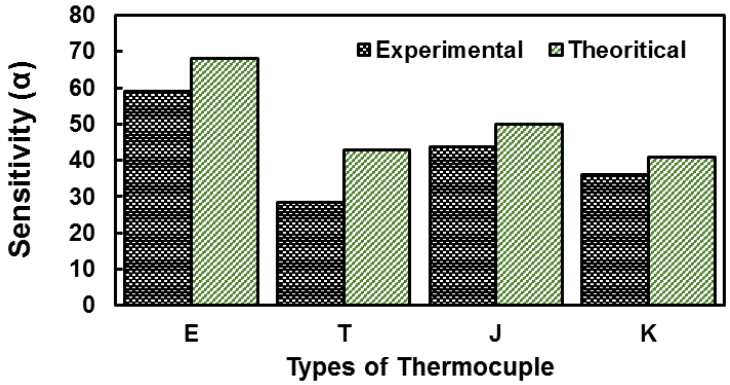

(e)

Fig. 4.7: Calibration graph showing variation of voltage with temperature of (a) E-type, (b) J-type, (c) T-type, and (d) K-Type CSJTs; (e) the bar chart showing the comparison of sensitivity value

Table 4.1: Comparison of sensitivity between in-house developed coaxial surface junction thermocouple and the conventional thermocouple

Sl. No.	Types of Thermocouple	Experimental Sensitivity of CSJT (μV/°C)	Ideal Sensitivity of thermocouple (μV/°C) [*ASTM, 1993*]
1.	E-type	58.96	68
2.	T-type	28.47	43
3.	J-type	43.82	50
4.	K-type	36.02	41

4.4.2 Constant source of heat flux

For short duration impulse facilities, the dynamical based calibration is not very well established. Generally, the model experiences step load for a very short duration of timescale. Before utilizing the sensor in the impulse facilities, it is essential to calibrate the thermal probe with the similar nature of heat load in order to account for the error in the case of the actual experiment. The method includes exposing the thermal probe to a known input wattage using laser source. Further, the surface temperature history is obtained and compared with the theoretical estimate. The present study includes laser-based calibration study exposing the fabricated thermal sensors to a known wattage in the range of 1.5-6 W respectively with a time interval of 40 s. The obtained temperature history from the sensor is utilized to obtain the input wattage using various analytical techniques. The current thesis work is focussed on the radiation-based calibration of various in-house fabricated coaxial surface junction thermocouple namely, E, J and T-type respectively.

4.4.2.1 Radiation Based Calibration

Most of the ground-based impulse facilities such as shock tube/shock tunnels/ expansion tubes are utilized to simulate the near realistic flight condition in laboratory scale where the experimental timescale is of the order of few milliseconds or even lesser than that [*Srinivasan et al., 2016; Irimpan et al., 2015; Jagadeesh et al., 2000*]. In general, the convective heating rate is studied by mounting the thermal sensors on the aerodynamic model, where the model experiences sudden heating load. In order to simulate the thermal sensor for such flow conditions, the sensors are calibrated by applying similar step load condition on the sensor. *Figure 4.8* shows the schematic of the experimental set-up, which includes a continuous wave (CW) laser source (*Make: Coherent, USA*), CSJT mounted on the stand, thermocouple amplifier and a PC-based data acquisition system.

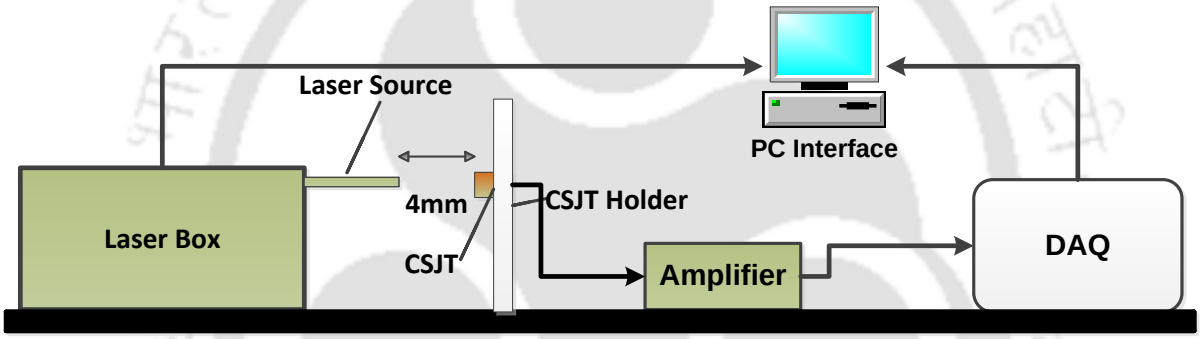

Fig. 4.8: Schematic of the Laser-based calibration set-up for conducting the radiation based calibration for coaxial thermocouple

The thermal sensor and the laser source are kept 4 mm apart. The laser has been tuned for various input wattage of 1.5, 3, 4 and 6 W respectively. Three different types of coaxial surface junction thermocouple namely, E, J and K-type have been considered for the desired experiments. A step heat load is applied to the sensing surface of the sensor by projecting the laser source on to the sensing surface. The experiments have been conducted by exposing all the sensors to different input wattage of the laser source. The change in voltage has been captured as the output for the all the sensors (*Figs. 4.9-a, 4.10-a,* and *4.11-a*). The sensor responded well to the input heat load; however, it is observed that the signal from the J-type CSJT kept on rising considering the other types of CSJT. The temperature-time history of the obtained voltage signal has been plotted using the sensitivity of the thermal probe (*Figs. 4.9-b, 4.10-b,* and *4.11-b*). Considering the thermal

properties of the coaxial sensors as constant, the heat flux $q_S(t)$ passing through the surface is calculated using the Duhamel's superposition integral as given below [*Taler, 1996*].

$$q_s(t) = \frac{\beta}{\sqrt{\pi}} \int_0^t \frac{1}{\sqrt{t-\tau}} \frac{d\{T_s(\tau)\}}{dt} d\tau \;;\; \beta = \sqrt{\rho c k} \tag{4.2}$$

For using the above-mentioned *Eq. (4.2)*, it is desirable to have an appropriate closed form solution of transient temperature data and the estimation of the value of the thermal product (β). As a qualitative measure, the thermal product value is considered from literature as cited in *Table 5.2* of *Chapter 5*. *Eq. (3.13)* is considered to estimate the surface heat flux from the obtained temperature-time history. As described in *Chapter 3*, an in-house developed MATLAB® code has

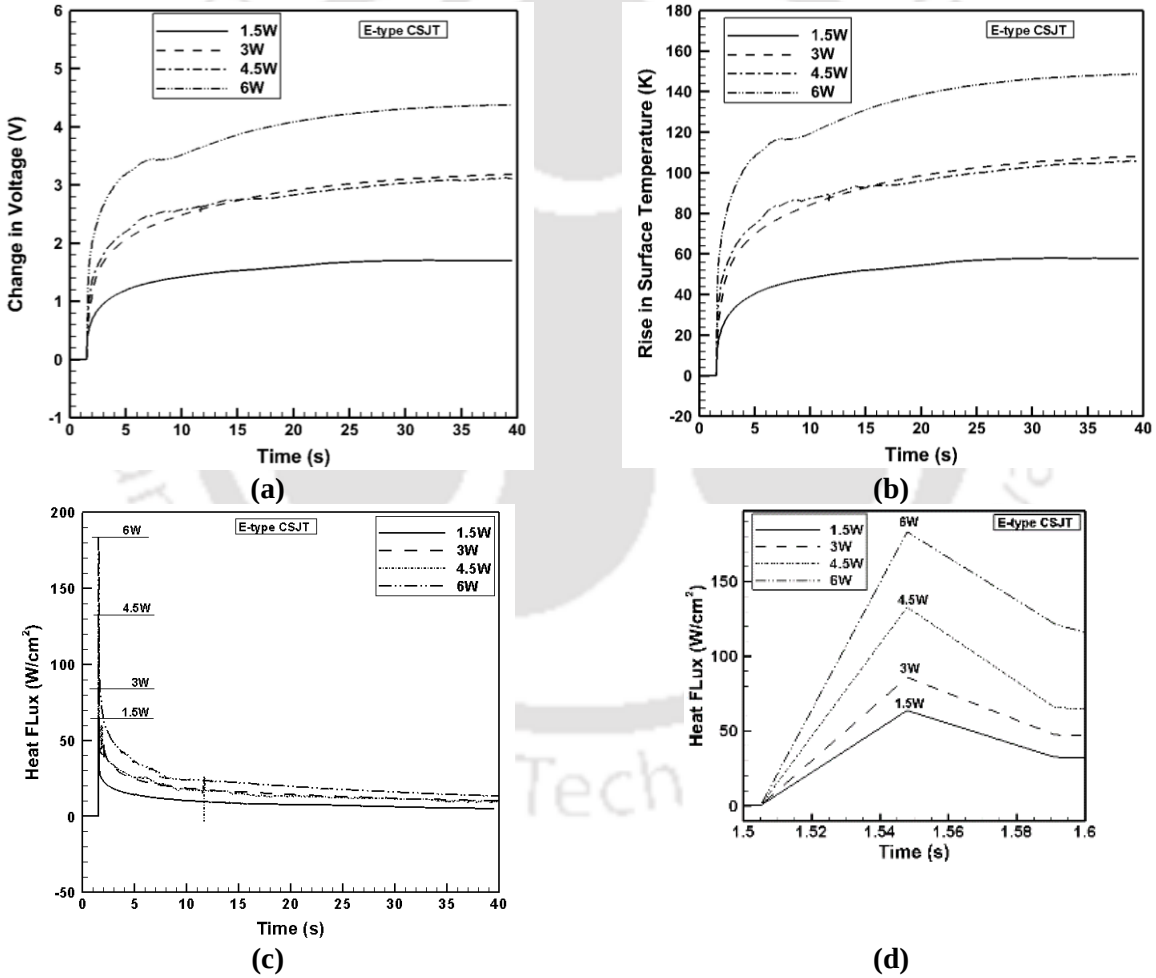

Fig. 4.9: (a) Variation in the change in voltage captured using laser-based set-up for E-type, (b) Rise in surface junction temperature obtained from obtained voltage signal for E-type, (c) Heat flux history extracted from the temperature-time history for E-type, and (d) being the zoomed portion of the graph (c) focussing the peak region

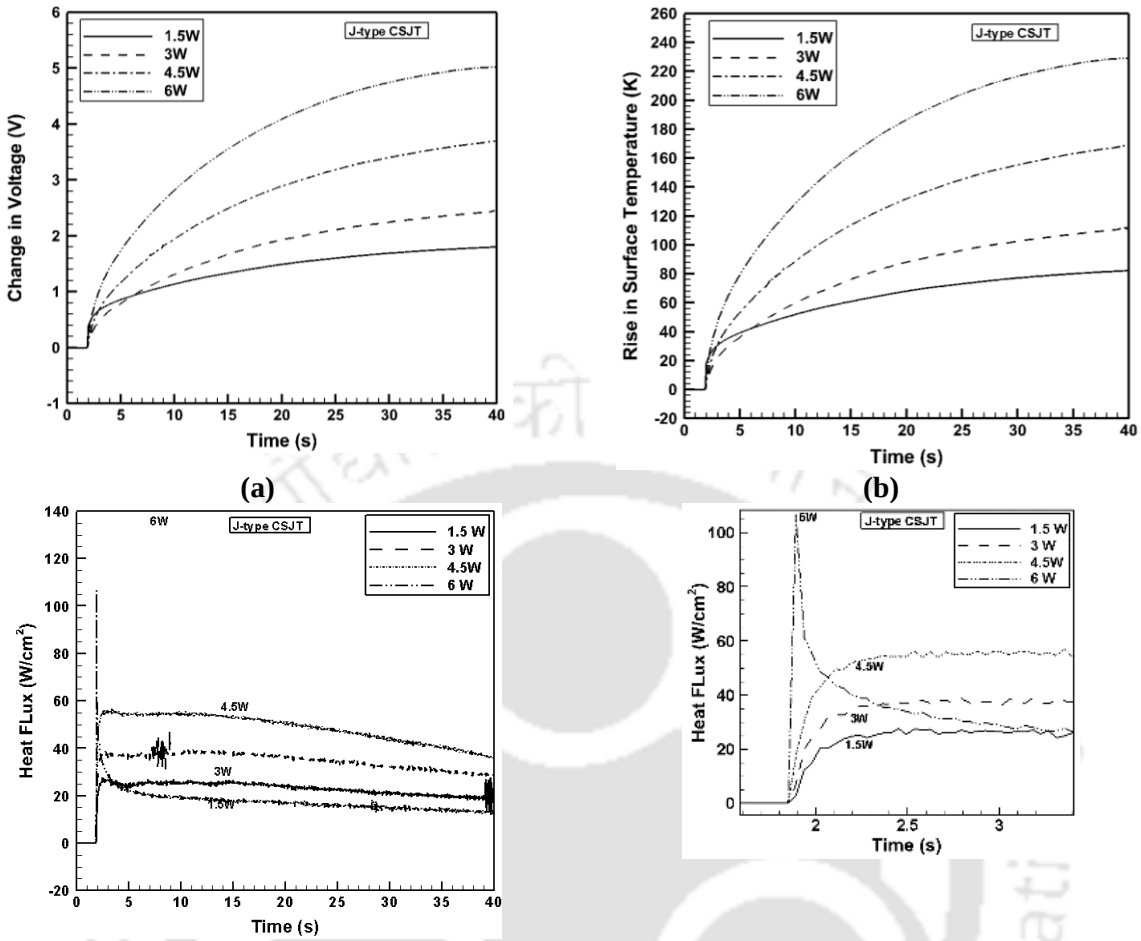

Fig. 4.10: (a) Variation in the change in voltage captured using laser-based set-up for J-type, (b) Rise in surface junction temperature obtained from obtained voltage signal for J-type, (c) Heat flux history extracted from the temperature-time history for J-type, and (d) being the zoomed portion of the graph (c) focussing the peak region

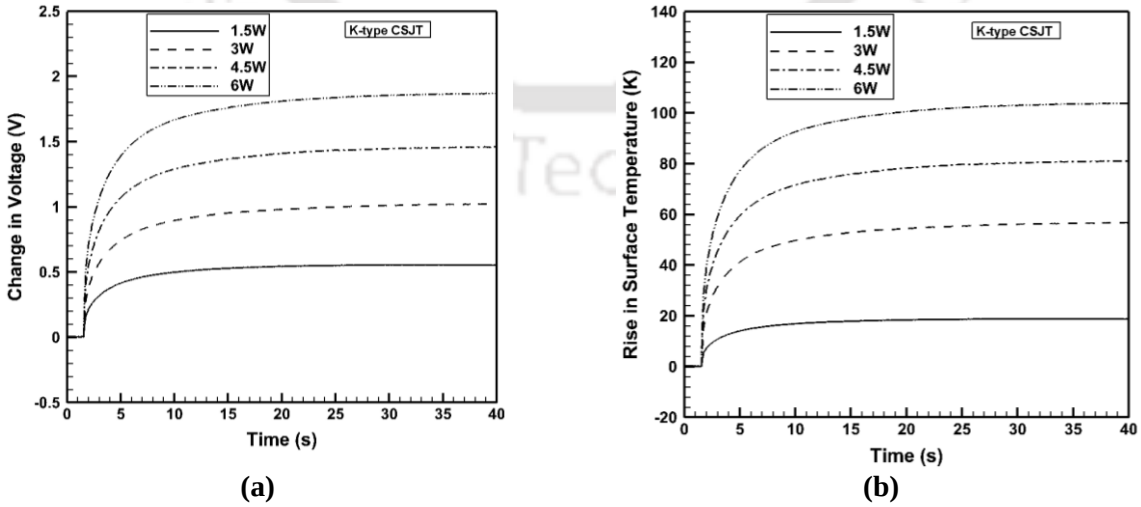

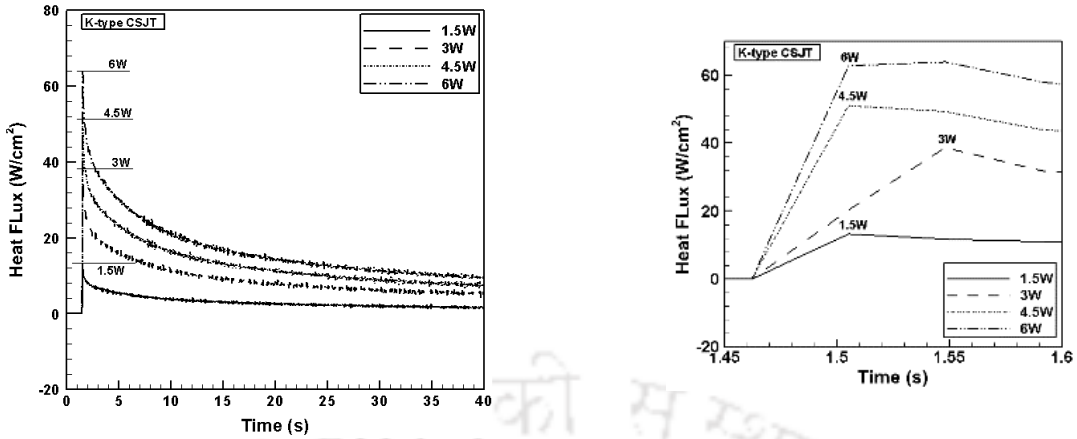

Fig. 4.11: (a) Variation in the change in voltage captured using laser-based set-up for K-type, (b) Rise in surface junction temperature obtained from obtained voltage signal for K-type, (c) Heat flux history extracted from the temperature-time history for K-type, and (d) being the zoomed portion of the graph (c) focussing the peak region

been utilized for discretization of temperature data and subsequent computation of heat flux using the algorithm as seen in *Fig. 4.9(c)*, *Figs. 4.10(c)* and *Fig. 4.11(c)* respectively. The obtained heat flux is in close agreement with the input wattage fed to the sensor, justifying the successful implementation of the radiation-based methodology to dynamically, calibrate the in-house fabricated sensor. However, the work carried out is just a preliminary step taken to highlight the usage of the laser of known wattage as a source of calibration. Further, experiments need to be carried out in order to justify the timescale of application is concerned as the present experiments cater a time domain of 40 seconds, which needs to be curtailed down to few millisecond/microsecond timescale. The experiments are the preliminary studies, which needs further tuning for desired timescale of application. The developed set-up would be very handy in utilizing to create near analogous heating environment experienced by aerodynamic models in impulse facilities.

4.5 Summary

The chapter focuses on the fabrication, characterization and calibration methodology of the coaxial surface junction thermocouple. Firstly, the detailed fabrication procedure and difficulties involved has been elaborated successfully Few thermocouples namely, E, T, J and K-type respectively were fabricated. Once the fabrication process has been completed, an XRD analysis is employed to check the deformation of one thermocouple over the other. As explained, the junction at the surface

of the thermal sensor is created because of the plastic deformation of one thermocouple material with the other thermocouple material. In order to visualize the obtained deformation, XRD analysis has been carried out and a different peak is clearly observed justifying the deformation due to abrasion of the material. After the characterization of the thermal sensor, calibration has been carried out using constant temperature and constant heat flux methodology. The constant temperature process basically involves calculating the sensitivity of the fabricated thermal sensors using the oil-bath technique (static calibration). The process involves checking the linearity of the voltage signal with respect to the change in the temperature. An oil-bath calibration technique was used to provide the necessary gradual temperature required for calibration. A good linear trend has been observed from the calibration run. A lag in both heating and cooling has been observed in the calibration, which can be attributed to the hysteresis losses. The hysteresis losses cannot be minimized but definitely, it can be controlled by minimizing the thermal equilibrium in the beaker. The static calibration run yielded sensitivity value of *58.96* μV/°C, *28.47* μV/°C, *43.82* μV/°C and *36.02* μV/°C respectively for E, T, J and K-type thermal probe. Further, the calibration using constant heat flux methodology involves exposing the thermal probe to a similar environment as faced by the sensors in real time experiment such as impulse facilities (i.e., replicating the desired facility in laboratory scale before being exposed to real environment, to check the error that could occur, when the sensor faces the actual flow field). The desired environment has been created using the laser source of variable wattage. Three fabricated thermal sensors have been exposed to different laser wattage namely, 1.5, 3, 4.5 and 6 W respectively. The obtained results have successfully demonstrated the practical implication of the usage of laser wattage set-up as a source to calibrate the thermal probe. However, the laser results needs further experimental validation by minimizing timescale of application.

CHAPTER 5

Experimental Techniques for Thermal Product Estimation of CSJT

Compendium:

The short duration aerodynamic experiments demand the measurement of transient surface heat flux. Generally, the temperature histories are obtained by mounting the calorimetric gauges (such as thin-film sensors and coaxial surface junction thermocouple) on the aerodynamic surfaces. The appropriate form of one-dimensional heat conduction modeling is employed while recovering the surface heat fluxes from transient temperatures. Such prediction of surface heat flux depends on the correct estimation of thermal properties coined as "thermal product (TP)" of the substrate and also the surface temperature history. TP is defined mathematically as square root of the products of density, specific heat and thermal conductivity of the substrate of the gauge. Many a times, due to the nature/type of materials and gauge fabrication techniques, the values of the thermal product do change since the substrate of a CSJT always undergoes the plastic deformation. Unlike the other types of gauge, such as TFGs, the sensing surface always sits on the substrate and the substrate has fixed thermal property values. Thus, the quantification of TP values through experimental means, for CSJTs after gauge fabrication, is very essential. The present study intends to evaluate the thermal product values of the in-house fabricated CSJTs (E and J-types) for short duration experiments. The CSJTs are in-situ designed, fabricated and calibrated in the laboratory. The estimation of thermal product includes two laboratory designed experiments viz., "water droplet and water plunging" techniques. In both the experiments, the transient responses are acquired by exposing the CSJTs to impulse heat load for a duration of 8 ms. The experimental evaluation of TP values for both types of CSJTs are compared with the corresponding theoretical estimates. Eventually, the effects of TP values on surface heat fluxes are analyzed by comparing them with the peak and average heat loads. The experimental evidence highlights that the surface temperature histories and the average heat flux are in very good agreement.

5.1 Introduction

Transient surface temperature and heat flux measurement are very important requirements in umpteen heat transfer research. Many engineering applications do require precise information of time-varying short duration temperatures due to fast change in heat flux. The typical examples include rapid fluctuations of temperatures on the cylinder walls of internal combustion engines [*Nijeweme et al., 2001; Alkidas and Myers 1982*], convective surface heating rate variations on aerodynamic models exposed to high speed flow [*Sanderson and Sturtevant, 2002; Jagadeesh et al., 2001*] and boiling experiments [*Chen and Hsu, 1995*]. It calls for the need of compact fast response thermal sensors for capturing the rapid variation of temperatures. In general, they monitor temperature histories at selected points and then relate them to surface heat transfer rates in one particular spatial coordinates. During short duration time scale of measurement, the surface heat flux is obtained by using the one-dimensional, semi-infinite medium solution for a step change in temperature. For a known surface temperature history (T_s), the instantaneous heat flux (q_s) can be deduced from Duhamel's superposition integral [*Taler, 1996*].

$$q_s(t) = \frac{\beta}{\sqrt{\pi}} \int_0^t \frac{1}{\sqrt{t-\tau}} \frac{d\{T_s(\tau)\}}{dt} d\tau \;;\; \beta = \sqrt{\rho c k} \tag{5.1}$$

Here, 'ρ' is the density, 'c' is the specific heat capacity and 'k' is the thermal conductivity of the substrate material and 'β' is defined as the "thermal product (TP)" of the substrate material.

The thin film gauges (TFGs) and coaxial surface junction thermocouples (CSJTs) are potential candidates to capture the highly transient temperature histories because they have a response time in the range of microseconds as discussed in presiding *Chapters 3 and 4* [*Schultz and Jones, 1973*]. Both the TFGs and CSJTs can be mounted in flush with any arbitrary surface. Subsequently, heat fluxes can be calculated from temperature histories by using *Eq. (5.1)*. However, the value of 'β' does not change for TFGs because thin films are coated on a particular substrate. But, in case of CSJTs, the sensing element is a "surface junction" which is formed by eroding the thermocouple materials. Hence, the value of 'β' do change, because of the nature of surfaces formed during fabrications.

Over the years, researchers have discussed the variation in TP value on surface heat flux estimation, during short duration time scale measurements [*James, 1990; Lyons and Gai, 1988;*

Miller, 1985]. In addition, researchers have adopted different techniques to measure thermal product values. In certain cases, experimental correlations are deduced for determination of TP at a reference temperature and a given rise surface temperature [*Miller, 1985*]. Using electrical methods, the determination of TP from measured temperature history is possible for TFGs, by providing a constant step input current to the gauge. Since it has a resistive heating element, the TP can be determined with knowledge of input heat flux. High frequency calorimetric gauges have also been explored to perform unsteady heat transfer experiments in an open circuit wind tunnel. The TP of the gauge substrate is determined by electrical methods and experimental correlations. Unsteady surface temperature histories and TP values are used to predict unsteady surface heating rates in the wake region of rotor mounted in the test section of wind tunnel [*James, 1990*]. Further, a novel optical technique has been illustrated that uses a continuous-wave, argon-ion laser of known input power. By using this technique, the TP determination for both thin-film type and thermocouple gauges becomes possible with the knowledge of input heat fluxes and measured surface temperature histories [*Lyons and Gai, 1988*]. Another significant experimental investigation highlights the thermal response and effective TP determination of a 'K-type' CSJT [*Buttsworth, 2001*]. A 'water droplet calibration' technique is implemented for millisecond time scale experiments while 'shock tube method' is used for microsecond time scale experiments. In the similar line, an experimental technique to evaluate the thermal product of a miniature 'K-type' thermocouple has been investigated at high enthalpy environment by using a shock tube facility [*[1]Mohammed et al., 2011*]. Further, the effect of using different methods of plastic deformation of the surface junction on the TP values has been studied. It has been further emphasized that individual dynamic calibration for each CSJT is highly desired for accurate estimation of TP because uncertainties up to 25% can be introduced when the thermophysical values of junction materials are directly taken from the literature [*Mohammed et al., 2008; Mohammed et al., 2007*].

In the backdrop of surface heat flux computations from short duration transient temperatures using *Eq. (5.1),* the accuracy of estimation of heat flux is highly dependent on TP values. Whatever may be the thermal sensor, thin-film on a substrate or a surface thermocouple on conducting metals, the basic calibration is very much essential to convert the measured temperature with respect to surface heating rates (*Eq. 5.1*) through accurate determination of TP (β) value. For TFGs, the substrate is essentially an insulator (typically quartz, pyrex, Macor etc.)

and the thermal properties $(\rho, c \text{ and } k)$ do not change significantly during measurement time scales even with different sensing elements [*[1]Sarma et al., 2016; Kumar et al., 2012; Kumar et al., 2011; Jagadeesh et al., 2001*]. In contrast, the value of β is very unique for a particular CSJT because it depends on the thermal properties of the metallic plating formed during its preparation through plastic deformation by grinding the junction surface. While fabricating CSJTs, the micro-scratches formed during plastic deformation helps in the sensor to respond immediately to thermal load during short duration experiments. As a qualitative estimate, average thermal properties values $(\rho, c \text{ and } k)$ of junction materials are obtained from the literature. Subsequently, TP of the surface junction is calculated by considering the appropriate weighing factor of each metallic element [*Sahoo and Kumar, 2015; Kumar and Sahoo, 2013*]. However, this method may not always replicate the correctness of the surface junction's thermal properties for CSJTs. Moreover, the plastic deformation at the surface junction also varies with the method of preparation and purity of material of CSJTs available locally. In some situations, when the CSJTs are fabricated with alloys of metal (such as Alumel, Nicrosil, Nisil etc.) the literature values of thermal properties are only the average estimates of TPs. Considering these factors, it is felt that the TP values of CSJTs should be determined experimentally in the similar time-scale of measurements, to rule out ambiguities of theoretical assumptions.

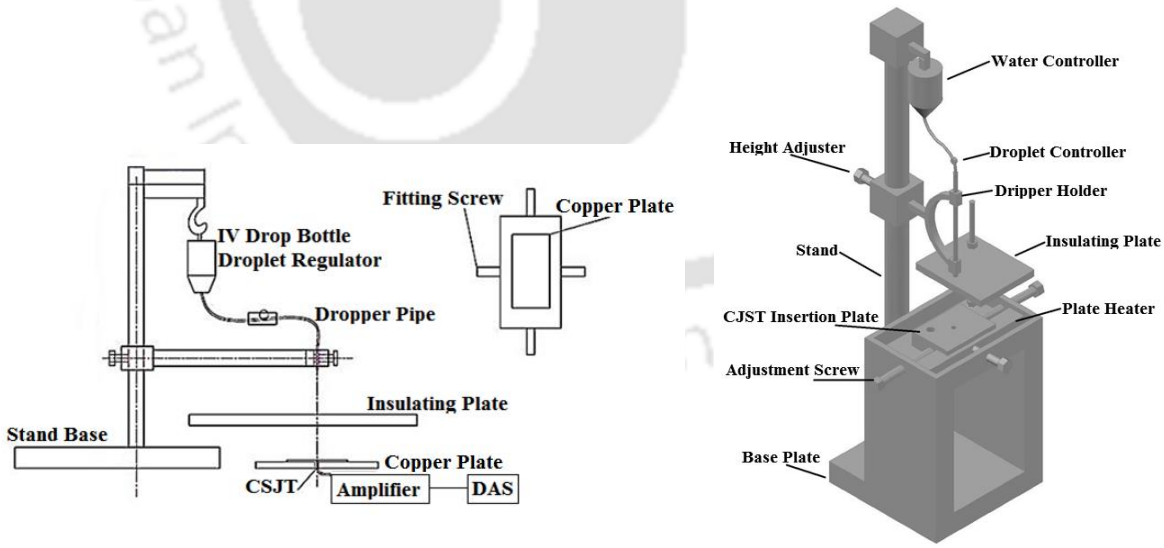

(a) Water droplet technique

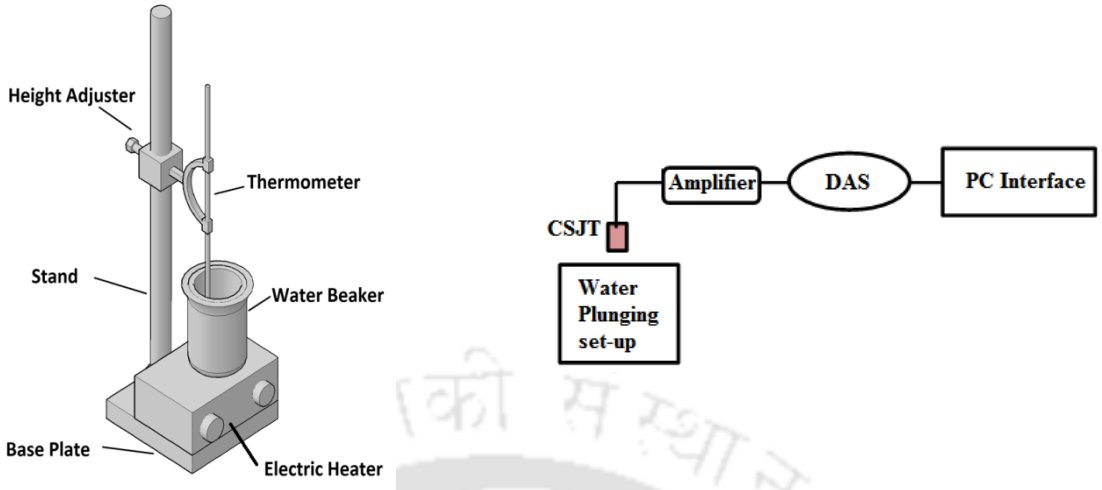

(b) Water plunging technique

Fig. 5.1: Experimental arrangement CSJTs for determination of thermal product: (a) water droplet technique; (b) water plunging technique. (*More details with complete pictorial representation of the experimental set-ups are given in "Appendix D"*).

In this investigation, simple laboratory experiments (*Fig. 5.1*) are introduced to measure TP values of two different types of CSJTs (E-type and J-type) in the short duration time scales (8 ms). For the first experiment (commonly known as "water-droplet" technique), the CSJTs are exposed to a heating environment with a plate heater and very small water droplets at ambient temperature are allowed to impact on the surface of the gauge in a controlled manner (*Fig. 5.1-a*). Subsequently, the transient temperature responses from CSJTs are monitored. The other method uses 'water-plunging' where the CSJTs are dipped into the hot-water bath and side by side their instantaneous transient responses are captured (*Fig. 5.1-b*). The feasibility of both techniques in terms of estimating the TP value is explored. A comparative analysis for surface heat flux determination is also made for both the techniques with reference to theoretical predictions to ascertain the effectiveness of the surface junction.

5.2 THERMAL PRODUCT DETERMINATION – EXPERIMENTAL METHOD

The thermocouples are the best suited universal techniques for measuring the temperature since many years. It has the capability of operating over a wide range of temperature and is reasonably cheap. The junction quality is the most important factor, which determines the performance of the thermocouple such as accuracy, repeatability and response time etc. The difference in the conventional and the coaxial thermal sensors are highlighted in *Chapter 3 and 4*. The complete

fabrication and static calibration methodology comprising the coaxial thermal sensors are elaborated in *Chapter 4* respectively.

The calorimetric gauges work on the principle of one-dimensional transient heat conduction and surface heat fluxes are obtained with an assumption of negligible thermal penetration within the measurement time scale. The accuracy of surface heat flux determination (*Eq. 4.1*), mainly depends on the precise measurement of temperature history and the correctness of TP(β). In general, the theoretical estimation of the thermal product (β_t) requires the information of thermal property values of materials from which the surface junction is prepared. Since the junction point of thermocouple materials (viz. chromel-constantan-epoxy for E-type and iron-constantan-epoxy for J-type) is being deformed to a surface during its fabrication, it is very likely to have a plastic deformation of three different materials. In the present case, they are fabricated from available materials of different sizes as mentioned in *Table 5.1* and β_t is calculated by considering the appropriate weighing factor of 0.5 for property values of each thermocouple materials [*Caldwell, 1962*].

Table 5.1: Thermal properties of junction material properties for theoretical determination of TP values [*Caldwell, 1962*]

Types of CSJT	**Constituents**	**Density** (ρ) (Kg/m^3)	**Specific Heat** (c) (J/kg-K)	**Thermal Conductivity** (k) (W/m-K)	**Thermal Product** $(\beta_t = \sqrt{\rho c k})$ (Jm^{-2}s$^{-1/2}$K^{-1})	**Sensitivity S** (μV/°C)
E-Type	Chromel (3.25 mm)	8730	448	17.8	8695	58.96
	Constantan (0.813 mm)	8922	407	22.5		
J-Type	Constantan (0.813 mm)	8922	407	22.5	13605	43.82
	Iron (2.5 mm)	7870	450	80.4		

In CSJTs, the junction surface is the consequence of plastic deformation of three different materials. Thus, estimation of β by considering the average values of each material property may not replicate the correct behaviour of the surface junction. In addition, the micro-scratches developed through such deformation is an indicative measure of short duration thermal response [*Buttsworth, 2001*]. Based on the assumptions of the fact of low thermal inertia at the surface of the substrate and a homogeneous semi-infinite substrate, the heat flux is obtained from *Eq. (5.1)*.

Thus, it is always advisable to have the experimental determination of β, for all types, CSJTs fabricated in-house to ascertain the effectiveness of surface junction. The present investigation is carried out by two independent experimental methods (i.e. water droplet technique and water plunging technique) for determination of TP values both types of CSJT. Moreover, a comparative assessment of TP values is made to calculate the percentage deviation from its theoretical estimates. The feasibility of both techniques is explored by using these experimental TP values for calculation of surface heat flux from *Eq. (5.1)*.

5.2.1 Water Droplet Technique

The experimental arrangement consists of a copper plate (100 mm × 50 mm) having 5 mm thickness in which the CSJT can be flush-mounted with the surface. This plate is mounted on a base stand, has provisions of lateral and longitudinal movement through adjustable screws (*Fig. 5.1-a*). The other important component of the setup is the "water droplet mechanism" which is attached to the base stand. The flow rate of water is controlled by "droplet regulator" while the 'height adjuster' maintains an adequate distance between the plate and water droplet. The water dropper is held perfectly above the CSJT with help of a stainless steel (SS) pipe, which is fixed by the jaw of base stand. The CSJTs are mounted in flush on the copper plate with its surface facing towards water droplet. During the experiment, the heat is applied to the CSJT by heating the copper plate with an electric heater. An insulating plate placed between the copper plate and the water droplet mechanism isolates thermal influence between the heated plate and water temperature. The temperature of the plate is monitored by CSJT through a data acquisition system (DAS). It comprises of voltage amplifier (*INA 128*; Texas make; up to gain factor of 500) of CSJT, DC power supply (*PCD 3303*; *Scientific make*; with a range of ±15 V) for the amplifier and high frequency rating oscilloscope (*TBS 1072B-EDU*; *Tektronix make*). After heating the plate, the temperature is monitored from CSJT and insulating plate is removed so that a drop of water at ambient temperature (26 °C) is allowed to impact on junction surface. The instantaneous response of CSJT in the form of the voltage signal is recorded in DAS.

For the known values of water droplet temperature (T_w) and the surface temperature of the plate (T_s), the value of β can be obtained from the instantaneous temperature (T) as recorded from CSJT [[3]*Mohammed et al., 2011*],

$$\frac{T-T_s}{T_s-T_w}=\frac{\beta_w}{\beta_w+\beta} \tag{5.2}$$

Here, β_w (= 1643 $Jm^{-2}s^{-1/2}K^{-1}$) is the TP of water and its value is taken from reference [[2]*Mohammed et al., 2011*]. It may be emphasized that "distilled water" has been used for all the experiments and it is expected that TP value will not alter drastically with respect to literature reported data. Further, it is assumed that heat is conducted only in one-dimension for droplet as well as a thermocouple and there is no rebound of a water droplet on the sensor surface so that instantaneous heat transfer takes place in one dimension. For all the experiments, distilled water has been used and transient responses from CSJTs are captured only once for a single droplet in the form of voltage signal with time duration of 8 ms. The sample voltage signals from both CSJTs are amplified adequately and captured in the oscilloscope (*Fig. 5.2*).

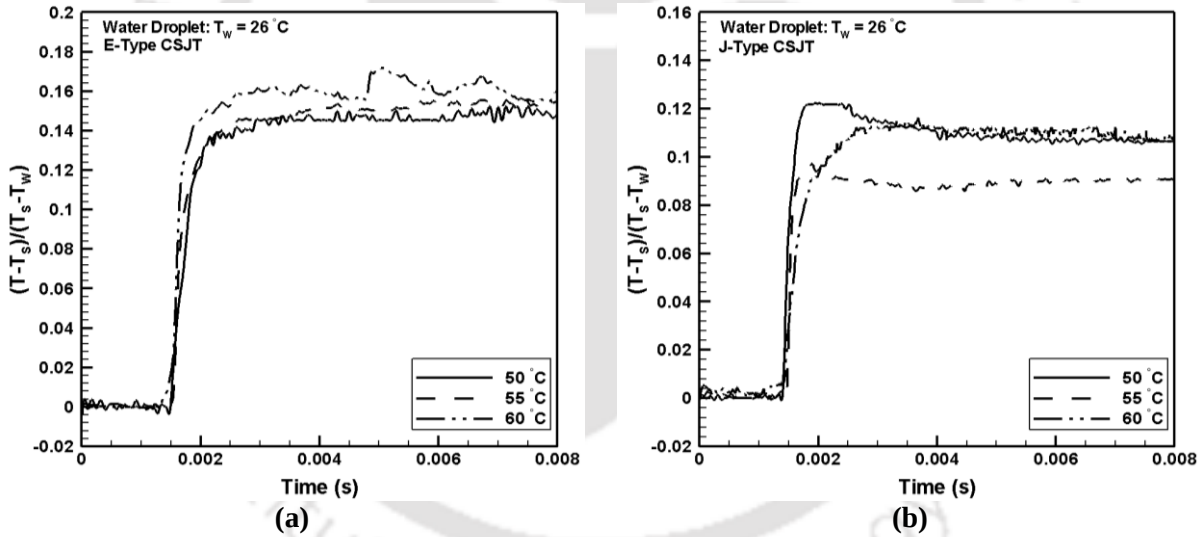

Fig. 5.2: Transient variations of non-dimensional temperature ratio $\left(\{T-T_s\}/\{T_s-T_w\}\right)$ for CSJTs during water droplet (WD) technique at different surface temperatures (T_s) of the plate: (a) E-type; (b) J-type

The water droplet experiments are performed at a fixed ambient temperature of the water (T_w = 26 °C) with three different surface temperatures of the plate (T_s = 50 °C, 55 °C, 60 °C). Ideally, the TP value can be obtained by maintaining one particular temperature difference (T_s-T_w). In this case, different sets of temperature are explored mainly to reduce the experimental uncertainties. However, the highest temperature is limited by the electrical heater which is being

employed for heating the copper plate. The voltage signals from the thermal gauge are converted to a non-dimensional form of temperature ratio by considering the 'sensitivity' of each CSJT (*Fig. 4.7*) and are plotted in *Fig. 5.2*. It clearly shows a step-rise in temperature during the time scale of 8 ms. For each temperature difference $(T_s - T_w)$, the TP values of each CSJT (E-type; J-type) are calculated by *Eq. (5.2)*. These values are ensured with an average of several trials while maintaining a very good repeatability of signals (*Table 5.2*). For E-type CSJT, the average value of β during water droplet calibration experiment is found to be 8883 $Jm^{-2}s^{-1/2}K^{-1}$. This is in line with a closed agreement (accuracy of 2%) with a literature reported data [*Irimpan et al. 2015*].

In a similar manner, the non-dimensional form temperature history is plotted in *Fig. 5.2(b)* for J-type CSJT and the average value of β is obtained during water droplet calibration as, 13580 $Jm^{-2}s^{-1/2}K^{-1}$ (*Table 5.2*). It is in very good agreement (0.18%) with a theoretical average of TP (*Table 5.1*), calculated through property values of thermocouple elements.

Table 5.2: Experimental techniques for thermal products of CSJTs

Types of CSJT and their specifications	**Water Droplet (WD)**			**Water Plunging (WP)**		
E-Type S **= 58.96 µV/°C** $\beta_{t,E}$ **= 8695** $Jm^{-2}s^{-1/2}K^{-1}$	T_w **= 26 °C**			T_s **= = 26 °C**		
	T_s **= 50 °C**	T_s **= 55 °C**	T_s **= 60 °C**	T_w **= 50 °C**	T_w **= 55 °C**	T_w **= 60 °C**
	8993	**8892**	**8764**	**8322**	**8382**	**8654**
	$(\beta_{e,E})_{WD}$ **= 8883** $Jm^{-2}s^{-1/2}K^{-1}$			$(\beta_{e,E})_{WP}$ **= 8452** $Jm^{-2}s^{-1/2}K^{-1}$		
Percentage deviation for β	$\frac{\beta_{t,E} - (\beta_{e,E})_{WD}}{\beta_{t,E}} = -2.1\%$			$\frac{\beta_{t,E} - (\beta_{e,E})_{WP}}{\beta_{t,E}} = 2.8\%$		
J-Type S **= 43.82 µV/°C** $\beta_{t,E}$ **= 13605** $Jm^{-2}s^{-1/2}K^{-1}$	T_w **= 26 °C**			T_s **= = 26 °C**		
	T_s **= 50 °C**	T_s **= 55 °C**	T_s **= 60 °C**	T_w **= 50 °C**	T_w **= 55 °C**	T_w **= 60 °C**
	11935	**15795**	**13010**	**9943**	**9630**	**9181**
	$(\beta_{e,J})_{WD}$ **= 13580** $Jm^{-2}s^{-1/2}K^{-1}$			$(\beta_{e,J})_{WP}$ **= 9585** $Jm^{-2}s^{-1/2}K^{-1}$		
Percentage deviation for β	$\frac{\beta_{t,J} - (\beta_{e,J})_{WD}}{\beta_{t,J}} = -0.18\%$			$\frac{\beta_{t,J} - (\beta_{e,J})_{WP}}{\beta_{t,J}} = 29.5\ \%$		

5.2.2 Water Plunging Technique

Water plunging calibration is another independent technique where the CSJTs are exposed to the sudden heating environment during the experimental time scale. The set-up consists of a heater,

the beaker containing distilled water, thermometer and CSJT along with its instrumentation as shown in *Fig. 5.1(b)*. The working principle is analogous to that of 'water droplet technique' except the fact that CSJTs are instantaneously dipped into the preheated distilled water while constantly monitoring the temperature of the water by a conventional thermocouple. Initially, the CSJTs are at room temperature (T_s) and the distilled water in a beaker is heated to a predefined temperature (T_w). When the CSJT is dipped instantaneously in the water, a step rise in temperature is experienced at the junction surface and a voltage signal is generated. It is captured through DAS in the similar manner as discussed in *Section 5.2.1*. The temperature histories expressed in the non-dimensional form are shown in *Fig. 5.3*. For each temperature difference $(T_w - T_s)$, the TP values of each CSJT (E-type; J-type) are calculated using *Eq. (5.2)* and are summarized in *Table 5.2*. In this case, also, the average value of β is found to be 8452 $Jm^{-2}s^{-1/2}K^{-1}$ for E-type CSJT that matches very well (3%), when compared with the literature reported data of 8695 $J.m^{-2}.K^{-1}.s^{-0.5}$ [*Irimpan et al., 2015*]. However, for J-type TFG, the average value of β (9585 $Jm^{-2}s^{-1/2}K^{-1}$) is under-predicted by about 29% from its theoretical estimate (13605 $Jm^{-2}s^{-1/2}K^{-1}$), as mentioned in *Table 5.1*. It may be emphasized here that one of the elements in J-type CSJT is 'iron'. When it is dipped in water, there are likely chances of oxidation on the surface junction and thereby it can degrade its TP values. However, this situation is not severe in case of water droplet technique because the droplets are allowed to impact upon the surface junction in a controlled manner. The experimental data for TP determination from "water-droplet and water-plunging technique" (*Table 5.2*) shows a very good match for both types of CSJT except for the case when TP from J-type CSJT obtained through "water-plunging" technique.

5.2.3 Comparative Assessment of Thermal Products

In the previous sections, the TP values of CSJTs are determined through independent experiments under a different set of heat flux conditions while maintaining the same temperature difference between the surface and water. In order to have a comparison of both the techniques, the transient responses of non-dimensional temperature ratio for "water-droplet and water-plunging" techniques is replotted in *Fig. 5.4*. At a given temperature difference and for both the experimental

techniques, it is seen to have sharp step-rise at about 1.8 ms followed by steady signals for rest of the time scale till *8* ms while the peak temperature ratios have the range of *0.12 to 0.15*. Thus, the feasibility of both the techniques for short duration measurements is justified by the fact of the step-rise in temperature for short duration heat loads to CSJTs. The comparative average TP values of CSJTs determined from these techniques are given in *Table 5.3*.

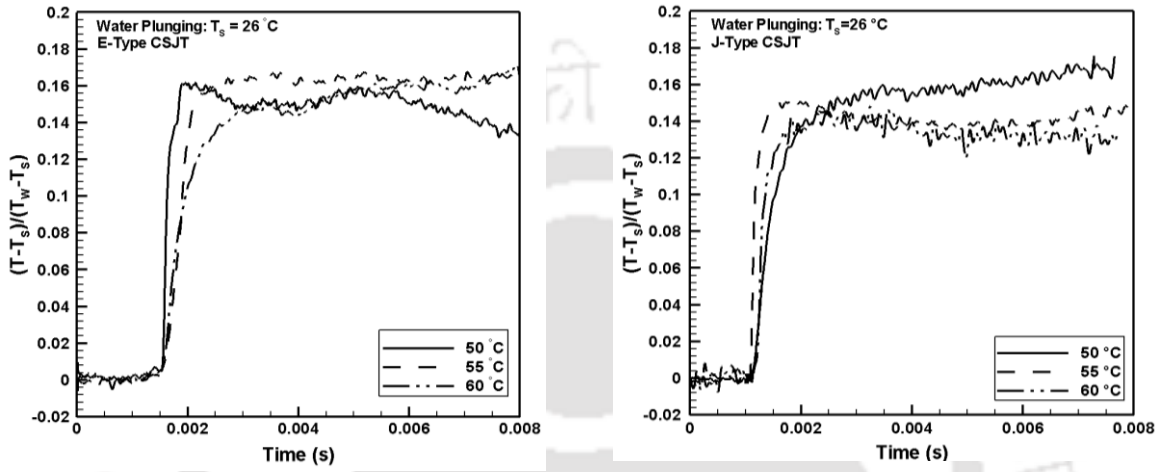

Fig. 5.3: Transient variations of non-dimensional temperature ratio $\left(\{T-T_s\}/\{T_w-T_s\}\right)$ for CSJTs during water plunging (WP) technique at different surface temperatures $\left(T_s\right)$ of the plate: (a) E-type; (b) J-type

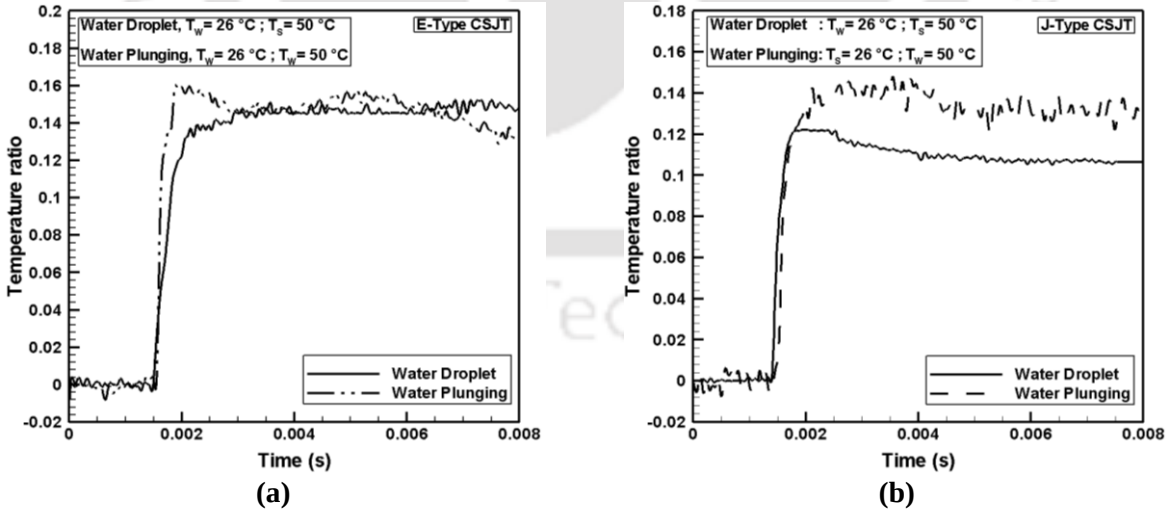

Fig. 5.4: Transient variations of non-dimensional temperature ratio for CSJTs during water droplet (WD) and water plunging (WP) technique at fixed water temperature and surface temperature of the plate: (a) E-type; (b) J-type

Table 5.3: Comparative assessment thermal product and surface heat flux for CSJTs

Types of CSJT	E-Type				J-Type			
	Theoretical estimate (WD)	**Water-droplet method**	**Theoretical estimate (WP)**	**Water-plunging method**	**Theoretical estimate (WD)**	**Water-droplet method**	**Theoretical estimate (WP)**	**Water-plunging method**
Thermal product β ($Jm^{-2}s^{-1/2}K^{-1}$)	$\beta_{t,E} = 8695$	$\left(\beta_{e,E}\right)_{WD} = 8883$	$\beta_{t,E} = 8695$	$\left(\beta_{e,E}\right)_{WP} = 8452$	$\beta_{t,J} = 13605$	$\left(\beta_{e,J}\right)_{WD} = 13580$	$\left(\beta_{e,J}\right)_{WD} = 13580$	$\left(\beta_{e,J}\right)_{WP} = 9585$
Peak Heat Flux (W/cm^2)	$\left(q_{t,E}\right)_{WD} = 5.64$	$\left(q_{e,E}\right)_{WD} = 5.76$	$\left(q_{t,E}\right)_{WP} = 11.15$	$\left(q_{e,E}\right)_{WP} = 10.81$	$q_{t,J} = 9.65$	$\left(q_{e,J}\right)_{WD} = 9.61$	$\left(q_{t,J}\right)_{WP} = 12.7$	$\left(q_{e,J}\right)_{WP} = 8.94$

It is observed that the experimental determination of TP through both the technique has a close resemblance (within ±3% accuracy) as compared to theoretical TP estimate for E-type CSJT. However, it is not true for J-type CJST where a significant deviation (about 29%) is found when the theoretical TP values are compared with experimentally determined values from "water-plunging" technique. As mentioned earlier, it is further emphasized that average theoretical estimation of TP (as given in *Table 5.1*), does not really replicate its correctness rather an appropriate experimental method should be followed to justify the surface junction's thermal properties in short duration time scales. The type of material and its purity, formation of plastic deformation between the materials at the surface are some of the critical factors that affect the thermal properties of the surface junction.

5.3 Determination of Instantaneous Surface Heat Flux

All the calorimetric gauges rely on transient surface temperature histories for prediction of short surface heat flux by using *Eq. (5.1)*. In many instances, the TP values are generally assumed from theoretical estimates which are either thermal properties of the substrate (in the case of thin film gauges) or the surface junction (for CSJTs). In any case, the accuracy of heat flux predictions mainly depends on the correctness of TP values as well as the acquisition of transient surface histories from CSJTs. With this objective, the subsequent investigation involves predictions of surface heat fluxes through acquired temperature signals and the corresponding TP determination of respective experimental techniques (i.e. water-droplet and water plunging methods). In short time scales, the surface heating rates from transient temperatures can be recovered through appropriate modelling of *Eq. (3.1)* with the assumption of one-dimensional heat conduction [*Taler, 1996; Schultz and Jones, 1973*]. The complete elaboration related to the modelling of surface heat flux is described in *Chapter 3*.

The results indicate that the transient surface heat flux variation resembles the nature of 'impulse' heat load for "water-droplet" method (*Fig. 5.5-a*). This is in line with the experimental case in which heat is being transferred from the plate surface to the water-droplet during its impact. For an E-type CSJT, it is seen that there is a sharp rise in heat flux immediately after the droplet impact to a peak heat flux values of about *6* W/cm^2 within 0.3 ms. During the same time scale, the peak heat flux value is seen to be *10* W/cm^2 for J-type CSJT. However, the TP values determined

experimentally $\left[\left(\beta_{e,E}\right)_{WD}$ and $\left(\beta_{e,J}\right)_{WD}\right]$ and theoretically through thermal properties average, $\left(\beta_{t,E}\right.$ and $\left.\beta_{t,J}\right)$ do not affect the peak values of surface heat fluxes in both cases.

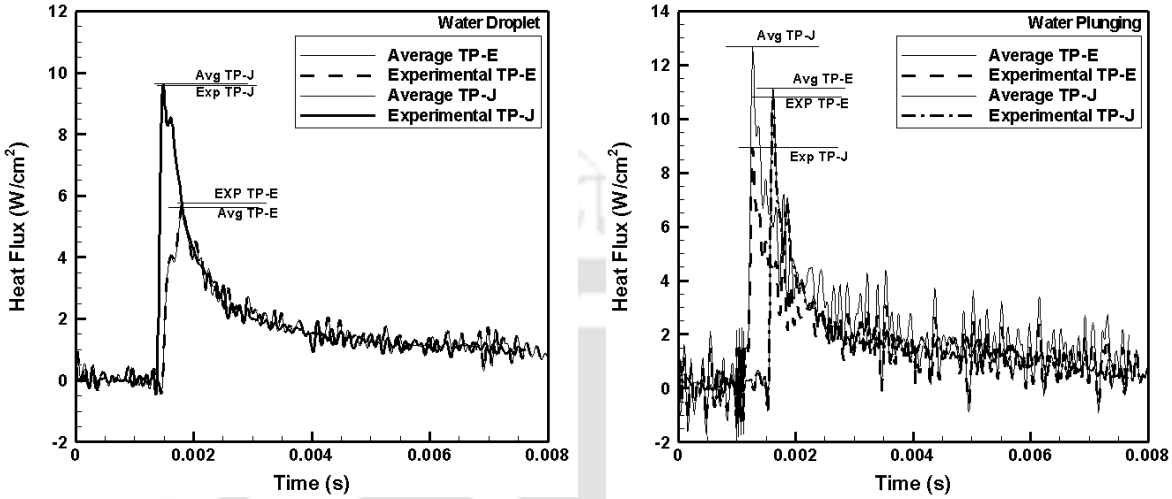

(a) **(b)**

Fig. 5.5: Comparative assessment of surface heat flux histories for CSJTs: (a) water droplet technique; (b) water plunging method

Although the experiments for both types of CSJTs are conducted in a similar environment, the deviation of *4* W/cm^2 does not seem to be promising. When the results for "water-plunging" techniques are compared, the surface heat fluxes also show the similar trends of "impulse heat load". For E-type CSJTs, the peak heat flux is found to be about *11* W/cm^2 with experimental and theoretical values of TP. However, a significant deviation of peak surface heat flux of *4* W/cm^2 is seen for J-type CSJT which is mainly due to under-prediction of TP values (29%) during "water-plunging" experiments. In both experiments, it is interesting to note that the average heat flux is computed as, *1.8* W/cm^2, after an initial period of *4* ms (*Fig. 5.5*). Irrespective of nature of experiments, TP values do not affect average heat flux calculation and hence one can assume this to be the theoretical estimate without conducting any experiments. This approach is essentially followed for predictions of surface heat fluxes from CSJTs during short experimental time scales such as shock tunnels [*Irimpan et al., 2015*]. It may be emphasized that E-type CSJTs have higher sensitivity value as compared to J-type CSJTs and it leads to higher magnitude of voltage signals for same values of heat loads. Hence, they are mostly used as routine experiments involving short duration timescales without any ambiguity. However, the importance of "water-droplet and water-plunging" techniques are realized for experimental TP determination when the CSJTs are prepared

with different sets of materials (such as Alumel, Nicrosil, Nisil etc.) for which junction properties are likely to change during its fabrication process. Another attempt has been made to estimate Thermal Product of different coaxial thermocouples using the shock tube technology. A brief study has been highlighted in the appendix section (*Appendix D*).

5.4 Summary

The present investigation aims at determination of "thermal product" in short duration timescale, for coaxial surface junction thermocouples through laboratory experiments. For this purpose, two types of fabricated CSJTs (E and J) are chosen as elaborated in *Chapter 4*. Experimentally, the TP values are determined through "water-droplet and water-plunging techniques", both of which are exposed to impulse heat loads. The corresponding transient temperature histories are captured and subsequently, TP values are calculated. While comparing them with theoretical estimates, the results show encouraging agreements except for a particular case in which the TP value was underpredicted in 'water-plunging" experiment for J-type CSJT. Further, the temperature histories are used to calculate the surface heat flux and a very good comparing is found among all the experimental results. All the experimental results of sensitivity, temperature and the surface heat fluxes are found to be accurate within an experimental uncertainty of ±5%. The experimental outcome of TP values for E-type CSJTs are in close resemblance (within ±3% accuracy) whilst a significant under-prediction of about 29% is observed for experimentally determined TP values with respect to its theoretical estimates for J-type CSJT during 'water-plunging" experiments. Consequently, it influences the peak heat flux predictions from the surface temperature histories. Based on the outcome of the experiments, the E-type CSJTs are found to be efficient in comparison to its counterpart J-type CSJTs in terms of its sensitivity and consistency in predicting surface heat flux accurately. The techniques discussed in this Chapter has a great significance in determining TP values experimentally for short durations particularly for CSJTs fabricated from metallic alloys for which there are not any exact theoretical estimates.

CHAPTER 6

Measurement of Instantaneous Heat flux using Surface Junction Probe in a Shock Tube

Compendium:

This chapter aims at comprehensive investigations towards installation of a shock tube and its experimental calibration. Additionally, the shock tube is utilised to estimate the heat flux in the supersonic environment using in-house developed coaxial surface junction thermocouples (CSJTs). A moderate size shock tube of 7 m long with inner diameter of 55 mm and thickness of 11 mm has been is designed in-house and installed successfully in the Mechanical Engineering department of Indian Institute of Technology Guwahati. The low-pressure air as 'test gas' is considered in the 5 m long driven section of the shock tube while the driver section has a length of 2 m and is filled with high pressure nitrogen/ helium gas. Shock waves are generated through appropriate rupture of aluminium diaphragm (1.2 mm thickness) while maintaining suitable pressure ratios across the driver and driven section. All necessary instrumentations have been incorporated for measuring shock speeds and pressure rise across primary as well as reflected shock. Subsequently, reflected shock Mach number and temperature rise across primary and reflected shock are estimated through one-dimensional shock tube relations. Further, the prepared coaxial surface junction thermocouples (CSJTs) namely, E, T and J-types (as elaborated in the earlier chapters) are used to calibrate the installed shock tube. These are mounted on a specially-designed end-flange for measuring the surface temperature rise and subsequent estimation of the stagnation heat flux of the test gas. The maximum rate of temperature rise recorded by the presently designed thermocouple is noted to be 7800 K/s. This limiting value is marked to be a characteristic constant of the sensor since it is found to be independent of the magnitude of the step change in temperature. The calibration of shock tube also involves comparative assessments of shock tube parameters obtained through experimental results and analytical calculations. The experimental evidence shows a reasonable agreement between theoretical and analytical results. In addition, the stagnation point heat flux is measured at the end flange of the shock tube by mounting the thermal sensors on a 10 mm radius hemispherical model. The experiment intends for a comparative assessment among different thermal sensor in a low supersonic highly transient environment. The obtained results have shown reasonable accuracy among the different thermal sensor justifying the usability of thermal sensor in low supersonic region.

6.1 Introduction

Shock waves are considered to be an integral part of flow field features in the area of high-speed aerodynamics. The typical phenomena of shock wave carry a significant amount of energy and they have the ability to propagate in conventional mediums (solid, liquid and gas) as well as through plasma and electromagnetic field. It further leads to compression of the medium that can drastically change the properties of the medium. The capability of shock waves to generate an instantaneous rise in pressure and temperature pulses in the medium suits its usage in many research areas of space engineering, high-temperature materials, chemical kinetics, medical and industrial applications. In the middle of the eighteenth century, after a series of studies and experiments, it was realized that the waves from explosions travel faster than the speed of the sound waves. Recently, there have been major revolutions pertaining to the industrial application of shock waves as such cell transformation, preservative injection into bamboos, sandal oil extraction, removal of dust from silicon wafer surfaces etc. [*Jagadeesh, 2008*]. Later, shock tubes are fabricated from low-cost materials that can produce pressure pulses through explosives [*Duff and Blackwell, 1966*]. With respect to the aerodynamic point of view, the high speed and high altitude flows were simulated by using conventional facilities such as supersonic/hypersonic wind tunnel [*Rose et al., 2015; Muntz et al., 1999*]. With the realization of shock wave capabilities, high enthalpy short duration impulse facilities came into existence to understand the problem of re-entry and scramjet engines. However, due to lack of high speed sensors and flow diagnostic instrumentation, these facilities provided limited data. With recent developments in high speed data acquisition, it is possible to generate hypersonic flows by using a moderate size impulse facility for very short time duration with the test time of few milliseconds. Although there are difficulties in the processing of data acquisition for short test times, the modern high speed instrumentation and flow diagnostics techniques enable required solution for the intended time duration. The main attraction of such short duration facilities is that it can provide a high-enthalpy slug of test gas at a very reasonable cost. The facilities include large and small scale developments in shock tunnels, free-piston shock tunnel and explosion tubes over last few decades [*McMillan, 2004; Itoh et al., 2001; Doolan and Morgan, 1999; Lu and Wilson 1994; Modarres and Azzazy, 1988*].

A shock tube is the simplest form of device that can generate moving shock waves by allowing a high pressure region to suddenly come in contact with a low pressure region. Since

shock waves can be generated under controlled conditions, many analogous natural occurring phenomena related to shock-associated/shock wave physics can be studied experimentally by using "shock tube" as a laboratory tool. Basically, it is a closed tube having a driver (*region '4'*) and driven section (*region '1'*) separated by a diaphragm (*Fig. 6.1*). Both sections have substantially different fill pressures so that the diaphragm opens suddenly, at a point depending on the rupture pressure of the material. Typically, shock tubes are fabricated from stainless steel while diaphragms are made out of cellophane, aluminium, or steel etc. depending on the strength of shock wave requirement. Thus, the gas from the high pressure (driver) section expands into the low pressure (driven) section of the tube, which contains the test gas. On the sudden rupture of the diaphragm, pressure waves originating from the diaphragm section coalesce to form the shock front, which propagates into the low pressure section. It is known as "*primary shock*" which followed by a "contact surface" which is an imaginary line acting as an interface between the driven and driver gases (*region '2' and '3'*) in the medium (*Fig. 6.1*). The moving primary shock travelling towards a driven section of the tube has a velocity greater than the sonic velocity of the undisturbed test gas. It leads to compression, heating and accelerating the test gas for which there is a sudden rise in pressure and temperature (*region '2'*) as shown in *Figs. 6.1(a-b)*.

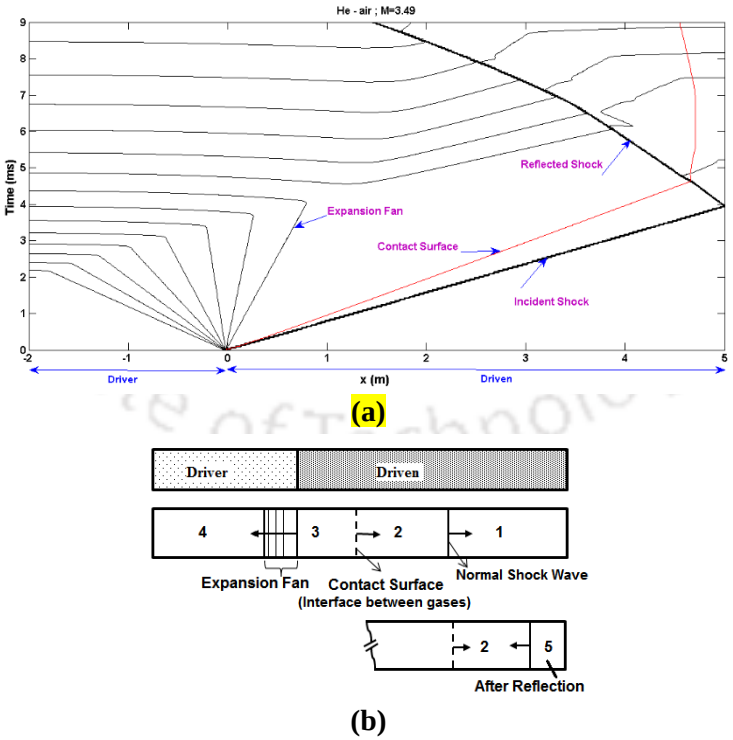

Fig. 6.1: Schematic representation of a conventional shock tube and its working principle as per the data obtained in the calibration run [*Takayama et al., 2014*]

The shock wave typically has a thickness of a few mean free paths and the compressed medium reaches its equilibrium values of pressure, density and temperature in this distance. Upon reaching the end of the tube, the incident primary shock wave reflects and travels backward. At this point, the test gas has acquired the properties corresponding to region '2'. Immediately upon the reflection from the end flange of the driven section, the gas particles have zero velocity so that the test gases are modelled as a slug of "stagnant gas" for a very short test time [*Takayama et al., 2014*]. Subsequently, when the reflected shock travels backwards, the medium (test gas) is further compressed and heated (region '5'). On the other side of the diaphragm, a series of expansion waves are initiated upon rupture of the diaphragm. They propagate towards driver section of the tube and get reflected from the end wall of the high pressure section [*Takayama et al., 2014*]. Thus, the appropriate length ratio of the driver and the driven section is maintained so that the driver gases do not contaminate the test gases during test flow durations. The test medium under sudden compressed and heated conditions (region '2' and '5') invites many interesting mechanical applications in the areas of chemical kinetics [*Bhaskaran and Roth, 2001*], ignition delay measurements for fuels [*Spadaccini and Colket, 1994*], impact assessment on structures [*Andreotti et al., 2015*] and shock assisted deformation studies [*Ray et al., 2015*].

In this backdrop, the present investigations are aimed at the development of a moderate size shock tube (7 m long, with 55 mm inner diameter) suited for a variety of interdisciplinary applications and in turn determine the stagnation heat flux by using in-house fabricated coaxial surface junction thermocouple. Measurement of stagnation point heat flux has been aimed by flush mounting a thermocouple at the driven end of the shock tube mainly by two approaches. In the first approach, the thermal sensors are flush mounted directly on the end flange, while in the second approach, the sensors are flush mounted on a hemispherical model (*radius 10 mm*) fitted at the end flange. The first technique is utilized to calibrate the shock tube and demonstrate it as an additional measurement diagnostic for calibrating the thermal sensors. Further, the second methodology is aimed at measuring the stagnation point heat using different in-house fabricated thermal sensors. Essentially, mounting of the thermocouple on the end flange would suddenly expose it to a high temperature bath created behind the reflected shock during operation of the shock tube. Such an exposure of a thermal sensor to step change in temperature is possible in very few devices like shock tube. Thus, shock tube is helpful in creating a high temperature bath for a very short duration

which can be utilized not only for measurement of stagnation heat flux but also for calibration of the thermal sensor. Hence, one can find out the maximum rate of temperature rise which it can sense by any thermal sensors. In view of this, a shock tube of 7 m long is made out of stainless steel tube of 55 mm inner diameter having a thickness of 11 mm. This chapter depicts a complete investigation towards calibration methodologies with different instrumentation and also, using in-house fabricated thermal sensors as explained in *Chapter 4* in a comprehensive and systematic manner. Further, the thermal sensors mounted on the hemispherical model fitted at the end flange of the shock tube are utilized to capture the instantaneous heat flux to get a comparative assessment of the CSJTs in the low supersonic environment.

6.2 Installation of Shock Tube

A 7 m long shock tube is made out of stainless steel with each tube having 1 m in length. The assembly is such that there are two tubes in the driver section and five tubes on the driven section respectively (*Fig. 6.2*). The longer driven section ensures the fact that the attenuation of the shock fronts does not become a major factor when it is reflected from the end wall. The inner diameter of the tube is 55 mm with a thickness of 11 mm. A metallic diaphragm mounted on the flange separates the driver and driven sections of the tube (*Fig. 6.3 and Fig. 6.4*). All the geometrical parameters for the assembly of shock tube and its part component are shown in *Fig. 6.3*. Aluminum sheet with a diameter of 100 mm, thickness 1.2 mm is used to fabricate the diaphragms for the shock tube (*Fig. 6.4*).

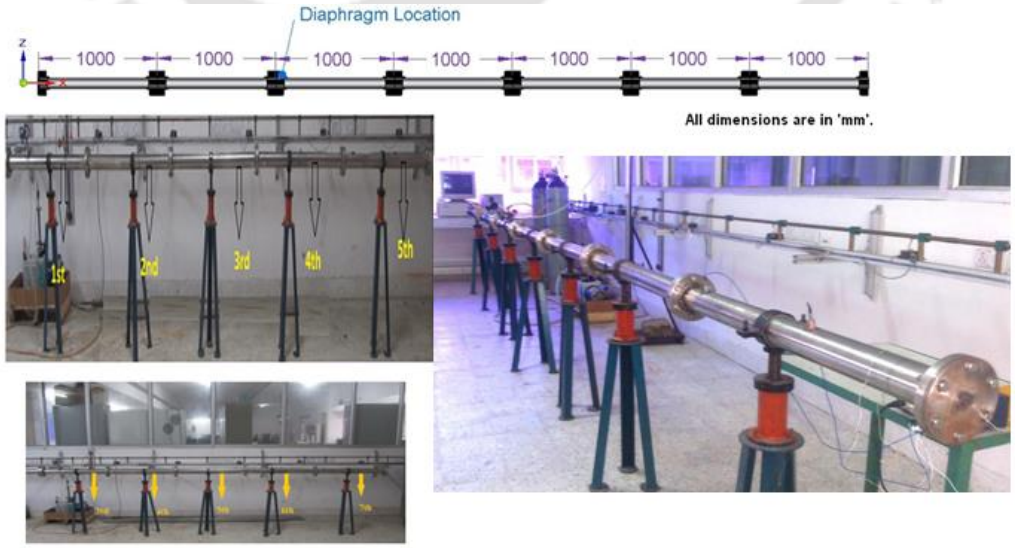

Fig. 6.2: Photograph of shock tube assembly

In order to have a controlled rupture of diaphragm and generation of the shock wave, V-grooves are made with one-third of the total thickness of diaphragm [*Takayama et al., 2014*]. It ensures the fact of localized rupture at the point with lowest stress concentration factor [*Timoshenko, 1956*]. The driver section consists of high pressure gas cylinder, pressure regulator,

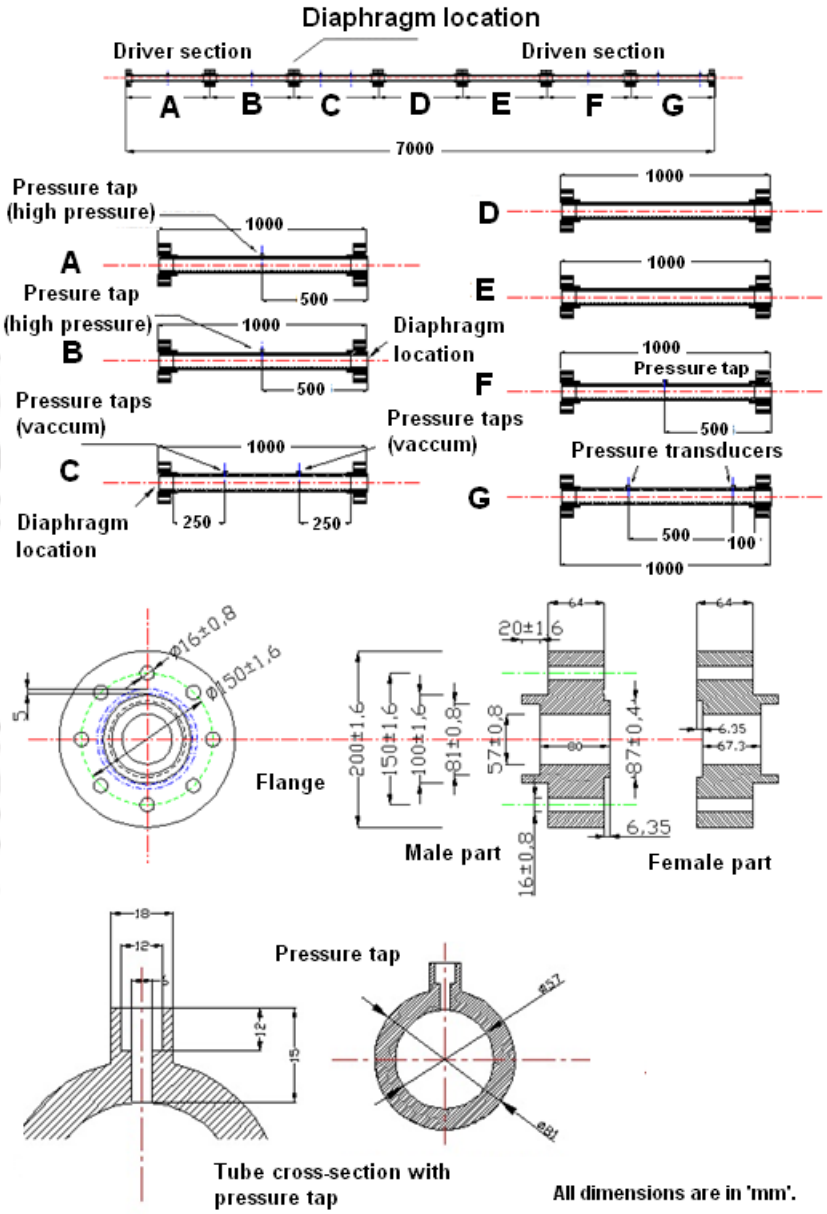

Fig. 6.3: Design and geometrical parameters for shock tube assembly

pressure gauges (analog and digital) with an adequate number of valves for regulation of gas (*Fig. 6.5-a*). It is of 2 m length to which the high pressure gas enters through a ball valve. The gas cylinder is attached to the pressure regulator so that the pressure inside the driver section and mass flow rate of the gas can be easily controlled. At the opening of the cylinder two ball

valves are placed; one for the entry of the high pressure gas inside the cylinder and other for the discharge of gas from the cylinder to the atmosphere. The driven section of the shock tube (*5 m*

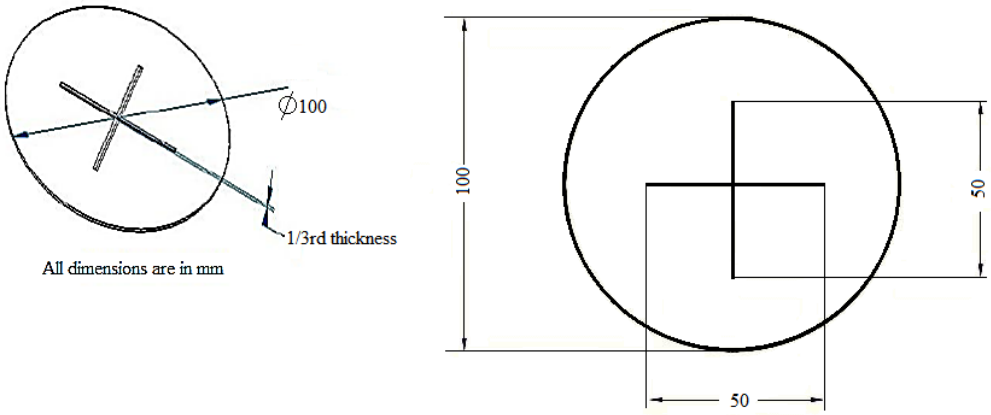

Fig. 6.4: Design of metallic diaphragm for shock tube experiments

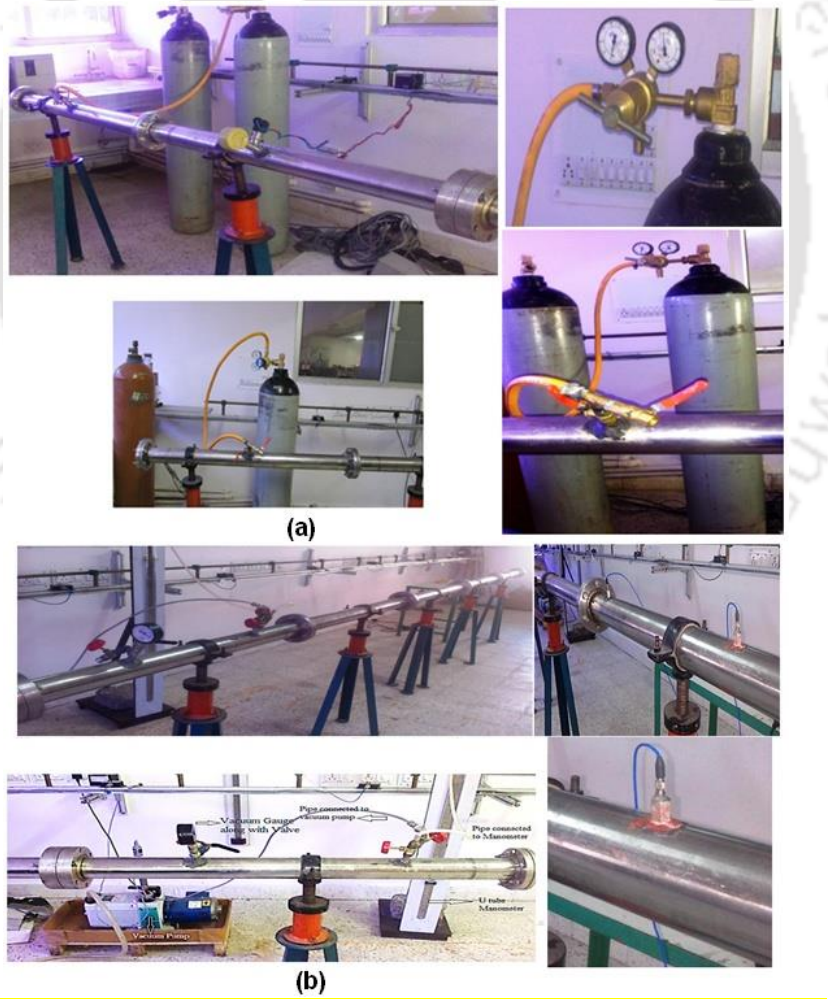

Fig. 6.5: Components of shock tube: (a) driver section; (b) driven section

long) consists of a vacuum pump (*Rotary type; ED6 series; HHV Pumps Private Ltd., Bangalore*), vacuum gauge and a U-tube manometer (*Fig. 6.5-b*). In the first tube of the driven section, there are provision of two openings, one for the connection to the vacuum pump so that low pressures can be created inside the driven section and another is connected to the vacuum gauge and a U-

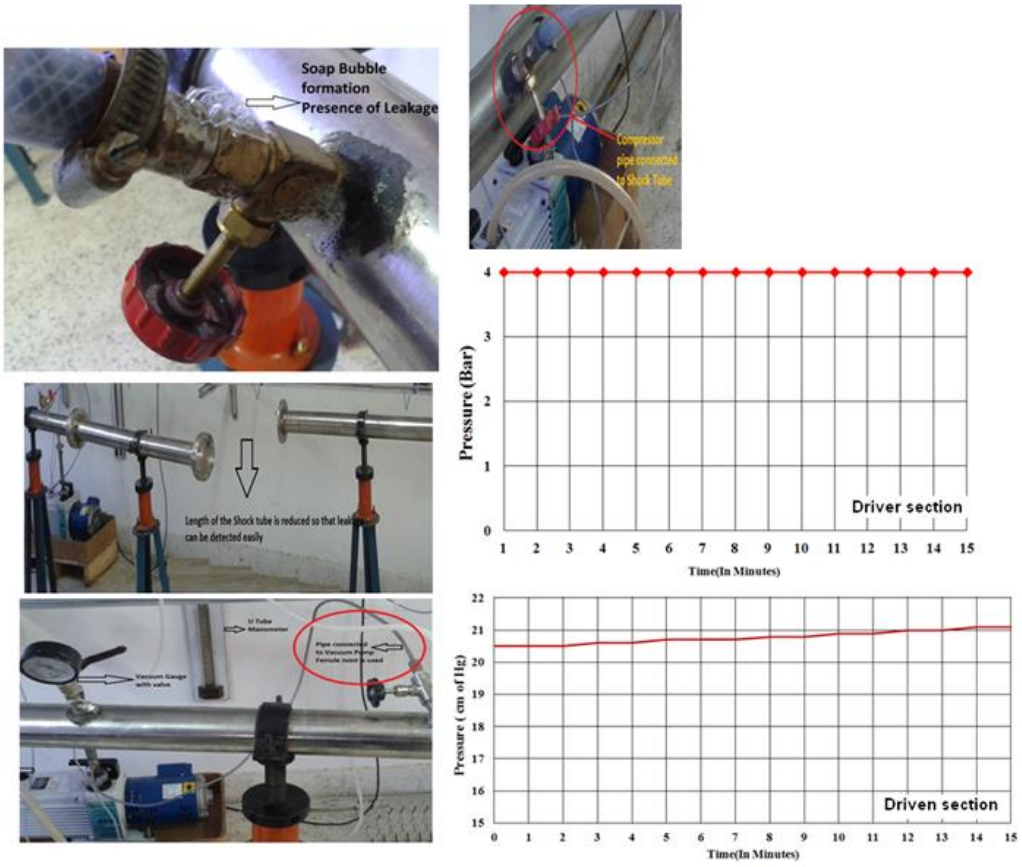

Fig. 6.6: Leakage test experiments in the shock tube

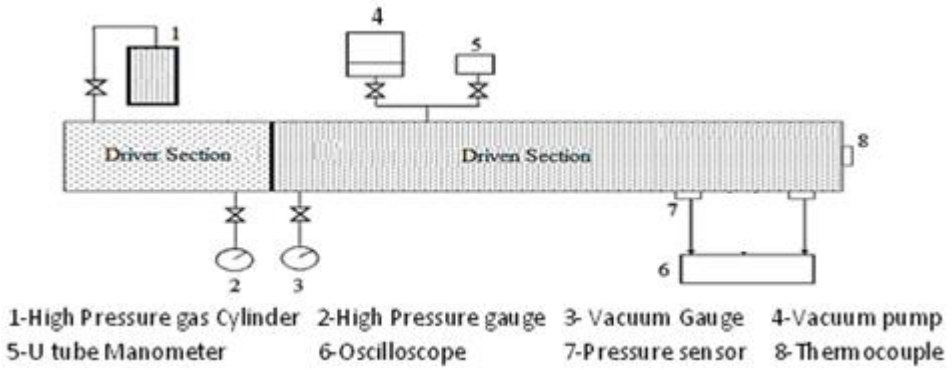

Fig. 6.7: Line diagram of shock tube with different components and its operation

tube manometer. In order to check the repeatability of the vacuum gauge is connected along with the U-tube manometer (via a T-joint). The fourth and fifth tubes are fully closed, while having

provisions of placing pressure transducers and thermal sensors. Being a low pressure region, the driven section is more prone towards leakage of atmospheric air into the tube. So, the leakage test is conducted for the shock tube in order to have complete leak-proof experiments during the test duration and its performance is shown in *Fig. 6.6*. The overview of all the instrumentation and data reduction techniques of shock tube operation is shown in the line diagram (*Fig. 6.7*).

6.3 Instrumentation for the Shock Tube

In the entire process of calibration and experiments in a shock tube, there are certain prime requirements such as maintaining appropriate pressure ratios across the diaphragm (i.e. between the driver and driven section), measuring shock speed and pressure rise across the shock waves. The driver side pressure (p_4) is monitored on the control console through a high pressure gauge as shown in *Fig. 6.5(a)*. The driven section initial pressure (p_1) is obtained through parallel measurements from a precision vacuum gauge as well as a mercury manometer. The temperatures in the driver and driven sections $(T_1$ and $T_4)$ are considered as room temperature of 25 ºC. Two pressure transducers (*PCB Piezotronics, USA; Model 113B22*) are mounted at the locations of pressure taps in the last segment of driven side of the shock tube (*Fig. 6.8*). A stainless steel holder (*1/4" BSP thread*) used over 10.8 mm length (approximately equal to the thickness of shock tube) houses the pressure transducers, thereby flush mounted with inner tube surface. The pressure sensor mounted in flush with the inner surface of the shock tube, measure the pressure jump behind primary as well as reflected shock waves due to rupture of the diaphragm. Whenever the primary shock passes over the two sensors, a step change in the voltage signals is seen in the oscilloscope (*Make: Yokogawa, having a bandwidth of 200MHz and a sampling rate of 2.5 GS/s*), corresponding to pressure jump across the shock wave (*region '2'*). Subsequently, when the shock waves reflect from the end flange of the driven section, there is a further rise in pressure (*region '5'*) because the reflected shock pass through the already elevated medium of higher pressure. The coaxial surface junction thermocouples (CSJT) are intended to capture stagnation temperature rise across the reflected shocks. In this setup, an in-house designed E-type thermal sensor (*Chapter 4*) is installed at the end of the driven tube in a specially designed end-plate attachment made out of stainless steel (*Fig. 6.9-a and Fig. 6.10-a*) . In order to mount the thermocouple, in the end- flange,

the thermocouple holders are designed so that it can be mounted in flush with the inner surface of the end flange (*Fig. 6.9-a*).

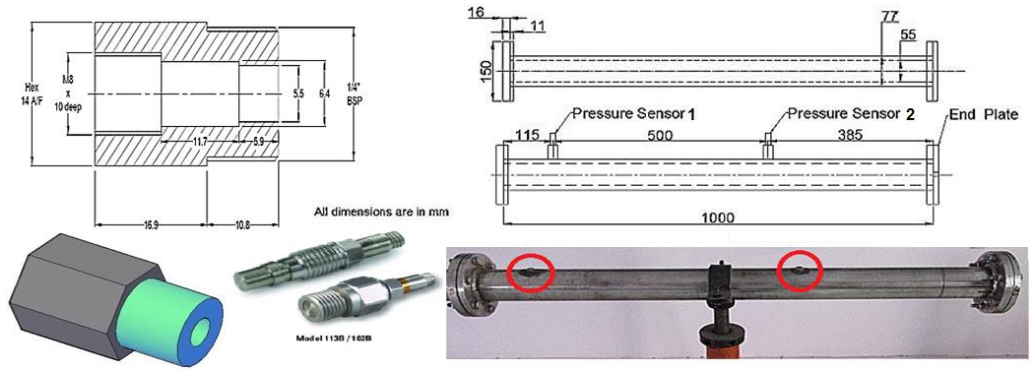

Fig. 6.8: Design, fabrication of pressure sensor holder and its mountings in the driven section of the shock tube

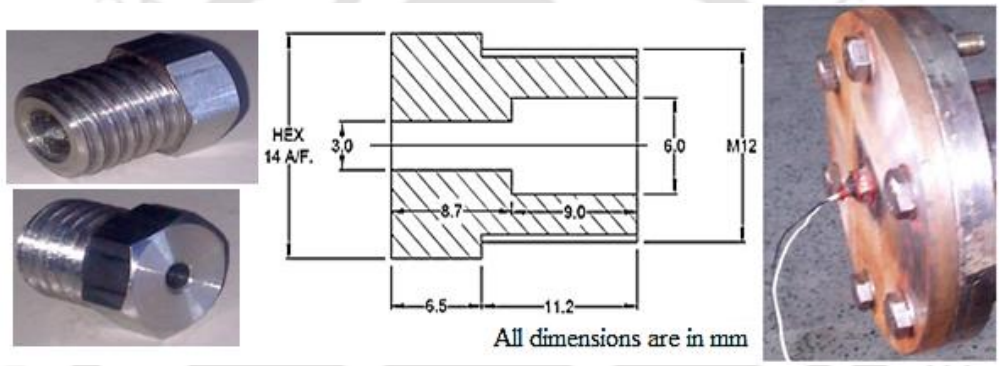

(a)

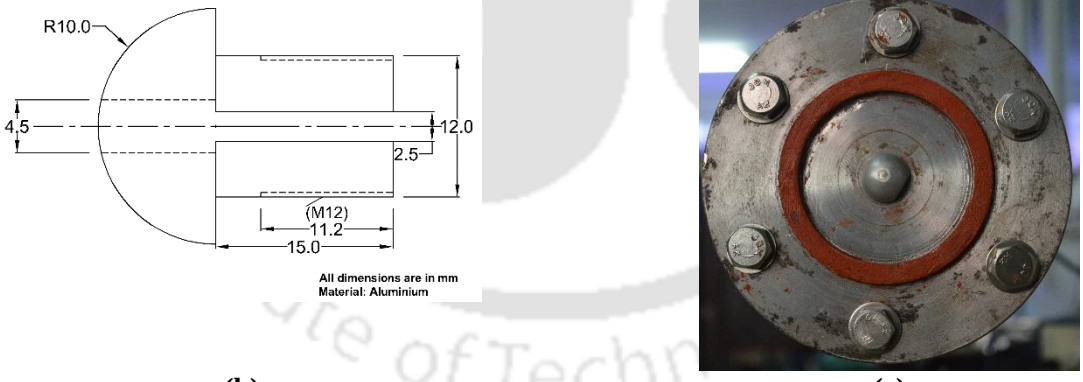

(b) **(c)**

Fig. 6.9: (a) Design and fabrication of thermocouple inserts and its mounting on the endplate of the shock tube; (b) Schematic of the hemispherical model mounted in the end flange of the shock tube; (c) End flange of the shock tube showing the mounted model

The material for thermocouple holder is also stainless steel which is similar to the pressure transducer holders. Here, a hole of 6 mm diameter and 9 mm depth is provided to hold the CSJT (*Fig. 6.9-a*). Another, 3 mm hole is provided for electrical connection from the sensing element to the amplifier of the thermocouple. The gap between the thermocouple and holder is filled by

wrapping Teflon on the thermocouple and the sensor gets insulated from the end plate of the shock tube. Once the first set of experiment is completed, few in-house thermal sensors namely, E, T and J-types respectively as elaborated in *chapter 4*, are utilized to capture the stagnation point heat flux (*Fig. 6.10-b*). A hemispherical model of 10 mm radius with 25 mm overall length is chosen to house the thermal sensor for measuring the stagnation point heat flux as explained in *Fig. 6.9-b*. For the case of the hemispherical model, the thermal sensor is flush mounted on the hemisphere model, which is fitted on the end flange of the shock tube. The schematic and the mounting assembly for the thermal sensors in the end section of the shock tube are shown in *Fig. 6.9-b* and *Fig. 6.10-b* respectively. Normally, CSJT works on the principle of "Seebeck effect" in which a voltage signal is produced corresponding to a temperature change at the surface junction. Thus, for capturing this time varying signal, the CSJT is instrumented with a voltage amplifier (*INA 128; Techno Science Instruments; Bangalore*) with adequate gain factors (in this case 500).

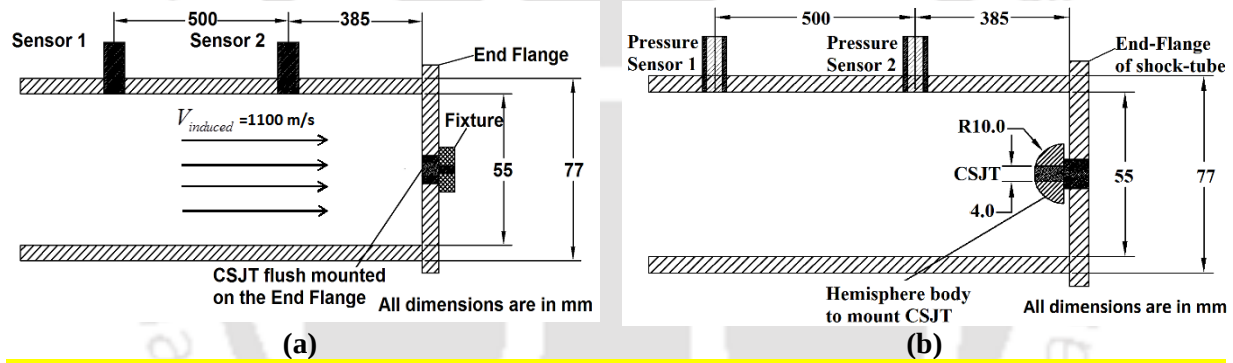

Fig. 6.10: Schematic of the shock tube section showing the mounting assembly of the CSJT (a) onto the end-flange of the shock tube; (b) over a hemispherical model

6.4 Calibration of Shock Tube

The constant area shock tube is a laboratory tool that creates a plane shock wave by the sudden rupture of diaphragm separating the high (*driver*) and low (*driven*) pressure region of the tube. When the diaphragm suddenly bursts, the high pressure gas rushes into the low pressure test gas. It induces a series of compression and expansion waves that propagate into driven and driver section of the shock tube. The compression waves travelling towards low pressure region coalesce to form a strong normal shock while a series of expansion waves travel to the high pressure region (*Fig. 6.1*). At the same time, the interface between the test gas and driver gas also travels into the low pressure section. When the shock wave reaches the end of a tube, it gets reflected from the end flange and travelling back into the driven section. The gas between the shock wave and the interface is the "test gas" with high pressure, temperature and velocity with respect to the tube as

a consequence of string moving shock. This moving slug of the gas column at high temperature and pressure can be used as impulsive heat/force for simulating aerodynamic flow fields. However, the test duration for such uniform flow is limited to few milliseconds. Since shock waves can be generated under controlled conditions, many analogous natural occurring phenomena related to shock-associated/shock wave physics can be simulated experimentally by using "shock tube" as a laboratory tool. Because of simplicity and low cost of operations, shock tube is treated as a unique laboratory tool for many other engineering applications as well. Prior to its usage in practical applications, the performance of the shock tube needs to be evaluated with respect to its ideal behaviour.

6.4.1 Shock tube relations

The ideal behavior of a shock tube is predicted through *one-dimensional Rankine-Hugonoit* relations [*Anderson, 2004*]. Considering the shock tube sketched in *Fig. 6.1*, where the high pressure gas having specific heat ratio (γ_4) is separated from low pressure gas with specific heat ratio (γ_1) by a diaphragm.

$$\frac{p_2}{p_1} = 1 + \frac{2\gamma_1}{\gamma_1 + 1}\left(M_s^2 - 1\right);\ \frac{T_2}{T_1} = \frac{1 + \left(\frac{\gamma_1 - 1}{\gamma_1 + 1}\right)\frac{p_2}{p_1}}{1 + \left(\frac{\gamma_1 - 1}{\gamma_1 + 1}\right)\frac{p_1}{p_2}} \tag{6.1}$$

$$\frac{T_2}{T_1} = \frac{1 + \left(\frac{\gamma_1 - 1}{\gamma_1 + 1}\right)\frac{p_2}{p_1}}{1 + \left(\frac{\gamma_1 - 1}{\gamma_1 + 1}\right)\frac{p_1}{p_2}} \tag{6.2}$$

$$\frac{p_4}{p_1} = \left(\frac{p_2}{p_1}\right)\left[1 - \frac{\left(\gamma_4 - 1\right)\left(a_1/a_4\right)\left(\frac{p_2}{p_1} - 1\right)}{\left(\sqrt{2\gamma_1}\right)\left(\sqrt{\left(2\gamma_1\right) + \left(\gamma_1 + 1\right)\left(\frac{p_2}{p_1} - 1\right)}\right)}\right]^{\frac{-2\gamma_4}{(\gamma_4 - 1)}} \tag{6.3}$$

$$u_2 = u_3;\ p_2 = p_3;\ a_1 = \sqrt{\gamma_1 R_1 T_1};\ a_4 = \sqrt{\gamma_4 R_4 T_4} \tag{6.4}$$

$$\frac{p_5}{p_1} = \left[\frac{2\gamma_1 M_s^2 - \left(\gamma_1 - 1\right)}{\left(\gamma_1 + 1\right)}\right]\left[\frac{-2\left(\gamma_1 - 1\right) + M_s^2\left(3\gamma_1 - 1\right)}{2 + M_s^2\left(\gamma_1 - 1\right)}\right] \tag{6.5}$$

$$\frac{T_5}{T_1}=\left(\frac{\left[2(\gamma_1-1)M_s^2+3-\gamma_1\right]\left[(3\gamma_1-1)M_s^2-2(\gamma_1-1)\right]}{(\gamma_1+1)^2 M_s^2}\right) \tag{6.6}$$

$$\frac{M_R}{M_R^2-1}=\frac{M_s}{M_s^2-1}\sqrt{1+\frac{2(\gamma_1-1)}{(\gamma_1+1)^2}\left(M_s^2-1\right)\left(\gamma+\frac{1}{M_s^2}\right)} \tag{6.7}$$

The shock tube's performance is entirely based upon the pressure ratios (p_4/p_1) and the ratio of speeds of sound (a_4/a_1) for the driver and driven section. Referring to the notations used for various regions of shock tube at different time instants (*Fig. 6.1*), the mathematical expressions for calculating pressure and temperature rise across primary shock $(p_2/p_1$ and $T_2/T_1)$, pressure and temperature rise across reflected shock $(p_5/p_1$ and $T_5/T_1)$, reflected shock Mach number (M_R), can be expressed as a function of primary shock Mach number (M_s).

6.4.2 Experimental procedure for shock tube operation

Initially, an aluminium diaphragm of 1.2 mm thickness separates the driver and driven section of the shock tube (*Figs. 6.11 (a-b)*). Since the strength of the shock increases with increase in the ratio of speeds of sound, it is desirable to have a driver gas with a low molecular weight.

Conversely, driven gas should have high molecular weight. So, the strongest shock wave is obtained by using a heavy driven gas and a light driver gas. While meeting these requirements, the present investigation is aimed for two driver gases (*nitrogen and helium*) with air in the driven section of the shock tube. At the beginning of the experiment, the pressure inside the driven section (p_1) is maintained at *0.18* bar and all the valves are closed. The driver section (p_4) is filled with nitrogen/helium through a high pressure cylinder and the diaphragm ruptures at a pressure of approximately *20* bar. The sudden rupture of the diaphragm (due to the pressure difference between the driver and driven section of the tube) creates a shock wave that propagates into the driven section. The critical factor in designing the V-groove on the diaphragm plays an important role during the rupture process as shown in *Fig. 6.11*. If the diaphragm does not rupture instantaneously, then it leads to the only formation of compression waves as observed in *Figs. 6.11(c-e)*. Studies have shown that most often the crack in the diaphragm starts at the center and

spreads to the edges [*Takayama et al., 2014*]. Therefore, the gas flow starts as a jet initially followed by a subsequent mass flow of driver gas after the petal like complete rupture of the

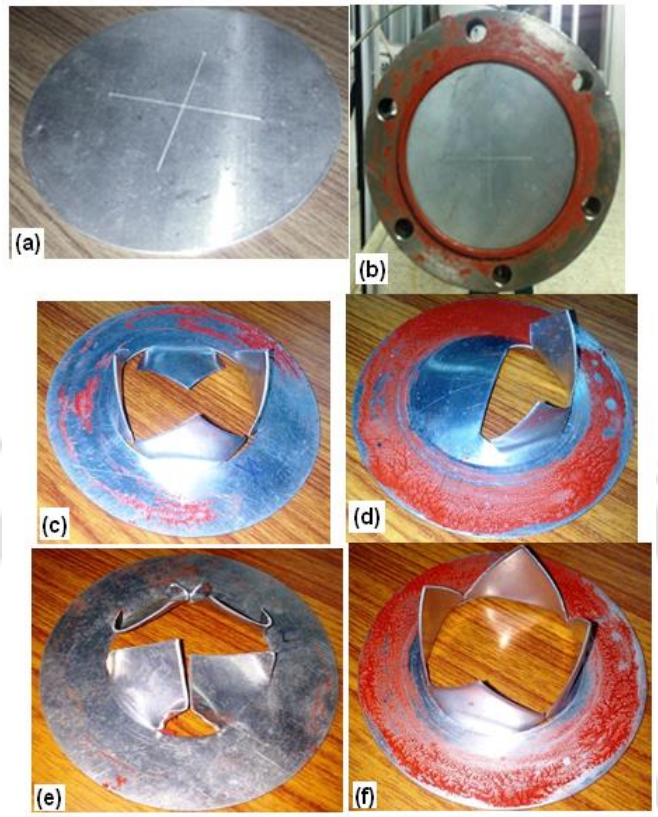

Fig. 6.11: Diaphragm rupture process in the shock tube

diaphragm (*Fig. 6.11-f*). Often this controlled nature of diaphragm rupture resembles the formation of shock wave as a consequence of coalescence of series of compression waves. The sudden rise

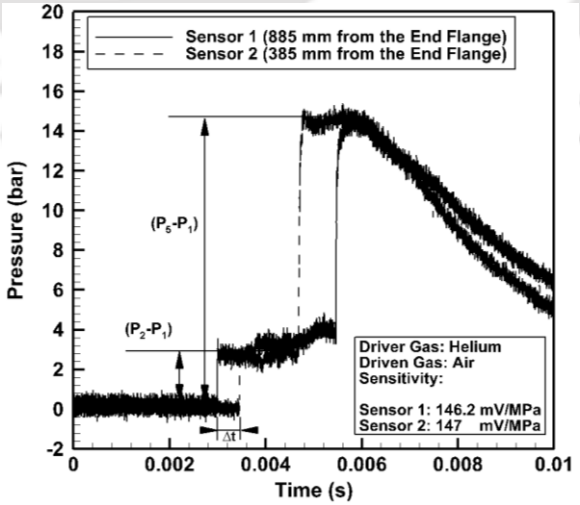

Fig. 6.12: Pressure rise across primary and reflected shock in the shock tube

in pressures across the shock wave induces mass motion of the driven gas (air). The primary shock gets reflected from the end plate, thus forming the reflected shock. The pressure jumps across the primary as well as a reflected shock are captured from the pressure transducers mounted at the last segment of the driven tube in the form of voltage signals (*Fig. 6.5-b*). The typical voltage signal is noted from the pressure sensor with 'nitrogen/helium' as driver gas and 'air' as driven gas. Based on the 'sensitivity' information as supplied by the manufacturer, the pressure rise across the primary and reflected shocks are measured (*Fig. 6.12*). With the knowledge of the distance between the pressure taps (ΔS) and the time taken by the shock waves (Δt) to travel this distance (obtained from pressure signals) as shown in *Fig. 6.12*, the speed of sound in the "region 1" (a_1), the shock wave velocity (V_s) and the experimental shock Mach number $(M_{s,e})$ can be calculated from *Eq. (6.8)*.

$$V_s = \frac{\Delta S}{\Delta t};\quad a_1 = \sqrt{\gamma R T_1};\quad M_{s,e} = \frac{V_s}{a_1} \tag{6.8}$$

Table 6.1: Comparison of shock Mach numbers between analytical calculations and experiments

Sl. No.	M_s		(p_2/p_1)		(p_5/p_1)		(T_2/T_1)		(T_5/T_1)	
	Theory $(M_{s,t})$	Exp. $(M_{s,e})$	Theory $(p_2/p_1)_t$	Exp. $(p_2/p_1)_e$	Theory $(p_5/p_1)_t$	Exp. $(p_5/p_1)_e$	Theory $(T_2/T_1)_t$	Exp. $(T_2/T_1)_e$	Theory $(T_5/T_1)_t$	Exp. $(T_5/T_1)_e$
	Driver Gas: **Nitrogen**; Driven Gas: **Air** $p_1 = 0.18$ bar; $\gamma_1 = 1.4$; $\gamma_4 = 1.4$; $R_1 = 287$ J/(kg.K); $R_4 = 297$ J/(kg.K)									
1	2.42	2.24	6.66	6.38	27.53	28.31	2.04	1.90	3.34	2.98
2	2.38	2.17	6.44	6.31	26.16	29.51	2.02	1.84	3.25	2.84
3	2.39	2.26	6.51	5.85	26.50	22.92	2.03	1.91	3.28	3.01
4	2.42	2.23	6.69	6.01	27.71	29.06	2.06	1.89	3.35	2.96
5	2.43	2.26	6.72	6.18	27.85	24.92	2.07	1.91	3.36	3.0
	Driver Gas: **Helium**; Driven Gas: **Air** $p_1 = 0.18$ bar; $\gamma_1 = 1.4$; $\gamma_4 = 1.66$; $R_1 = 287$ J/(kg.K); $R_4 = 2077$ J/(kg.K)									
6	3.68	3.49	15.63	11.53	89.65	82.84	3.56	3.30	6.78	6.17
7	3.65	3.34	15.43	8.96	88.14	67.99	3.53	3.10	6.70	5.71
8	3.52	3.35	14.26	12.50	79.62	76.03	3.33	3.12	6.25	5.76
9	3.62	3.42	15.11	11.36	85.83	75.92	3.48	3.20	6.58	5.95
10	3.67	3.22	15.59	16.73	89.34	76.03	3.56	2.95	6.76	5.37

Further, the theoretical shock Mach number $(M_{s,t})$ is obtained from initial pressure ratios (p_4/p_1) across the diaphragm using *Eq. (6.3)*. The *detailed parametric analysis is available in Appendix B*. With helium and nitrogen as driver gases (*region '4'*) and air as driven gas (region '1'), the

comparative assessment of shock Mach numbers $\left(M_{s,t} \text{ and } M_{s,e}\right)$ is obtained from both the methods (*Table 6.1 and Fig. 6.13*). Using the values of $M_{s,t}$ and $M_{s,e}$, one-dimensional shock tube relations (*Eqs. (6.2-6.7)*) have been used to compute the theoretical and experimental values of pressure and temperature ratios across both primary shock $\left[\left(p_2/p_1\right) \text{ and } \left(T_2/T_1\right)\right]$ and reflected shock $\left[\left(p_5/p_1\right) \text{ and } \left(T_5/T_1\right)\right]$. These values are calculated for five set of experiments for both nitrogen (N_2) and helium (He) as driver gas and the comparative behaviours are given in *Table 6.1* and *Figs. 6.14(a-b)*).

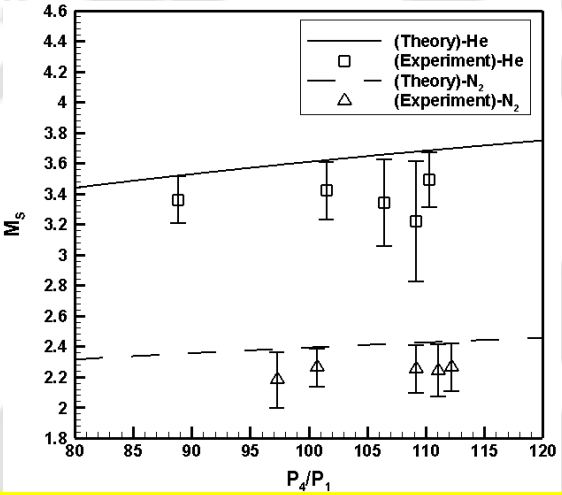

Fig. 6.13: Comparison of shock Mach numbers (experiment and theory) as a function of pressure ratio $\left(p_4/p_1\right)$

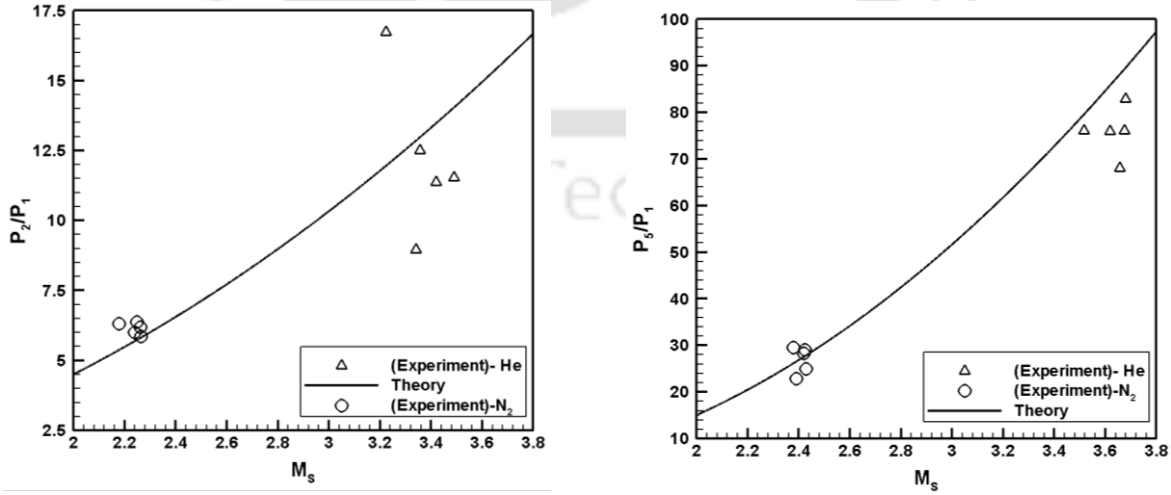

Fig. 6.14: (a) Pressure rise across primary and reflected shocks as a function of shock Mach numbers

Upon reaching the end flange of the driven tube, the shock wave gets reflected at much lower speed than the primary shock. With the knowledge of primary shock Mach number $\left(M_{s,t} \text{ and } M_{s,e}\right)$, it is possible to calculate the reflected shock Mach numbers $\left(M_{R,t} \text{ and } M_{R,e}\right)$

Table 6.2: Calculation of shock tube parameters using Nitrogen and Helium as driven gas

Sl. No.	$P_4\,(bar)$	P_4 / P_1	M_S		M_R	
			Theory	Exp.	Theory	Exp.
	Driver Gas: **Nitrogen**; Driven Gas: **Air** $p_1 = 0.18$ bar; $\gamma_1 = 1.4$; $\gamma_4 = 1.4$; $R_1 = 287$ J/(kg.K); $R_4 = 297$ J/(kg.K)					
1	19.65	109.17	2.42	2.25	1.97	1.37
2	17.51	97.28	2.38	2.18	1.91	1.35
3	18.13	100.72	2.39	2.26	1.93	1.39
4	19.99	111.05	2.425	2.24	1.98	1.43
5	20.2	112.22	2.429	2.26	1.99	1.41
	Driver Gas: **Helium**; Driven Gas: **Air** $p_1 = 0.18$ bar; $\gamma_1 = 1.4$; $\gamma_4 = 1.66$; $R_1 = 287$ J/(kg.K); $R_4 = 2077$ J/(kg.K)					
6	19.856	110.31	3.68	3.49	2.25	1.95
7	19.167	106.48	3.65	3.34	2.24	2.29
8	15.995	88.861	3.52	3.36	2.22	1.85
9	18.271	101.51	3.62	3.42	2.24	2.50
10	19.65	109.17	3.67	3.22	2.25	1.76

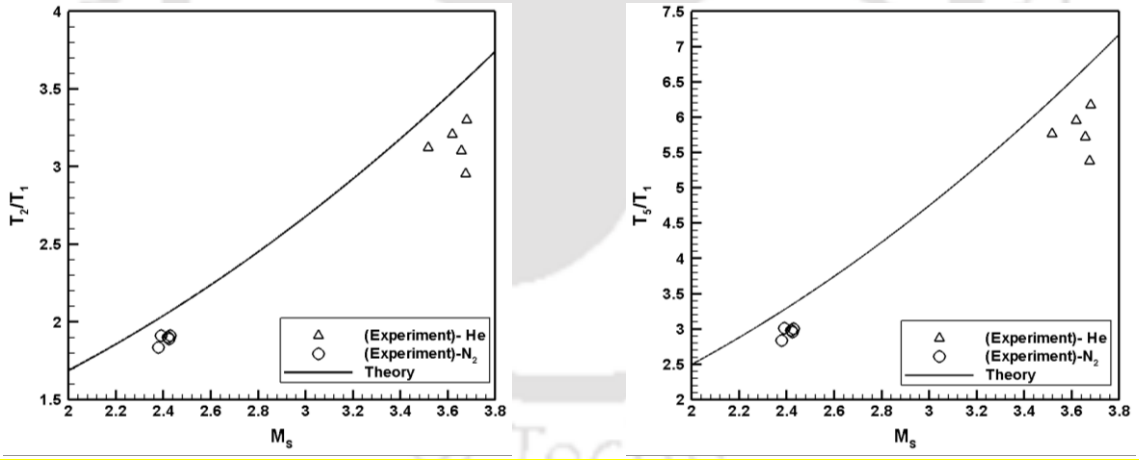

Fig. 6.14: (b) Temperature rise across primary and reflected shocks as a function of shock Mach numbers

by using *Eq. (6.7)*. The values of $M_{R,t}$ and $M_{R,e}$ are given in *Table 6.2*, while the trend of the plot is shown in *Fig. 6.15*. In addition, the percentage of deviation for each of the measured and calculated parameter of the shock tube is illustrated in *Table 6.3*. All these calibration curves (*Fig. 6.13, Figs. 6.14 (a-b) and Fig. 6.15*) show a reasonably good agreement (within *± 12 %*) between the theory and experiments for nitrogen driver. However, the deviation seems to be higher for

helium driver in certain test cases, which may be due to its lighter weight and higher shock Mach number [*Persico et al., 2005*]. Since most of the shock tube parameters depend on the square of the shock Mach number, the deviation seems to be amplified. It may also be emphasized that material of the diaphragm and its groove also plays a critical role in the calculation of shock Mach number from the pressure ratio $\left(p_4/p_1\right)$.

Table 6.3: Percentage deviation of shock tube parameters during its calibration

Sl. No.	**Driver Gas:** Nitrogen				
	Error % of deviation from Theory				
	$\frac{\left(M_{s,t}-M_{s,e}\right)}{M_{s,t}}$	$\frac{\left(p_2/p_1\right)_t-\left(p_2/p_1\right)_e}{\left(p_2/p_1\right)_t}$	$\frac{\left(p_5/p_1\right)_t-\left(p_5/p_1\right)_e}{\left(p_5/p_1\right)_t}$	$\frac{\left(T_2/T_1\right)_t-\left(T_2/T_1\right)_e}{\left(T_2/T_1\right)_t}$	$\frac{\left(T_5/T_1\right)_t-\left(T_5/T_1\right)_e}{\left(T_5/T_1\right)_t}$
1	7.02	4.2	-2.8	6.86	10.78
2	8.4	2.01	-12.8	8.91	12.61
3	5.44	10.13	13.5	5.91	8.23
4	7.63	10.16	-4.8	8.25	11.64
5	6.95	8.03	10.52	7.73	10.71
	Driver Gas: Helium				
6	5.16	26.2	7.59	7.45	8.95
7	8.49	41.9	22.86	12.22	14.71
8	4.54	12.34	4.5	6.47	7.88
9	5.52	24.81	11.54	7.9	9.53
10	12.26	-7.31	14.89	17.08	20.51

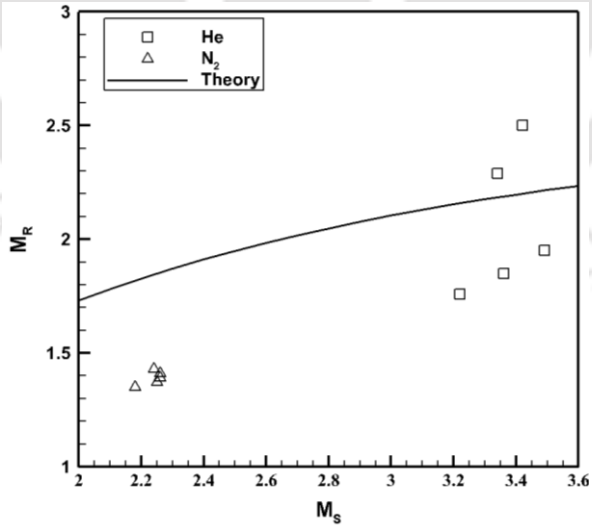

Fig. 6.15: Reflected shock Mach number as a function of primary shock Mach number

6.4.3 Stagnation heat flux measurement in the shock tube

6.4.3.1 Signal Processing

In order to mount the fabricated CSJT in the end-flange, the thermocouple holders are designed so that it can be fixed in flush with the inner surface of the end flange as discussed in *section 6.3*. During the shock tube experiments (*Fig. 6.16*), the transient rise in temperature is captured using the E-type CSJT with nitrogen and helium as the driver gases. The typical voltage-time histories and rise in temperatures $\left[T_s(t)\right]$ for three different tests are plotted in *Figs. 6.17 (a-b)* and *Figs. 6.18 (a-b)*. The surface temperature history resembles nature of 'ramp', with the rise in temperature of 4 ºC and 25 ºC, for nitrogen and helium driver, respectively. From this plot, the temperature gradient $\left(\Delta T_s/\Delta t\right)$ can be calculated as 7941 K/s and 7679 K/s with for nitrogen and helium driver, respectively. Thus, the in-house designed thermocouple is found to be capable to respond a very high rate of temperature rise. Contrarily, the rate of temperature rise felt by the sensor during static calibration is very small. Further, it is interesting to see that the rate of temperature rise resembles similar trends in experiments with Nitrogen and Helium drivers. As noted from the experimental data in *Table 6.1*, the expected temperature behind the reflected shock for nitrogen driver is 900 K while for helium driver this value is approximately 1800 K.

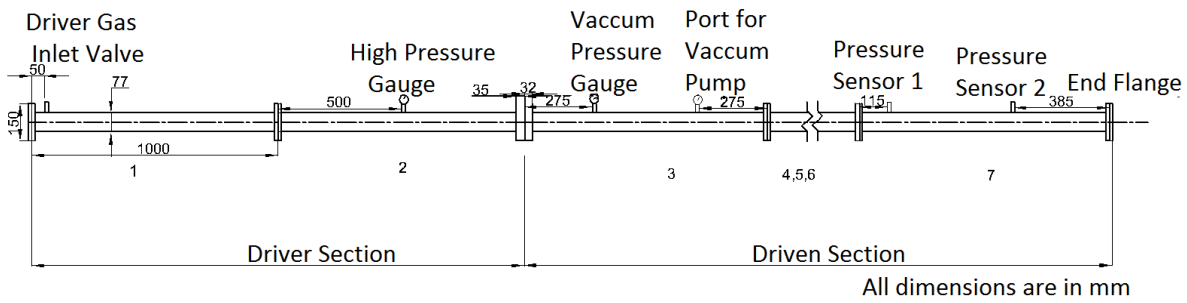

Fig. 6.16: Schematic of the shock tube facility at IIT Guwahati

Furthermore, the transient responses from the thermocouples (*Fig. 6.17 and Fig. 6.18*) depict the fact that the rate of temperature rise is independent of step height i.e. the rate of rise of temperature signal is same for both nitrogen and helium driver. After the sudden rise in temperature, in both the signals (*Fig. 6.17 and Fig. 6.18*), there is a change in slope of the temperature signal. In case of nitrogen driver, the rate of rise decreases, while in case of helium driver, rate of rise becomes negative. These alterations in the temperature signal are indications of the end of the test time in the shock tube and arrival of multiple waves and their complicated

interactions. Further, the occurrence of any interaction between different waves depends upon the shock tube driving conditions, which is accounted for the change in the pattern of the temperature signals. The interpretation of such phenomena through temperature signals from surface junction thermocouples is one of the strong outcomes of this experimental investigation.

Once the installed shock tube is benchmarked for calibration of the thermal probe, the fabricated thermal sensors as described in *Chapter 4* namely, E, T and J-types respectively are utilized to measure stagnation point heat flux using hemispherical model having a radius of 10 mm fitted at the end-flange of the shock tube as seen in *Fig. 6.10 (b).* Through the experiment, an attempt has been made to measure transient heat flux in the highly transient environment of the shock tube (*Fig. 6.16*). Attainment of thermal equilibrium between the test object and the fluid flow is not possible due to small test duration. The performance of the fabricated sensors are tested by measuring the stagnation point heat flux inside the shock-tube facility. The thermal sensor is flush mounted one by one on the hemispherical model fitted at the end-flange. The schematic of the mounting assembly is shown in *Figs. 6.9(a-b)* and *Fig. 6.10-b*. A hot shock layer is formed due to convective heat transfer on the supersonic model resulting in transient temperature rise at the model surface. An isothermal ambience was maintained during the test time by wrapping the connecting leads of the sensor and the cold junction of the thermal sensor in the hemisphere. An op-amp instrumentation amplifier (*TEXAS make, INA 128*) was used to amplify the output of the CSJT. The amplifier has a gain factor of 500 with an operating bandwidth frequency in the range of 1-40 kHz, which was sufficient for the familiarizing with the shock tube environment. The experiments are conducted using both nitrogen and helium as driver gas for all the thermal sensors (*E, T and J-type*); the typical voltage signal and rise in temperature signals (computed using sensitivity value) obtained for all the sensors are plotted in *Fig. 6.19*. The coaxial thermal sensor always gives the signal in the form of voltage as it works on the principle of Seebeck effect. A typical parabolic trend has been observed from the obtained signals, which signifies the typical case of constant heat flux of the semi-infinite theory of slab heat conduction (*Figs. 6.20(a-b)*). The experiments are conducted for three number of runs for all the thermal sensors, in order to check the repeatability of the thermal sensor.

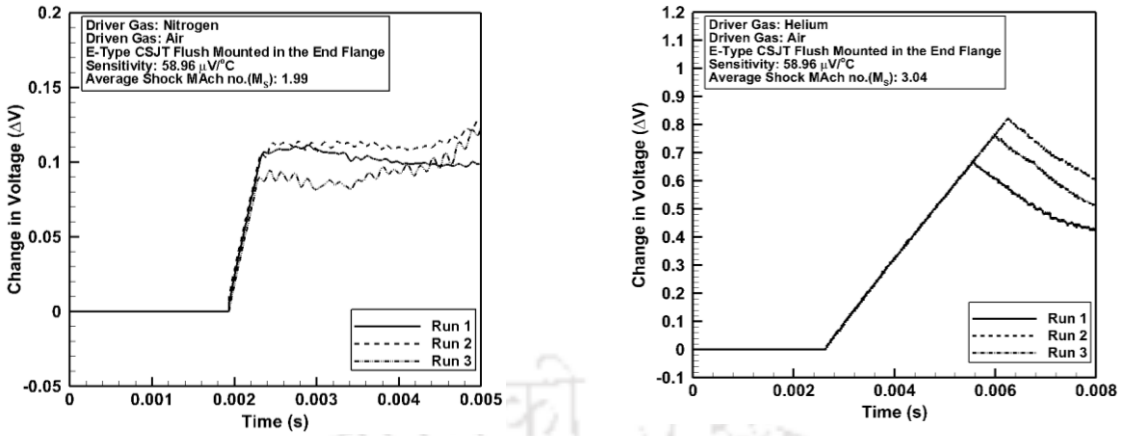

(a) **(b)**

Fig. 6.17: Typical voltage histories captured from E-type CSJT mounted on the end flange of the shock tube obtained using nitrogen and helium as driver gas

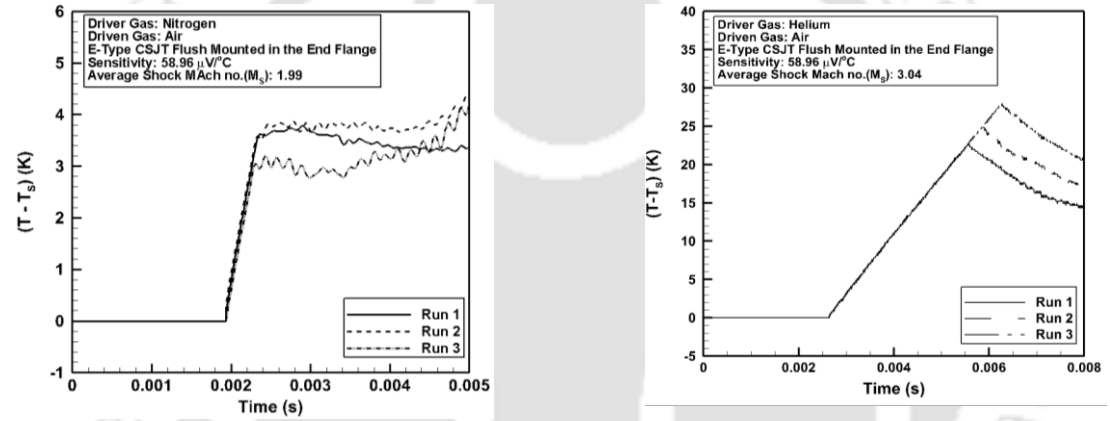

(a) **(b)**

Fig. 6.18: Typical voltage histories captured from E-type CSJT mounted on the end flange of the shock tube obtained using nitrogen and helium as driver gas

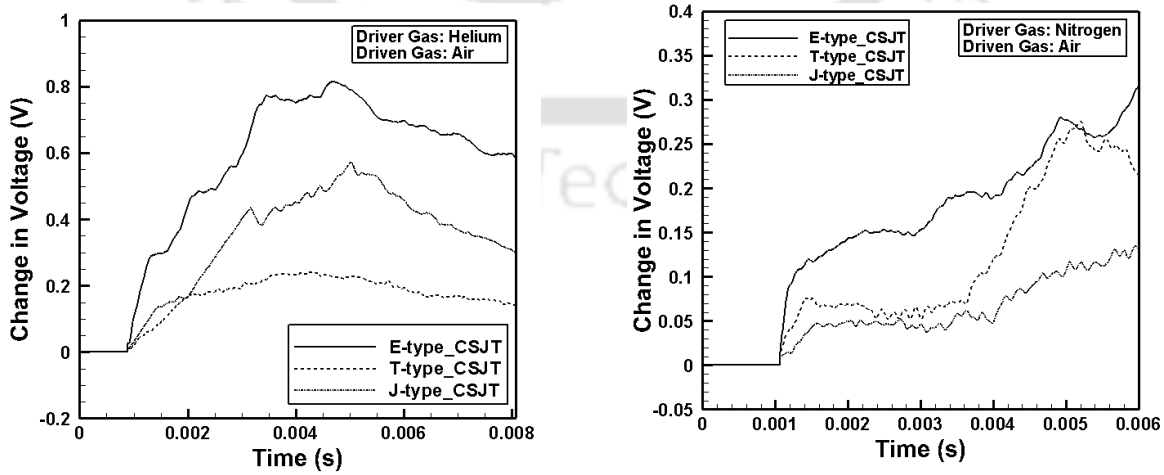

(a) **(b)**

Fig. 6.19: Typical voltage histories captured from CSJT mounted on the end flange of the shock tube

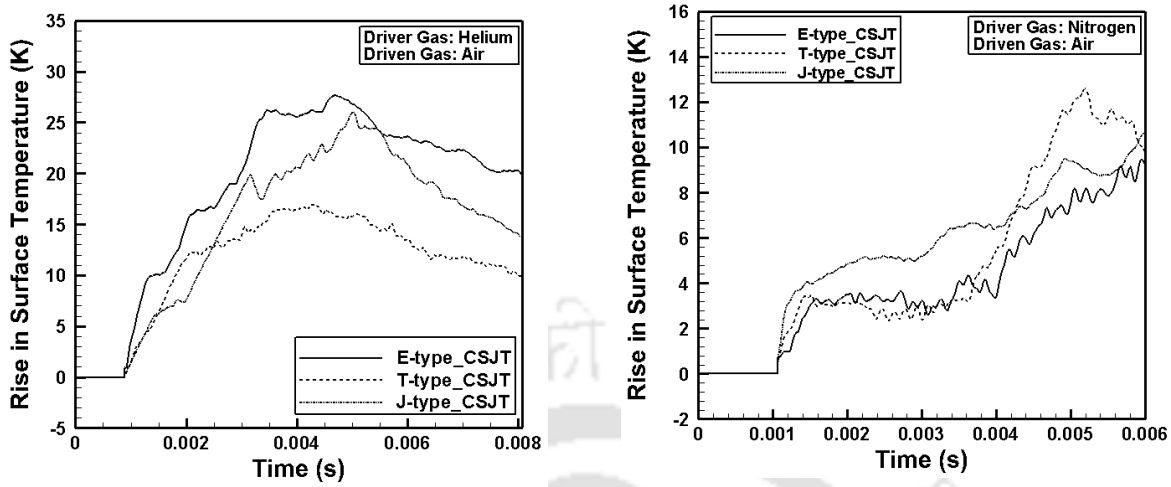

(a) (b)

Fig. 6.20: Typical rise in transient surface temperature from CSJT mounted on the end flange of the shock tube

6.4.3.2 Heat Flux Estimation

The obtained temperature signals are then used for evaluating the respective stagnation heat flux. Here, thermal properties of the substrate are treated as constant and the surface heat flux $\dot{q}_s(t)$ is calculated using Duhamel's superposition integral as explained in detailed in *chapter 3*. The surface heat flux computed by using *Eq. (3.4)*. For the present case, the thermal product is chosen from an experiment conducted as depicted in *chapter 5*. The obtained heat flux for all the tests (nitrogen and helium driver) which includes CSJT mounted as flush on the end flange as well as on the hemispherical model are plotted in *Figs. 6.21(a-b)* and *Figs. 6.22(a-b)*.

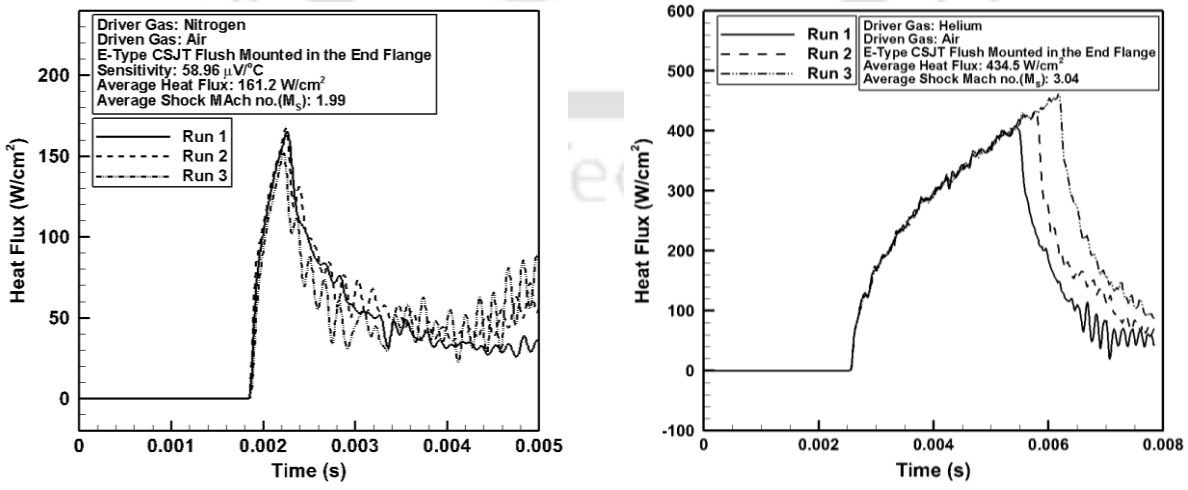

(a) (b)

Fig. 6.21: Surface heat flux histories from E-type CSJT mounted on the end flange of the shock tube

Considering *Figs. 6.21(a-b)*, similar trends of surface heat flux are seen with different peak heat flux values as, *160* W/cm^2 and *434* W/cm^2, with nitrogen and helium driver gas, respectively. This "similarity nature" in the heat flux signal can be marked as the property of the sensor since the maximum rate of temperature rise is same for both driving conditions. Further, different interactions may be responsible for the change in heat flux signal after the test time such as interaction between reflected shock and contact surface, reflected shock and expansion fan etc. Thus, present studies are found essential in evaluating the maximum rate of temperature rise for a given thermal sensor, thus considered as the property of sensing surface. In this case, the CSJT fabricated in-house has a potential of capturing highly transient phenomena of temperature rise in a shock tube. With another viewpoint, current investigations also recommend the use of shock tube as calibrating facility of any transient thermal sensors for evaluating the maximum rate of temperature rise. From the flow as captured from the hemispherical model, it is expected to form a bow shock over the model for the free stream flow. It has been observed that E and T-type thermal sensors predict the value of heat flux in close agreement with each other (*Figs. 6.22(a-b)*). *Table 6.4* gives the comparative assessment of the heat flux predicted for three number of repeated shots for all the thermal sensors. However, the J-type thermal probe slightly overpredicts the values as compared with the other two types considering both the gases (*Table 6.4*). The thermal product value of J-type CSJT could be one such reasons for the over-prediction in heat flux value. In addition, the purity in the construction process, purity of the thermocouple material etc. may also lead to the uncertainty in the heat flux values as compared to its counterparts. In continuation, a

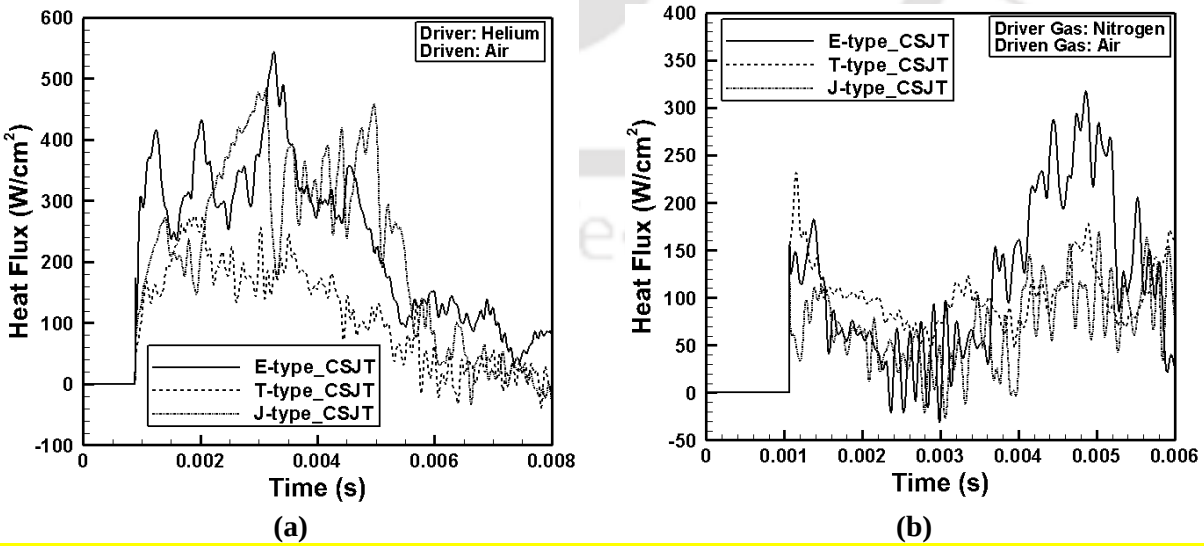

Fig. 6.22: Heat flux signal obtained from the temperature history of CSJTs flush mounted on the hemispherical model fitted at the end-flange

similarity in heat flux value with the steady region can be observed from the flow containing helium as the driver gas for all the thermal sensors. However, it is difficult to observe a similar phenomenon in case of nitrogen as driver gas. Besides to validate the obtained CSJTs results, an experiment has been conducted using Silver thin-film gauge (STFG), fabricated in-house. The brief details of the study is mentioned in *Appendix F*. The experiments using the CSJTs is justified from the heat flux value as estimated using the STFG.

Table 6.4: Comparative Chart showing the heat flux obtained using hemispherical model

Sl. No.	Types of CSJT	Experimental				
		Incident Shock Mach Number (M_S)		Average Heat Flux (W/cm^2)		Average Heat Flux (W/cm^2)
		Helium	Nitrogen	Helium	Nitrogen	STFG
1.	E	3.56	2.04	465 ± 1.8%	179 ± 3.75%	449.8
2.	J	3.55	2.38	582 ± 4.6%	232 ± 4.15%	
3.	T	3.77	2.42	445 ± 3.5%	100 ± 5%	

Further, the uncertainty analysis has been performed (based on *Appendix E*) for the calculations of shock Mach number and subsequently its effect on reflected shock Mach number, pressure and temperature ratios across primary and reflected shocks. Similarly, uncertainties for temperature measurements and heat flux calculation are also estimated during shock tube calibration. The average values of overall uncertainties for each of the parameters are given in *Table 6.5*.

Table 6.5: Uncertainty values for shock tube parameters during calibration

Shock tube parameters	Average value of uncertainty	
	Nitrogen	Helium
M_s	±0.1%	±0.11%
(p_2/p_1)	±0.19%	±0.22%
(p_5/p_1)	±1.6%	±9.17%
(T_2/T_1)	±1.97%	±2.99%
(T_5/T_1)	±2.68%	±9.23%
$T_s(t)$	±0.16%	±0.24%
$\dot{q}_S(t)$	±0.55%	±0.2%

6.5 Summary

A moderate size shock tube (7 m) has been installed successfully by measuring and estimating shock tube parameters. The parametric studies are achieved through experiments and analytical

calculations with an average deviation of ±12%. For nitrogen driver, these deviations seem to be less (within ±8%). Further, with helium driver, all the shock tube parameters are significantly high that makes it suitable for short duration application studies. Moreover, the in-house designed CSJTs help in estimating maximum rate of temperature rise and stagnation heat flux. It has been found that the maximum rate of temperature rise recorded by the E-type CJST, during a step change in temperature for a very short duration, is around 7800 K/s. This parameter is noted to be independent of the magnitude of the step; since it has been regarded as the property of the sensor. As a consequence of this fact, the nature of the heat flux signal in all the experiments is found to be similar. Further, shock tube is recommended for evaluating this constant parameter of any thermal sensor, since it can provide the necessary high temperature bath of any magnitude for a very short duration. All experimental data are accurate in the uncertainty level of ± 9 %. Most of the components and instrumentation of this shock tube are indigenously designed and fabricated. The strengths of shock waves can be substantially increased by employing driver gases with lower molecular weights (such as helium) and thicker diaphragms. The shock tube once calibrated using the CSJT, a hemispherical model of 10 mm radius is utilized to give a comparative assessment by measuring the stagnation point heat flux. The sensors were able to successfully capture the heat flux with E and T-type CSJT falling in close range to each other, with slight overprediction in value using the J-type. The jump in heat flux value can be coined in terms of the thermal product of the CSJT. Moreover, purity in thermocouple material during the preparation phase can be another reason for the disparity. Being modular in nature, the future scope of this facility development is inclined towards many interesting mechanical applications in the areas of impact assessment on structures and shock assisted deformation studies on generic models, chemical kinetics, ignition delay measurements for potential biofuels.

CHAPTER 7

Probe for Heat Flux Measurement in the Hypersonic Facility

Compendium:

The presence of high enthalpy flows over the test model for a short span of time (~ 1 ms) makes the aerodynamic environment very hostile in the test section of the hypersonic tunnel. The flow field becomes more complicated due to the presence of thin-shear layer, viscous interaction and high temperature. In such harsh environment, the heat flux measurements demand fast response probes. In these conditions, coaxial surface junction thermocouples (CSJTs) have potentials to respond faster to capture the transient temperature data during the short duration hypersonic flows in the test section of the tunnel. In previous chapter, effectiveness of CSJTs have been studied experimentally, while capturing stagnation heat fluxes with high pressures (~ 15 bar) and high density (~ 3 kg/m^3) flows prevailing at the end flange in a shock tube. Now, it is felt to extend the study in a hypersonic shock tunnel, where the flow is expanded in a nozzle that produces free stream Mach number of 8.2 with free stream pressure and temperatures of 155 Pa and 90 K, respectively, in the test section. In this Chapter, a comparative performance assessment has been made for three different surface junction probes (E, J and T-types) by exposing them in the above flow environments. The first experiment includes mounting of all the CSJTs along with Pitot tube on a hemispherical model in a single plane inside the test section of the shock tunnel. All the sensors are exposed to a slug of high enthalpy test gas prevailing for 1 ms test time. The second set of experiment encompasses a total of 9 CSJTs flush mounted over a 30° wedge at a location 4 mm, 24 mm and 44 mm respectively away from the leading edge of the body. Abreast, experimental results are complemented with numerical and analytical modellings under same flow conditions prevailing in the test section of the tunnel. The estimated surface heat flux for E and T-type CSJTs from both set of experiments are recovered well within reasonable accuracy, compared with numerical solutions. Further, the first set of experimental result for stagnation heat flux, are in comparable range with the analytical solution. Howbeit, under the prevailing short timescale of measurements in the shock tunnel, the probes are quite sensitive in capturing the transient data. Besides, the performance index (sensitivity and response time) for E-type probe are found to be 58.96 µV/ºC *and 21 µs as compared to 43.82* µV/°C and *29 µs for J-type and 28.47* µV/°C and *24 µs for T-type, respectively.*

7.1 Introduction

In short duration timescale, the capturing of transient temperature becomes challenging, which necessitates the demand for highly sensitive/fast response sensors. The survival of measuring devices becomes more critical due to the high stagnation enthalpies of such flows [*Stalker et al., 2005; Lu and Wilson, 1994*]. The test flow durations are limited to few hundreds of microseconds or even lesser than that for ground-based impulse facilities [*Morgan, 1997; Reddy et al., 1996; Rabinowicz, 1957*], due to various constraints (e.g. shock tubes/shock tunnels/expansion tubes). Concurrently, the measurement of transient surface temperature and thereafter heat transfer rate becomes commanding issues for the design of high speed flight vehicles. In many applications, the data from the ground-based impulse facilities experiments needs to be supported by the design of the heat flux sensors. Surface coating of models with encapsulated thermocronic liquid crystals [*Babinsky and Edwards, 1996; Robert and East, 1996*] is the classical approach for measuring the surface temperatures in the wind tunnel. The working principle is such that the crystal reflects depending on the detected surface temperatures and the responses are visible in the form colour based on the different temperatures. Employing temperature sensitive paints (TSP) over the surface of the model, one can also measure the transient surface temperature on the aerodynamic surfaces in the high speed facilities [*Peng et al., 2016; Liu et al., 2009; Ohmi et al., 2008; Hubner et al., 2002*]. It works on the principle of oxygen quenching of luminescence from the paint. The emitted light intensity by the paint is estimated by photo-detector and successively correlated with the variations in the transient temperatures. Of lately, a typical preference to capture the short duration transient surface temperatures is the use of nickel/platinum thin film gauges (TFGs), the response time of which falls in the range of ~1 μs with a typical thickness of the order of few micrometers [*Sarma, 2017; [1]Sarma et al., 2016; [2]Sarma et al., 2016; Kumar and Sahoo, 2012*]. The base metals in the form of paste/ink supported on an insulating substrate constituent the basic methodology of these sensors [*Kumar et al., 2011; Sahoo et al., 2005; Jagadeesh et al., 2000; Stewart and Chen, 1994*]. The sensor when energized by a suitable power source, the resistance of the base metal changes with temperature. During shock tunnel experiments, the thin film gauges loses its adequate resistance because of the unexpected heat loads. These phenomena make frequent replacement of the sensors making it unwieldy affecting the accuracy and repeatability of measurements. In nutshell, being the residues of paints, all the measuring techniques become prone to wear and tear on the sensing surface on the impact of the high speed test gases.

A surface junction probe instead of the metal-insulating substrate combination can overcome the limitations as described in the previous section. Underlining the need for imminent short duration time scale measurements and severe test flow conditions in impulse facilities, the surface junction probes are preferred candidates for capturing transient temperature as compared to other techniques. The response time of such sensors is in comparable range with TFGs [*Kumar and Sahoo, 2013; Kumar et al., 2011; Menezes and Bhat, 2010; [3]Mohammed et al., 2010; Mohammed et al., 2008; Sanderson and Sturtevent, 2002*]. The probes are generally prepared from the metallic elements known as "coaxial surface junction thermocouple (CSJT)". The sensing element in a CSJT is a surface junction is of few micron thicknesses, while it is only a point junction in case of conventional thermocouple [*Chapter 1*]. The fabrication of CSJT involves two metallic elements through a surface junction formed using the grinding process. The small-scale plastic deformation of the junction allows the fast response characteristics and makes it suitable for short duration transient study [*Desikan et al., 2016; Irimpan et al., 2015; Mohammed et al., 2010; Mohammed et al., 2008*]. In continuation, the changes in the temperature in the high speed flow correspond to the voltage change across the metallic elements can be suitably captured by the data acquisition system. The ability to flush mount on the model surfaces being the distinct feature of the CSJT. The design trait and methods of fabrication of different types of thermocouples have been discussed in the open literature [*Li et al., 2017; Anbuselvan and Reddy, 2016; Desikan et al., 2016; Kumar and Sahoo, 2013; Menezes and Bhat, 2010; Mohammed et al., 2008; Sanderson and Sturtevent, 2002*]. With a perspective of measuring surface temperature history on aeroan dynamic bodies in a shock tunnel facilities, an E-type (chromel-constantan) and K-type (chromel-alumel) CSJTs have been employed separately [*Menezes and Bhat, 2010; Mohammed et al., 2010; Sanderson and Sturtevent, 2002*]. Nonetheless, the effective comparisons of different types of CSJTs in shock tunnel flow with simultaneous exposure to high temperature slug of test gases can provide a better insight about the surface junction probe's characterization (such as response time, prediction of surface heat flux). Indeed, knowledge of these parameters is very imperative for a factual estimate of surface heat flux and they are seldom tackled in the reported literature. In the current work, an effort has been made to delve into different types of surface junction probes and address their comparative performances in shock tunnel experiments. Simultaneously, the probes experience step heat loads and the corresponding transient temperature responses are noted to address their comparative performances.

Considering the above arguments, the study intends towards characterization (sensitivity, thermal product and response times) and thereafter predicting surface heat fluxes using different types of surface junction probes (*E-type, T-type and J-type*). All the probe sees a Mach flow of 8.2 in the test section of the hypersonic shock tunnel, having a test time of nearly 1 ms. Two number of experiments have been carried out. The first experiment consist of hemispherical models mounted in a rake assembly flush mounted with a pitot tube and three different types of CSJTs, which are mounted in a single plane inside the test section. The probes experience a step rise of heat loads within the test flow duration. The second experiment includes measurement of low heat flux on a flat plate inclined at 30º (compression ramp) using coaxial thermal probes in the hypersonic flow environment of shock tunnel. Furthermore, once estimating the leading edge heat flux, it has been thought of to study the impact of high speed flow at different x-location over the compression corner using few more thermocouples. Basically, for re-entry vehicles, compression ramp represents the two-dimensional inlets and deflected control surfaces [*Marini, 2001; Kendall, 1957*]. A unique flow pattern for shock wave boundary layer interaction studies can be observed on the compression ramp flows when it is encountered by hypersonic flow environment. Therefore, to obtain an optimum design, it is very much essential to grasp the knowledge of various flow phenomenon encountered by such geometries. Prior to the shock tunnel testing, the sensitivity of each thermocouple (i.e. the variation of voltage with respect to temperature) is determined through the calibration experiments (Chapter 4). The transient temperatures from shock tunnel experiments are recorded from each probe and subsequently surface heat fluxes are obtained through one-dimensional heat conduction analysis. Simultaneously, the experimental surface heat fluxes obtained from stagnation point from all the probes are compared with analytical expressions. In addition, the results from both the experiments are compared numerically with the in-house developed solver. The details of shock tunnel experiments and computation studies are described in the subsequent section.

7.2 Experiments in Shock Tunnel

In Impulsive facilities such as shock tunnel, the test gas flow in the test section only for a few milliseconds or even lesser. Considering this, the surface junction probes must have a fast response time as well it should be suitable for the rapidly varying flow conditions. Hence, the CSJTs should be able to withstand such destructive high stagnation enthalpies test flow environment and be able

to shred information on the transient temperatures captured within the short test window [*Schultz and Jones, 1973*]. The present investigation serves the utilization of three CSJTs namely, E-type (chromel-constantan), T-type (copper-constantan) and J-type (iron-constantan) for experiments in a shock tunnel. The constantan wire (*0.8128 mm in diameter*) is used as an inner material for all the CSJTs, while chromel/copper (*3.25 mm diameter*) and iron (*2.5 mm diameter*) being the outer material (*Fig. 4.1-a and Figs. 4.1 (c-d)*). In continuation, the thorough fabrication and sensitivity calibration methodology of the CSJTs has been elaborated in *Chapter 3* and *Chapter 4* respectively.

7.2.1 Test Facility

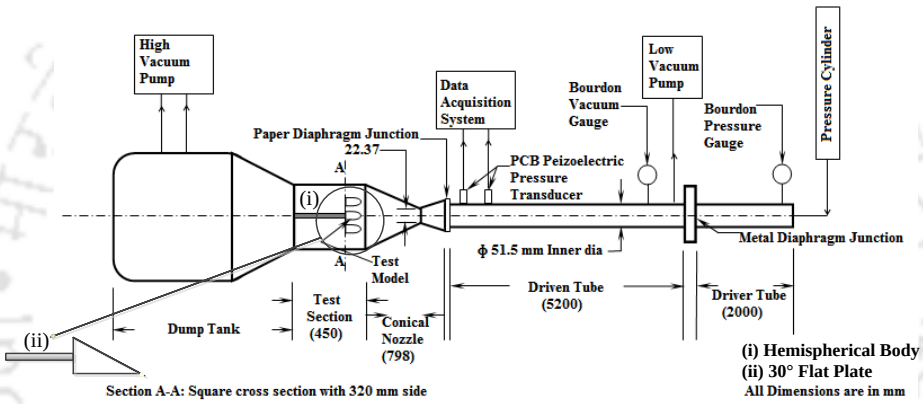

Fig. 7.1: Hypersonic shock tunnel experimental facility

The high speed flow experiments are carried out in the hypersonic shock tunnel facility of IIT Bombay (*Fig. 7.1*). The temperature probes experiences step heat loads at high stagnation enthalpies from the test gas with a flow Mach number of 8.2. The *shock tube section* separated by a paper diaphragm (Miler paper) with a converging-diverging nozzle, followed by a rectangular test section (*300 mm × 300 mm cross-section and 450 mm long*) and a dump tank (*1 m diameter*) attached to the highly efficient multi-stage vacuum pump (*up to* 10^{-6} *mbar*) constitute the major assembly of the shock tunnel facility. The shock tube section of the tunnel has a driver (*high pressure*) and a driven (*low-pressure region*) section separated by a metallic diaphragm (*aluminium alloy of 1.2 mm thickness*). The operation of the tunnel is such that the driver section is pumped with high pressure gas (*helium*) so that the metallic diaphragm ruptures suddenly. Thus, generating a shock wave that propagates into the driven section of the tube, compressing the test gas (*air*) inside it. Subsequently, the test gas gets heated due to the sudden rise in temperature across the shock wave. Once the test gas reaches the end of the driven section, the primary shock

encounters reflection and propagates back into a medium, where the test gas is already at elevated temperature and pressure. This leads to further enrichment of the temperature and pressure of the test gas. As the gas motion behind the reflected shock is almost zero, the slug of the test gas in the driven section experiences a momentary reservoir of high temperature and pressure. As a result the paper diaphragm (Miler paper) rupture and the complete slug of test gas experiences expansion in the nozzle, establishing a free stream flow (*Table 7.1*) in the test section for a typical time duration of 1 ms. *Figure 7.1* highlights the schematic of the hypersonic shock tunnel facility of IIT Bombay, with all its dimensions along with the mounting assembly of both test models in the test section.

Table 7.1: Free stream flow conditions in the test section of the shock tunnel

Mach no. (M_∞)	**Static pressure** P_∞ (Pa)	**Static temperature** T_∞ (K)	**Unit Reynolds number,** $\mathrm{Re}_\infty\,(\mathrm{m}^{-1})$	**Stagnation enthalpy** (MJ/kg)
8.2 ± 2.5%	155 ± 5%	90 ± 3%	$(1.48 \times 10^6) \pm 1\%$	1.41 ± 3%

7.2.2 Test Model and Instrumentation

The determination of shock speed, nozzle supply pressure and effective time duration of the slug of the gas passing over the test model are some of the key diagnostic characteristics in the shock tunnel. To enable the measurement of primary shock speed and reservoir/nozzle supply pressure, two pressure transducers (*Model: 102A08, Make: PCB Piezotronics, USA*) are mounted *505 mm* apart at the end part of the driven section. Another transducer in the form of pitot tube is mounted in the test section to measure the test gas flow pressure history. The study comprises of two separate experiments with same free stream conditions. The first test model involves 4 number of the hemispherical model (made out of brass) of radius 12.2 mm and length 35 mm mounted in a rake assembly with their leading edges in the same vertical plane at the exit of the nozzle (*Fig. 7.2-a*). The hemispherical models are flush mounted with three CSJTs and a pitot sensor. As specified by the manufacturer, the pitot probe has a response time of the order of 1 µs. Further, it ensures the fact that all the CSJTs and the Pitot probe encounters same test flow conditions at the same time during the experiments. Moreover, the dimensions of the rake are chosen such that all the measurements are performed in the core flow regions of the test gas. The latter part of the experiment includes a flat-plate/wedge-body (*made of brass*) inclined at an angle of 30^o. Three number of CSJTs (*E-type, T-type and J-type*) are aligned flush mounted on the surface at a particular *x*-location with 4 mm away from the leading edge of the plate (*Fig. 7.2-c*). Rest of the

CSJTs are housed on the surface of the wedge at a distance of *24 mm* and *44 mm* away from the leading edge. Thus, every x-location encompasses all the three CSJTs as shown in *Fig. 7.2 (c)*.

In the first case, considering the experimental flow conditions and geometrical shape of the hemispherical model, a bow shock appears for a Mach number of 8.2. As a result, there is a sudden rise in temperature leading to a significant increase in surface heat flux in the vicinity of surface junction probes [*Anderson, 2004; Anderson, 2000*]. Hence, the hemispherical model housing the CSJTs may also be called as "stagnation probe". Likewise, for the second case, considering the geometrical shape of the test model, an oblique shock appears for a Mach number of 8.2 measuring the peak heat flux at the sharp leading edge of the wedge. During the test time, an isothermal ambience has been maintained by wrapping the connecting leads of the sensor and the cold junction of the thermal sensor in the hemisphere as well as in the wedge. The output obtained from all the thermal sensors (*E, T and J-types*) have been amplified using an op-amp instrumentation amplifier (*INA 128*). The amplifier (*Appendix: Fig. C.4*) has a gain factor of 500 with an operating frequency bandwidth in the range of 1-40 kHz, which is found to be sufficient for amplifying the voltage signals in the shock tunnel flow environment (typically *1 kHz* frequency). After suitable amplification, all the signals from the sensors are acquired using a PC-based data acquisition system armed with *NI-PCI-6115 S-series* cards. The card has a sampling rate of about 1 MS/s. The acquired signals are further post-processed through a 4^{th} order IIR low-pass filter having a cut-off frequency of about 10 kHz.

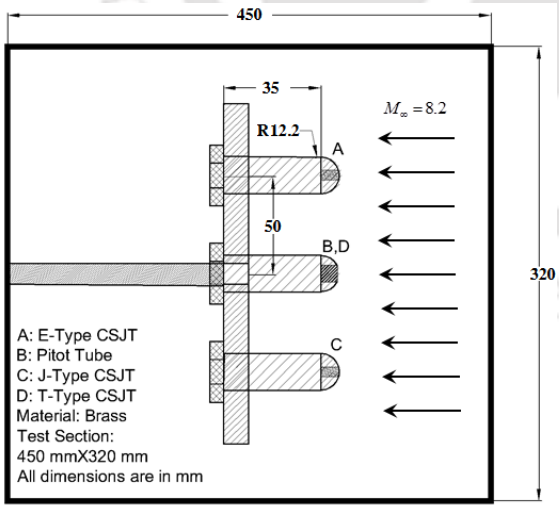

(a)

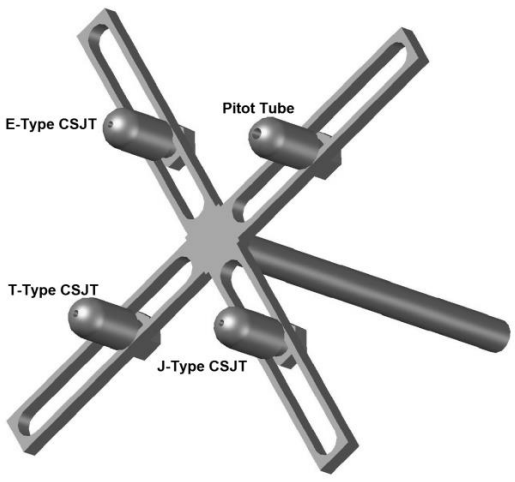

(b)

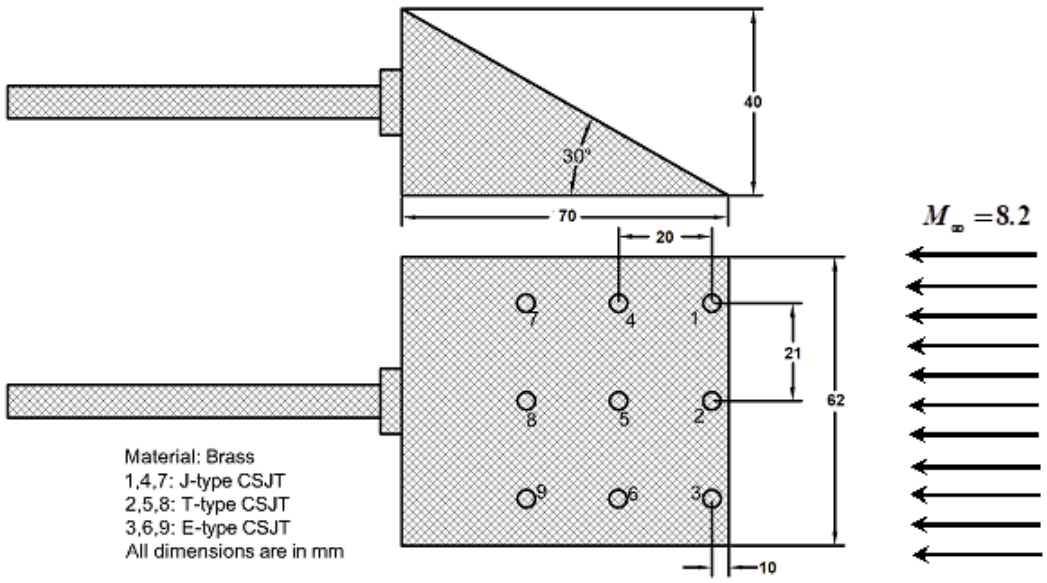

(c)

Fig. 7.2: Hemispherical model housing surface junction probes and pitot pressure transducer for shock tunnel experiments: (a) geometrical details; (b) photograph of the rake; (c) schematic of the 30º inclined flat plate

7.2.3 Experimental Data Interpretation

7.2.3.1 Hemispherical Body

The measurement of transient responses from the pitot probe and the surface junction thermal probe helps one to ascertain the quality of free stream flow in the test section at Mach number of 8.2.. For the hemispherical model, considering the free stream flow (*Table 7.1*), a bow shock appears over the hemispherical body [*Anderson, 2004*]. A normal shock behaviour is found along the axis of each probe such that the Pitot probe experiences a stagnation pressure drop across the shock. *Figure 7.3(a)* shows the effective test duration of the flow inside the tunnel signified by the time during which the Pitot signal remains steady (~1 ms). The same plot also highlights the typical time histories of the surface temperature change $\left[T_s(t)\right]$ recorded from the surface junction probe (*Fig. 7.3-c*) so that the experimental data can be interpreted during the test flow duration. The entire signal follows a parabolic trend depicting the quintessential characteristics feature of thermal sensors in shock tunnel flows. By correlating the time domain for Pitot probe and thermal probes, it is found that the "response time" of all the surface junction probe is in the range of few microseconds (*Table 7.2*). Since all the sensors are mounted in a single plane (*Fig. 7.2-b*) and keeping the Pitot probe as a benchmark reference sensor, the response time of each CSJTs are calculated (E-type: *21 μs*; J-type: *29 μs*; T-type: *24 μs*) using the time lag as shown in *Fig. 7.3(b)*.

These times seems to be adequate for ultra-short duration experiments [*Desikan et al., 2016; Srinivasan et al., 2016; Irimpan et al., 2015*]. In continuation, the parabolic trend of the voltage history from surface junction probes is observed with almost similar time domain from the Pitot history. This evidence rationalizes the usability and applicability of CSJTs for recovering transient temperature change during microsecond time scale in hypersonic flow environment. With the knowledge of "sensitivity" of each probe (*Table 7.2*), the temperature rise experienced by the thermocouples during the test time is plotted in *Fig. 7.3(c)*. From this plot, the temperature gradient $\left(\Delta T_s/\Delta t\right)$ is obtained as, *1779 K/s* (E-type) and *1951 K/s* (T-type) and *1862 K/s* (J-type). It justifies the fact that microscopic thickness of surface junction (*~ 20-24 µm* as per *Irimpan et al., 2015*) probes have adequate thermal inertia on shock tunnel flow time scales. Besides, the calorimetric principle of heat flux gauges is utilized for surface heat flux prediction, as the thermal penetration of heat into the probe is negligible during the shock tunnel experimental time scale [*Taler, 1996; Schultz and Jones, 1973*]. Nonetheless, during the test time, the actual temperature rise is only in the range of *3 K* to *5.5 K*, despite the test gas temperature being *1780 K* at the stagnation point.

Table 7.2: Characteristics and performance indicators for surface junction probes

Tunnel Characteristics (based on Pitot signal, *Figs. 7.3 (a-b)*): Test Time= 1 ms				
Types of CSJT	**Materials and size**	**Thermal product [*Chapter 5*] ($Jm^{-2}s^{-1/2}K^{-1}$)**	**Sensitivity [*Chapter 4*] (µV/°C)**	**Response time [*Fig. 7.4-b*] (µs)**
E	Chromel (outer element; 3.25 mm diameter) Constantan(inner element; 0.813 mm diameter)	8452	59	21
J	Iron (outer element; 2.5 mm diameter) Constantan (inner element; 0.813 mm diameter)	9585	44	29
T	Copper (outer element; 3.25 mm diameter) Constantan (inner element; 0.813 mm diameter)	7046	28	24

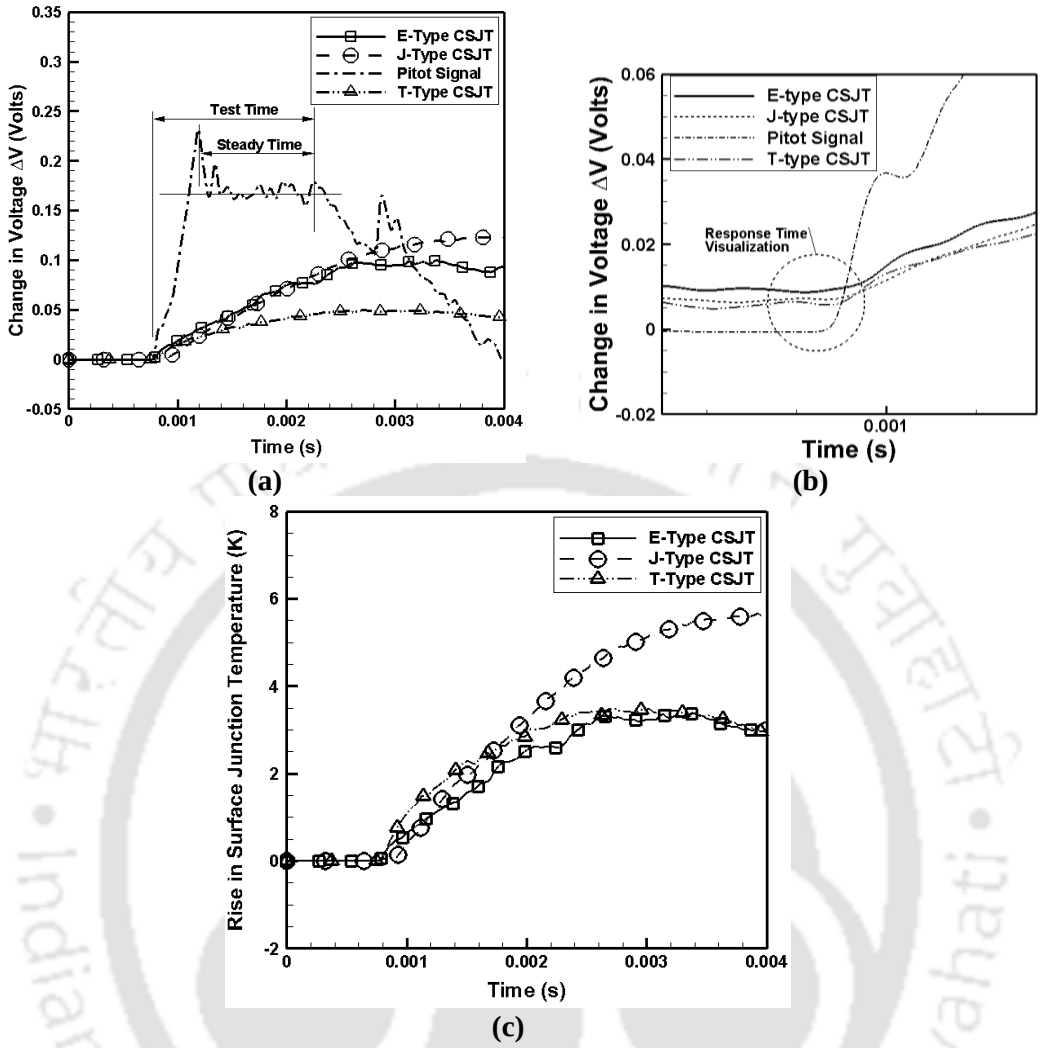

Fig. 7.3. (a) The voltage signal from Pitot transducer and thermal probe during shock tunnel experiments; (b) Enlarged view of voltage signals of CSJTs and pitot transducer; (c) Rise in surface temperature history from surface junction probes

7.3.2.2 Wedge Body Experiments

Considering the second test model (*Fig. 7.2-c*), for the same free stream test conditions (*Table 7.1*), an oblique shock is formed at the leading edge of the wedge body [*Anderson, 2004*]. The experiments have been planned in such a way that at three different *x*-locations on the wedge body heat flux history could be studied (*Fig. 7.2-c*). The objective of the experiment is to study the flow physics around the wedge body by acquiring the heat flux value. For the given flow conditions as depicted in *Table 7.1*, all the thermal sensors have been able to capture the desired signals. However, the sensor at location 9 (E-type), failed to capture the signal, which is due to the problem in the instrumentation. The acquired signal from the thermal probes at 4 mm, 24 mm and 44 mm away from the leading edge respectively, are shown in Figs. 7.4-7.6.

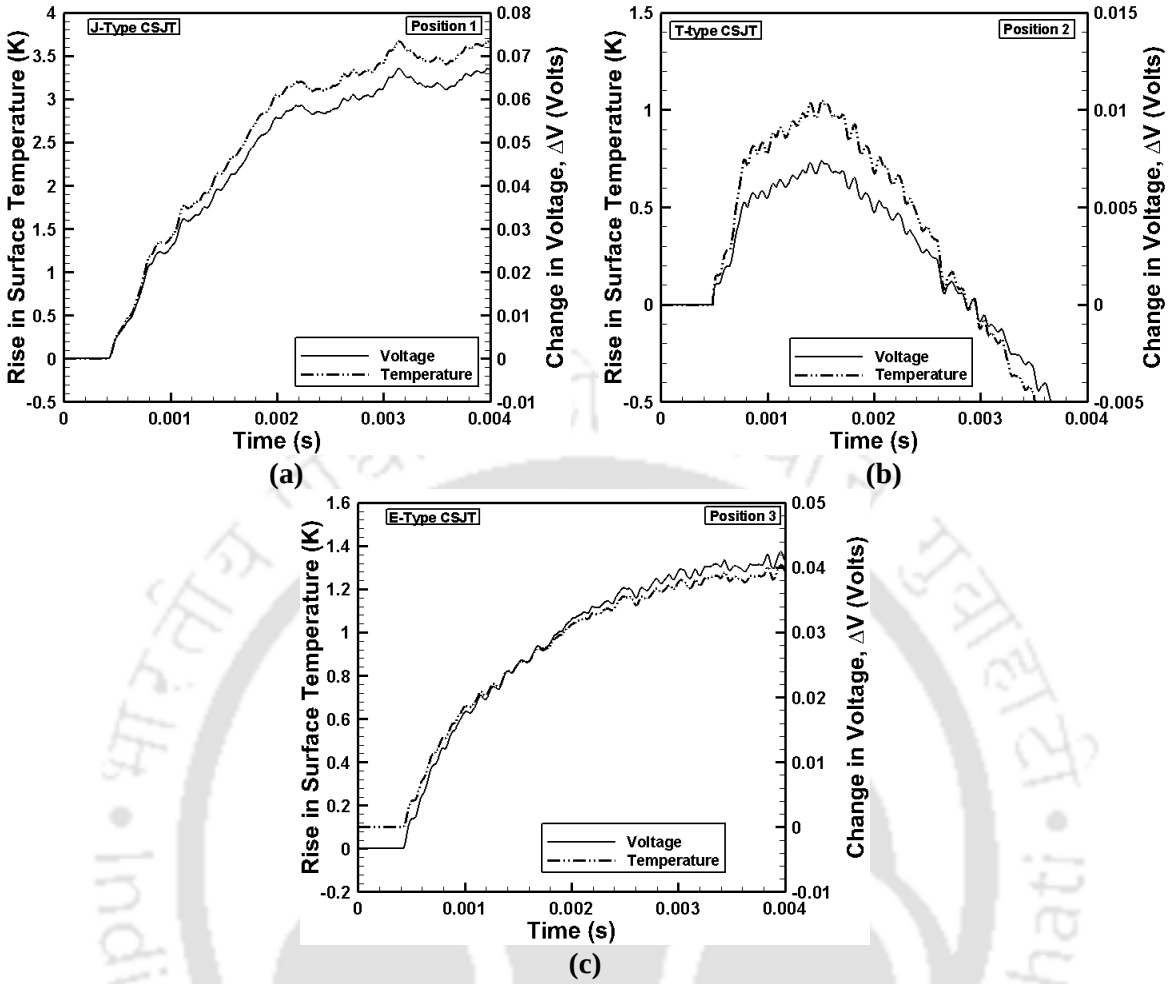

Fig. 7.4 Signal captured from the wedge shape body at 4 mm away from the leading edge of the body using (a) J-type, (b) T-type, and (c) E-type CSJTs

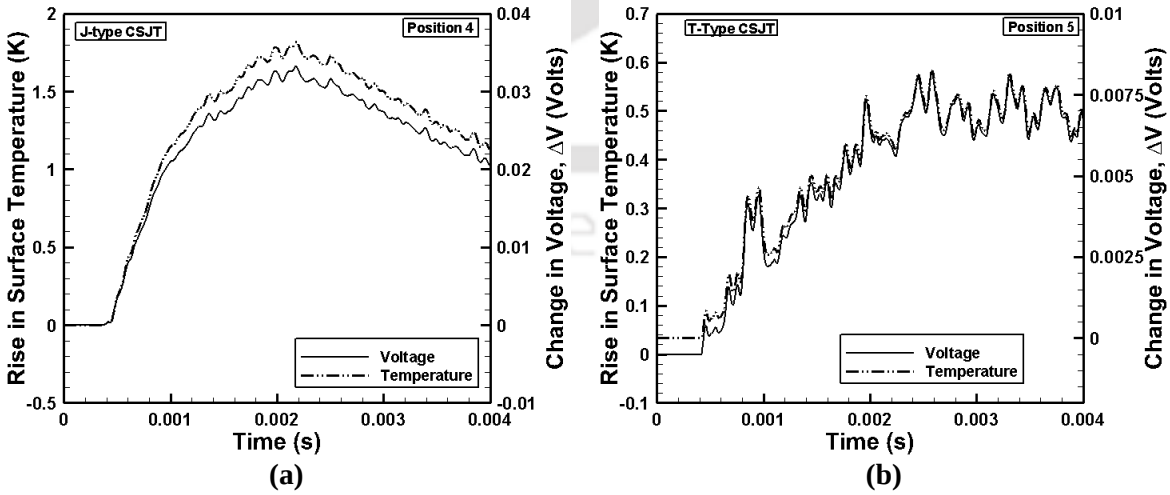

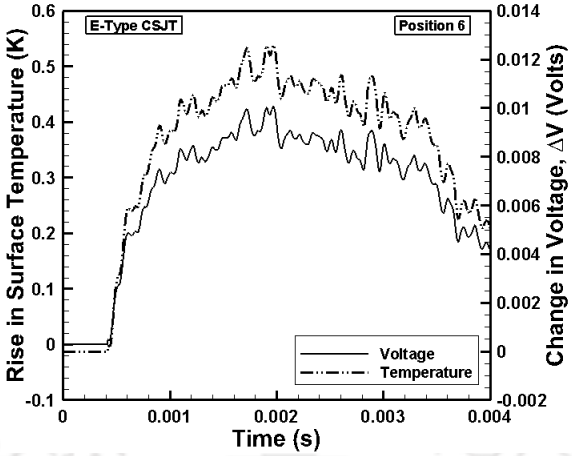

(c)

Fig. 7.5: Signal captured from the wedge shape body at 24 mm away from the leading edge of the body using (a) J-type, (b) T-type, and (c) E-type CSJTs

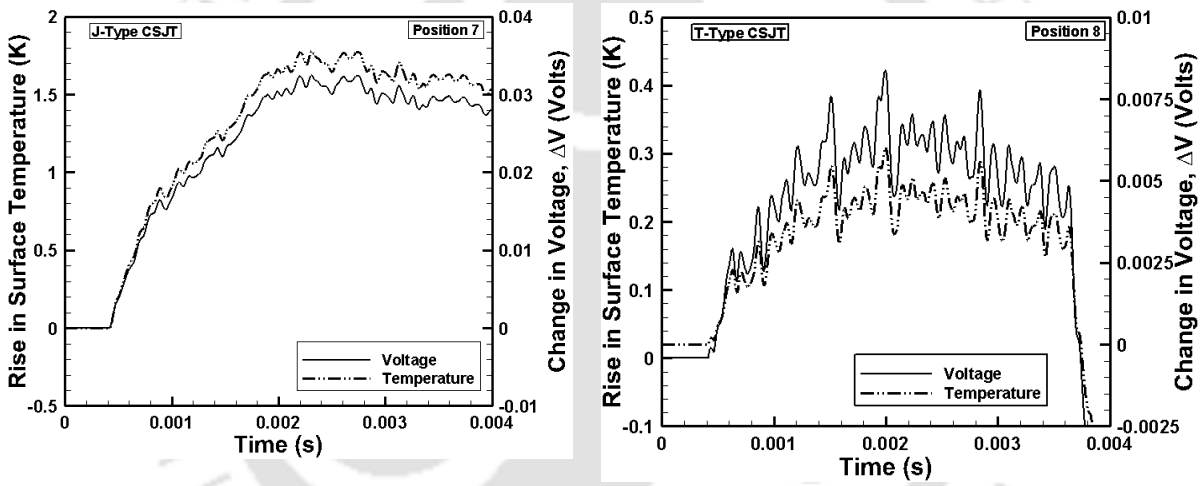

(a) **(b)**

Fig. 7.6: Signal captured from the wedge shape body at 44 mm away from the leading edge of the body using (a) J-type, and (b) T-type CSJTs

7.3 Computations of Surface Heat Flux

7.3.1 Prediction of Stagnation Heat Flux Based on Correlation for the Stagnation Point

The test gases in the shock tunnel have very high stagnation enthalpies. At the same time, during experimental test window of 1 ms, the flow encounters "*step rise*" in heat flux at the surface junction probe. Meanwhile, the heat flux at the stagnation point of the model can be estimated by the theoretical approach using "*Fay and Riddell*" correlation [*Anderson, 2000; Fay and Riddell, 1958*]. Moreover, there exist modified version of this correlation at high enthalpy test conditions in the literature that caters dissociation flow fields [*Desikan et al., 2016; Srinivasan et al., 2016*]. In this case, the simple expression (*Eq. 7.1)* is used to calculate the stagnation heat flux

corresponding to test flow conditions in the shock tunnel, which are also adopted in the literature [*Fay and Riddell, 1958*].

$$q_o = 0.763\, Pr^{-0.6} \left(\rho_e \mu_e\right)^{0.5} \frac{1}{\sqrt{R_n}} \left[\frac{2\left(p_e - p_\infty\right)}{\rho_e}\right]^{1/4} \left[c_p \left(T_o - T_w\right)\right] \tag{7.1}$$

Here, 'Pr' represents Prandtl number of the test gas (= *0.71* for air), 'p_e', 'ρ_e' and 'μ_e' are the static pressure, static density and dynamic viscosity, respectively at the edge of the boundary layer. Likewise, 'p_∞' is the free stream static pressure, 'c_p' is the specific heat capacity of the test gas at constant pressure, 'T_o' and 'T_w' are the free stream total temperature, and model wall temperature, respectively and 'R_n' is the nose radius of the blunt body. The average value of stagnation heat flux is estimated as, *37 W/cm*^{2} with repeatability margin of ±*3 W/cm*^{2} from the conducted study (*Table 7.4*).

7.3.2 Numerical computations for surface heat flux prediction

7.3.2.1 Numerical Methodology

In order to compare the experimental studies, a numerical non-equilibrium compressible flow solver has been used to perform the numerical simulation with a second order accuracy. Essentially, it is an upgraded version of "unstructured solver for hypersonic aerothermodynamics simulations (USHAS)" developed in-house [*Desai et al. 2017; Desai et al. 2016*]. The governing equations (*mass, momentum, energy and species conservation*) are solved for two-dimensional axisymmetric laminar flow in finite volume formulation were eleven prominent chemical reactions of dissociation of air and associated five species (N_2, O_2, NO, N, O) are accounted. This solver employs AUSM scheme for inviscid flux computations and second-order accuracy has been achieved by using Venkakrishnan limiter [*John et al., 2014*]. The idea for the present simulation study has been taken from the literature *John et al.,* 2014. More details of the calculations for high-temperature reaction kinetics, transport properties and thermodynamic properties may be found in references [*Gordon and McBride, 1994; Dunn and Kang, 1973*].

7.3.2.2 Numerical Computation

The numerical strategy is applied to two test models (hemisphere and wedge body) as the test flow conditions for both the models are similar (*Fig. 7.7 and Fig. 7.8*). The simulations are performed

to compliment the present experimental studies with the freestream flow conditions (*Table 7.1*) for the thermal probe. It may be noted that the initial pressure (before the arrival of the hypersonic flow) in the test section of the shock tunnel is of the order of 0.1 Pa. This condition leads to the very high Knusden number and thus makes it difficult for simulation by using conventional Navier Stokes solver. Therefore, numerical simulations are generally initiated with hypersonic freestream conditions in the computational domain. Such simulations can give only the steady state results and not the temporal variation of any property. The typical computational domain for both the test models along with the boundary conditions is shown in *Fig. 7.7* and *Fig. 7.8*.

In addition, no-slip boundary, isothermal wall condition (300 K) is considered for both the test cases i.e. hemisphere as well as the compression ramp. In order to carry out the essential mesh independence study, different meshes of size 280×100, 320×140, 360×180 are employed for hemispherical body and 90×240, 140×290, 190×340 for wedge body to carry out the simulations as mentioned in *Table 7.3*. The convergence histories obtained for the grid independence study for both hemisphere and wedge body are shown in *Figs. 7.9(a-b)*, where the steady-state convergence is assumed when the residual becomes lesser than 10^{-6}. The stagnation heat fluxes are computed for each of the mesh sizes and encouraging match in values is noticed with a medium level mesh of size 320×140. Subsequently, the temperature and Mach number contours on this grid are plotted in *Fig. 7.10 and Fig. 7.11*, respectively. For the hemispherical body, the mesh size (320×140), the average value of stagnation point heat flux is obtained as, *50.6* W/cm^2 (*Table 7.3*). Considering the wedge body, the obtained results from different simulations with the considered meshes are given in *Table 7.3*. In continuation, *Fig. 7.12 and Fig. 7.13* depicts the Mach and temperature contour of the wedge body. Surprisingly, all these simulations with different grid sizes from the wedge body show the heat flux values closer to the leading edge. Therefore, a solution obtained from 190×340 grid can be considered as a mesh independent solution, which gives an average heat flux value of *16.7* W/cm^2. Further, no alteration in chemical composition due to chemical reactions among the flow particles observed in all the simulations. Temperature contours (*Fig. 7.10 and Fig. 7.12*) clearly depict this fact where maximum temperature in the domain is seen to be lower than the probable temperature of dissociation reactions. The results from the in-house solver are compared with the outcome of the experiment. The experimental study has been validated using the numerical in-house solver developed by *Desai et al. (2016)*. The details of the numerical

methods have been elaborated in the reference *Desai et al. (2017)* and *Desai et al. (2016)*. The equations in the coupled manner are as follows:

$$\frac{\partial U}{\partial t}+\frac{\partial EI}{\partial x}+\frac{\partial FI}{\partial y}+S+\alpha\left(S_I+S_V\right)=\frac{\partial Ev}{\partial x}+\frac{\partial Fv}{\partial y} \tag{7.2}$$

Where,

$$U=\begin{pmatrix}\rho\\ \rho u\\ \rho v\\ \rho E\\ C_1\\ C_2\\ C_3\\ C_4\end{pmatrix}, E_1=\begin{pmatrix}\rho u\\ \rho u^2+p\\ \rho uv\\ \left(\rho E+p\right)u\\ uC_1\\ uC_2\\ uC_3\\ uC_4\end{pmatrix}, F_1=\begin{pmatrix}\rho v\\ \rho uv\\ \rho u^2+p\\ \left(\rho E+p\right)v\\ vC_1\\ vC_2\\ vC_3\\ vC_4\end{pmatrix}, E_v=\begin{pmatrix}0\\ \tau_{xx}\\ \tau_{xy}\\ u\tau_{xx}+v\tau_{xy}-q_x-\sum_{i=1}^{N}h_iC_i\overset{:}{u}_i\\ -C_1\overset{:}{u}_1\\ -C_2\overset{:}{u}_2\\ -C_3\overset{:}{u}_3\\ -C_4\overset{:}{u}_4\end{pmatrix},$$

$$F_v=\begin{pmatrix}0\\ \tau_{xy}\\ \tau_{yy}\\ u\tau_{xy}+v\tau_{yy}-q_y-\sum_{i=1}^{N}h_iC_i\overset{:}{v}_i\\ -C_1\overset{:}{v}_i\\ -C_2\overset{:}{v}_2\\ -C_2\overset{:}{v}_3\\ -C_4\overset{:}{v}_4\end{pmatrix},$$

$$S_1 = \frac{1}{y}\begin{pmatrix} \rho v \\ \rho uv \\ \rho u^2 + p \\ (\rho E + p)v \\ vC_1 \\ vC_2 \\ vC_3 \\ vC_4 \end{pmatrix}, S_v = \frac{1}{y}\begin{pmatrix} 0 \\ \tau\tau_{xy} - \frac{2}{3}y\frac{\partial(\mu v / y)}{\partial x} \\ \tau_{yy} - \tau_{\theta\theta} - \frac{2}{3}y\frac{\partial(\mu v / y)}{\partial y} \\ u\tau_{xy} + v\tau_{yy} - q_y - \frac{2}{3}y\frac{\partial(\mu v^2 / y)}{\partial y} - \frac{2}{3}y\frac{\partial(\mu uv / y)}{\partial x} - \sum_{i=1}^{N} h_i C_i \dot{v}_i \\ -C_1 \dot{v}_1 \\ -C_2 \dot{v}_2 \\ -C_3 \dot{v}_3 \\ -C_4 \dot{v}_4 \end{pmatrix},$$

$$S = \begin{pmatrix} 0 \\ 0 \\ 0 \\ 0 \\ S_1 \\ S_2 \\ S_3 \\ S_4 \end{pmatrix}$$

Here, α is a constant (α = 1 for 2*D* axi-symmetric, α = 0 for 2*D* problem).

Internal energy and total energy is calculated as $e = \sum_{i=1}^{N} e_i \frac{C_i}{\rho MW_i}$ and $E = e + 1/2\left(u^2 + v^2\right) E = e$ + 1/2 (u^2 + v^2) respectively, where, $e_i = h_{fi}^0 + \int_{TR}^{T} C_{pi} dT - R_u T$ which represents the molar internal energy of i^{th} species. Different shear stress components are as follows:-

$$\tau_{xx} = \mu\left(\frac{4}{3}\frac{\partial u}{\partial x} - \frac{2}{3}\frac{\partial v}{\partial y}\right), \tau_{yy} = \mu\left(\frac{4}{3}\frac{\partial v}{\partial y} - \frac{2}{3}\frac{\partial u}{\partial x}\right), \tau_{xy} = \mu\left(\frac{\partial u}{\partial y} + \frac{\partial v}{\partial x}\right),$$

$$\tau_{\theta\theta} = \mu\left(-\frac{2}{3}\left(\frac{\partial u}{\partial y} + \frac{\partial v}{\partial x}\right) + \frac{4v}{3y}\right)$$

Heat fluxes are $q_x = -k\frac{\partial T}{\partial x}$ and $q_y = -k\frac{\partial T}{\partial y}$.

$$Y_i \tilde{u}_i = -D_{im} \frac{\partial Y_i}{\partial x}, Y_i \tilde{v}_i = -D_{im} \frac{\partial Y_i}{\partial y},$$

$D_{im} = 5 \times 10^{-5}\, m^2/s$, is the effective binary diffusivity of species *i* in the mixture.

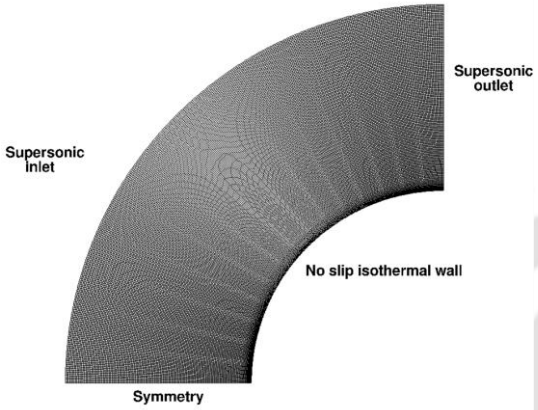

Fig 7.7: Computational domain and associated boundary conditions for flow over thermal probe

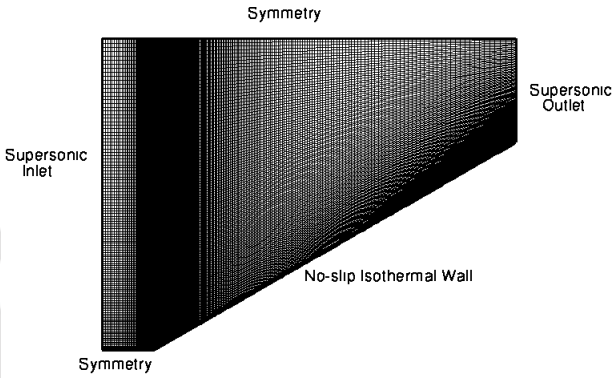

Fig 7.8: Computational domain and associated boundary conditions for flow over flat plate inclined at 30°

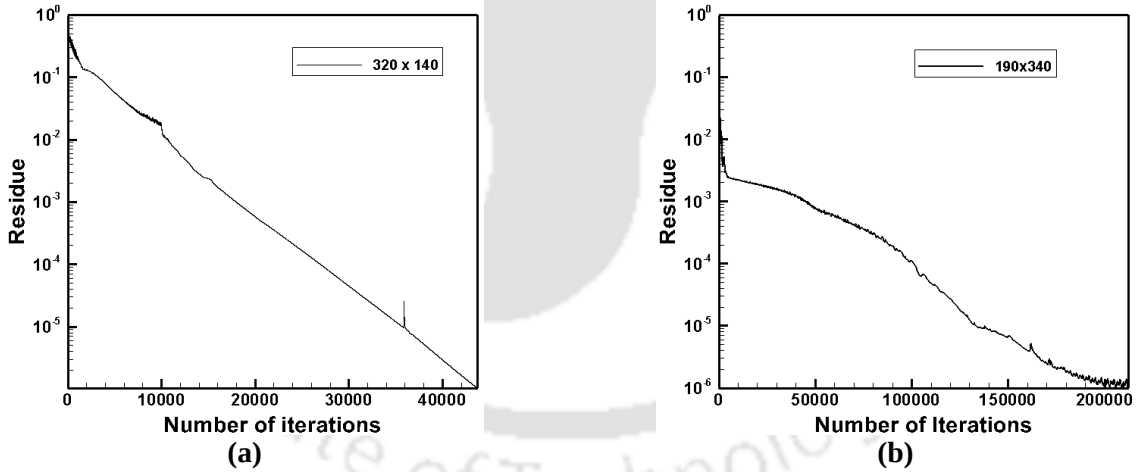

Fig 7.9: Convergence history for the grid independence solution for (a) hemispherical body, and (b) wedge shaped body

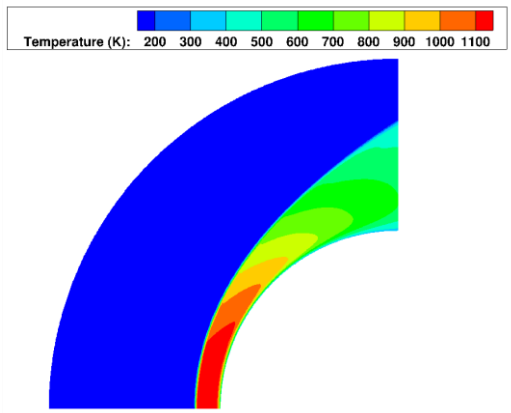

Fig. 7.10: Temperature contours obtained from numerical simulation

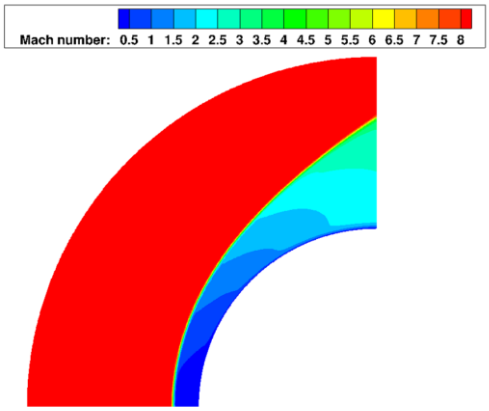

Fig. 7.11: Mach number contours achieved from numerical simulation

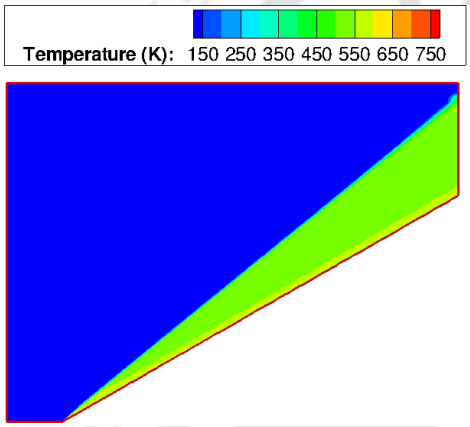

Fig. 7.12: Temperature contour obtained from the Numerical Simulation

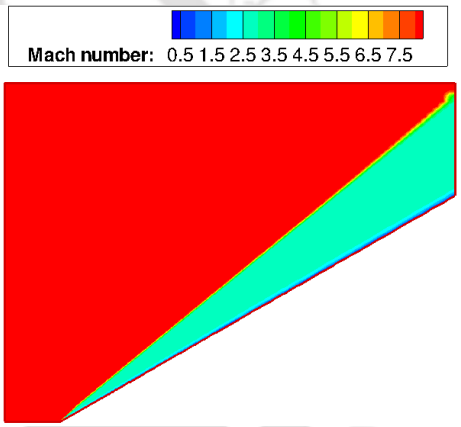

Fig. 7.13: Mach contour obtained out of Numerical Simulation

Table 7.3: Surface heat fluxes computed in the Hypersonic Shock Tunnel

Model Construction	**Grid size**	**ΔY_{min} (m)**	**ΔX_{min} (m)**	**Stagnation Point for Hemispherical Body (W/cm^2)**
Hemispherical Body	280 × 100	6.84×10^{-5}	2.7×10^{-5}	39.52
	320 × 140	6×10^{-5}	1.2×10^{-5}	50.57
	360 × 180	5.35×10^{-5}	9×10^{-6}	51.48
				Leading Edge Heat Flux (W/cm^2)
Wedge Body	240 × 90	8.0×10^{-6}	4.78×10^{-5}	17.6
	290 × 140	5.0×10^{-6}	2.83×10^{-5}	17.9
	340 × 190	2.0×10^{-6}	1.7×10^{-5}	16.7

7.4 Recovery of Surface Heat Flux during Experiment

In shock tunnel tests, the standard approach of governing one-dimensional heat conduction formulation has been used while predicting surface heat flux from transient temperatures [*Irimpan et al. 2015; Kumar et al., 2011; Menezes and Bhat, 2010; [3]Mohammed et al., 2010; Taler, 1996; Schultz and Jones, 1973*]. The physical model into consideration assumes the fact that lateral heat conduction during the experimental time scale (~ 1 ms) is negligible and the heat is conducted only in the direction normal to the surface. In the present situation, all the surface junction probes are prepared with metals, which are good conductors and the formed junction has a thickness of the order of few micrometre (~ 20-24 μm). Likewise, the thermal penetration distance during the experimental run-times is negligible as compared to the linear dimension of the thermal sensor (10 mm). Thus, it is quite reasonable to assume that the rise in mean temperature is same as that of surface temperature history $\left[T_s(t)\right]$ as acquired by junction probe (*Fig. 3.6*). *Chapter 3* elaborates the complete methodology behind the estimation of surface heat flux.

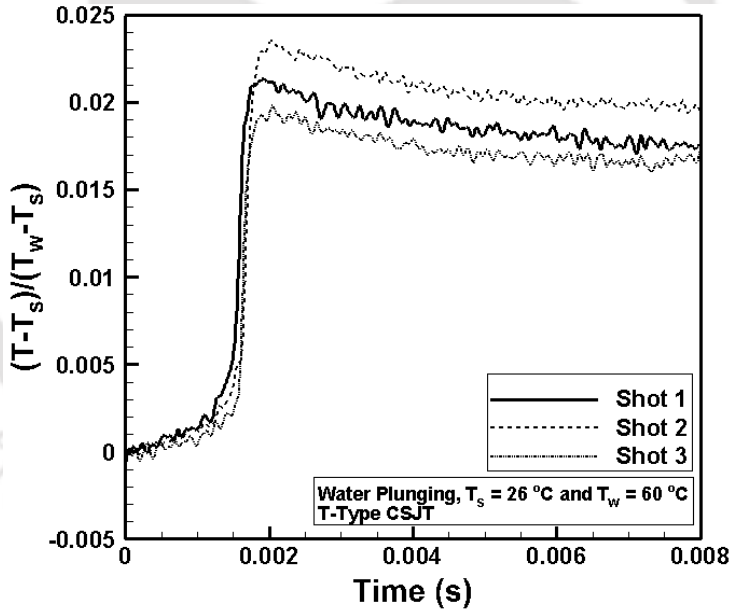

Fig. 7.14: Transient variations of non-dimensional temperature ratio for T-type CSJT during water plunging (WP) technique at fixed water temperature and surface temperature of the plate

The sensing surface of the CSJTs is prepared through plastic deformation of two different metals and it is unique for each type of CSJT as described in *Chapter 4*. In the current investigation, the "thermal product (β)" (for E and J type) have been determined experimentally using "water plunging technique" as reported in *Chapter 5*. Additionally, an effort has been made to determine

the thermal product for *T-type* CSJT using *water plunging technique* as elaborated in *section 5.2.2*. The experiments have been repeated at 60°C and the results are plotted in *Fig. 7.14*. Three number of experiments have been repeated and an average thermal product value of 7046 $Jm^{-2}s^{-1/2}K^{-1}$ has been obtained. For each of the surface junction probe, these values are mentioned in *Table 7.2*.

Further, the discretization of temperature signal and subsequent computation of surface heat flux follows a time step of the order of 1 μs as shown in *Eq. (3.11)*. All the obtained temperature signals from the surface junction probes during shock tunnel experiments are analyzed to infer heat flux at stagnation point of hemisphere as well as over the periphery of the wedge body. The transient temperature distributions extracted from temperature discretization technique for the stagnation probe are compared with experimental temperature history. For a closed form solution of temperature history, all the signals show excellent recovery of analytical distribution of surface temperature rise through cubic spline fitting. *Figure 7.15* show the comparison of experimental signals and discretized data for the stagnation probe. Afterwards, surface heat fluxes have been predicted using *Eq. (3.13)*, and are plotted in *Fig. 7.16*. The average values of surface heat fluxes computed within the steady flow duration, repeated for three tests have been addressed in *Table 7.5*. The predicted surface heating rates by the temperature discretization data show excellent agreement within an experimental uncertainty of ± 2%.

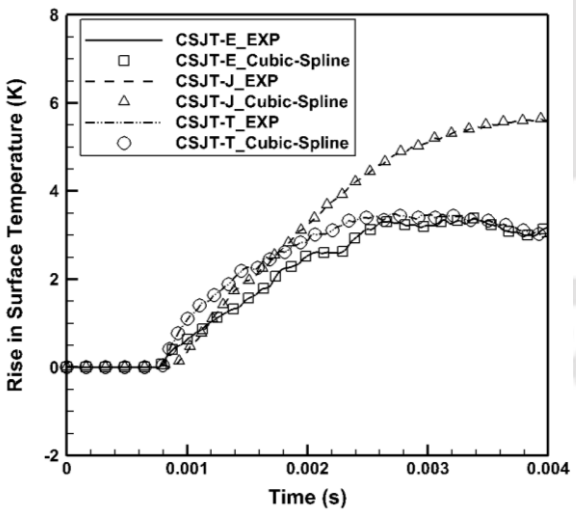

Fig. 7.15: Comparison of experimental signals from surface junction probes with discretized temperature data.

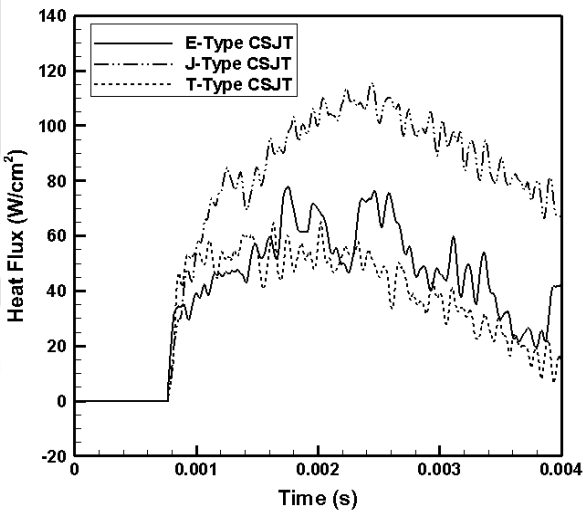

Fig. 7.16: Experimental heat flux recovery from surface junction probes during from shock tunnel tests

Table 7.4: Comparison assessment of average values of surface heat fluxes from stagnation probe

Types of CSJT	Experimental TP (β_e) ($Jm^{-2}s^{-1/2}K^{-1}$)	Experimental Stagnation Heat Flux (*Eq. 3.9*) (W/cm^2)	Fay and Riddell (*Eq. 7.1*) (W/cm^2)	Numerical Simulation (W/cm^2)
E	8452	53 ± 2%	36 ± 7 %	50.6
T	7046	57 ± 2%		
J	9585	89 ± 2%		

Table 7.5: Comparison of average heat fluxes at 4 mm away from the leading edge

Sl. No.	Experimental TP (β_e)	Type of CSJT	Experimental Heat Flux (W/cm^2)	Numerical Heat Flux (W/cm^2)
1	8452	E	11 ± 8.2%	16.7
2	7046	T	13 ± 6.8%	
3	9585	J	35.79 ± 7%	

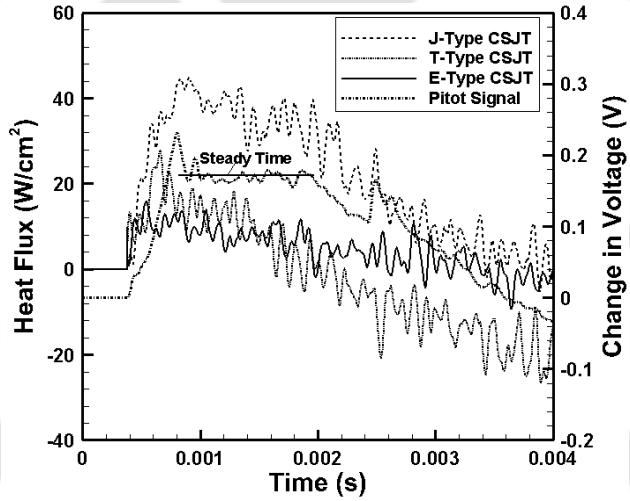

Fig. 7.17: Heat flux signals captured from the wedge shape body acquired at 4 mm away from the leading edge using E, T and J-type thermal sensors, superimposed with the typical pitot signal

Table 7.6: Comparison of average heat fluxes at 24 mm and 44 mm away from the leading edge

Sl. No.	Type of CSJT	Position (x= 24 mm)	Heat Flux (W/cm^2)	Position (x= 44 mm)	Heat Flux (W/cm^2)
1	J	Position 4	42.3 ± 7.2%	Position 7	32.3 ± 6.28%
2	T	Position 5	5.49 ± 5.2%	Position 8	3.4 ± 5.38%
3	E	Position 6	9.44 ± 8.18%	Position 9	-

As explained in the previous section, considering similar process and assumptions, the heat flux distribution over the wedge body is estimated from all the CSJTs. As mentioned, the obtained temporal signals from all the CSJTs over the wedge model during the shock tunnel experiments are analyzed to infer surface heat flux at the leading edge. The heat flux is predicted using *Eq.*

(3.13) and are plotted in *Fig. 7.17*. The figure shows the heat flux captured at 4 mm away from the leading edge of the wedge body. In addition, *Fig 7.17* shows the typical pitot signal representing the usual characteristics of the shock tunnel. A close look at the signal shows a 'rise time' of about 0.34 ms. The average values of surface heat fluxes computed within the test flow duration of 1 ms repeated for three tests are tabulated in *Table 7.5*. From the flow phenomenon as captured by Pitot sensor (*Fig. 7.3-a*), a steady flow duration of 1 ms is observed and during this time frame, the signal captured by the CSJT show a parabolic rise in surface temperature highlighting the usual characteristics of a thermal sensor [*Taler, 1996*]. All the surface thermal probe were successfully able to capture the flow as generated due to oblique shock occurring at the sharp leading edge of the compression corner. However, the surface thermal probe at position '9' did not respond due to the dismantling of the wiring in the sensor. The plan of applying thermal sensor over the whole surface of the flat plate is to estimate the varying heat flux over the surface at a particular *x*-location subjected to strong hypersonic flow (*Fig. 7.4*). The captured results suggested the successful implementation of the thermal sensor having the capability of capturing low heat flux.

7.5 Performance Assessment of Surface Junction Probes

From the predicted flow phenomena by the Pitot pressure history (*Fig. 7.3-a*), it is observed that there is a steady test flow of 1 ms duration, during which all the surface junction probes from both the experiments show a parabolic rise in surface temperature. During this timescale, the CSJTs in the hemispherical model show an average heat flux value of *53* W/cm^2, *57* W/cm^2 and *89* W/cm^2, for *E, T* and *J-types* probes, respectively. Additionally, at the leading edge using the wedge model, an average heat flux value of *11* W/cm^2, *13* W/cm^2 and *35.79* W/cm^2 respectively have been predicted for *E, T* and *J-types* of CSJTs.

Pertaining to *Fig. 7.16* and *Fig. 7.17*, the heat flux histories are seen to have a steady region (~ 1 ms) for E and T-type probes, analogous to experimental test times observed in the pitot pressure history. When the average values on this timescale are compared, the recovery in surface heat fluxes has an excellent match for stagnation probes E-type (*53* W/cm^2) and T-type (*57* W/cm^2) with respect to numerical simulation (*50.6* W/cm^2) and over predicts for J-type probe (89 W/cm^2). Under same test flow conditions, the "*Fay and Riddell*" expression for stagnation heat flux under-predicts the values (*37* W/cm^2). The similar values of leading edge heat flux (x = 4 mm) are, *11* W/cm^2 (E-type), 13 W/cm^2 (T-type) and 35.8 W/cm^2 (J-type), with respect to values obtained from

numerical simulation *16.7* W/cm^2. When the similar comparison is made for the J-type probe at stagnation point and leading edge on the plate, there is a significant over-prediction of average surface heat flux during the shock tunnel experimental time scale for both the experimental models. Moreover, J-type probe sees only a rising trend during same time scale and no steady region is found for average surface heat flux estimation. It essentially means that "thermal product of surface junction" does not fall in the line of shock tunnel time scale of experiments. It may be noted here that the diameter of outer element of thermocouple material is 2.5 mm for the J-type probe in contrast with 3.25 mm for other two probes. Being slight oversize in diameter and with bridge thickness of 20-24 µm, it may not be possible to achieve adequate response time with respect to shock tunnel flows. Further, the effective proximity of the junction to the insulation between thermocouple materials and their purity during its construction process can also be a source of uncertainty in thermal product estimation. In the end, these issues lead to a discrepancy in heat flux signals, for the J-type probe in comparison with its counterparts. Furthermore, it has been emphasized that slight variation in size and effective junction depth can affect the "*response time and thermal product*" of surface junction probes [*Buttsworth, 2001*]. In this investigation, a slightly higher size CSJTs are explored due to lack of availability of same size materials locally. Thus, from the present study, it may be inferred that E and T-type surface junction probes are found to be suitable for shock tunnel experiments while measuring transient temperatures and predicting surface heat fluxes in both the cases. In this case, the experimental temperature histories during shock tunnel tests reproduce transient surface heat fluxes through analytical technique only for stagnation heat flux as well as by numerical simulation for both the test cases with reasonable accuracy. Besides, it bears higher sensitivity values and an admissible "thermal product" for the ultrashort duration of time scales prevailing in shock tunnel experiments. For J-type of the probe, the performance indicators (such as rise and response times) seem to be quite promising in twain cases, while acquiring transient temperature data for shock tunnel application. However, size of the thermocouple elements and adequate method of creating plastic deformation at the junction surface plays a crucial role in shock tunnel experiments.

7.6 Summary

Three surface junction probes (*E, J* and *T-type*) have been constructed in-house for their usage in capturing highly transient temperatures in ultra-short duration shock tunnel flows. They are

mounted simultaneously on a rake along with the Pitot pressure transducer as well as on the flat plate inclined at an angle of 30º in the test section of the shock tunnel. When these stagnation probes and Pitot transducer experience the same free stream flow in the shock tunnel, the time responses from CSJTs are compared with Pitot signal. The quick response time of the surface junctions (*21 µs for E-type, 29 µs for J-type and 24 µs for T-type*) reveal their suitability in capturing transient temperature data for millisecond duration flows in a shock tunnel. While recovering surface heat flux from transient temperature history from the hemispherical and wedge model, the *E-type* and *T-type* probe are found to be most suitable as it bears suitable thermal product for ultra-short duration time scales prevailing in shock tunnel experiments. The inconsistency in surface heat flux prediction from the J-type probe is mainly due to the discrepancy in the estimate of the effective thermal product of the sensing junction. The ruggedness, ease of fabrication and cost-effectiveness, make the CSJTs more lucrative for experiments in shock tunnels. Besides, they can be flush mounted on miniature aerodynamic model shapes due to their small sizes while measuring transient temperatures. The intention behind the research is to bring about the comparative behaviour of in-house developed surface junction probes for the shock-tunnel experiment. The performance indicators of surface junction probes are quite encouraging and very promising with respect to their future applications in the shock tunnels if the purity of junction elements, bridge thickness and thermal product estimation of junction probes are addressed properly.

CHAPTER 8

Thermal Probe for Application in Internal Combustion Engine

Compendium:

The previous chapters include the design and fabrication of various CSJTs and their calibration experiments to measure performance indicators such as, sensitivity and thermal product. Some of these CSJTs were exposed to high enthalpy flows in shock tubes and shock tunnels for evaluating their effectiveness in terms of rise time and response time. Further, it is felt that exposure of these sensors to cyclic heat loads can provide better insight in terms of thermal endurance and continuous exposure to high temperature ambience. In addition, the measurement of instantaneous heat flux in the internal combustion (IC) engine can provide information of "hot-spot" region and necessity for exploring new materials. In order to carry out such measurement, an E-type (Chromel-Constantan) coaxial surface junction thermocouple was chosen. The intended study aims at in-house fabrication of a surface junction thermal probe for assessing its capability in the highly transient thermal environment for measuring surface temperature and subsequently its heat flux. The experiments are intended to evaluate the measurement capability and endurance of the sensor for a periodic change in heat load. The experiments also include measurement of exhaust gas heat flux and combustion chamber heat flux using the fabricated coaxial thermal sensor. For the first set of experiment, the thermal sensor is placed at the exhaust of the IC engine and eventually estimating the heat flux. Considering the next experimental set-up, the engine head has been redesigned with a port to accommodate the sensor. Both the experiments have been conducted and the results have shown satisfactory trend, and magnitude. The obtained results from the combustion chamber have been compared with the similar work attempted by the previous researchers.

8.1. Introduction

The transient measurement of heat transfer rates is very much predominant applications such as, high-speed flows, internal combustion (IC) engine applications etc. Recent advances have led to the development of ground based impulse facilities such as shock tunnels, free-piston shock tunnels, and expansion tubes [*Kulkarni and Reddy, 2008; Morgan, 1997; Reddy et al., 1996*]. The basic fact of these facilities lies in its very short duration test time, which is of the order of few milliseconds and thermal ambience of step/impulsive heat loads. During this ultra-short duration test time, the steady-state concept of heat flux predictions is no longer valid. In addition, measuring short duration transient temperatures and thereafter, predicting heat fluxes with appropriate modelling becomes a challenging task. Pertaining to IC engines, the measurement of temperatures in the combustion chambers and exhaust gases are vital parameters where the temperatures are expected to be in the range of 350 °C to 700 °C. In this line, Mattavi (1974) attempted a miniature sensor for measuring steady-state heat transfer rates in the engine. It may be noted that the thermal loads in the combustion chamber are cyclic in nature during which the pressure also varies with crank angle. Moreover, the exhaust of the IC engine resembles the pulsating nature of the flow. In nutshell, quantification of heat content in the combustion chamber and exhaust of the IC engine is very crucial. Many times, it is almost difficult to fix any kind of thermal probe to capture the variation of heat loads. One of the estimates is to predict the heat load variation as a function of crank-angle from the measured "pressure-crank angle" data [*Chun and Heywood, 1987*]. Such measurement can be useful to understand the issues related to combustion efficiency and evolvement of new materials for using alternative fuel in the combustion chamber of the engine. Further, it plays a strong influence on the engine emission characteristics and in turn defines the cooling requirement for the engine. Heat transfer characteristics at "hot-spot" locations on the engine head, play an important role in estimating heat release rate and on other engine parametric studies.

In the backdrop, the determination of exhaust gas temperature (EGT) can help us calculate the engine's air-fuel ratio (AFR) which is one of the most important performance parameters of IC engines [*Barlett and Whalley, 1998*]. If enough fuel is not injected into the cylinders during the combustion process, the exhaust gas will be much hotter. This condition is known as a "lean" air-fuel ratio. On the other hand, if there is too much fuel in the combustion process, the exhaust gas will be cooler, which is a typical case of a "rich" air fuel ratio. Too lean or rich an air-fuel ratio

can result in loss of performance of the engine. Thus, engine's performance can be optimized by proper determination of the EGT. Many previous researchers have carried out work on the measurement of heat transfer rate in the internal combustion engine as well exhaust gas temperature. *Caton and Heywood (1981)* experimentally measured instantaneous cylinder pressure and EGT for a range of engine operating conditions. *Quadais (1997)* introduced a theoretical model for predicting the instantaneous EGTs and velocities of a single-cylinder diesel engine to compare instantaneous exhaust velocities and temperatures with the corresponding measured parameters. *Rakopoulos and Mavropoulos (2001)* performed an experimental analysis to study the transient engine surface temperature and instantaneous heat fluxes in the combustion chamber walls of a direct injection (DI), air cooled, four-stroke diesel engine. *Alkidas and Myers (1982)* measured the transient heat flux in the cylinder head of a spark ignition engine. Furthermore, a chromel-alumel overlapping thin-film thermocouple have been developed for measuring the heat transfer in the ceramically coated combustion chamber [*Assanis and Friedman (1993)*]. Although, the previous measurements do highlight the studies on heat transfer measurements, still there is a scope of improvements in the modern era of instrumentation. For instance, the studies show usage of conventional thermal probes along with associated accessories for receiving signals. Though the available instruments certainly meet the requirements, but they are often complicated and difficulties are associated with maintaining the set-up.

Keeping all these difficulties in view, a simple cost-effective coaxial surface junction thermocouple of E-type is proposed. Being developed and fabricated in-house, the sensor can capture the time-varying temperature signals within a very short span of time. The sensor has a high response time of the order of few microseconds. The proposed work includes capturing the instantaneous surface heat flux from transient temperature data through one-dimensional heat conduction modelling in the combustion chamber as well as the exhaust of the spark ignition engine and in turn test its applicability. The cylinder head of the engine is modelled as the wall where the thermal probe is mounted while facing the combusted gases. Further, the choice of insulation among the thermocouple elements is very challenging since it has to sustain a high temperature ambience in the combustion chamber. The applicability of usage of this sensor is also evaluated through the experimental studies. The study also encompasses the design and in-house fabrication of engine head.

8.2 Experiment of Thermal Sensor in the Combustion Chamber

8.2.1 Fabrication of Coaxial Surface Junction Thermocouple

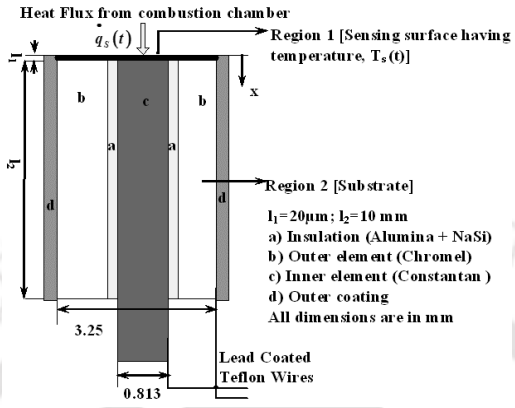

Fig. 8.1: Schematic of the CSJT fabricated for its application in the combustion chamber of the internal combustion engine

The measurement of instantaneous heat flux inside the combustion chamber becomes very challenging accounting the design feature of the engine. Considering this aspect, a chromel-constantan coaxial surface junction thermocouple (CSJT) of E-type is designed and fabricated in-house; from the available thermocouple material. A thin layer of ceramic paste (a mixture of alumina and sodium silicate) has been used to separate the thermocouple wires. The design methodology is similar to as explained in *chapter 3*, except that the insulation used for housing the thermocouple material is completely different. The complete assembly is allowed to dry naturally at room temperature such that a bond is developed among the inserted material. The main reason behind using this insulation is such that the paste of this mixture (Alumina and NaSi) can resist very high temperature and it can electrically insulate the thermocouple wires. The mixture has low thermal conductivity and has very high structural stability. Once the assembly gets hardened naturally, the continuity between the two wires is checked using a multimeter, to ascertain whether the used solution had actually created the electrical insulation. Further, after confirming that there is no electrical connectivity between the two wires, the extra layer of the epoxy paste is cleaned using the scalpel blade. The surface junction is created similarly as explained in *Chapter 4*. The junction formed on the surface has a junction thickness of around 20-24 µm [*Irimpan et al., 2015; Menezes and Bhat, 2010*]. Further, the connecting leads were spot welded on to the thermocouple wires using the spot welding machine [*Fig. C.8 in Appendix:C*]. The dimension of the

thermocouple is chosen based on the thermal penetration depth by using the concept of semi-infinite theory for heat conduction.

Figure 8.1 shows the schematic of the fabricated coaxial surface junction thermocouple. A detailed design methodology of the fabrication process has been explained in *Chapter 4*. The only difference in the fabrication assembly now lies with the use of *ceramic mixture* as oppose to the previous choice of *epoxy resin* (Araldite), as an insulation. The calibration technique of CSJT involves oil-bath experiments in which the relationship between changes in temperature and corresponding change in voltage are obtained. In this case, a linear relationship has been observed for the chosen thermocouple materials (i.e. chromel and constantan). Referring to *Fig. 4.1(a)*, the slope of the curve is the "sensitivity" of the thermocouple i.e. *58.96* μV/°C. The complete details of the calibration methodology are similar to as explained in *Chapter 4*.

8.2.2 Experimental Facility

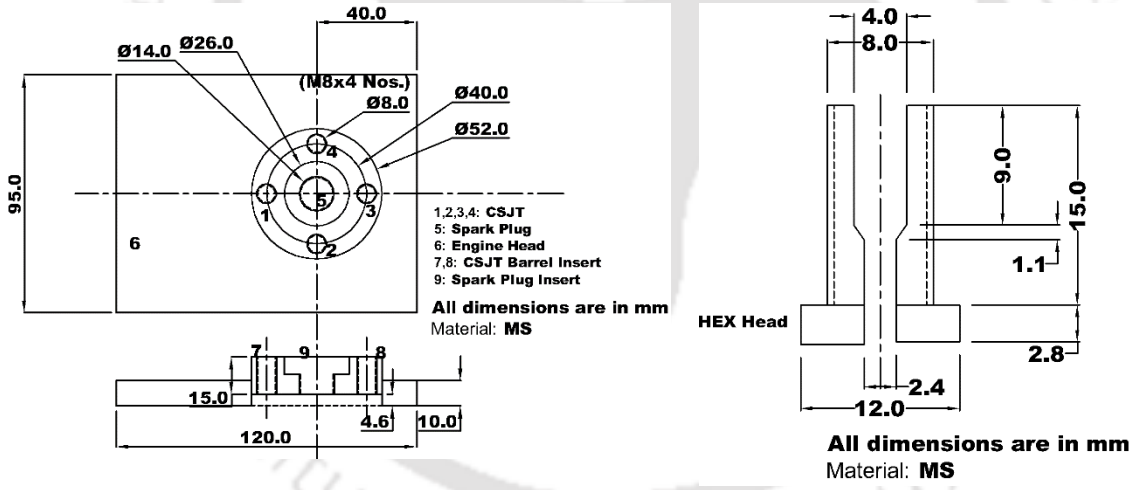

Fig. 8.2. Schematic of the (a) engine head, and (b) CSJT insert for mounting on the engine head

The experimental facility includes a four stroke, air-cooled GK100 Honda engine, having a horizontal shaft, side valve and a single cylinder. The engine has a compression ratio of 4.8. At a rated speed (3000 RPM), the engine has the power of 1.3 kW and a maximum rated torque of 3.92 N.m. For measuring the instantaneous heat flux inside the combustion chamber of the spark ignition engine, an engine head design is suitably modified and fabricated having a dimension of 120 mm × 95 mm × 10 mm. This head has a provision for holding four number of the thermal

sensor at a time; but for the current set of experiments, only one port out of the four has been chosen (*Fig. 8.2-a*). The centre of the engine head has a provision for fitting the spark plug.

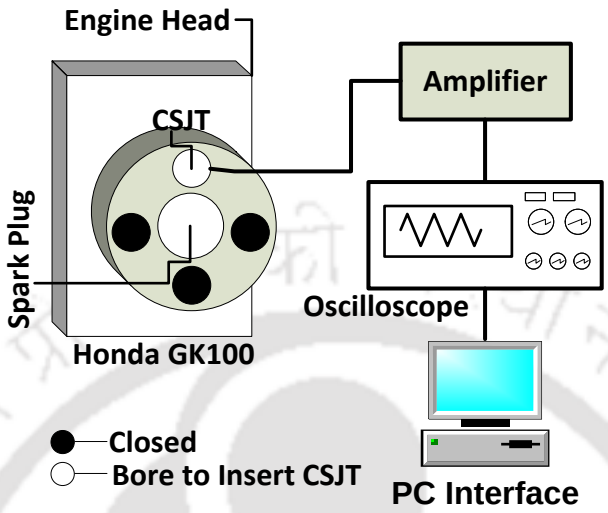

Fig. 8.3: Layout of the CSJT fitted on the engine head along with its accessories

Table 8.1: Specifications of the experimental engine

Type	**Side Valve, 4 Stroke, Air Cooled, Horizontal Shaft, Single Cylinder**
Displacement (cc)	97
Air-Fuel ratio	14.7
Bore x stroke(mm)	52 x 46
Compression Ratio	4.8:1
Rated Horse Power/Speed	1.4 HP / 3600 RPM
Maximum Horse Power	1.8 HP / 4200 RPM
Maximum Torque/Speed	0.4 Kg-m / 3000 RPM
Ignition System	TCI
Ignition Timing	20° BTDC

The detail specifications of the engine are presented in *Table 8.1*. Furthermore, the barrel for holding the CSJT sensor has been constructed with an insert of 8 mm diameter and an internal hole of 4 mm as shown in *Fig. 8.2(b)*. The sensor is kept flush mounted on the cylinder head, so that the junction is exposed to cyclic heat load as expected in the combustion chamber of the engine [*Fig. C.13 in Appendix:C*]. The engine head has been fitted in such a way that the combustion chamber was maintained air-tight with the surrounding. *Figure 8.*3 highlights the complete schematic layout of the proposed experiment. The assembly includes INA 128 Amplifier (*gain*

factor of 500; frequency 1-40 kHz; Make - Texas, USA), an oscilloscope (*sampling frequency of 1 GS/s; Make- Tektronix, USA*) and a PC-based LabVIEW interface to visualize the acquired data.

8.2.3 Results and Discussion

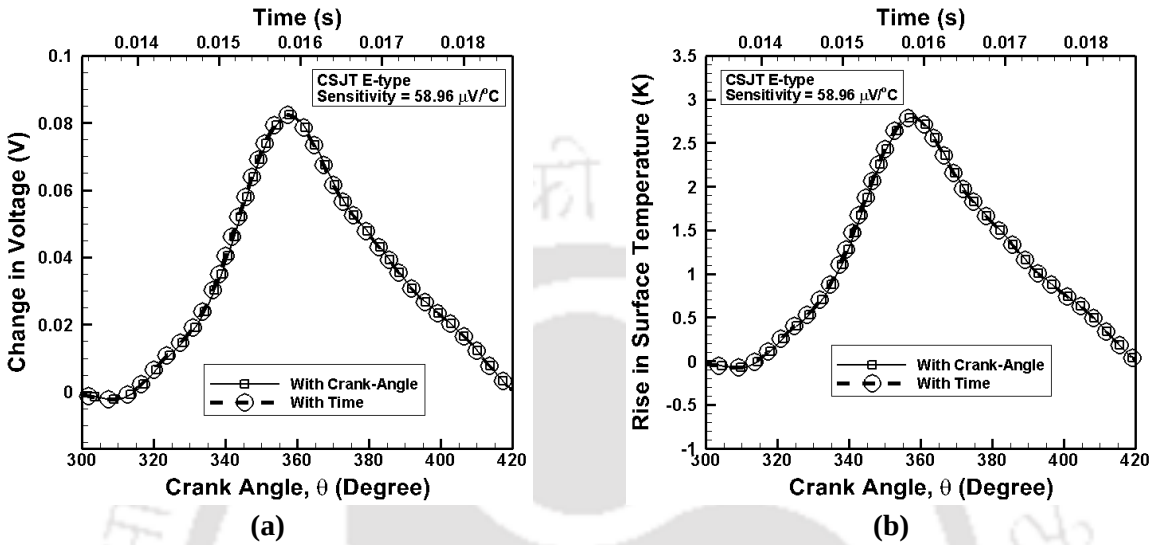

Fig. 8.4: Transient signal (a) change in voltage, (b) rise in surface temperature captured using the CSJT flush mounted on the engine head

Once the calibration and fabrication of the coaxial thermal sensor are over, the sensor is explored to measure instantaneous heat flux inside the combustion chamber. The thermal sensor is flush mounted with the inner surface of the engine head facing the combustion chamber. An isothermal ambience has been maintained throughout the experiment, by wrapping the complete sensor with the layer of alumina and NaSi. Initially, engine is started and as it achieves the steady state condition, the thermal sensor is employed to record the data. The obtained transient variation in voltage signal and the temperature data using the in-house built thermal sensor are plotted in *Figs. 8.4 (a-b)*. Here, the temperature-time history is estimated using the sensitivity value of the E-type thermal sensor as mentioned in *Chapter 4* (*Fig. 4.7*). A sharp peak has been observed from the obtained temporal data depicting the combustion schedule of the engine; which signifies that as soon as the combustion takes place inside the combustion chamber, the thermal sensor captures a sharp shoot. The obtained sharp shoot is kept on repeating after every cycle. Furthermore, the engine has been set to run at a particular fixed RPM (3000 rpm).

In addition, the heat flux data pertaining to cyclic load inside the reciprocating internal combustion engine can be measured using the time-averaged cyclic temperature variation. The principal assumption for calculating heat flux is such that the heat flow through the sensor wall

should be one-dimensional. The experimental temperature data in the present case are discretized using the cubic spline method as discussed in *Chapter 3* (*Eq. 3.9*). The TP values i.e. $(\rho ck)^{1/2}$ plays an important role while predicting the surface heat flux value from *Eq. (3.9)*. The thermal product (TP) value for E-type CSJT in *Eq. (3.9)* is chosen from the experiment conducted as reported in *Chapter 5*. Further, using the techniques as mentioned, the surface heat flux histories are predicted from the obtained temperature histories by a numerical algorithm developed in-house [*Chapter 3*].

Figure 8.5 shows the variation of heat flux with respect to crank angle as well as time in the region of compression and expansion stroke in the combustion chamber. This region is the zone of interest in the heat transfer studies considering maximum heat flux. The obtained results have been compared with the work attempted by previous researchers such as *Alkidas and Myers (1982), Alkidas and Cole (1985), and Assanis and Friedmann (1993)*. The trend of the obtained result matched well with the previous attempted work; thereby validating the use of the developed cost-effective coaxial thermal sensor in the combustion chamber environment of the internal combustion engine. An approximate value of about *2.17* MW/m^2 have been obtained from the experiment with an error of ±3 %. The rate of increase in the heat flux and the magnitude of the peak heat flux are the result of gas pressure and temperature of the burnt gases.

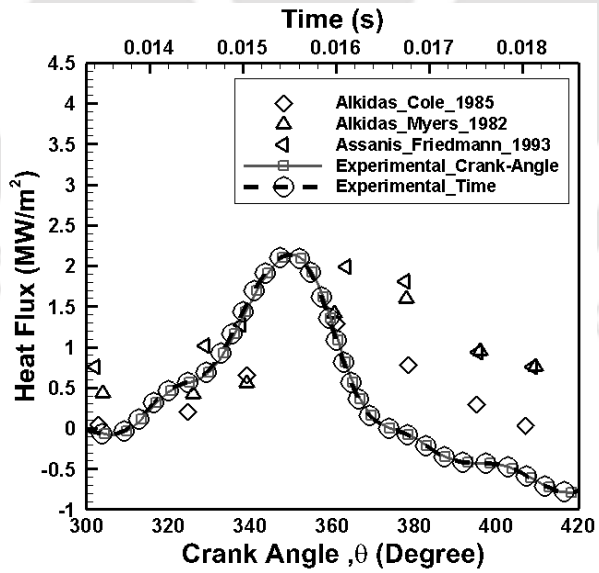

Fig. 8.5: Instantaneous heat flux obtained from the temperature history captured at the head of the combustion chamber of the internal combustion engine

8.3 Experiment in the Exhaust of the Internal Combustion Engine

8.3.1 Test Facilities

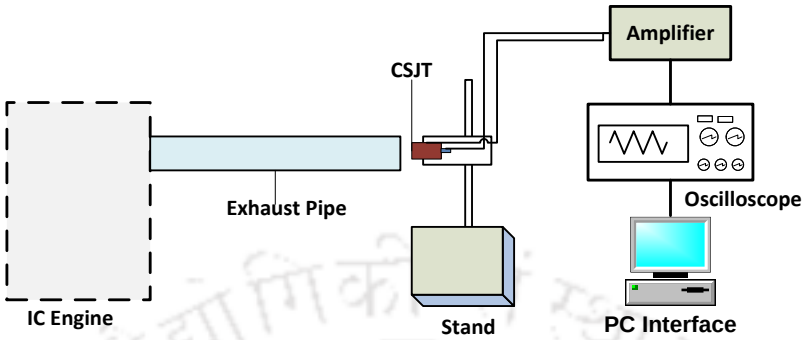

Fig. 8.6: Schematic representation of experimental setup for measuring exhaust gas temperature using a coaxial surface junction thermocouple.

The current experimental facility consists of a single cylinder, four-stroke, direct injection, water-cooled 3.5 kW, variable compression ratio (VCR) diesel engine (*Make: Kirloskar, India*) [*Bora et al., 2014*]. The data acquisition for the experimental analysis consists of similar set-up as described in *section 8.2.2*. The reason for considering two separate engines in two particular experiments lies purely on the fact of difficulty in mounting the sensor in the existing GK Honda engine. The previously considered engine as described in section 8.2.2 is smaller and the heat content out of the exhaust would be very small. Moreover, the GK100 engine does not have the provision for measuring the EGT. Further, it is planned in the future scope of work to estimate heat flux in the combustion of the VCR diesel engine. The engine set-up has an exhaust pipe, which is of radius 19 mm and the maximum velocity attained during a complete cycle is 6 m/s which is *measured using Hot Wire Anemometer*. At the beginning, the engine is run at no load condition in order to warm it up to an optimal level for a proper combustion of fuel followed by a gradual increase (20%, 40%, 60%, 80% and 100%) of the load. At any particular specified load condition, the engine is allowed to run for few minutes and the temperatures at the outlet of cooling water and exhaust gas are monitored closely at the computer display until it reaches a steady state condition. This indicates that the combustion inside the cylinder becomes steady and is ready for data acquisition. For the measurement of exhaust gas temperature, the experiments are carried out for various load conditions as discussed, although only 80% engine load is considered for further analysis as it gives the maximum brake thermal efficiency [*Sahoo, 2011*]. The coaxial thermocouple (CSJT) is placed in-line with the help of stand (about *5 mm* distance) just outside the exhaust outlet of the engine (*Fig. 8.6*). The thermocouple is connected to a data acquisition

system (DAS) and the temperature is recorded as a voltage change in the DAS. The front surface of the thermocouple acts as the sensing junction with the other end being dipped to ice-water to maintain the reference frame. The experimental set up along with the placement of thermocouple for EGT measurement has been shown in *Fig. 8.6*.

8.3.2 Signal Processing

Once the assembly to measure the exhaust gas heat flux is ready, the experiments are conducted and the typical voltage signal are acquired from the thermocouple for the experimental run time of 50 ms as shown in *Figs. 8.7(a-f)*. The flow from the exhaust port of the engine seem to be of periodic nature and the thermal sensor is able to predict the flow successfully; characterized as pulsating flow at the outlet of an IC engine exhaust manifold [*Gonzales, 2008*]. The typical signal obtained at 80% load condition has been considered for further analysis as discussed in *section 8.3.1*. In order to estimate the heat flux from the voltage signal through one-dimensional heat conduction modelling, only a fraction of the signal (5 ms) is considered where the parabolic nature is observed. The fraction of the voltage and temperature signal for the duration of 5 ms has been shown in *Fig. 8.8*.

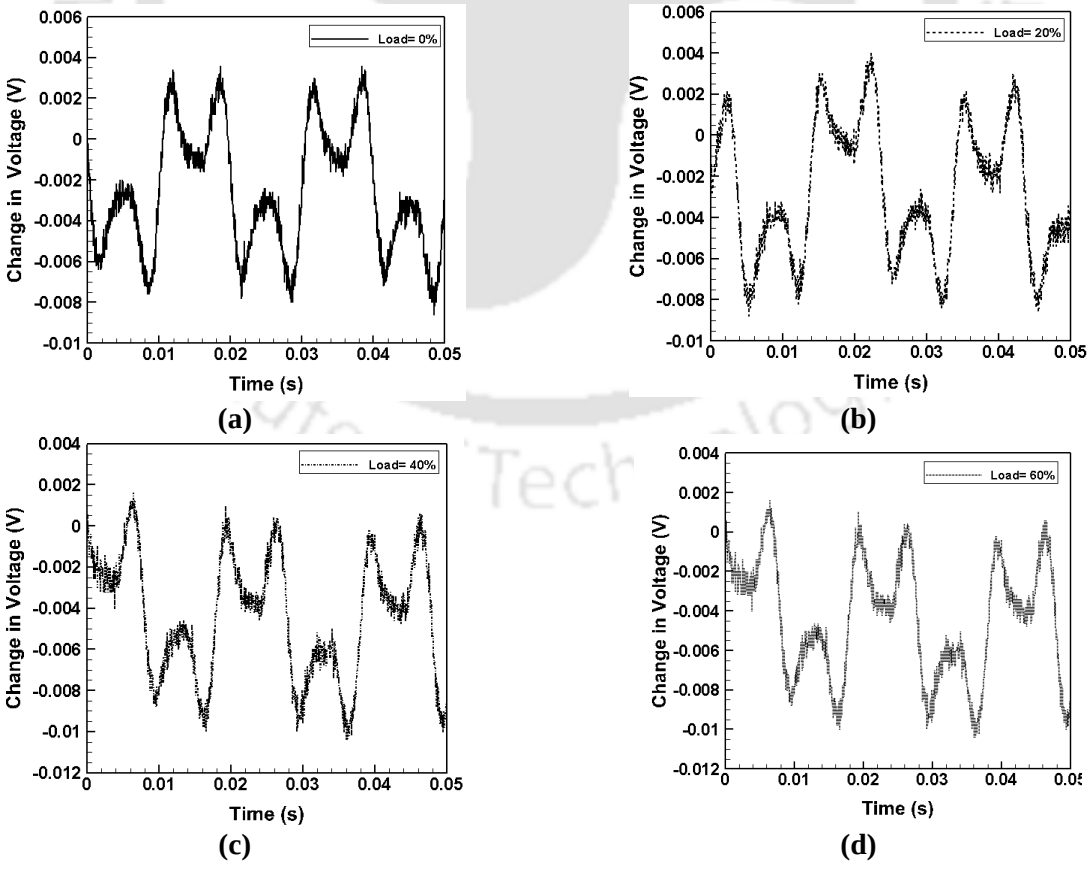

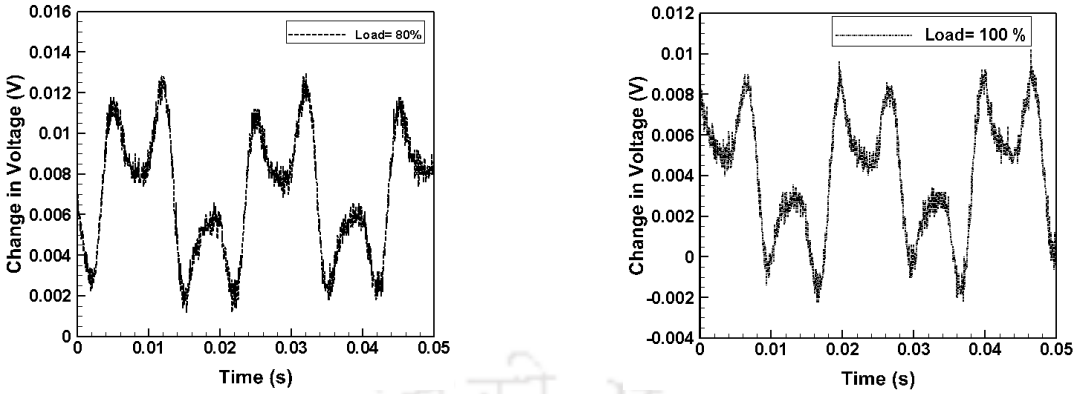

Fig. 8.7: Typical voltage-time signal captured from CSJT for internal combustion engine at various load conditions (a) 0%, (b) 20%, (c) 40%, (d) 60%, (e) 80%, (f) 100%

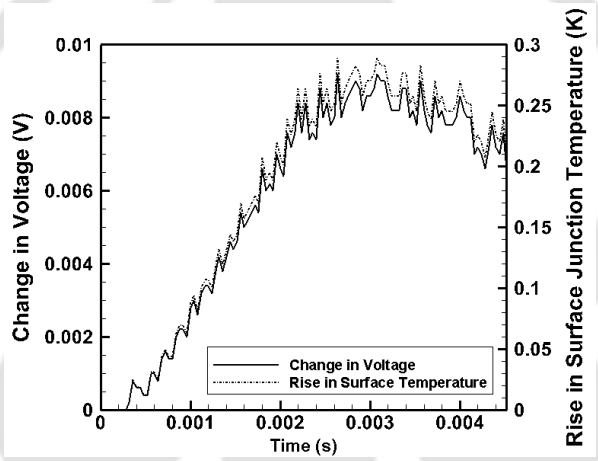

Fig. 8.8: Transient voltage and temperature signals obtained from coaxial surface junction thermocouple at the exhaust of the IC engine.

8.3.3 Estimation of Heat Flux

The performability of the thermal sensor can only be accessed once the heat flux is predicted. The method as described in *section 8.2.3* is considered for further post processing of the obtained temperature-time signal using one-dimensional heat conduction modelling. The heat flux signal corresponding to the temperature changes as shown in *Fig. 8.8* is obtained using *Eq. (3.13)* and are plotted in *Fig. 8.9***.** The signal seems to have a step-rise of heat flux with an approximate average value of 0.0287 MW/m^2 with ±6.19% [obtained using *Eq. (E.1) in Appendix: E*] uncertainty. The experiments conducted demonstrates the successful use of a coaxial thermal sensor to capture the periodic and pulsating load corresponding to the harsh environment such as that of the internal combustion engine.

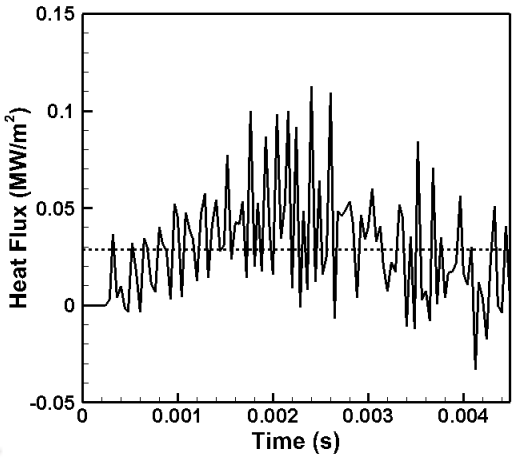

Fig. 8.9: Transient heat flux signal derived from temperature history by using one-dimensional heat conduction modelling.

8.4 Summary

An in-house attempt has been made designing and fabricating E-type coaxial surface junction thermocouple for checking the feasibility and workability of the sensor in the harsh environment such as that of internal combustion engine. The designed thermal sensor is calibrated to obtain the sensitivity (58.96 μV/°C). Further, the CSJT is utilized to capture the heat flux inside the combustion chamber of the internal combustion engine as well as at the exhaust of the engine. The combustion experiment is carried out using a GK100 Honda engine whose head is redesigned and fabricated with a provision to flush mount the thermal sensor. Further, a barrel has been designed to hold the thermal sensor. The experiments are conducted and a desirable trend is captured by the thermal sensor validating the use of the thermal sensor in the combustion chamber of the internal combustion engine. In addition, the obtained results are validated with the results obtained by the previous researchers with a good match of the trend. The second set of experiments has been conducted with the exhaust port using a 3.5 kW Kirloskar make variable compression ratio (VCR) diesel engine. The experiments have shown a desirable trend in turn validating the use of the thermal sensor. Both, the study has shown the feasibility of the development of a cost-effective, rugged, robust and reusable E-type coaxial thermal sensor for its application in the internal combustion engine. In addition, the study suggests that the same thermal sensor as explained in *Chapter 3* can be used in different applications with just slight alteration in its epoxy material.

CHAPTER 9

Coaxial Thermal Probe for Transient Measurement in an Indigenous Gas Turbine Engine#

Compendium:

With the advancement of aerospace industries, the success of man's desire to fly faster and higher depends on suitable engine technology. At higher speeds, the additional problems such as aero-thermodynamic heating, combustion instability in the engine becomes predominant because they are vital design parameters for exploring future generation materials. The precise location of the "hot-spot region" can be detected by estimating instantaneous surface heat flux from the temperature histories with appropriate heat transfer modelling. Keeping this entire vista in mind, the present chapter explores the designing and fabrication of a special type of K-type coaxial surface junction thermocouple along with its implementation in the indigenous afterburner turbofan engine to detect the combustion instability (screech phenomenon). After the fabrication, a packaging assembly is formed for the developed sensor, which includes few curing process and fabrication of barrel to house the thermal sensor. Until now, the author has demonstrated real-time application with experiments in shock tube, shock tunnels, IC engines by using in-house fabricated surface junction thermocouples (E, T, J and K-type). Each experimental facility has their unique flow ambiences and challenges while acquiring transient responses from thermal sensors. In this chapter, the author intends to utilize this sensor as "product oriented thermal probe" for industrial application. The focus is inclined towards mounting the thermal sensor in the "jet pipe section" of the large-scale gas turbine engine where the expected temperature is more than 1000 ℃. Few preliminary experiments has been performed for checking the feasibility of the developed sensor before its application in the high-temperature environment of the gas turbine engine. Two sets of engine experiments were attempted, one with a screech and the other without screech. The recovered signals from both the experiments have shown some interesting results depicting the usability of the thermal sensor for capturing the transient phenomenon in the jet pipe.

Most of the data collected during experiments are treated as, classified and not intended for public access. Only, schematic and photographic representation of the data are presented in this chapter.

9.1 Introduction

The gas turbine is the heart of the turbomachinery. The turbine is utilized in several ways like the power generation, process plants, oil and gas industry, aviation, and many smaller industries. The compressor module compresses the air and in turn, the fuel gets ignite in the combustor module. The expansion of the resulting gases takes place in the turbine module. Being on the same shaft, the turbine shaft continues to rotate and drive the compressor. The gas turbine contains a separate starter unit to provide the first starter motion; which is drive until the turbine reaches its design speed and the whole unit continues to run. The compressor, combustor, and turbine are the primary modules of the gas turbine. Further, inlet and exhaust module too are included in the gas turbine structure. In general, one or more shafts connect the compressor, combustor, and turbine and they are collectively termed as a gas generator. Largely most advanced and recent gas turbines are of axial compressor type rather than the earlier compact gas turbine design, which operated on centrifugal compressors. An axial compressor stage may not give high compression ratio as that of centrifugal compressor; a multistage compressor could provide more pressure ratio than its counterpart. In a recent development, even the compressor and turbine module split into smaller sub-module in order to exert lesser stress on the individual component and yield higher efficiency. *Figure 9.1* typically illustrates the basic mechanism of a gas turbine engine.

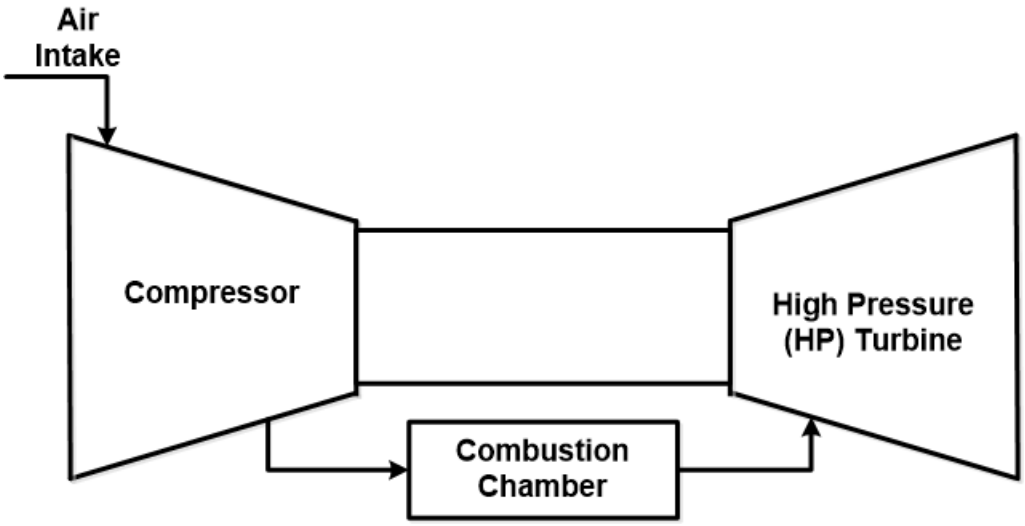

Fig. 9.1: Schematic of the basic principle of a gas turbine engine

As early as 1900's, the first step for the development of gas turbine engine were initiated with pioneering work in Germany. Several countries contributed to the development of the gas turbine research. In this view different thought process led to the development of the first gas

turbine, flight [*Whittle, 1941*]. *Holzwarth (1931)* carried the pioneering work on series of models in between 1908-1933. His work led to the development of first commercial available gas turbine.

The gas turbine engine component (such as blades, vanes, discs, and combustor) experience very severe heating environments in particular the afterburner section, involving high thermal and mechanical loads [*Ashirvadam, 2009*]. Afterburner also known as reheat thrust augmenter, provides additional thrust in cases such as emergencies, take off, combat, in supersonic flight of high performance. Additionally, it provides low-capital cost method, light-weight, to increase the engine thrust. During the reheat development, one of the most persistent problem is development of high frequency screech [*Ashirvadam, 2009*]. It is characterized by peculiar violence, which can lead to the tear of sheet metal, mechanical failure; mild screech can lead to breakage of bolts and abatement of nuts. Generally, in gas turbine afterburner, two types of instabilities are frequently encountered. One being the low frequency self-excited oscillations known as the reheat buzz (occurs over a certain fuel-air ratio) and the other is the screech, which is usually followed by high frequency pressure oscillations that could cause degradation of burner. Screech also coined as combustion instability could be some form of resonant oscillations. The inlet condition of afterburner at which screech occurs is not a fixed quantity, it varies along with the design of the afterburner. As per the previous studies, the identification of combustion driven flow oscillations (mostly occur in combustors and afterburners) are really tough. A massive effort is needed to find ways of preventing/reducing the occurrence of screech because of its destructive nature. Mostly, the screech phenomenon are associated with the transverse oscillations, which could lead to the deterioration of the perforated liners of afterburner in suppressing the oscillations.

Hence, in-situ capturing various operational parameters like strain, pressure, temperature, and vibration from hot section components is a great technical challenge. These are addressed through developmental activities involving high-temperature sensor materials, appropriate sensor design practices, processing techniques for sensor embedment, assessment of sensor response and life under harsh environments and advanced remote signal/data acquisition. These sensors are very important both for the performance evaluation of developmental engines and the health monitoring of engines. Some of the general requirements for the sensors (namely: strain, flow, temperature, exhaust gas composition etc.) and their substrate needs attention while exploring them in typical temperature and pressure ranges of aero engines (*Fig. 9.2*). A afterburning turbofan, which is

representative of the indigenous engine on which experiments have been carried out is shown in *Fig. 9.2*.

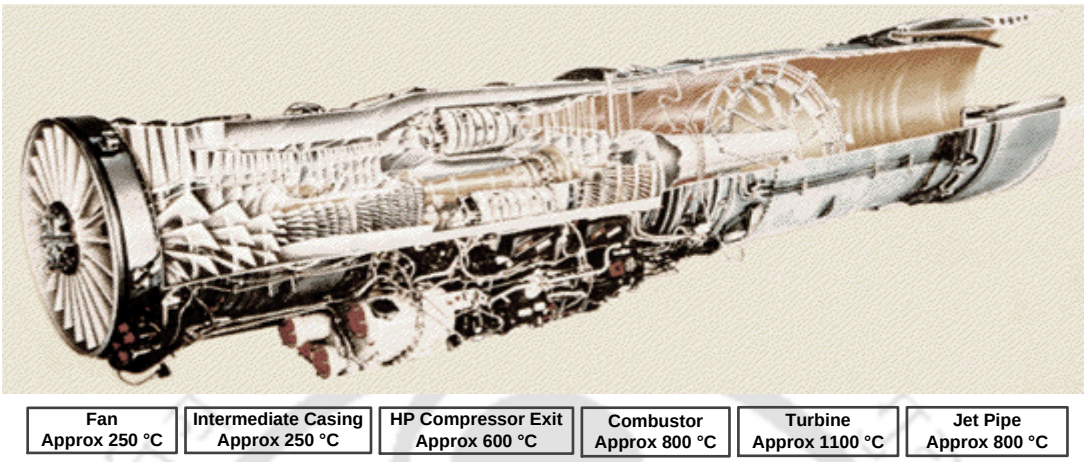

Fig. 9.2: Schematic of the afterburner turbofan gas turbine engine assembly utilized for mounting the developed CSJTs [*Pratt and Whitney, 1960*].

In this backdrop, the outline of the proposed plan is to explore the effectiveness and potential of coaxial surface junction thermocouple (CSJT) under a hostile thermal environment of a gas turbine engine. In this line, a special K-type CSJT (chromel-alumel) was successfully fabricated, at IIT Guwahati. The calibration of the sensors and their effectiveness in terms of high response time (few microseconds), in acquiring rise in temperature in the combustion chamber of an internal combustion (IC) engine has been successfully explored [*chapter 8*]. It is now proposed, to use this CSJT as a potential thermal sensor at various locations in the gas turbine engine as shown in *Fig. 9.2*. This particular study is aimed at the following objectives:

- Response and rise time of the sensor
- Effectiveness of insulation material (sodium silicate & alumina mixture)
- Acquisition of voltage signal with variation of temperature at different locations
- Measuring instantaneous transient heat flux
- Thermal endurance of the CSJT in high-temperature environment
- Potentially developing CSJT as a product oriented Sensor

9.2 Fabrication of Coaxial Surface Junction Thermocouple

A K-type Coaxial Surface Junction Thermocouple (chromel-alumel) shown in *Fig. 9.3*, has been developed and suitably amassed for gas turbine engine. The design constituents a chromel material

of *2.5* mm in diameter and an alumel wire of *0.813* mm diameter. The design methodology is similar to as elucidated in *section 8.2.1*. On confirming the connectivity of the designed surface

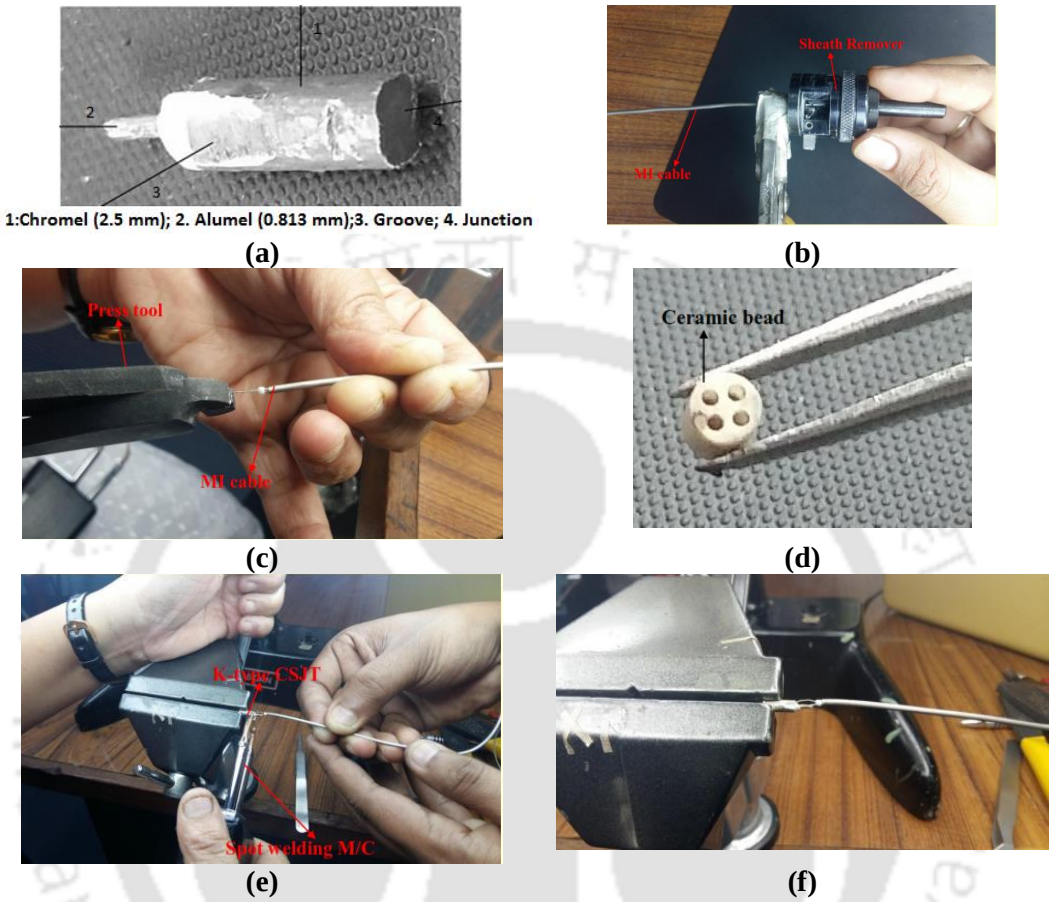

Fig. 9.3: Fabrication procedure of specially designed K-type CSJT: (a) surface junction assembly; (b) preparation of M-type MI cable using sheath cutter; (c) MI cable connection to CSJT; (d) Ceramic bead separating chromel and alumel wire of MI cable; (e) spot welding of MI cable wires to CSJT; (f) assembly of MI cable welded to CSJT.

junction thermocouple, a provision is made on the exposed chromel and alumel wire, to house the connecting wires as shown in *Fig. 9.3(a)*. The diameter of the bottom half of the chromel wire is reduced by few millimeters in order to make complete assembly as a tapered one keeping it in mind that the scalpel does not damage the bonding between two wires. A mineral insulated (MI) cable of K-type (Make: *Omega, USA*), is utilized as connecting leads over the two thermocouple wires. For connecting the MI cable, the outer sheath of the cable is removed using the sheath cutter as seen in the *Fig. 9.3(b-c).* After the removal of the sheath, between the two exposed wires of the cable a ceramic bead is inserted (*Fig. 9.3-d*). The two wires of the MI cable is pressed using the press tool such that the wires can be spot-welded onto the CSJT assembly (*Fig. 9.3-e*). The pressed

MI cable wire is then spot-welded onto the CSJT assembly using spot welding machine as seen in *Fig. 9.3(f)*. The entire additional exercise by use of MI cable is the need for K-type CSJT for exploring the high-temperature environment of the gas turbine engine. The complete sensor assembly including the MI cable should fall in the range of *30-33* Ω.

9.2.1 Packaging of Surface Junction Thermocouple

A barrel having a depth 0.8 mm with an outer thread (M5) is chosen to house the thermal sensor (*Fig. 9.4-a*). The barrel is a modified design of pressure mounting probe that is used in gas turbine engine (*Fig. 9.4-b*). All the unwanted wires that exist inside the pressure sensor is removed by heat treatment. In order to house the developed thermal sensor, the sensor has to undergo a few round of curing process. A two round of curing process was carried out for the CSJT assembly. For the curing process, a ceramic adhesive is applied on the outer casing of the probe, so that the surface becomes insulated from the barrel which is to be housed (*Fig. 9.4-c*). The curing process involves few rounds of the heating process. Firstly, once the ceramic cement is applied on the outer periphery of the sensor followed by natural drying at room temperature for around 30 min. Further, the assembly is kept inside the furnace and it is heated for nearly three round of heating cycle (*Fig. 9.4-d*). This process involves heating at 90 °C for 30 min, at 175 °C for another 30 min and finally at 315 °C for next 1 hour . Once the curing process is over, the sensor assembly is taken out and necessary steps are taken to develop a packaging assembly for the miniature thermals sensor as shown in *Fig. 9.4(b)*. In order to house the thermal probe inside the barrel, firstly, a layer of ceramic cement is applied on the cured sensor. After the application of ceramic cement, the assembly is housed in the barrel as seen in *Fig. 9.4(e)*. The complete assembly is taken for another round of curing in exactly similar fashion as described earlier. The process helps in creating an adhesive bonding between the sensor and the barrel assembly. The ceramic cement paste can resist temperature as high as 870 °C. Once the curing process is completed, a normal adhesive bond is

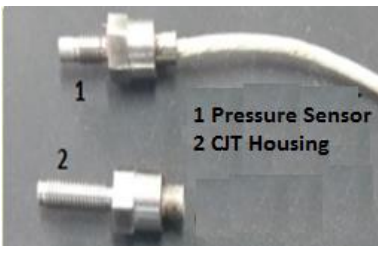

(a)

(b)

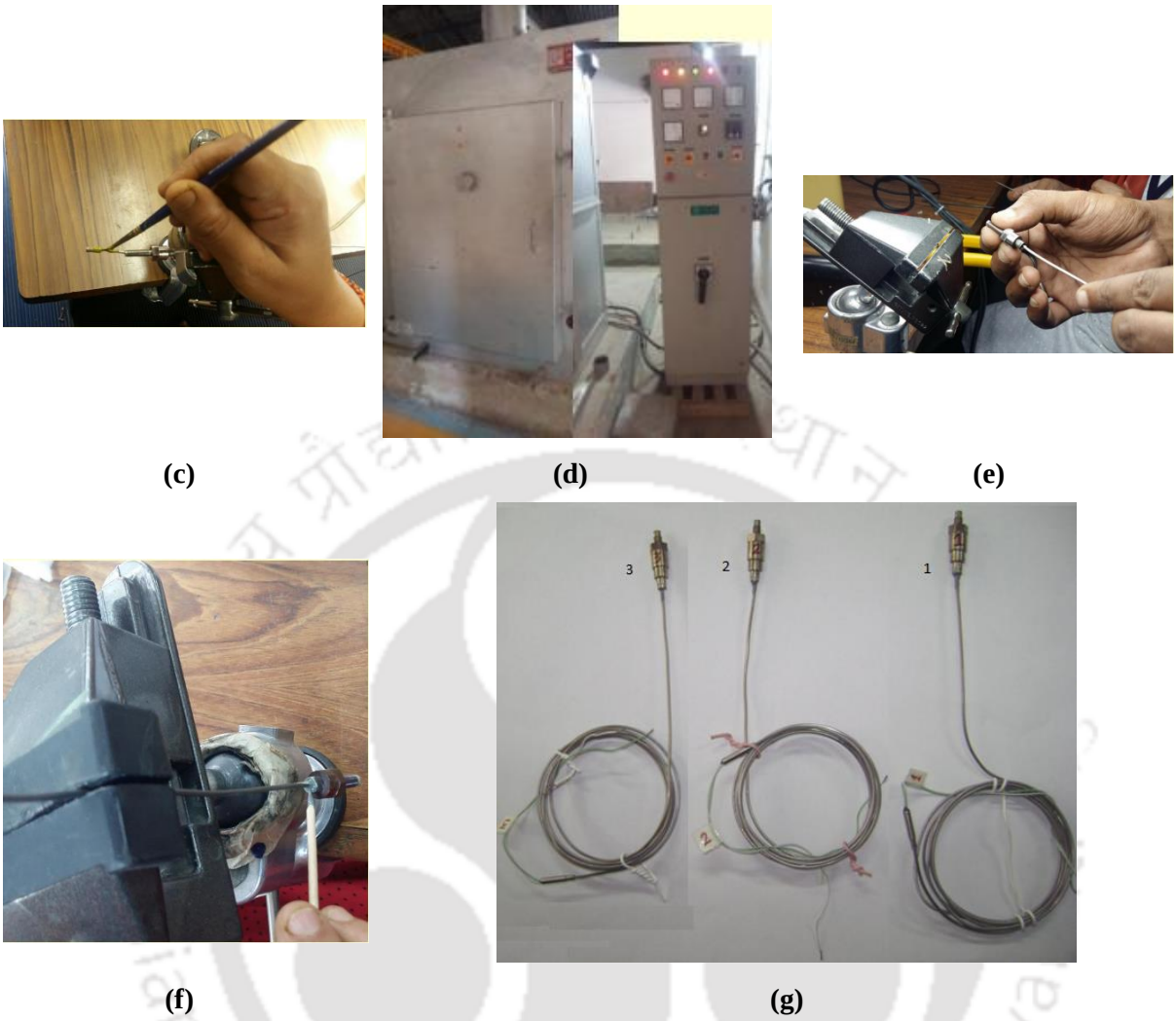

Fig. 9.4: Packaging procedure: (a) barrel for CSJT probe; (b) miniature CSJT probe housed in a barrel; (c) application of ceramic cement for pre-curing of CSJT; (d) furnace for curing CSJT probe; (e) insertion of CSJT in the barrel; (f) application of adhesive for final packaging; (g) packaged sensors for gas turbine engine testing.

filled on the lower assembly in order to give grip to the final assembly (*Fig. 9.4-f*). The bonded assembly is cooled naturally at room temperature for few hours. Once the bonding is created between the barrel and the sensor assembly, the thermal probe is ready to be utilized for capturing transient response in the high-temperature region. Three numbers thermal probes have been developed and packaged for its application in the very high-temperature environment in gas turbine engine (*Fig. 9.4-g*).

9.3 Static Calibration of surface Junction Probe

The static calibration is essential to check the linearity in the variation of the voltage signal of the developed sensor with respect to the temperature and to obtain its "sensitivity" [*Kumar and Sahoo*

2013]. For this purpose, an alumina powder based fluidized bath is utilized as shown in *Fig. 9.5(a)*. It has a provision for heating up to a temperature of 550 °C, starting from room temperature. Before carrying out this process, the calibration for INA 128 thermocouple amplifier has been performed, because the instrumentation for capturing signal from CSJT includes an amplifier along with PC-based data acquisition system. The amplifier has 6-ports with fixed gain factor of 500 in four of them and 1000 in the other two ports. For the calibration run, a known value of DC voltage is given as input using DC calibrator to the connected wires (*Fig. 9.5-b*). The calibration was carried out at gain factor of 500, for which a fixed value DC input was fed and an amplified output was obtained as tabulated in *Table 9.1*. The graph is obtained for the given DC input to the corresponding amplified DC output as shown in *Fig. 9.5(c)*. The obtained output values are in close agreement with the given input, depicting the successful calibration of the thermocouple amplifier.

The static calibration set-up includes an alumina-based fluidized bath, a conventional thermocouple (TC) of K-type, the CSJT probe (K-type), a thermocouple amplifier box, a PC-based data recorder, and analyzer. The conventional TC along with CSJT probe was dipped inside the alumina powder up to a depth of 25 mm as seen in the *Fig. 9.5(a)* maintaining the tip of both the sensors at the same position. *Figure 9.6* shows the complete assembly of the fluidized based static calibration set-up. The temperature of the bath is regulated from 30 °C to 550 °C and a corresponding change in voltage output from the CSJT probe and conventional TC is captured using the data recorder and analyzer (*Make: MIC 355M, Russia*). The data recorder and analyzer has a sampling frequency of around 54 kHz. The voltage variation captured in the data recorder for both the sensing probes is shown in *Fig. 9.5(d)*. The variation in CSJT probe as seen in *Fig 9.5(e)*, becomes stagnant after reaching a temperature variation of around 270 °C. It was due to the fact that the captured voltage signal for CSJT probe has crossed the total limiter set for

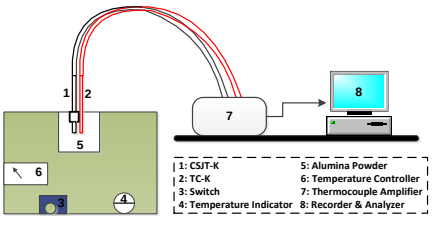

(a)

(b)

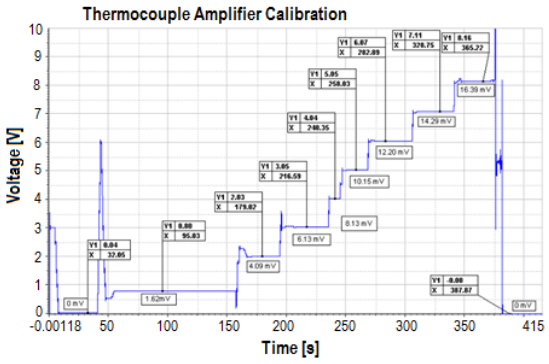

(c)

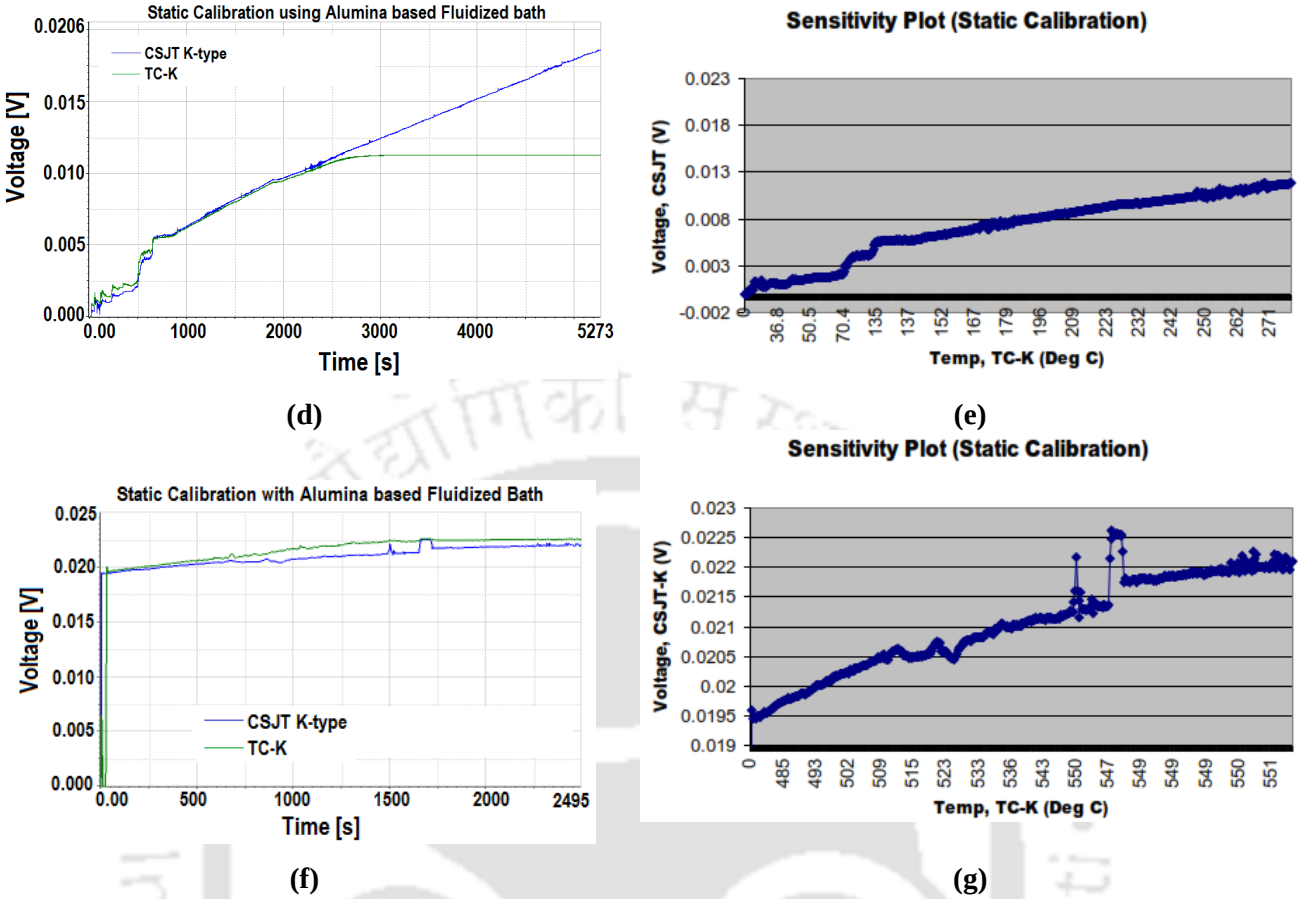

Fig. 9.5: Alumina based fluidized bath calibration experiments: (a) schematic representation of alumina base fluidized bath; (b) DC calibrator; (c) calibration graph for amplifier; (d) voltage variation with time for a time for temperature up to 270 °C; (e) voltage variation with temperature up to 270 °C; (f) voltage variation with time for a time temperature up to 480 °C; (g) voltage variation with temperature up to 480 °C.

acquiring the data. For that specific reason, the calibration was stopped, the limiter was reset, and further, the data were acquired after 480 °C as seen in *Figs. 9.5(f-g)*. The graph (*Fig. 9.5-e*) shows a linear variation for the voltage signal with respect to the fed temperature as captured by CSJT probe for temperature up to 270 °C. The linear variation of change in voltage signal as captured

Table 9.1: Data chart for calibration of thermocouple amplifier

Sl. No.	Input DC Voltage (mV)	Amplifier Gain	Output DC Voltage (V)
1.	1.62	500	0.8
2.	4.09		2.03
3.	6.13		3.06
4.	8.13		4.04
5.	10.15		5.05
6.	12.2		8.07
7.	14.29		7.11
8.	16.39		8.16

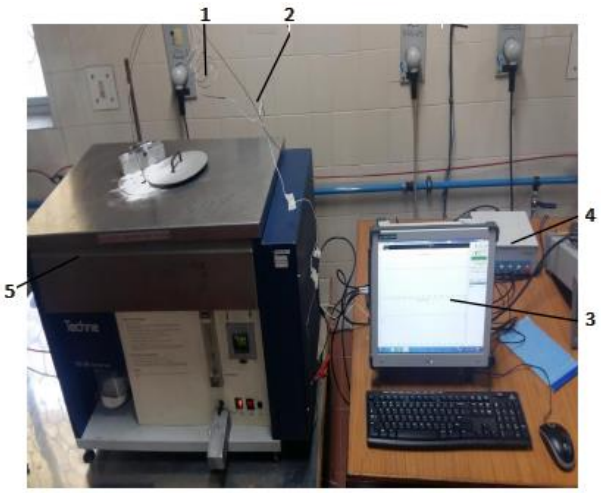

Fig. 9.6: Photograph of Fluidized bed static calibration setup.

by CSJT-K and TC-K corresponding to the temperature variation from 480 °C to 550 °C are shown in *Figs. 9.5(f-g)*. The sensitivity value obtained out of the experiment is about 41 µV/°C, which is in close agreement with the cited value in the literature.

9.4 Oil-Plunging Technique

The oil-plunging technique is carried out to access the thermal product as well as to know how fast the thermal sensor responds to a given heat source. It is basically similar to the one explained by *Buttsworth (2001)*, with an exception that in this experiment silicon oil is used instead of distilled water. The reason behind using silicon oil ahead of distilled water is the fact that the silicon has a higher boiling point, act as a perfect electrical insulator. Further, silicon oil has greater temperature stability, has good heat transfer characteristics as compared to distilled water. The set-up used has

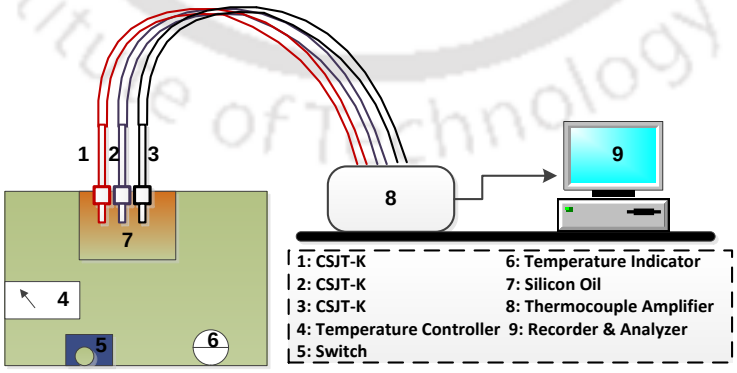

(a)

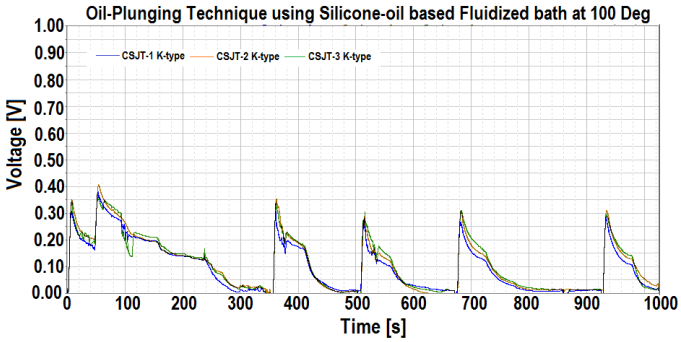

(b)

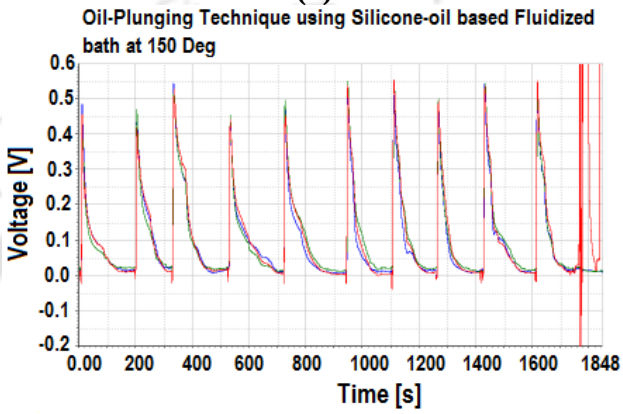

(C)

Fig. 9.7: Silicon oil based fluidized bath plunging experiments: (a) schematic representation; (b) voltage signals from CSJT probes at temperature of 100 °C; (c) voltage signals from CSJT probes at temperature of 150 °C.

a limitation that it cannot be used beyond 150 °C. For the current set of experiments, three developed CSJT probes as described earlier has been chosen. The set-up consists of silicon oil based fluidized bath, thermocouple amplifier and data recorder and analyser as seen in *Fig. 9.7(a)*. The three CSJT were exposed in such way that the tip of all the sensors is at the same position. All the sensors are coupled to data recorder and analyser through thermocouple amplifiers. The data recorder and analyser had a sampling frequency of 54 kHz. The experiments were conducted mainly for two sets of temperature reading viz., 100 °C and 150 °C. Firstly, the oil was heated to 100 °C till its stabilization, which was ascertained by dipping the conventional thermocouple. Once the temperature reaches 100 °C, the CSJTs are directly dipped into the heated silicone oil and is taken out instantly. The entire process was repeated for at least five times in order to ascertain the repeatability of the developed sensors. The voltage signals are captured as shown in *Fig. 9.7(b)*. The graph depicts the instantaneous response of the thermal sensors. In addition, the experiments were repeated for another three sets of reading by keeping the oil temperature at 150 °C. It has

been observed from the graph that all the sensors responded very well corresponding to the exposed heated source (*Fig. 9.7-c*).

9.5 Transient Experiment Using Gas Torch

A gas torch assembly was chosen to carry out the transient experiment in order to check the quick response of the CSJT probes. The experiment was carried with one of the developed sensor clubbed with two numbers of conventional thermocouples; whose tip was kept at the same position as that of the CSJT. The schematic representation of the complete gas torch assembly is shown in *Fig. 9.8(a)*. The sensors were fixed at a particular position and experiments were performed in such a way that the gas torch was lit and exposed to the sensors just for a fraction of a second and the readings were captured. The acquiring set-up comprises of the similar assembly as described in "oil-plunging technique". The attained change in voltage signal from the thermal probe and two other conventional thermocouples were shown in *Fig. 9.8(b)*. A good comparison study can be noted from the conducted experiment. The graphical representation depicts the fast response characteristics of the thermal probe as compared to the conventional thermocouple. The voltage curve of CSJT starts falling at about 3.95 s, whereas, the conventional probe resembles the trend at about 4 s. It may be emphasized here that conventional thermocouples mostly suit to study the variation in temperature where time domain is immaterial. But, for the CSJT probe, the fast response characteristics is essential to the predict surface heat flux.

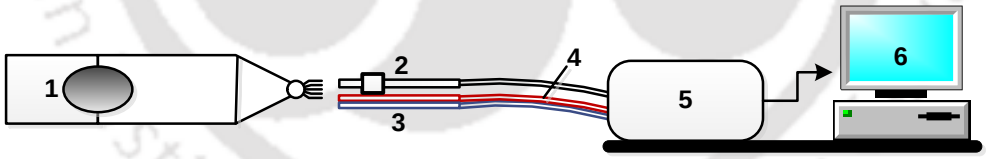

1: Gas Torch 2: CSJT-K 3: TC-K1 4: TC-K2 5: Thermocouple Amplifier 6: Data Recorder & Analyzer

(a)

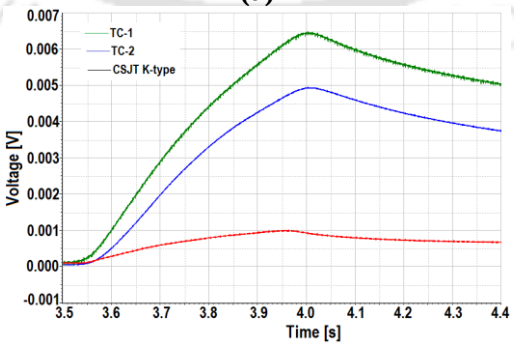

(b)

Fig. 9.8: Experiments of CSJT probes with a gas torch: (a) schematic representation of experimental setup; (b) voltage-time signals obtained from the experiments.

9.6 Experiments in the Indigenous Turbofan Turbine Engine

Once all the necessary preliminary studies are completed, the potential of thermal probes is tested by exposing them in the ambiance of gas turbine engines to capture the transient response. The specification and the characteristics of the afterburning turbofan, which is representative of the indigenous engine on which experiments have been carried out are elaborated in *Table 9.2*. The intended study is to capture "screech phenomena" in the jet pipe section of the gas turbine engine as shown in *Fig. 9.2*. The "screech" in the gas turbine is termed as "combustion instability" with an expected temperature of 1000 °C. For carrying out the experiments, two numbers of developed CSJTs were mounted in the jet pipe section at the 3 O'clock and 11 O'clock position from the rear end of the gas turbine engine (*Figs. 9.9(a-b)*). The tip of the sensors has not been exposed directly to the inner line flow rather located at a distance of 24 mm away from the inner line of the jet pipe because of the experimental limitations. The two sets of experiments were conducted; firstly the engine was run at speed (NH 14000 rpm) where the inner line jet temperature reached up to 750 °C and secondly the speed of the engine (NH 15000 rpm) is increased till the "screech region" where the inner line temperature was as high as close to 1000 °C. For the first set of experiment, the necessary instrumentation set-up is completely similar to the one used in acquiring the signal as described earlier sections. In the second set of experiment, the instrumentation acquired the date with a slight difference.

The input signal from both the CSJTs split into two half; one was clubbed with the "Kulite Pressure sensor" where the signal is intended to be captured in both AC and DC coupling, and the other wire from the CSJT signal was fitted in a similar manner to the data recorder and analyser (*Fig. 9.9-c*). The Kulite pressure sensor as mentioned is housed at a similar distance from the inner line of the jet pipe. This pressure sensor is suited to high-temperature ambiance and is rugged transducer with the capability to capture the screech frequency, thus measuring instability in the engine environment. Therefore, mounting the CSJT probes along with the pressure sensor would help us to get a comparative assessment. So, it is planned to acquire screech frequency using the CSJTs which gives us an advantage in many aspects such that along with screech frequency, the sensor can give us the information of "rise in temperature" and subsequently "heat flux" at that particular condition of screech phenomenon. The mounted CSJTs at 3 O'clock and 11 O'clock position from the rear end at the jet pipe section of the gas turbine engine (*Figs. 9.9(a-b)*), are situated beyond the "afterburner section". The voltage signals captured from the CSJTs are

Table 9.2: General specifications and characteristics of the Gas turbine engine

Type	Afterburning Turbofan
Length	3,490.0 mm
Diameter	909.3 mm
Dry weight	1,236 kg
Airflow	78 kg/s
Bypass ratio	0.16:1
Overall pressure ratio	21.5:1
LP Compressor pressure ratio	3.4:1
HP Compressor pressure ratio	6.4:1
Turbine entry Temperature	1214-1427 °C
Components	
Compressor	Two-spool, with low-pressure (LP) and high-pressure (HP) axial compressors
Combustors	Annular, with dump diffuser and air-blast fuel atomizers
Turbine	1 LP stage and 1 HP stage
Performance	
Maximum Thrust	Military thrust (throttled): 52 kN Full afterburner: 81 kN
Specific Fuel Consumption	Military thrust (throttled): 79.52 kg/(kN·h) Full afterburner: 207.00 kg/(kN·h)
Thrust to weight ratio	7.8:1 (76.0 N/kg)

processed with a low-pass filter having a cut-off frequency of 10 Hz (*Fig. 9.9-d*). The signal is compared along with the NH value, which is nothing but the high-pressure compressor speed. The graph clearly shows the successfully acquired data with every variation in the NH value.

A second set of experiments were attempted, where the engine runs were monitored until the "screech region". The comparative variation in the signal acquired from the Kulite pressure transducer, CSJT data for both AC and DC coupling along with the NH (compressor) and NL (turbine) values in terms of their speeds, respectively, are shown in *Figs. 9.10(a-e)*. These signals were filtered using band pass and low pass filter. The Kulite pressure signal was filtered with a band pass filter in the frequency range of 2000-2400 Hz; while the DC coupled signal was passed to a low pass filter having a cut-off frequency of 5 Hz. The AC coupled signal helps one to capture the frequency variation as captured by CSJTs and on the other hand, DC coupled helps one to acquire only the change in voltage signal from the CSJTs. The signal captured demonstrated some interesting finding. At the peak region, both the CSJT and Kulite pressure transducer responded typically at the same time as seen in the enlarged version of the figure (*Figs. 9.11(a-e)*). The spectrogram of the Kulite pressure signal along with CSJT-AC coupling was plotted as seen in *Figs. 9.12(a-b)*. During screech occurrence, both pressure signals and thermal probe see a

frequency 2200 Hz indicating the capability of the thermal probes to sustain high-temperature endurance. Further, the voltage signal from CSJTs can be utilized to predict surface heat flux with appropriate modeling. In nutshell, the study reveals that K-type coaxial surface junction probes are successful candidates for the ambiance gas turbine engine in terms of predicting temperature, heat fluxes and have potentials to sustain thermal endurance.

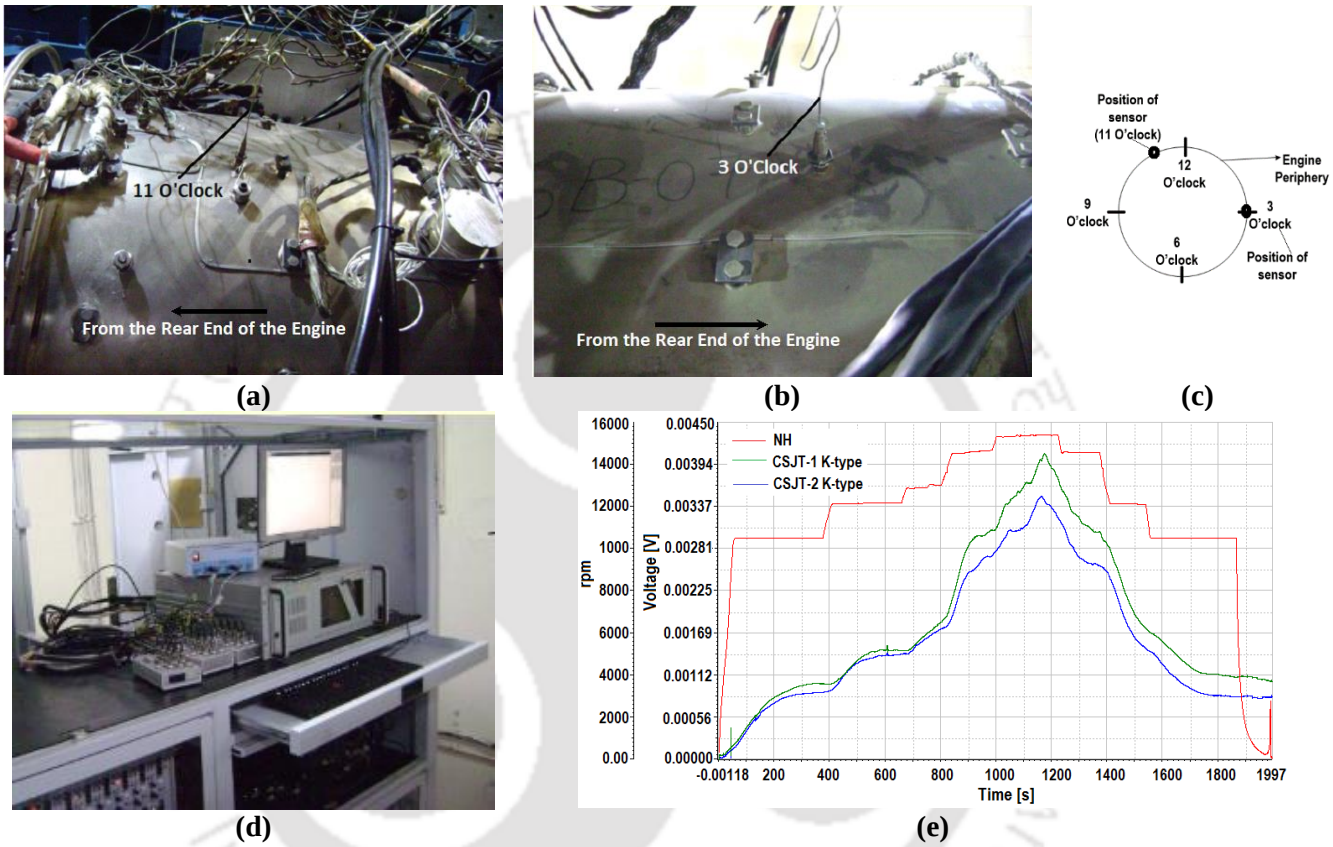

Fig. 9.9: Experiments with CSJT probes on the jet pipe of the gas turbine engine: (a) mounting at3 O'clock position; (b) mounting at 11 O'clock position; (c) position with respect to clock; (d) data acquisition system; (e) voltage signals from CSJT probes along with their NH values

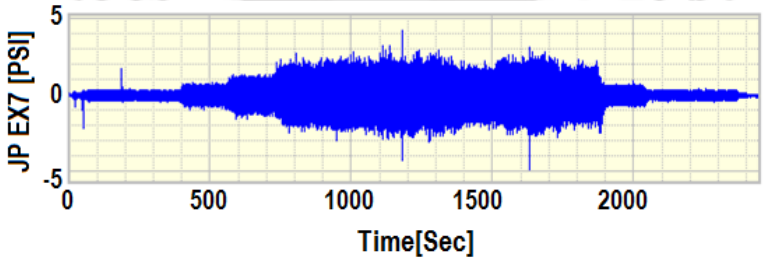

(a)

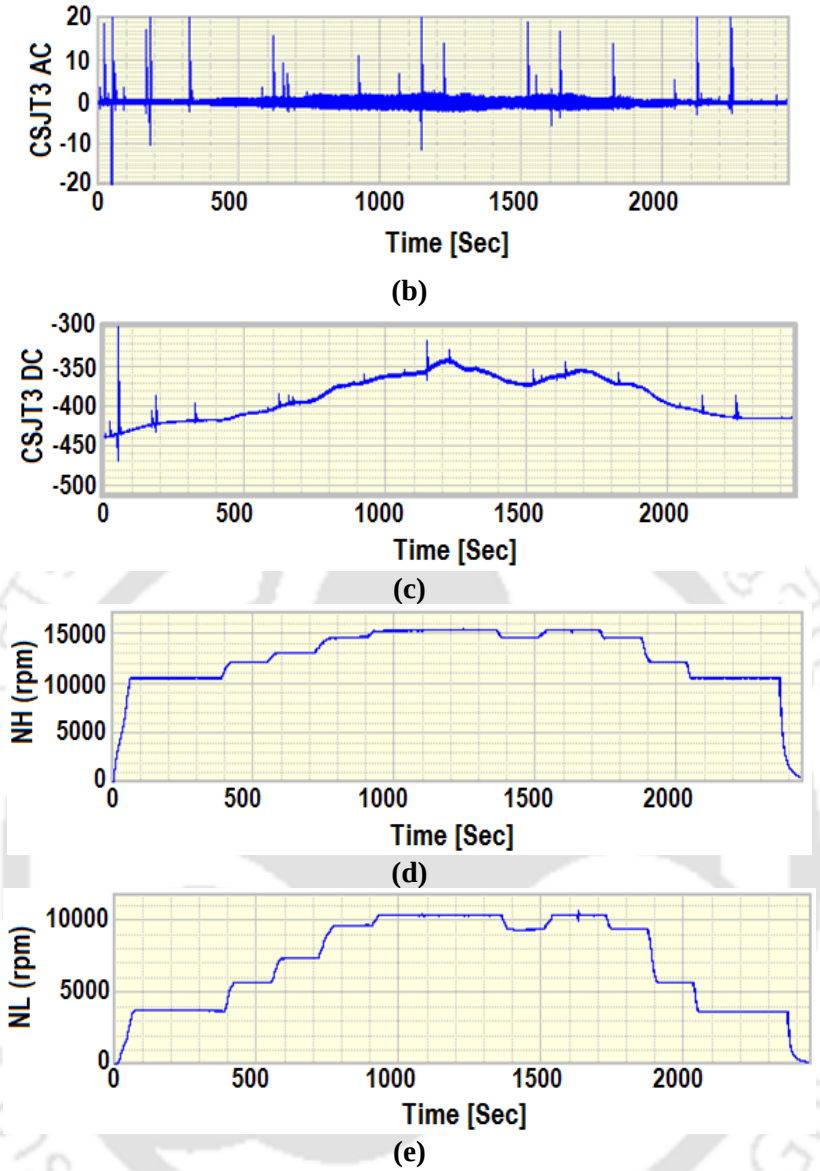

Fig. 9.10: Various signals acquired during gas turbine experiments: (a) pressure transducer; (b) AC coupled CSJT signal; (c) DC coupled CSJT signal; (d) fan speed; (e) high-pressure compressor speed.

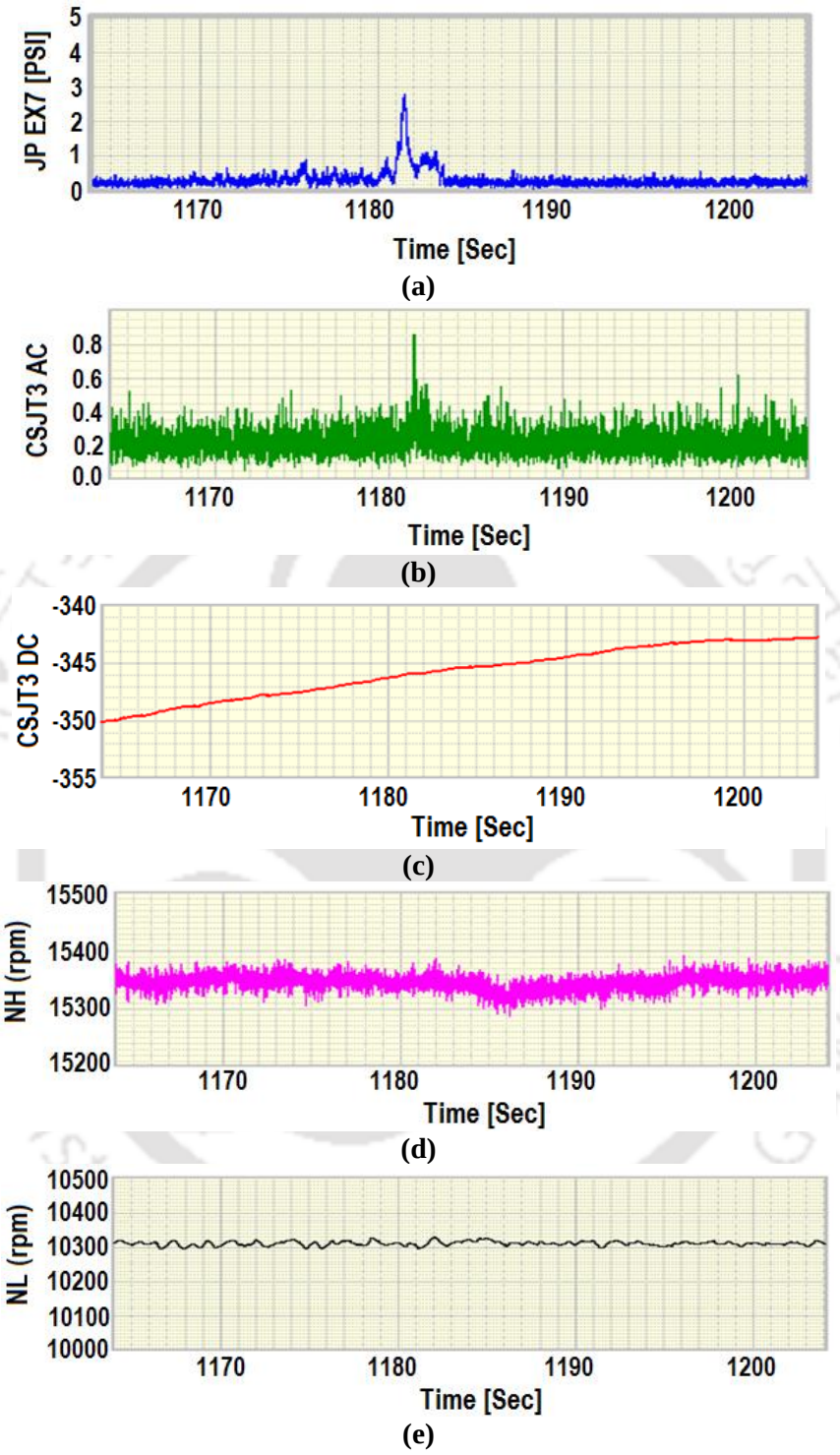

Fig. 9.11: Enlarged view of signals highlighting "screech" region: (a) pressure transducer; (b) AC coupled CSJT signal; (c) DC coupled CSJT signal; (d) fan speed; (e) high-pressure compressor speed.

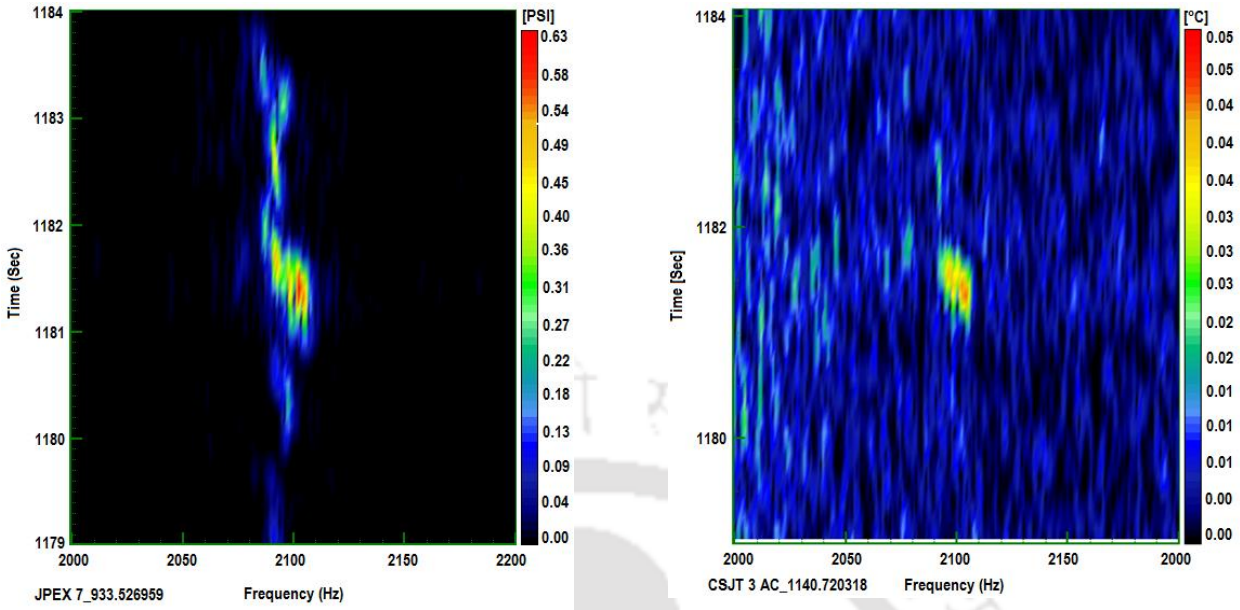

(a) **(b)**

Fig. 9.12: Spectrogram showing screech phenomena in a gas turbine engine: (a) pressure transducer; (b) In-house developed surface junction probe

9.7 Summary

The unsteady flow phenomena remain one of the basic turbomachinery problems of interest. One such phenomenon in a gas turbine engine are characterized as “screech” which essentially known as “combustion instability”. Typically, it occurs at the higher speed of the engine (14000 rpm) with a temperature around 1000 °C. Generally, robust pressure transducers are employed to capture the “screech frequency” along with the pressure data. The present investigation is focused on designing and fabricating a low cost K-type coaxial surface junction probe for its application in the gas turbine engine in order to capture the “screech phenomenon” and quantify them in terms of temperature as well as frequency. The entire packaging of the thermal probes with their respective MI cables are carried out for experiments in a gas turbine engine. After successful sensor characterization and calibration experiments, the probes have been housed at a location of “jet pipe” section of gas turbine engines at locations of 3 O’clock and 11 O’clock position (when viewed from rear end). Side by side, the pressure transducer is mounted at the same location to compare the data of thermal probe (*as seen by ‘red’ colour in Fig 9.12*). The engine is run at speeds so as to have screech phenomena, signals are acquired from both thermal probe and pressure transducer. The encouraging agreement was found from both the sensors were “screech” phenomena are detected at same locations from both the sensors. The screech frequency is obtained

as 2200 Hz at a temperature of 1000 °C when the engine speed is about 15000 rpm of pressure preliminary experiments on calibrating the thermal sensors were attempted successfully. In nutshell, packaged K-type thermal probe justifies its utility and potential in high-temperature gas turbine ambiance in terms its response and thermal endurance and further its capability to measure beyond heat flux.

CHAPTER 10

Conclusions and Scope of Future Work

10.1 Conclusion

Growing interest in unsteady flows has led to the intensive development of fast response measurement techniques towards the flow diagnostics. The focal point of the present study is designing, in-house fabrication, calibration of Coaxial Surface Junction Thermocouple (CSJT) for real-time applications in transient flow environment, which is successfully achieved in the due course of the research investigation. Various coaxial thermal sensors were fabricated in-house, with detailed calibration study including the constant temperature (static calibration) and constant heat flux (dynamic mode) based technology. The study also included determination of thermal product using experimental methods i.e. water droplet and water plunging technique. Further, sensors were exposed to real-time environments such as that of the shock tube, shock tunnel, internal combustion engine for heat flux estimation and gas turbine for detecting the combustion instability as well as temporal-time history. All the major objectives were achieved during the research investigation. Some of the important outcomes that can be drawn out of the study are listed as follows:

a) The assumed dimension for the fabrication of CSJT is well within the scope for the validation of one-dimension heat conduction equation for the semi-infinite body. The overall length of 10 mm height can be successfully utilized for a flow duration of up to 1s, beyond which one has to utilize the cold compensation factor for calculation of heat flux. Further, it was observed that there are construction difficulties in connection with the fabrication of T-type CSJT because of its highly conductive nature, leading to the difficulty in machining as well as in joining the connecting wires with the help of soldering/spot welding. One can achieve spot welding type connection for connecting wires for T-type CSJT using a machine having the energy level of close to *1000 J*.

b) It has been observed that static calibration achieved through both the methods i.e., oil-bath based calibration and alumina powder based fluidized bath are effective in their own way. However, former seemed to more effective because of the linear trend of the voltage versus temporal curve achieved as seen in *Fig. 9.5(e)* and *Fig. 9.5(g)*. However, considering CSJT

one need to be careful that same material should be used for connecting the lead wires while taking the calibration, else it will result in an erroneous result.

c) Experimentally, the TP values are determined through ‘‘water-droplet and water-plunging techniques” in which both types of CSJTs are exposed to impulse heat loads. The corresponding transient temperature histories are captured and subsequently, TP values are calculated. While comparing them with theoretical estimates, the results show encouraging agreements except for a particular case in which the TP value was under-predicted in ‘‘water-plunging” experiment for J-type CSJT. It is observed that the experimental determination of TP through both the technique has a close resemblance (within ±3 % accuracy) as compared to theoretical TP estimate for E-type CSJT. However, it is not true for J-type CJST where a significant deviation (about 29%) is found from ‘‘water-plunging” technique when the theoretical TP values are compared with experimentally determined values. The type of material (particularly ‘‘iron” in J-type CSJT) and its purity, the formation of plastic deformation between the materials at the surface, are some of the critical factors that affect the thermal properties of surface junction during its preparation.

d) It was observed that cubic-spline based curve fitting discretization technique is best suited for a present set of experimental results as compared to piece-wise linear and least square techniques, which can be highlighted from *Fig. (D.5)* [*Appendix D*]. This technique is successful for obtaining surface heat flux from the transient temperature data.

e) A thorough experimental description and methodology have been reported with respect to the calibration of the shock tube. The parametric studies are achieved through experiments and analytical calculations with an average deviation of ±12 %. For nitrogen driver, these deviations seem to be less (within ±8 %). Moreover, the in-house designed CSJTs help in estimating maximum rate of temperature rise and stagnation heat flux. It has been found that the maximum rate of temperature rise recorded by the current CJST, during a step change in temperature for a very short duration, is around 7800 K/s. This parameter is noted to be independent of the magnitude of the step; since it has been regarded as the property of the sensor. Further, shock tube is recommended for evaluating this constant parameter of any thermal sensor, since it can provide the necessary high temperature bath of any magnitude for a very short duration.

f) The fabricated coaxial thermal sensors (E, T and J-type) were utilized to capture the stagnation point heat flux using a hemispherical model and flush mounting on the end-flange of the shock tube. It was observed that the heat flux captured with E and T-type were in close agreement with each other, while it slightly overpredicted in case of J-type CSJT.

g) A comparative study was carried out using E, T and J-type CSJT in the shock tunnel using hemispherical by exposing it to a flow of Mach number 8.2 along with the pitot sensor. A response time of *21 µs* for *E-type*, *29 µs* for *J-type* and *24 µs* for *T-type* were obtained revealing their suitability in capturing transient temperature data for millisecond duration flows in a shock tunnel.

h) While recovering surface heat flux from transient temperature history from the *hemispherical model*, the E-type and T-type probe are found to be most suitable as it bears suitable thermal product for ultra-short duration time scales prevailing in shock tunnel experiments. The inconsistency in surface heat flux prediction where observed for a J-type probe which is mainly due to the discrepancy in the theoretical estimate of the effective thermal product of the sensing junction.

i) Another study was carried out using *30° ramp body* (*flat plate*), with nine thermal sensors fitted to the body in order to capture low heat flux. A similar observation was made as seen with the hemispherical model that E and T-type CSJT predicted heat flux well within comparable range, while J-type over predicting the value; leading to the conclusion that E and T-type are better choices for high-speed flow heat flux estimation. The study proved the capability of a thermal sensor to capture low heat flux as obtained in this case.

j) Heat flux estimation in the combustion chamber and exhaust flow were successfully carried out using the E-type CSJT; Fabricated with slight modification in the epoxy resin as insulation between thermocouple materials, makes it suitable for high temperature application. The trend of the results from the combustion chamber was in comparable range with the work carried out by the previous researchers, that examines its effectiveness in cyclic heat load environment. It can be inferred that with just slight modification during fabrication process (as in this case), the thermal sensor can be utilized in any harsh environment.

k) Lastly, the sensor is utilized for capturing screech phenomenon in the afterburner section of the gas turbine. For conducting the experiments, the sensors were successfully modified and a complete packaging assembly was carried out successfully for meeting the high temperature

demand. The sensor (K-type) was favourably demonstrated to capture the qualitative information about combustion instability and justifying its capability for its utilization beyond heat flux measurements.

Concisely, major sensor characteristics of the present thesis work has been listed as follows:

Table 10.1: Thermal probe characteristics

[a] E-type CSJT		
Characteristics		**Remarks**
Dimension	Height (10 mm) Diameter (OD/ID) (3.25/0.813 mm)	- One-dimensional numerical simulation (Chapter 3) - Availability of the material (Chapter 4)
Plastic Deformation		- Qualitatively based on XRD results (Chapter 4)
Sensitivity	(58 – 68) µV/°C	- Based on the oil-bath calibration (Chapter 4)
Thermal Product	(8450 – 8890) $Jm^{-2}s^{-1/2}K^{-1}$	- Based on water droplet and water plunging techniques (Chapter 5)
Response time	(20 – 24) µs	- Based on the shock tunnel experiments (Chapter 7)
[b] T-type CSJT		
Characteristics		**Remarks**
Dimension	Height (10 mm) Diameter (OD/ID) (3.25/0.813 mm)	- One-dimensional numerical simulation (Chapter 3) - Availability of the material (Chapter 4)
Sensitivity	(28 – 43) µV/°C	- Based on the oil-bath calibration (Chapter 4)
Thermal Product	(7000 – 9000) $Jm^{-2}s^{-1/2}K^{-1}$	- Based on water plunging technique (Chapter 7)
Response time	(24 – 28) µs	- Based on the shock tunnel experiments (Chapter 7)
[c] J-type CSJT		
Characteristics		**Remarks**
Dimension	Height (10 mm) Diameter (OD/ID) (2.5/0.813 mm)	- One-dimensional numerical simulation (Chapter 3) - Availability of the material (Chapter 4)
Sensitivity	(43 – 50) µV/°C	- Based on the oil-bath calibration (Chapter 4)
Thermal Product	(9580 – 13650) $Jm^{-2}s^{-1/2}K^{-1}$	- Based on water droplet and water plunging technique (Chapter 5)
Response time	(29 – 33) µs	- Based on the shock tunnel experiments (Chapter 7)
[d] K-type CSJT		
Characteristics		**Remarks**
Dimension	Height (10 mm) Diameter (OD/ID) (2.2/0.813 mm)	- One-dimensional numerical simulation (Chapter 3) - Availability of the material (Chapter 4)
Sensitivity	(36 – 41) µV/°C	- Based on the oil-bath calibration (Chapter 4) and on alumina based fluidized bath (Chapter 9)
Thermal Product	(9393 – 11450) $Jm^{-2}s^{-1/2}K^{-1}$	- Based on water droplet technique (Reference Buttsworth, 2001)
Combustion Instability Study	Screech frequency 2200 Hz	- Based on experiments conducted in gas turbine engine (Chapter 9)
Probe	Packaged as a product for sensor trial in gas turbine engine (Chapter 9)	

10.2 Future work

Having exhaustively investigated surface junction thermocouples, there are still scopes for future improvements and enhancement in capturing the experimental data. Some of them are illustrated below:

1. Exploring possible design fabrication procedure for CSJT such as a tapered probe, small size probe (less than 2 mm diameter) and preparing junction with abrasive grit. The main intention behind such fabrication methodology is to achieve a good decay time (*fast response decay time*), which is very essential for longer duration measurement.
2. Surface Morphology (plastic deformation to response time relation) would help one to dwell deep into the deformation characteristics of the junction of the CSJT. One can also link the deformation behaviour of junction probe to the usual response time for the thermal sensor.
3. Thermal product estimation for using shock tube is another area in which surface junction probes can be calibrated. The determination of this value will justify heat flux calculations in the very short duration impulse facilities with experimental run times less than milliseconds. It plays a very important role in the hypersonic environment for accurate estimation of heat flux.
4. Dynamic calibration of thermal sensors with radiation mode of heat transfer can ascertain the uncertainty involved in the heat flux measurement in the real-time environment with radiative heat loads.
5. Inverse modelling of the thermal sensor, it would help one to infer heat flux where direct measurement of heat flux is not feasible.
6. Multidimensional heat transfer modelling application considering continuous mode data acquisition. As was visualized from the experimental study, one-dimensional heat conduction equation (Eq. 3.1) for the semi-infinite body would no longer be valid for longer duration study.
7. With respect experiments in internal combustion engines, adaptability of such thermal probe will essentially quantify combustion temperatures and heat flux estimation directly under cyclic heat loads.
8. Studying the feasibility of alloy type thermal probes (N, B, R and S types) can be good exercise for gas turbine engine applications

References

Abu-Qudais MD (1997) Instantaneous exhaust-gas temperature and velocity for a diesel engine, *Applied energy*, 56(1), 59-70

Alkidas AC (1980) Heat transfer characteristics of a spark-ignition engine, *Journal of Heat Transfer*, 102(2), 189–193

Alkidas AC (1989) Heat transfer characteristics of a spark – ignition engine, *Trans. ASME, J Heat transfer*, 102(2), 189-193

Alkidas AC and Cole RM (1985) Transient heat flux measurements in a divided-chamber diesel engine, *Journal of Heat Transfer*, 107(2), 439-444

Alkidas AC and Myers JP (1982) Transient heat-flux measurements in the combustion chamber of a spark-ignition engine, *Journal of Heat Transfer*, 104(1), 62–67

Anbuselvan KKN and Reddy KPJ (2016) Measurement of heat-flux for magneto-aerodynamic interaction studies in a hypersonic flow, *47th AIAA Plasmadynamics and Lasers Conference*, 4143

Anderson JD (2000) *Hypersonic and High Temperature Gas Dynamics*, AIAA

Anderson JD Jr (2004) Modern compressible flow with historical perspective, *3rd edition (New York: McGraw-Hill)*

Andreotti R, Colombo M, Guardone A, Martinelli P, Riganti G and Di Prisco M (2015) Performance of a shock tube facility for impact response of structures, *International Journal of Non-Linear Mechanics*, 72, 53–66

Ashirvadam K (2009) Combustion instability screech in gas turbine afterburner, *Doctoral dissertation*, Dept. of Aerospace, IISc Bengaluru

Assanis D and Badillo E (1989) Evaluation of alternative thermocouple designs for transient heat transfer measurements in metal and ceramic engines, *SAE Technical Paper*, 890571

Assanis DN, Friedmann FA, Hartnett CJP and Minkowycz WJ (1993) A thin-film thermocouple for transient heat transfer measurements in ceramic-coated combustion chambers, *International Communications in Heat and Mass Transfer*, 20(4), 459–468

ASTM STP 470 Manual on the Use of Thermocouples in Temperature Measurement *ASTM International* (1970)

Babinsky H and Edwards JA (1996) Automatic liquid crystal thermography for transient heat transfer measurements in hypersonic flow, *Experiments in Fluids* 21(4), 227-236

Barlett H and Whalley R (1998) Modelling and analysis of variable geometry exhaust gas systems, *Applied Mathematical Modelling*, 22, 545-567

Battisti L and Bertolazzi E (2001) Thin film heat transfer data reduction by means of some numerical techniques, *Tech. Rep. #15*, Dept. of Mechanical and Structures Engineering, Trento University, Italy

Bendersky D (1953) A special thermocouple for measuring transient temperatures, J. Mechanical Engineering, 75, 117-121

Bhaskaran K and Roth P (2002) Corrigendum to *"*The shock tube as wave reactor for kinetic studies and material systems, *Progress in Energy and Combustion Science*, 28

Bora BJ and Saha UK (2014) Effect of compression ratio on performance, combustion and emission characteristics of a dual fuel diesel engine run on raw biogas, *Energy Conversion and Management*, 87, 1000 – 1009

Bora BJ, Saha UK, Chatterjee S and Veer V (2014) Effect of compression ratio on performance, combustion and emission characteristics of a dual fuel diesel engine run on raw biogas, *Energy Conversion and Management*, 87, pp. 1000-1009

Buttsworth DR (2001) Assessment of effective thermal product of surface junction thermocouples on millisecond and microsecond time scales, *Experimental Thermal and Fluid Science*, 25(6), 409-420

Buttsworth DR, Stevens R and Stone CR (2005) Eroding ribbon thermocouples: impulse response and transient heat flux analysis, *Measurement Science and Technology*, 16(7), 1487–1494

Caldwell FR (1962) Thermocouple materials, temperature; its measurement and control in science and industry, *National Bureau of Standards Monograph 40, UNT Digital Library, Washington D.C., USA*, 2.

Carslaw HS, and Jaeger JC, (1959) Conduction of Heat in Solids, *Oxford University Press*, London, England, pp. 353-386

Caton JA and Heywood JB (1981) An experimental and analytical study of heat transfer in an engine exhaust port, *International Journal of Heat and Mass Transfer*, 24(4), 581-595

Chana KS, Wilson TS, Bryanston CP, Burnett M and Jones TV (2003) High bandwidth heat transfer measurements in an internal combustion engine under low load and motored conditions, *Heat Transfer and Cooling in Propulsion and Power Systems,*069, 7–11

Chang J, Güralp O, Filipi Z, Assanis D, Kuo TW, Najt P and Rask R (2004) New heat transfer correlation for an HCCI engine derived from measurements of instantaneous surface heat flux, *Society of Automotive Engineers*, Warrendale, PA, 2004-01-2996.

Charles E, Lorival R, Boyer A and Malbrunot P (1984) A fast-response, high-temperature high-pressure surface thermocouple, *Sensors and Actuators, 6(2),* 135–142

Chen JC and Hsu KK (1995) Heat transfer during liquid contact on superheated surfaces, *J. Heat Transfer*, 117, 693–697

Chun KM and Heywood JB (1987) Estimating heat-release and mass-of-mixture burned from spark-ignition engine pressure data, *Combustion Science and Technology*, 54(1-6), 133-143

Cobb HM (2010) *The history of stainless steel,* ASM International

Cook WJ and Felderman EJ (1966) Reduction of data from thin film heat transfer gauge: A concise numerical technique, *AIAA J*., 4(3), 561–562

Coulter GA (1967) Dynamic calibration of pressure transducers at the BRL shock tube facility, *U.S. Army Research Laboratories*, Report 1843

D'Aleo FP and Prasser HM (2012) Design, calibration and testing of a thin film temperature gauge array for temperature and heat flux measurements in fluid mixing experiments, *Flow Measurement and Instrumentation*, 24, 29–35

Desai S, Kulkarni V and Gadgil H (2016) Delusive influence of nondimensional numbers in canonical hypersonic nonequilibrium flows, *Journal of Aerospace Engineering*, 29(5), 04016030

Desai S, Kulkarni V, Gadgil H and John B (2017) Aerothermodynamic considerations for energy deposition based drag reduction technique, *Applied Thermal Engineering*, 122, 451-60

Desikan SLN, Suresh K, Srinivasan K and Raveendran PG (2016) Fast response co-axial thermocouple for short duration impulse facilities, *Applied Thermal Engineering*, 96, 48-56

Doolan CJ and Morgan RG (1999) A two-stage free piston driver, *Shock Waves*, 9, 239-243

Duff RE and Blackwell AN (1996) Explosive driven shock tubes, Review of Scientific Instruments, 37(5):579-586

Dunn MG and Kang SW (1973) Theoretical and experimental studies of re-entry plasmas, *NASA CR*, 2232

Dunn MG and Stoddard FJ (1979) Measurement of heat-transfer rate to a gas turbine stator, *Journal of Engineering for Power*, 101(2), 275-280

Ekkad SV and Han JC (2000) A transient liquid crystal thermography technique for gas turbine heat transfer measurements, *Measurement Science and Technology*, *11*(7), 957

Enomoto Y and Furuhama S (1986) Study on thin film thermocouple measuring instantaneous temperatures on surface of combustion chamber wall in internal combustion engine (2nd Report, Study on thin film thermocouples embedded in combustion chamber wall, *Bull. Jpn. Soc. Mech. Eng.*, 29 (256), 3434–3441

Ewing J A (2006) Development of a direct-measurement thin-film heat flux array, *Master's Thesis, Virginia Polytechnic Institute and State University*, 1-39

Fay JA and Riddell FR (1958) Theory of stagnation point heat transfer in dissociated air, *Journal of the Aeronautical Sciences*, 25(2)

Fultz B and Howe J (2008) *TEM and Diffractometry of Materials*, Springer-Verlag Berlin Heidelberg

Gai SL and Baird JP (1985) Stagnation point heat transfer in hypersonic high enthalpy flow, *AIAA 20th Thermophysics Conference*, Williamsburg Va, USA

Gatowski JA, Smith MK and Alkidas AC (1989) An experimental investigation of surface thermometry and heat flux, *Experimental Thermal and Fluid Science*, 2(3), 280–292

Glass II and Patterson GN (1955) A theoretical and experimental study of the shock tube, *Journal of the Aeronautical Sciences*, 22, 73-100

Gonzales RH (2008) Diesel exhaust emission system temperature test, *National Technology & Development Program, 5100—Fire Management*, 0851 1816—SDTDC

Gordon S and McBride BJ (1994) Computer program for calculation of complex chemical equilibrium composition and applications, *NASA*, 1331

Gruszczynski JS (1965) Shock tube instrumentation techniques for study of hypervelocity entry problems, *IEEE Transactions of Aerospace and Electronics Systems*, 1, 43–56

Gulhan A (1999) Heat flux measurements in high enthalpy flows, *Defense Technical Information Center Compilation Part Notice ADP010750 (unclassified)*, 25–29

Hager JM, Simmons S, Smith D, Onishi S, Langley LW and Diller TE (1990) Experimental performance of a heat flux microsensor, *ASME International Gas Turbine and Aeroengine Congress and Exposition*, V004T09A031-V004T09A031

Heichal Y, Chandra S and Bordatchev E (2005) A fast-response thin film thermocouple to measure rapid surface temperature changes, *Experimental Thermal and Fluid Science*, *30*(2), 153–159

Henshall BD (1960) Stagnation-point heat-transfer rate measurements in the unexpanded flow of the NPL hypersonic shock tunnel, *ARC Technical Report*, 468

Holman JP (2001) Heat transfer, Eighth SI Metric Edition

Holmberg DG and Diller TE (1995) High-frequency heat flux sensor calibration and modelling, *J. Fluids Eng.*, 117(4), 659-664

Hoersch H, Editor (1993) Manual on the Use of Thermocouples in Temperature Measurement, *ASTM Special Publication Manual 12*, fourth edition.

Holzwarth H (1931) Explosion turbine, U.S. *Patent No. 1,824,893*.

Hsu KK and Chen JC (1995) Heat transfer during liquid contact on superheated surfaces, *J. Heat Transfer, 117(3)*, 693-697

https://me-mechanicalengineering.com/modes-of-heat-transfer/

Hubble DO and Diller TE (2010) A hybrid method for measuring heat flux, *Journal of Heat Transfer*, *132*(3), 031602

Hubner JP, Carroll BF and Schanze KS (2002) Heat-transfer measurements in hypersonic flow using luminescent coating techniques, *Journal of thermophysics and heat transfer*, 16(4), 516-522

Ijaz UZ, Khambampati AK, Kim MC, Kim S and Kim, KY (2007) Estimation of time-dependent heat flux and measurement bias in two-dimensional inverse heat conduction problems. *International Journal of Heat and Mass Transfer*, 50(21-22), 4117–4130

Iliopoulou Vasiliki (2005) High frequency gas temperature and surface heat flux measurements, *Dissertation, Prom.: Arts, Tony; Wauters, Pierre*

Ireland PT and Jones TV (2000) Liquid crystal measurements of heat transfer and surface shear stress, *Measurement Science and Technology*, 11(7), 969

Irimpan KJ, Mannil N, Arya H and Menezes V (2015) Performance evaluation of coaxial thermocouple against platinum thin film gauge for heat flux measurement in shock tunnel, *Measurement*, 61, 291–298

Itoh K, Komuro T, Sato K, Tanno H and Ueda S (2001) Hypersonic aerodynamic research of HOPE using high enthalpy shock tunnel, *AIAA 10th International Space Planes and Hypersonic systems and Technologies Conference*, 24-27 April, Kyoto, Japan

Jagadeesh G (2008) Industrial applications of shock waves, *Proceedings of the Institution of Mechanical Engineers, Part G: Journal of Aerospace Engineering*, 222(5), 575-583

Jagadeesh G, Reddy NM, Nagashetty K and Reddy KPJ (2000) Fore body convective hypersonic heat transfer measurements over large angle blunt cones, *J. Spacecr. Rockets*, 37(1), 137-139

James EO (1990) A technique for measurement of instantaneous heat transfer in steady-flow ambient-temperature facilities, *Experimental Thermal and Fluid Science*, 3, 416-430

Jessen C and Gronig H (1990) A new method gauges for manufacture of thin film heat flux gauges, *Shock Waves 1*, 161–164

Jessen C, Vetter M and Grönig H (1993), Experimental studies in the Aachen hypersonic shock tunnel, *Zeitschrift Für Flugwissenschaften Und Weltraumforschung*, 17(2), 73–81

John B, Kulkarni VN and Natarajan G (2014) Shock wave boundary layer interactions in hypersonic flows, *International Journal of Heat and Mass Transfer*, 70, 81-90

Kar K, Roberts S, Stone R, Oldfield M and French B (2004) Instantaneous exhaust temperature measurements using thermocouple compensation techniques, *SAE Technical Paper* 2004-01-1418

Kendall DN and Dixon WP (1966) Heat transfer measurements in a hot shot wind tunnel, *IEEE Trans, Aerosp Electro Syst*., AES-3, 596–60

Kendall DN, Dixon WP and Schulte EH (1967) Semiconductor surface thermocouples for determining heat-transfer rates. *IEEE Transactions on Aerospace and Electronic Systems*, 4, 596-603

Kendall Jr JM (1957) An experimental investigation of leading-edge shock-wave-boundary-layer interaction at Mach 5.8, *J. Aero. Sci*, 24(1), 47-56

Khalid AH and Kontis K (2008) Thermographic phosphors for high temperature measurements: principles, current state of the art and recent applications, *Sensors*, 8(9), 5673-5744

Kidd CT (1985) Thin-skin technique heat-transfer measurement errors due to heat conduction into thermocouple wires, *ISA Transactions(ISSN 0019-0578)*, 24(2), 1-9

Kidd CT (1993) High heat flux measurements and experimental calibrations/characterizations, Tech. Rep. N93-13663, *Calspan Corporational AEDC Operations*

Kireyev VT (1962) On the shock wave motion for non-instantaneous shock tube diaphragm opening, *Izv. Akad. Nauk SSSR, OTN, Mekh. Mash.*, No. 6, 144-146

Kovacs A and Mesler RB (1964) Making and testing small surface thermocouples for fast response, *Review of Scientific Instruments*, 35(4), 485

Kulkarni V and Reddy KPJ (2008) Enhancement in counterflow drag reduction by supersonic jet in high enthalpy flows, *Physics of Fluids*, 20, 016103

Kumar R (2014) Design, fabrication and novel calibration techniques for heat transfer gauges during short-duration transient measurement, *Doctoral dissertation*, Dept. of ME, IIT Guwahati

Kumar R and Sahoo N (2013) Dynamic calibration of a coaxial thermocouples for short duration transient measurements, *J. Heat Transfer*, 135(12), 124502

Kumar R, Sahoo N and Kulkarni V (2010) Design, fabrication and calibration of heat transfer gauges for transient measurement, *Processing and Engineering Applications of Novel Materials*, IMECE2010-40253, 17–23

Kumar R, Sahoo N and Kulkarni V (2012) Conduction based calibration of handmade platinum thin film heat transfer gauges for transient measurements, *International Journal of Heat and Mass Transfer*, 55(9-10), 2707–2713

Kumar R, Sahoo N, Kulkarni V and Singh A (2011) Laser based calibration technique of thin film gauges for short duration transient measurements, *Journal of Thermal Science and Engineering Applications*, 3(4), 044504

Lawton B and Klingenberg G (1996) Transient temperature in engineering and science, *Oxford University Press, Oxford*

Ledford RL, Smotherman WE and Kidd CT (1968) Recent developments in heat-transfer-rate, pressure, and force measurements for hot-shot tunnels, *IEEE Transactions on Aerospace and Electronic Systems*, 2, 202-209

Lee LYW, Chen JC and Nelson RA (1982) Surface probe for measurement of liquid contact in film and transition boiling on high-temperature surfaces, *Review of Scientific Instruments*, 53(9), 1472

Lefebvre AH and Herbert MV (1960) Heat-transfer processes in gas-turbine combustion chambers, *Proceedings of the institution of Mechanical Engineers*, 174(1), 463-478

Li J, Chen H, Zhang S, Zhang X and Yu H (2017) On the response of coaxial surface thermocouples for transient aerodynamic heating measurements, *Experimental Thermal and Fluid Science*, 86, 141-148

Liu T and Sullivan J (2005) Pressure and temperature sensitive paints," *Experimental fluid mechanics, Springer*, ISBN: 9783540222415

Liu T, Cai Z, Lai J, Rubal J and Sullivan JP (2009) Analytical methods for determination of heat transfer fields from temperature sensitive paint measurements in hypersonic tunnels, *AIAA Paper*, *736*

Lu LK and Wilson DR (1994) Survey of Short duration, hypersonic and hypervelocity facilities, 18th *AIAA Aerospace Ground Testing Conference, Colorado Springs*

Lyons PRA and Gai SL (1988) A method for the accurate determination of the thermal product $(pck)^{1/2}$ for thin film heat transfer or surface thermocouple gauges, *J. Phys. E: Sci. Instrum.*, 21, 445

ASTM (1993) Manual on the use of thermocouples in temperature measurement (4th Edition), 48-51, ISBN 978-0-8031-1466-1

Marini M (2001) Analysis of hypersonic compression ramp laminar flows under sharp leading edge conditions, *Aerospace science and technology*, 5(4), 257-271

Marr M, Wallace JS, Chandra S, Pershin L and Mostaghimi J (2009) A fast response thermocouple for internal combustion engine surface temperature measurements, *Experimental Thermal and Fluid Science*, 34(2), 183–189

Martinez-Botas RF, Lock GD and Jones TV (1995) Heat transfer measurements in an annular cascade of transonic gas turbine blades using the transient liquid crystal technique, *Transactions-American Society of Mechanical Engineers Journal of Turbomachinery*, 117, 425-425

McMillan RJ (2004) Shock tube investigation of pressure and ion sensors used in pulse detonation engine research, *M.Sc. Thesis, Air Force Institute of Technology, Wright-Patterson Air Force Base, Ohio*

Menezes V and Bhat S (2010) A coaxial thermocouple for shock tunnel applications, *The Review of Scientific Instruments*, 81(10), 104905

Merski NR (1999) Global aeroheating wind-tunnel measurements using improved two-color phosphor thermography method, *Journal of Spacecraft and Rockets, 36*(2), 160-170

Miller CG (1985) Refinement of an 'alternate' method for measuring heating rates in hypersonic wind tunnels, *AIAA Journal*, 23(5), 810-812

Miller III CG (1981) Comparison of thin-film resistance heat-transfer gages with thin-skin transient calorimeter gages in conventional hypersonic wind tunnels

Milton D Van Dyke (1958) The similarity rules for second-order subsonic and supersonic flow, *NACA-report, 1374*

Modarres D and Azzazy M (1988) Modern experimental techniques for high speed flow measuremnets, *AIAA, 26th Aerospace Sciences Meeting, Nevada*

Moffat RJ (1985) Using uncertainty analysis in planning of an experiment, *ASME J. Fluids Engineering*, 107, 173-178

Mohammed H, Salleh H and Yusoff M (2007) The transient response for different types of erodable surface thermocouples using finite element analysis, *Thermal Science*, 11(4), 49–64

Mohammed H, Salleh H and Yusoff MZ (2008) Design and fabrication of coaxial surface junction thermocouples for transient heat transfer measurements, *International Communications in Heat and Mass Transfer*, 35(7), 853–859

[1]Mohammed H, Salleh H, Yusoff MZ and Campo A (2010) Thermal product of type-E fast response temperature sensors, *Journal of Thermal Science*, 19(4), 364–371

[2]Mohammed H, Salleh H and Yusoff MZ (2010) Thermal product of fast response temperature sensors for transient heat transfer applications with numerically determined surface heat flux history, *The Open Thermodynamics Journal*, 4(2), 36–49

[3]Mohammed H, Salleh H and Yusoff MZ (2010) Fast response surface temperature sensor for hypersonic vehicles1, *Instruments and Experimental Techniques*, 53(1), 153–159

[1]Mohammed H, Salleh H and Yusoff MZ (2011) Dynamic calibration and performance of reliable and fast-response coaxial temperature probes in a shock tube facility, *Experimental Heat Transfer*, 24(2), 109–132

[2]Mohammed H, Salleh H and Yusoff MZ (2011) The effect of scratch technique on the thermal-product value of temperature sensors, *Thermophysics and Aeromechanics*, 18(1), 51–64

[3]Mohammed H, Salleh H and Yusoff MZ (2011) Thermal product estimation method for aerodynamics experiments, *Journal of Engineering Physics and Thermophysics*, 84(4), 849–859

Monde M, Arima H, Liu W, Mitutake Y and Hammad J (2003) An analytical solution for two-dimensional inverse heat conduction problems using Laplace transform, *International Journal of Heat and Mass Transfer*, 46(12), 2135–2148

Morey F and Seers P (2010) Comparison of cycle-by-cycle variation of measured exhaust-gas temperature and in-cylinder pressure measurements, *Applied Thermal Engineering*, 30(5), 487–491

Morgan RG (1997) A review of the use of expansion tubes for creating superorbital flows. *AIAA Paper*, 97-0279

Muntz EP, Lutfy F, Ketsdever A, and Vargo S (1998) A Collaborative High Alitude Flow Facility (CHAFF): University Facility for Studies of High Altitude Propulsion Plumes, Liquids and Gas Releases, and Interactions, *University of Southern California Los Angeles Dept of Aerospace Engineering*

Nagai H, Ohmi S, Asai K and Nakakita K (2008) Effect of temperature-sensitive-paint thickness on global heat transfer measurement in hypersonic flow, *Journal of Thermophysics and Heat Transfer*, 22(3), 373-381

Nakakita K, Osafune T and Asai K (2003) Global heat transfer measurement in a hypersonic shock tunnel using temperature-sensitive paint, *41st Aerospace Sciences Meeting and Exhibit*, 743

Nijeweme DJO, Kok JBW, Stone CR and Wyszynski L (2001) Unsteady in-cylinder heat transfer in a spark ignition engine: experiments and modelling, *Proceedings of Institution of Mechanical Engineers, Part D, Journal of Automobile Engineering*, 215, 747-760

O'Brien JE (1990) A technique for measurement of instantaneous heat transfer in steady-flow ambient-temperature facilities, *Experimental Thermal and Fluid Science*, 3(4), 416-430

Oleg S (2013) Heat transfer inside internal combustion engine: modeling and comparison with experimental data, *Master's Thesis*, Lappeenranta University, Finland

Olivier H and Gronig H (1995) Instrument techniques of the Aachen shock tunnel TH2, *International Congress on Instrumentation in Aerospace Simulation Facilities, ICIASF 95*, July 18–21, Wright-Patterson AFB, CH3482-3489

Olivier H, Gronig H and Schulze B (1995) Instrumentation techniques of the Aachen shock tunnel TH2, *International Congress on Instrumentation in Aerospace Simulation Facilities*, 1/1–116

Payman W and Shepherd WCF (1946) Explosion waves and shock waves, Proc. Roy. Soc. A, 186, 293-321

Peetala RK, Sahoo N and Kulkarni V (2013) Prediction of short-duration transient surface heat flux using various analytical techniques, *Heat Transfer—Asian Research*, 42, 530–543

Peng D, Jiao L, Sun Z, Gu Y and Liu Y (2016) Simultaneous PSP and TSP measurements of transient flow in a long-duration hypersonic tunnel, *Experiments in Fluids*, 57(12), 188

Persico G, Gaetani P and Guardone A (2005) Dynamic calibration of fast-response probes in low-pressure shock tubes. *Measurement Science and Technology*, 16(9), 1751

Piccini E, Guo SM and Jones TV (2000) The development of a new direct-heat-flux gauge for heat-transfer facilities, *Measurement Science and Technology*, 11(4), 342

Powars CA, Kennedy WS and Rindal RA (1972) Heat flux measurement using swept null point calorimetry, *Journal Spacecraft*, 9(9), 668-672

Rabinowitz J (1957) Aerodynamic studies in the shock tube, *CALCIT Hypersonic Research Project Memo No. 38*

Rakopoulos CD and Mavropoulos GC (2000) Experimental instantaneous heat fluxes in the cylinder head and exhaust manifold of an air-cooled diesel engine, *Energy Conversion and Management*, 41, 1265–1281

Ray N, Jagadeesh G and Suwas S (2015) Response of shock wave deformation in AA5086 aluminum alloy, *Materials Science and Engineering: A*, 622, 219-227

Ray N, Jagadeesh G and Suwas S (2015) Response of shock wave deformation in AA5086 aluminum alloy, *Materials Science and Engineering A*, 622, 219–227

Reddy NM, Nagashetty K, Jagadeesh G and Reddy KPJ (1996) Review of hypersonic research investigations in IISc shock tunnel (HST1), *Sadhana*, 21(6), 741-773

Reinsch CH (1971) Smoothing by spline functions II, *Numer. Math.*, 16, 451–454

Roberts GT and East RA (1996) Liquid crystal thermography for heat transfer measurement in hypersonic flows: a review, *Journal of spacecraft and rockets*, 33(6), 761-768

Rose PH (1958) Development of the calorimeter heat transfer gauge for use in shock tubes, *Review of Scientific Instruments*, 29(7), 557

Rose JBR, Jinu GR and Brindha CJ (2015) A numerical optimization of high altitude testing facility for wind tunnel experiments, *Chinese Journal of Aeronautics*, 28(3), 636-648

Sahoo BB (2010) Clean development mechanism potential of compression ignition diesel engines using gaseous fuels in dual fuel mode, *Doctoral dissertation*, Dept. of ME, IIT Guwahati

Sahoo N (2007) Experiments on a blunt cone model in a hypersonic shock tunnel, *In: 16th Australasian Fluid Mechanics Conference, Gold Coast, Australia*, 503–506

Sahoo N and Peetala RK (2010) Transient temperature data analysis for a supersonic flight test, *ASME J. Heat Transfer*, 132, 084503-1-5

Sahoo N and Peetala RK (2011) Transient surface heating rates from a nickel film sensor using inverse analysis, *International Journal of Heat and Mass Transfer*, 54(5-6), 1297–1302

Sahoo N, Kulkarni V, Saravanan S, Jagadeesh G and Reddy KPJ (2005) Film cooling effectiveness on a large angle blunt cone flying at hypersonic speed, *Physics of Fluids*, 17(3), 036102

Sahoo N and Kumar R (2015) Performance assessment of thermal sensors during short-duration convective surface heating measurements, *Heat and Mass Transfer, Springer*, 1-9

Sahoo N, Saravanan S and Jagadeesh G (2006) Simultaneous measurement of aerodynamic and heat transfer data for large angle blunt cones in hypersonic shock tunnel, *Sadhana Academy Proceedings in Engineering Sciences*, 31(5), 557-581

Sanderson SR and Sturtevant B (2002) Transient heat flux measurement using a surface junction thermocouple, *Review of Scientific Instruments*, 73(7), 2781

Santos J, Oishi T and Martinez ER (2009) Null point calorimeter sweeps with comparisons to thermal FEA model predictions. *AIAA Paper*, 3758

Saravanamuttoo HIH, Rogers GFC and Cohen H (2001) *Gas turbine theory*, Pearson Education.

Saravanan S, Jagadeesh G and Reddy KPJ (2009) Convective heat-transfer rate distributions over a missile shaped body flying at hypersonic speeds, *Experimental Thermal and Fluid Science*, 33(4), 782–790

[1]Sarma S, Sahoo N and Unal A (2016) Calibration of a silver thin film gauge for short duration convective step heat load, *Sadhana*, 41(7), 787-794

[2]Sarma S, Unal A and Sahoo N (2016) Thin film gauges using carbon nanotubes as composite layers, *ASME Journal of Engineering Materials and Technology*, 138, 041014-1-8

Sarma S (2017) Thin film heat transfer gauges for short duration transient measurements, *Doctoral dissertation*, Dept. of ME, IIT Guwahati

Schooley JF (1986) Resistance thermometers, Thermometry, *CRC Press, Boca Raton*

Schreck E, Hiller B and Singh GP (1993) Calibration of micron-size thermocouples for measurements of surface temperature, *Review of Scientific Instruments*, 64(1), 218

Schrijer FFJ (2003) Transient heat transfer measurements in a short duration hypersonic facility on a blunted cone-flare using QIRT. *M.Sc. Thesis. Netherlands: TU Delft*

Schultz DL and Jones TV (1973) Heat transfer measurements in short duration hypersonic facilities, *AGARD-AG-165*

Seyfried H, Sarner G, Omrane A, Richter M, Schmidt H and Aldén M (2005) Optical diagnostics for characterization of a full-size fighter-jet afterburner, *ASME Turbo Expo 2005: Power for Land, Sea, and Air*, 813-819

Shelton S, Bergles A and Saha P (1973) Study of heat transfer and erosion in gun barrels, *AFATL-TR-73-69, Air Force Armament Laboratory*, Elgin Air Force Base: Florida

Simmons JM (1995) Measurement techniques in high-enthalpy hypersonic facilities, *Experimental thermal and fluid science*, 10(4), 454-469

Skinner GT (1962) A new method of calibrating thin film gauge backing materials, *Cornell Aeronautical Laboratory*, Buffalo, New York, CAL-105

Spadaccini LJ and Colket MB (1994) Ignition delay characteristics of methane fuels, *Progress in Energy and Combustion Science*, 20(5), 431–460

Srinivasan K, Desikan SLN, Saravanan R, Kumar A and Maurya PK (2016) Fore-body and base heat flux measurements on a typical crew module in short duration impulse facilities, *Applied Thermal Engineering*, 103, 842-854

Stalker RJ, Paull A, Mee DJ, Morgan RG and Jacobs PA (2005) Scramjets and shock tunnels – The Queeensland experience, *Progress in Aerospace Sciences*, 41, 471-513

Stalker RJ (1967) A study of the free-piston shock tunnel, *AIAA Journal*, 5, 2160

Stewart DA and Chen YK (1994) Hypersonic convective heat transfer over 140-deg blunt cones in different gases, *J. Spacecr. Rockets*, 31(5), 735-743

Sundqvist B (1992) Thermal diffusivity and thermal conductivity of Chromel, Alumel, and Constantan in the range 100–450 K, *Journal of applied physics*, 72(2): 539-545

Takayama K, Reddy KPJ and Kumar CS (2014) *Shock waves made simple*, Wiley India Pvt. Ltd., India.

Taler J (1996) Theory of transient experimental technique for surface heat transfer, *Int. J. Heat Mass Transfer*, 39, 3733-3748

Tashiro Y, Biwa T and Yazaki T (2007) Determination of a response function of a thermocouple using a short acoustic pulse, *The Journal of the Acoustical Society of America*, 121(4), 1956

Timoshenko S (1953) *History of strength of materials: with a brief account of the history of theory of elasticity and theory of structures*, Courier Corporation

Torregrosa AJ, Bermúdez V, Olmeda P and Fygueroa O (2012) Experimental assessment for instantaneous temperature and heat flux measurements under Diesel motored engine conditions, *Energy Conversion and Management*, 54(1), 57–66

Venkatakrishnan V (1993) On the accuracy of limiters and convergence to steady state solutions, *AIAA Paper*

Vidal RJ (1956) Model instrumentation techniques for heat transfer and force measurements in a hypersonic shock tunnel, *Cornell Aeronautical Laboratory, Report No. WADC TN56–315*

Wang TP (1990) Thermocouple materials, *ASM International, Metals Handbook, Tenth Edition*, 2, 869-888

Wei Y, Jian W and Guangxuan L (2006) Grid-independent issue in numerical heat transfer, *arXiv preprint math-ph/0609066*

Whittle F (1945) The first James Clayton lecture: the early history of the Whittle jet propulsion gas turbine, *Proceedings of the institution of mechanical engineers*, 152.1, 419-435.

Wilbur LH (1988) Re-entry aerodynamics (AIAA Education Series), *AIAA, Washington,* D.C

Woodbury KA and Gupta A (2008) A simple 1D sensor model to account for deterministic thermocouple errors (bias) in the solution of the inverse heat conduction problem, *Inverse Problems in Science and Engineering, Proceedings of the 5th international conference on inverse problems in engineering: theory and practice,* Cambridge, UK, 11-15th July

Woodfield PL, Monde M and Mitsutake Y (2006) Implementation of an analytical two-dimensional inverse heat conduction technique to practical problems, *International Journal of Heat and Mass Transfer*, 49(1-2), 187–197

Yusaf TF, Sye HF, Yusoff MZ and Hussein I (2005) Modelling of transient heat flux in spark ignition engine during combustion and comparisons with experiment, *American Journal of Applied Sciences*, 2(10), 1438-1444

Yust M and Kreider KG (1989) Transparent thin film thermocouple, *Thin Solid Films,* 176, 73–78

Appendix-A

Pressure Measurement in the Shock Tube

A. Driven Section

A U-tube Manometer is used as an auxiliary pressure-measuring device in the IITG- shock tube. In the driven section of the shock tube, a pressure of about 6 inches of Hg is kept, which is close to the vacuum state. The length of the U-tube manometer has been chosen based on the pressure inside the shock tube such that there is no outpour of the mercury. In the present case, the manometric height has been considered as 60 cm based on the obtained results.

$$P_1 = 6''of\ Hg$$
$$\Rightarrow P_1 = 6 \times 2.54\, cm\, of\ Hg$$
$$\Rightarrow P_1 = 0.1524\, m\, of\ Hg$$

Now,

$$P_1 = \rho g h$$
$$\Rightarrow P_1 = 13.6 \times 9.81 \times 0.1524$$
$$\Rightarrow P_1 = 20012.4\, Pa$$
$$\left[\Rightarrow P_1 = 0.2\, bar\right]$$

From the Fig. A.1,

$$P_1 + \rho g h = P_2$$
$$\Rightarrow 0.2 \times 10^5 + 13.6 \times 10^3 \times 9.81 \times h = 1.01325 \times 10^5$$
$$\Rightarrow h = 0.5999 m \approx 0.6 m$$
$$\left[\Rightarrow h = 60\, cm\right]$$

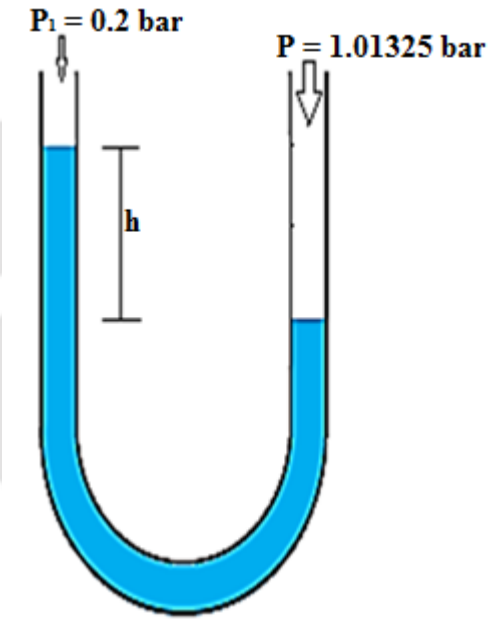

Fig. A.1: U-tube Manometer

The U-tube manometer length should be such that it has the capability to provide a minimum deflection of 60 cm. In the present study, a length of 2 m has been considered to fulfil the above requirement.

B. Driver Section

A high-pressure digital transducer with Paragon digital reader (Make: Wika, Germany) is utilized in the driver section to measure the driver section pressure (P_4) [Specification: 0-40 bar]

Appendix –B

B.1 Calculation of the Mach number, M_S (Analytically)

$$\frac{p_4}{p_1}=\frac{p_2}{p_1}\left[1-\frac{(\gamma_4-1)(a_1/a_4)(\frac{p_2}{p_1}-1)}{\sqrt{(2\gamma_1)}\left(\sqrt{(2\gamma_1+(\gamma_1+1)(\frac{p_2}{p_1}-1))}\right)}\right]^{\left(\frac{-2\gamma_4}{\gamma_4-1}\right)}$$

$$\Rightarrow \frac{p_4}{p_1}=\left[1+\frac{2\gamma_1}{\gamma_1+1}\left(M_S^2-1\right)\right]\left[1-\frac{(\gamma_4-1)\left(\sqrt{\frac{\gamma_1R_1T_1}{\gamma_4R_4T_4}}\right)\left(1+\frac{2\gamma_1}{\gamma_1+1}\left(M_S^2-1\right)-1\right)}{\sqrt{(2\gamma_1)}\left(\sqrt{(2\gamma_1+(\gamma_1+1)(1+\frac{2\gamma_1}{\gamma_1+1}\left(M_S^2-1\right)-1))}\right)}\right]^{\left(\frac{-2\gamma_4}{\gamma_4-1}\right)}$$

$$\Rightarrow \frac{19.65}{0.18}=\left[1+\frac{2\times1.4}{1.4+1}\left(M_S^2-1\right)\right]\left[1-\frac{(1.4-1)\left(\sqrt{\frac{1.4\times287\times298}{1.4\times296.92\times298}}\right)\left(1+\frac{2\times1.4}{1.4+1}\left(M_S^2-1\right)-1\right)}{\sqrt{(2\times1.4)}\left(\sqrt{(2\times1.4+(1.4+1)(1+\frac{2\times1.4}{1.4+1}\left(M_S^2-1\right)-1))}\right)}\right]^{\left(\frac{-2\times1.4}{1.4-1}\right)}$$

$$\Rightarrow 109.17=\left[1.167M_S^2-0.167\right]\left[1-\frac{0.4585\left(M_S^2-1\right)}{2.8M_S}\right]^{-7}$$

$$\left[\Rightarrow M_S=2.42\right]$$

B.2 Calculation of the value of P_2

$$\frac{p_2}{p_1}=\left[1+\frac{(2\gamma_1)}{(\gamma_1+1)}/(M_S^2-1)\right]$$

$$\Rightarrow \frac{p_2}{0.18}=\left[1+\frac{(2\times1.4)}{(1.4+1)}/(2.42^2-1)\right]$$

$$\left[\Rightarrow p_2=1.19bar\right]$$

B.3 Calculation of the value of P_5

$$\frac{p_5}{p_1}=\left[\frac{2\gamma_1M_s^2-(\gamma_1-1)}{(\gamma_1+1)}\right]\left[\frac{-2(\gamma_1-1)+M_s^2(3\gamma_1-1)}{2+M_s^2(\gamma_1-1)}\right]$$

$$\Rightarrow \frac{p_5}{0.18}=\left[\frac{2\times1.4\times2.42^2-(1.4-1)}{(1.4+1)}\right]\left[\frac{-2(1.4-1)+2.42^2(3\times1.4-1)}{2+2.42^2(1.4-1)}\right]$$

$$\left[\Rightarrow p_5=4.96bar\right]$$

B.4 Calculation of M_R

$$\frac{M_R}{M_R^2-1}=\frac{M_s}{M_s^2-1}\sqrt{1+\frac{2(\gamma-1)}{(\gamma+1)^2}\left(M_s^2-1\right)\left(\gamma+\frac{1}{M_s^2}\right)}$$

$$\Rightarrow \frac{M_R}{M_R^2-1}=\frac{2.42}{2.42^2-1}\sqrt{1+\frac{2(1.4-1)}{(1.4+1)^2}\left(2.42^2-1\right)\left(1.4+\frac{1}{2.42^2}\right)}$$

$$\Rightarrow \frac{M_R}{M_R^2-1}=0.6665$$

$$\left[\Rightarrow M_R=1.975\right]$$

B.5 Calculation of the Mach number, M_S (Experimentally)

PCB Piezotronics (Model: 113B22) make high frequency pressure sensors were installed at the end section of the shock tube with 0.5 m apart to measure the incident Mach number. The sensor has sensitivity of *146.2 mV/MPa* and *147.0 mV/MPa* respectively.

Distance between two pressure sensors is $x=0.50\,m$

Time duration between two initial peak rises,

$$\Delta t=t_2-t_1$$

From pressure signal graph,

$$\Delta t=6.33\times10^{-4}\ \text{sec}$$

$$Velocity, V=\frac{0.5}{6.33}\times10^4\ m/s$$

$$\left[\Rightarrow V=789.88\,m/s\right]$$

Speed of the sound in nitrogen medium at ambient temperature (i.e., 25 °C)

$$a=\sqrt{\gamma RT}$$

Where,

$$R=287\ J/kg-K\ \ for\ air$$

$$\therefore a=\sqrt{1.4\times287\times298}$$

$$\left[\Rightarrow a=346\,m/s\right]$$

$$\therefore \left(M_S\right)_{\text{exp}}=\frac{789.88}{346}$$

$$\left[\Rightarrow \left(M_S\right)_{\text{exp}}=2.28\right]$$

Appendix –C

C.1 Materials and Instruments utilized for the work

[Specification: Teflon TFE 0.6 mm multi-stranded wire**]**

(a)

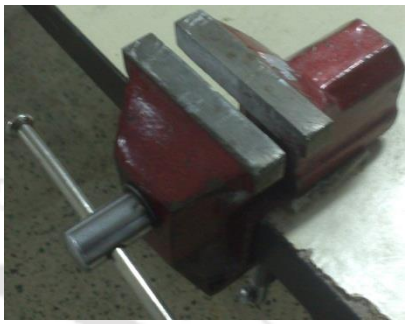

[Specification: Mini Table Bench Vice Cast Iron body with 35 mm thick and 36 mm jaw width**]**

(b)

Fig. C.1: (a) Teflon wire, (b) Mini-vice

[Specification: Araldite Klear-Two Component Fast Curing Epoxy Adhesive**]**

(a)

[Specification: HSS Parallel Shank Twist Drill (1 mm)**]**

(b)

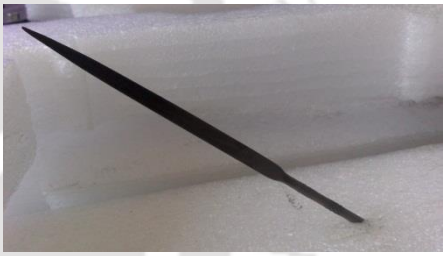

[Specification: Nicholson 100 mm Swiss pattern with natural finish Needle File**]**

(c)

Fig. C.2: (a) Araldite, (b) Drill bit, and (c) Needle file

[Specification: Make (Julabo GmbH, Germany), Hot water bath, -20 °C to 105 °C**]**

(a)

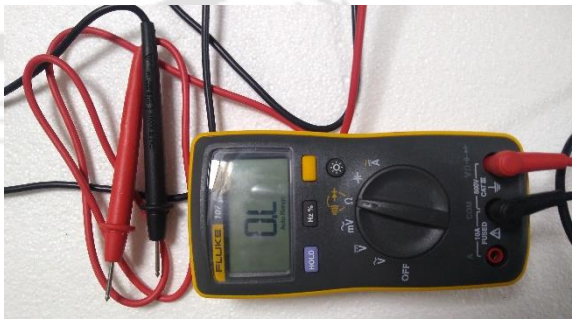

[Specification: Make (Fluke, China), Resistance max 40 MΩ, 600 V**]**

(b)

Fig. C.3: (a) Water bath, (b), and (c) Multimeter

[Specification: Make (Techno Science India Pvt Ltd, Bengaluru), 500 Gain (6 channel), INA 128**]**

(a)

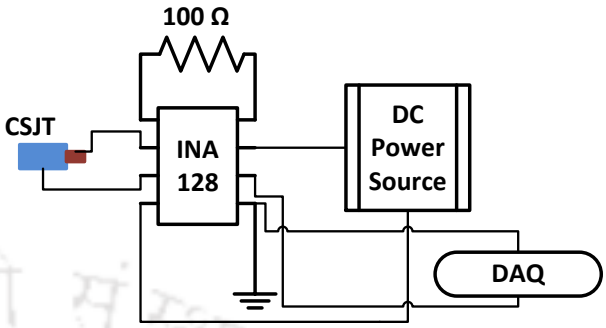

[Specification: Make (Texas, USA), INA 128 circuit**]**

(b)

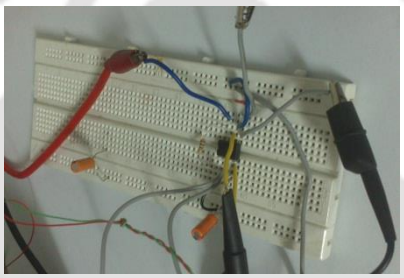

[Specification: Make (Texas, USA); **Model** (INA 128 Thermocouple amplifier (in-house))**]**

(c)

Fig. C.4: (a) Thermocouple Amplifier, (b) INA 128 Amplifier circuit, and (c) In-house designed INA 128 Amplifier

[Specification: (see Table C.1)**]**

[Specification: Make (RS Components & Controls (India) Ltd; **Model** (AT60D, 7998939), 220 V, AC 60 W**]**

(a) **(b)**

Fig. C.5: (a) Data Acquisition System (DAQ), and (b) Soldering station

[Specification: Make **(ScientiFic India)**; Model **(PSD3304);** 30V-2A, 0 to +/- 15V-1A, 5V-5A Multiple Power Supply**]**

Fig. C.6: DC power supply

[Specification: Make (Tektronix); **Model (**TDS2001C/TBS1072B-EDU); **Description: Bandwidth** : 50/70 MHz; **Channel** : 2 Analog Channels; **Sampling Rate** : 500 MS/s/ 1 GS/s; **Record Length**: 2.5k points at all-time bases**]**

Fig. C.7: Digital storage Oscilloscope

[Specification: Make (Bright Star Electronics, Pune, India); **Model** (CDWM 150)**]**

Fig. C.8: Capacitor discharge Spot welding machine

[Specification: Make: (PCB Peizotronics); **Model** (113B22)**]**

Fig C.9: High frequency pressure sensor

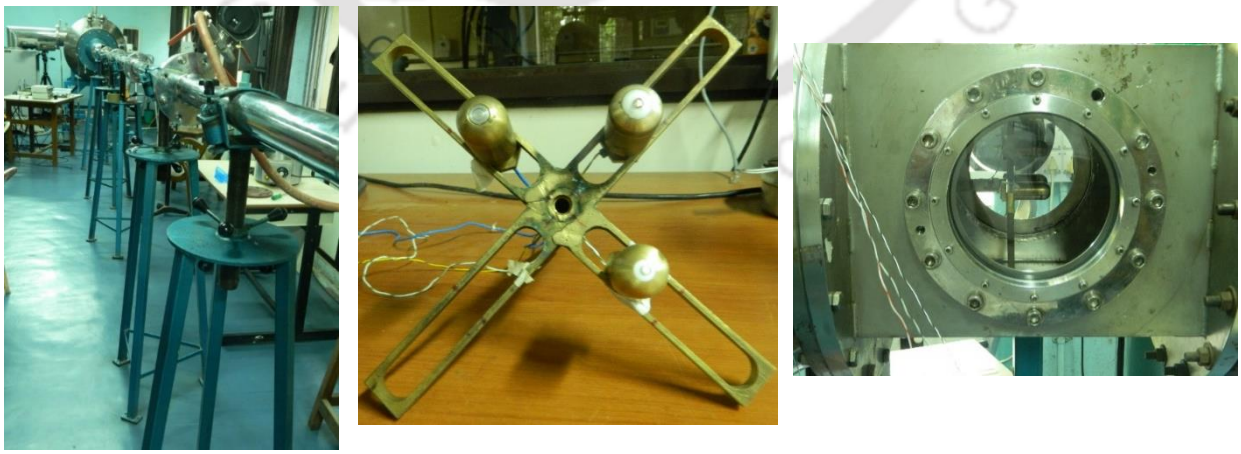

(a) **(b)** **(c)**

Fig. C.10: Pictorial view of (a) shock tunnel set at IITB, (b) the hemispherical model, and (c) mounting of hemispherical model in the test section of the shock tunnel

Material : Brass

(a)

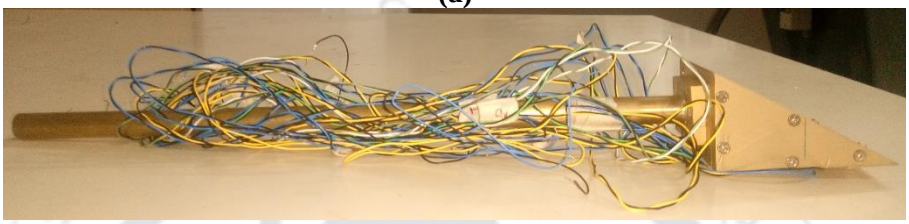

(b)

Fig. C.11: Pictorial view of the 30° wedge body for the shock tunnel application

(a)

(b)

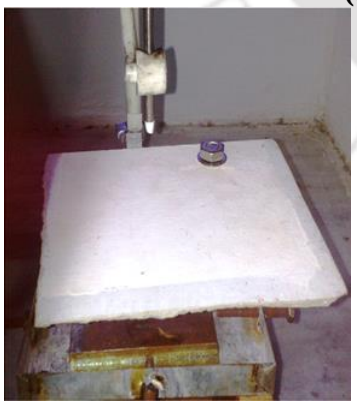

(c)

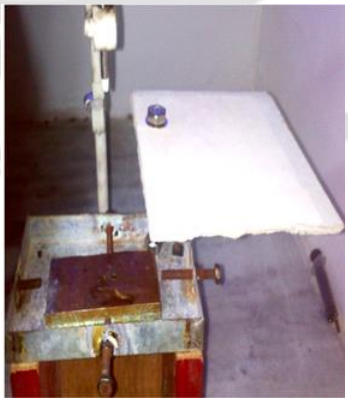

(d)

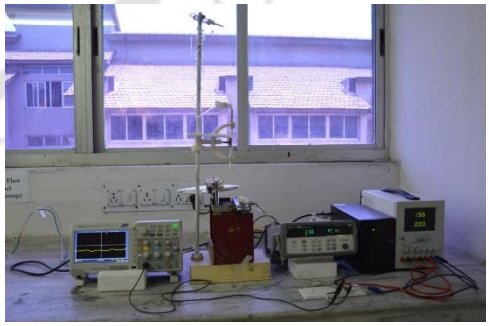

(e)

Fig. C.12: (a) water droplet set-up for thermal product estimation; (b) zoomed view showing the plate heater, copper plate and the insulating plate; Water droplet set-up showing (c) Insulating plate during heating, and (d) Insulating plate at the time of pouring; (e) Complete set-up for thermal product determination

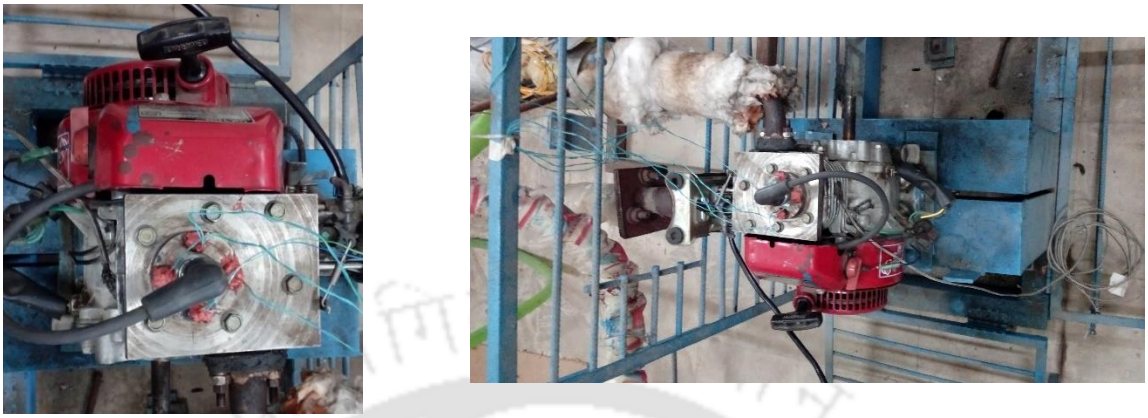

(a) **(b)**

Fig. C.13: Pictorial view of the experimental set-up showing the mounted coaxial thermal sensor

Table C.1: Specification of Instruments used for calibration

Equipment	Specifications	Remarks
Thermometer	Least count of 0.1 °C	Scientific, Analog, Water Resistant
Silicon Oil bath	Fluid can be used for the temperature -range	High viscosity index, high chemical and thermal stability and small change in properties for wide temperature range
Data Acquisition System (DAS)	Agilent 34970A Sl. No.-MY44033722, US	Measures and converts 11 different input signals: temperature with thermocouples, RTDs and thermistors; dc/ac volts; 2- and 4-wire resistance; frequency and period; dc/ac current

Appendix –D

D.1 Thermal Product Estimation using Shock Tube

In aerodynamic experiments, prediction of surface heat flux is very essential. The measurements are generally carried out by mounting the thermal sensors (such as thin-film, coaxial thermocouple) on the surfaces of aerodynamic bodies. The appropriate form of one-dimensional heat conduction modelling is employed for predicting the transient heat flux from the measured surface temperature histories as explained in *Chapter 3*. The correctness in the prediction of surface heat flux depends on the accuracy of acquired temperature history and further on the accuracy of the "Thermal Product (TP)" value. The TP value of the sensor does change due to the nature of the materials and during the fabrication process [*Chapter 5*]. The Thermal product of K-type CSJT varies in the range 4000-14000 as reported by [3]*Mohammed et al. (2011)*. In continuation, the measurement of surface heat flux during short duration timescale of measurement is estimated using the solution of the one-dimensional heat-conduction equation with a semi-infinite medium for a step change in surface temperature [*Taler, 1996*]. Additionally, for a known surface temperature history (T_s), the instantaneous surface heat flux (q_s) can be predicted from Duhamel's superposition integral [*Chapter 3*].

Keeping all this necessary condition for the prediction of surface heat flux, an attempt has been made for the prediction of thermal product using shock tube as a tool. The experimental procedure is such that an in-house fabricated CSJT is flush mounted as a static probe on the end section of the shock tube [*Fig. D.1*]. The flow physics of shock tube is similar to what has been explained in *Chapter 6* with helium as driver gas and air the driven gas.

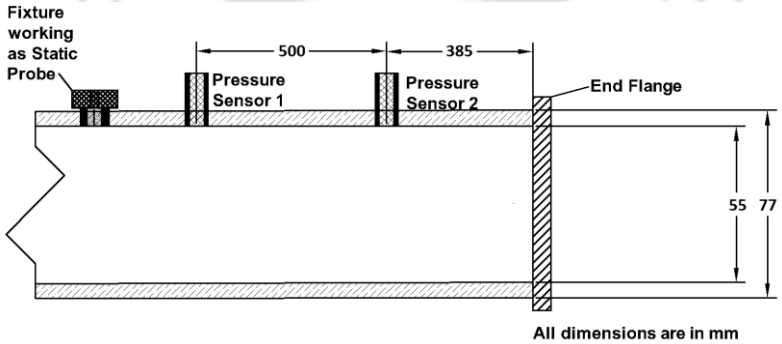

Fig. D.1: Schematic of the probe mounted on the shock tube-IITG for calculating the thermal product.

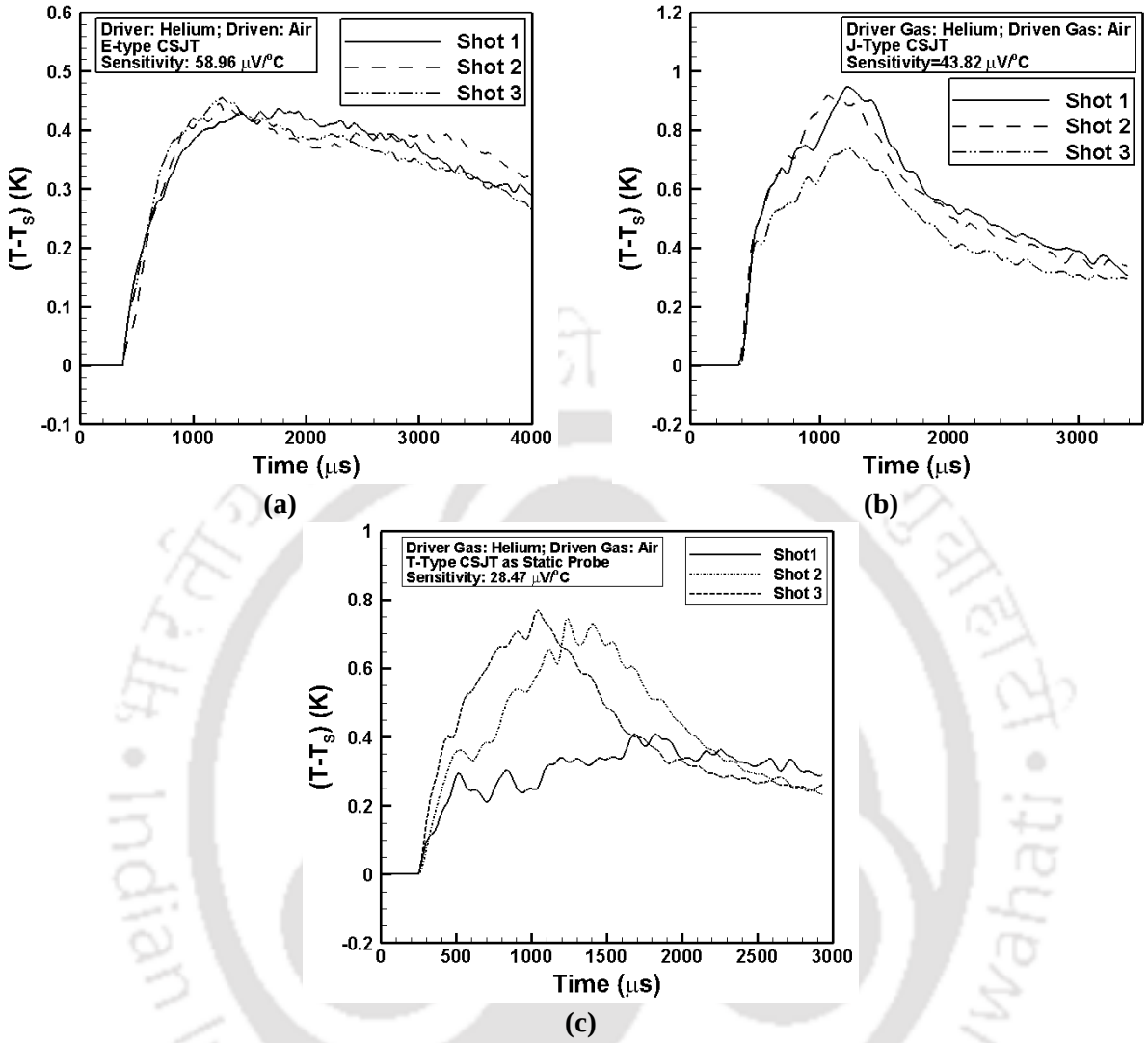

Fig. D.2: Temperature signal captured using the coaxial thermal sensors (a) E-type, (b) J-type and (c) T-type

Once the diaphragm gets a rupture, the thermal sensor is triggered with the initial slug of fluid in the form of the shock wave. *Figure D.2* shows the rise in surface temperature obtained from the thermal sensor. The signal resembles in the form of a sharp ramp signal as has been highlighted in *Chapter 5* while predicting the TP value using the 'Water droplet and Water plunging technique' respectively. Once we get the rise in surface temperature, the obtained temporal value is utilized to estimate the thermal product value from the *Eq. (D.1).*

Table D.1: Comparison of the thermal product of CSJT using Shock tube

Sl. No	CSJT Types	Thermal Conductivity (K) (W/m-K)	$(T_S - T_\infty)$	K_{room}	Density (ρ)	Specific Heat (c) (J/kg-K)	T_2 (K)	T_∞ (K)	Thermal Product, air (β_a) ($Jm^{-2}s^{-1/2}K^{-1}$)	Thermal Product , sensor (β_S) ($Jm^{-2}s^{-1/2}K^{-1}$)
1	E	0.061	0.43	0.026	0.92	1156	1063.09	300	8.07	14198.52
		0.063	0.41		0.97	1165	1114.99		8.45	16894.16
		0.062	0.42		0.92	1158	1071.68		8.11	14823.67
2	**J**	**0.058**	**0.74**	**0.026**	**0.89**	**1139**	**966.85**	**300**	**7.65**	**6893.58**
		0.08	**0.92**		**1.048**	**1236**	**1693.8**		**10.18**	**15415.17**
		0.081	**0.95**		**1.051**	**1238**	**1716.82**		**10.24**	**15318.89**
3	T	0.051	0.29	0.026	0.805	1099	787.18	300	6.72	10952.51
		0.051	0.72		0.806	1099	788.92		6.73	4527.41
		0.053	0.77		0.839	1114	852.23		7.07	5081.57

$$\frac{T_S - T_\infty}{T_a - T_\infty} = \frac{\beta_a}{\beta_S + \beta_a} \tag{D.1}$$

Where, T_a, T_S, T_∞ = Temperature of the shock wave, sensor and ambient respectively and, β_a, β_S = TP of the shock wave and sensor.

Using the value of β_a ($Jm^{-2}s^{-1/2}K^{-1}$), which is calculated based on the shock tube parameter, the thermal product value can be estimated from *Eq. (D.1)*. The obtained value for all the thermal sensor has been jotted down in *Table D.1*. Although the obtained results are just a preliminary estimate, it needs further intervention in the future as reported in the future work section (*Section 10.2*). A variation in the thermal product value has been observed for J and T-type CSJTs, but more experiments on this would result in a conclusive justification.

D.2 Discretization Technique Implementation for Heat Flux Estimation

As discussed in *Chapter 3*, on the discretization techniques such as Linear fit, polynomial fit and Cubic-Spline based techniques, a few attempt has been made to discretize experimental data obtained from the shock tube experiments as described in *Chapter 6*. The experiments were attempted on CSJT mainly for two cases (1) with sensor flush mounted on the end-flange, and (2) sensor flush mounted on the hemispherical model fitted at the end-flange of the shock tube. The experiments were conducted with helium as driver gas and air as the test gas with the same methodology as explained in *Section 6.2.3* and *Section 6.3.2*.

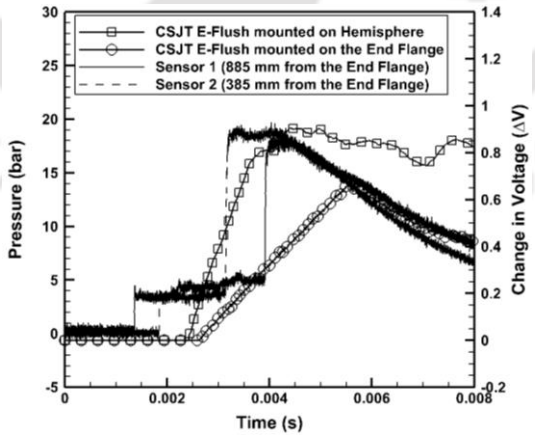

Fig. D.3: Change in voltage signal obtained with E-type CSJT flush mounted on the end flange and on the hemisphere fitted on the end flange and lastly, the obtained pressure signal using helium as the driver gas

The captured temperature data from the shock tube experiment are utilized to obtained one-dimensional surface heating rate by using analytical heat transfer modelling techniques. Firstly, the obtained temperature-time history are discretized using various curve fitting techniques namely, piecewise linear fit (*Eq. (3.6-3.8)*), Least square (polynomial fit) (*Eq. (3.9-3.10)*), cubic spline fit (*Eq. (3.11-3.12)*). In addition, the obtained temperature data from the discretization techniques are compared with the estimated experimental signal. *Figure D.3* shows the obtained pressure signal from the shock tube experiment; further, the change in voltage signal is superimposed with the pressure signal. The graph typically highlights the general flow physics of a typical shock-tube not concerning about the reflected portion of the shock from the end-flange. Further, the *Fig. D.3* is plotted to check the feasibility/correctness of the obtained signal. From the plot, it can be observed that the obtained signal from both the experiment seems to be very much logical with the rise of the thermocouple signal along with the pressure signal. Additionally, the obtained temperature data show a very good recovery of transient temperature data as seen in *Fig D.4(a)*. The basic difference between the two case studies as observed from the obtained temperature history is that in one case the sensor feels the conductive heat directly on the sensor surface, like the case of CSJT flush mounted on the end flange as a typical case of the infinite exposure area. On the other hand, the signal from CSJT flush mounted on the hemispherical model fitted at the end flange, the CSJT experiences partly convective and partly conductive due to the bow shock formation over the hemisphere (*Fig D.4(a-b)*). It shows the one-dimensional surface heating data produced by various discretization methods. It has been comprehended from case 1, that for the timescale of interest, the signal obtained from all the discretization technique, namely piecewise linear fit, polynomial fit and cubic spline fit shows good accuracy, the overall trend seems to follow a triangular form. So, it has been observed that, when the CSJT experiences ramp kind of input, the obtained temperature signal is of the form of triangular in nature and the heat flux predicted by all the three above mentioned process can be applied with polynomial approach slightly under-predicting the value. On the other hand, for the signal obtained from case 2, it is observed that surface heat flux obtained using all the given technique show a good trend, while cubic spline technique showing more accurate and smoother response compared to other technique. For the cubic-spline techniques to show the steady test timescale, seems quite logical from the consideration of the observed parabolic fit [*Holman, 2001*]. In general, cubic-spline

discretization techniques best suits for obtaining surface heating rate using coaxial surface junction thermocouple for the case of stagnation-point heat flux estimation, pertaining to high-velocity flow with a very small timescale of application. This section is just to highlight the discretization technique utilized to estimate the surface heat flux.

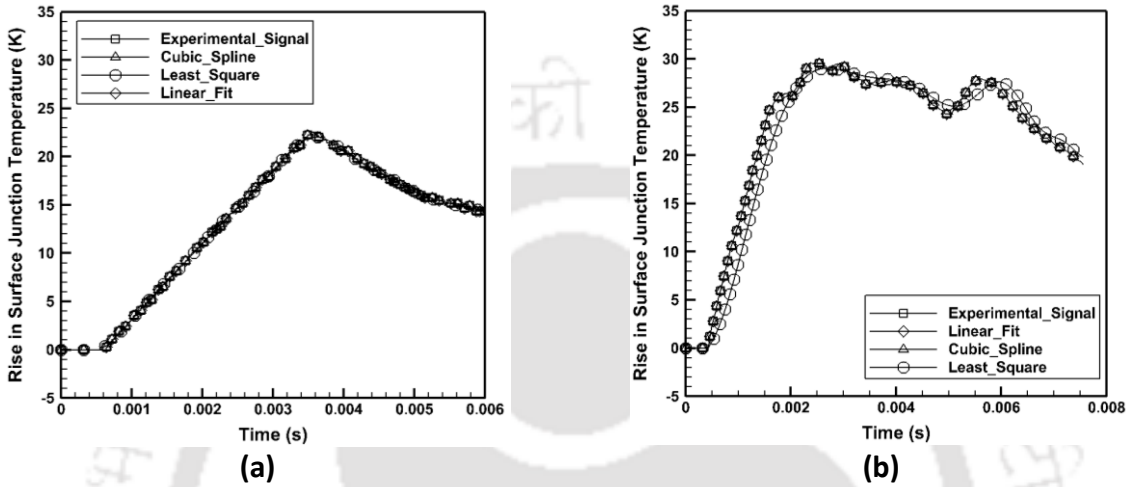

Fig. D.4: (a) Rise in transient surface temperature from CSJT mounted on the end flange of the shock tube; **(b)** rise in transient surface temperature from CSJT mounted on hemisphere fitted at the end flange of the shock tube

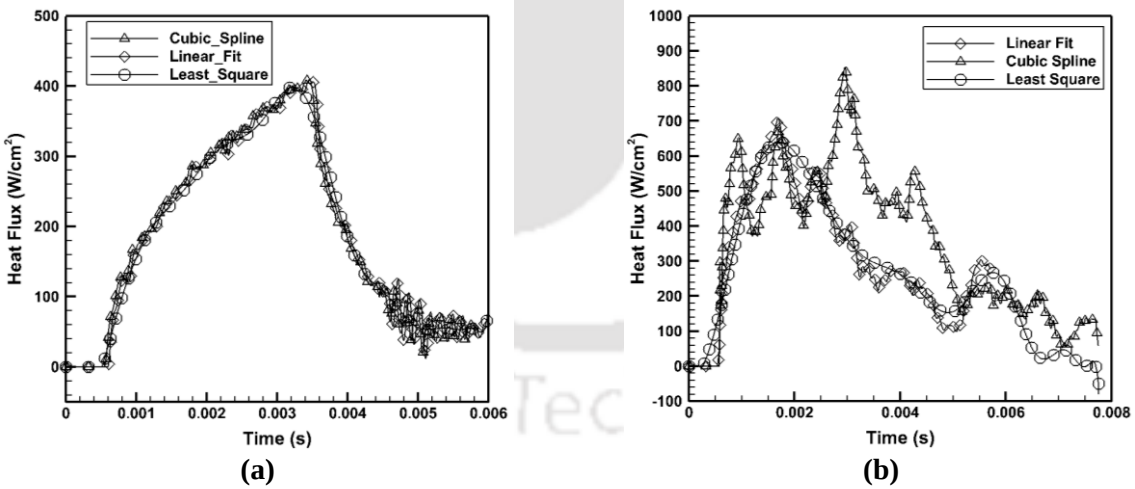

Fig. D.5: Surface heat flux histories obtained through one-dimensional heat conduction modelling from temperature histories of CSJT, mounted on the end flange of the shock tube

Appendix-E

E.1 Uncertainty Study

In any experimental investigation, the uncertainty assessment deals with the accuracies involved in the instruments and subsequently its effects in the global measurements as given by *Eq. (E.1)*. The method of sequential perturbation technique has been used for uncertainty calculation [*Moffat, 1985*]. The instruments used in the present investigations include pressure measurements through mercury manometer, digital pressure gauge and pressure transducers, transient temperature measurement through CSJT and subsequent estimation of heat flux histories. The data acquisition system involves necessary instrumentation such as power supply unit, voltage amplifier and oscilloscopes. Based on the manufacturer's specification the accuracy of these units is ±0.01 ˚C, ±0.015 %, ±0.015 %, ±0.02 %, ±0.01 % and ±0.12 % respectively. The uncertainty in accounting for calculation of sensitivity of CSJT was about ±0.345 %.

$$W_R = \left[\left(\frac{\partial R}{\partial x_1} w_1 \right)^2 + \left(\frac{\partial R}{\partial x_2} w_2 \right)^2 + ... + \left(\frac{\partial R}{\partial x_n} w_n \right)^2 \right] \quad \text{(E.1)}$$

Where R is a given function of the independent variable $x_1, x_2, x_3, ...x_n$, i.e., R= R $\left(x_1, x_2, x_3, ...x_n\right)$, W_R is the uncertainty for the parameter R, and $w_1, w_2, w_3, ...w_n$ are the uncertainty in the individual independent variables.

Appendix-F

F.1. Experiments with Silver Thin-Film gauge

TFGs and CSJTs are the two prime resistance temperature detector sensors which are suitable for measuring highly transient surface temperature data, as the response time of such sensors fall in the range of few microseconds. A thin-film gauge consists of a high conducting material in the form of thin-film (silver/platinum/nickel) painted or sputtered over a substrate material (pyrex/macor). The sensing material of the thin-film is available in the form of ink/paste form, which is then painted over the substrate with the use of paintbrush/sputtering as explained. The voltage change is further measured based on the change of the resistance occurred as a result of the change in temperature. On a general note, metals having a higher temperature coefficient of resistance (TCR) with high sensitivity are usually preferred as substrate material for the thin-film gauges.

In the backdrop, an attempt has been made to study the feasibility of in-house developed Silver thin-film gauge (STFG) in the highly transient environment of shock-tube. A pyrex substrate of 10 mm long and 6 mm diameter is chosen for the present study. The surface of the pyrex material is polished using grain silicon carbide sandpaper (wet and dry) to remove sharp irregularities such that the gauge material can stick properly on the substrate material. Afterwards a thin layer of silver ink is hand painted on the substrate which is then allowed to get dry naturally in a clean environment. Further, the gauge assembly is placed on a steel base and inserted inside the oven for about 10-15 mins at a preferred temperature (~ 350 °C). After the baking process, the gauge is not taken out until the temperature of the oven reaches the room temperature. The resistance of the gauge is checked using the multimeter. If the resistance does not fall in the desirable range of 10-100 Ω, a second layer of ink is painted and the whole process is repeated. The entire fabrication process can be accessed from references (*Sarma 2017 and Kumar 2014).*

If the resistance of the gauge falls in the desirable range, some regions of the same is painted with silver strips to facilitate connection of lead wires and further the gauge assembly is dried in the oven. Finally, the lead wires are soldered on the silver strips using the micro-solder machine as shown in *Fig. (F.1)*. After the fabrication process, the gauges are calibrated using the standard Oil-bath calibration method as explained in *Chapter 4*. The calibration of the thin-film

gauge is elaborated in detail in the literature *Sarma (2017)*. A TCR value of *0.0026/°C* is obtained from the static calibration of the silver thin-film.

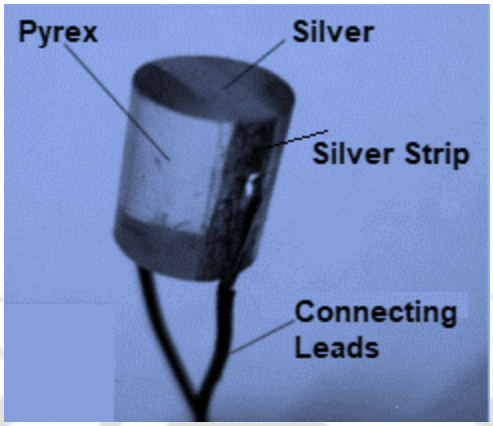

Fig. F.1: A typical silver thin film gauge fabricated in the laboratory (*Sarma 2017).*

After the fabrication and calibration of the STFG, the sensor is utilized to study its feasibility in the shock tube and to validate the working of the in-house developed coaxial surface junction thermocouples as explained in *Chapter 6*. The TFG is flush mounted at the end flange of the shock tube in a similar manner as mentioned in *Section 6.3* (*Fig. 6.10-a*). The experiments are conducted using helium as the driver gas and air as the driven gas (*Section 6.4.2*) separated by an aluminium diaphragm of 1.2 mm thickness (*Fig. 6.11*). The complete working principle and operation of shock tube is explained in *Chapter 6*. *Figure F.2* shows the typical STFG and pressure sensor response captured during the experimentation in shock tube. The graph clearly highlights two picks which signifies the temperature rise across incident shock and reflected shock. It can be emphasized from the graph that STFG is able to capture both incident and reflected shock as typically obtained during operation of the shock tube. On the other hand, CSJT as seen in *Fig. 6.17* only captures responses due to reflected shock, emphasizing that TFG are more sensitive than its counterpart. Additionally, the heat flux (*Eq. 3.13*) is computed from the captured response of the TFG with usage of one-dimensional heat conduction modelling elaborated in *Chapter 3*. *Figure F.3* shows the typical heat flux histories of the STFG highlighting effect of both the incident shock wave (ISW) and reflected shock wave (RSW). An average value close to *223 W/cm^2* for ISW and *449.8 W/cm^2* for RSW are obtained from the three repeated shots (±2.78 % uncertainty). The obtained values are in close agreement with the estimated values corresponding to *E, T and J-type* CSJTs in *Chapter 6*.

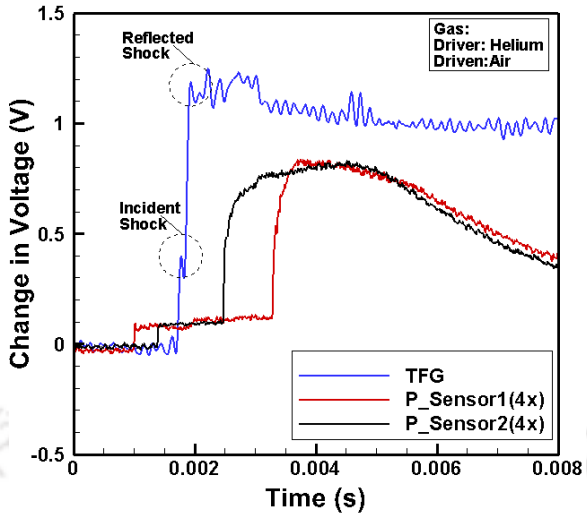

Fig. F.2: Typical voltage response captured from the STFG and the pressure sensors inside the shock tube for short duration study

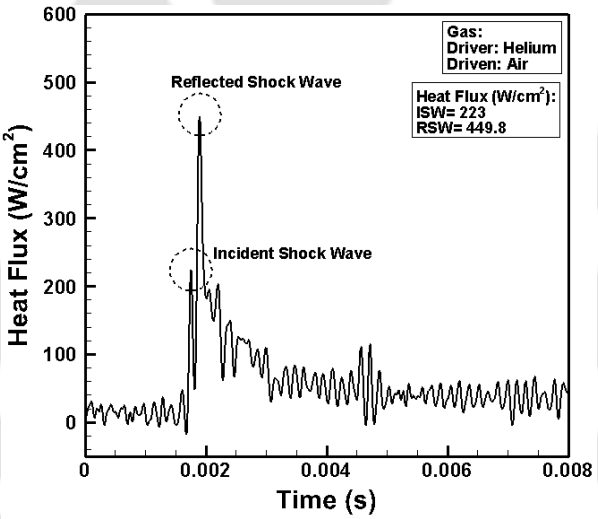

Fig. F.3: Heat flux histories estimated from the voltage response of the STFG for short duration study